UNIVERSITAT DE BARCELONA
FACULTAT DE QUÍMICA
DEPARTAMENT D'ENGINYERIA QUÍMICA I METAL·LÚRGIA

Fenton and UV-vis based advanced oxidation processes in wastewater treatment: Degradation, mineralization and biodegradability enhancement.

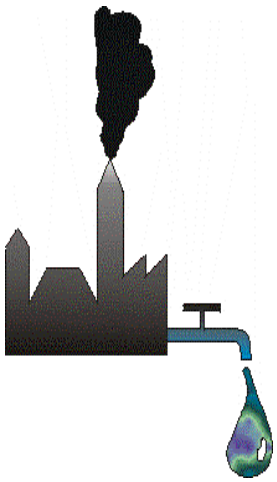

Miguel Rodríguez
Barcelona, April, 2003

Programa de Doctorado de Ingeniería Química Ambiental

Biennio 1998-2000

Memoria presentada por Miguel Rodríguez, Ingeniero Químico, para optar al grado de Doctor en Ingeniería Química

Miguel Rodríguez

La presente Tesis ha sido realizada en el Departamento de Ingeniería Química y Metalurgia de la Universidad de Barcelona, bajo la dirección del Dr. Santiago Esplugas Vidal, quien autoriza su presentación:

Dr. Santiago Esplugas Vidal

Barcelona, Abril de 2002

Al Prof. Sergio Miranda, pilar fundamental en mi transitar por la vida universitaria.

Por fortuna la vida está llena de momentos como estos. Por ello, nunca abandones, siempre será mejor perseverar y ver como al final todo llega, así como llega el sol cada mañana.

Miguel

En honor a la verdad, el espacio para los agradecimientos podría ocupar un capítulo de esta tesis, y más que una exageración es una manera de expresar el haber tenido la fortuna de trabajar y compartir con tanta gente y de quienes siempre recibí ayuda, aprecio, amistad y solidaridad razones por las cuales estoy muy agradecido. Trataré sin embargo, en un buen ejercicio de síntesis. resumir sin dejar a nadie en el olvido.

En primer lugar quiero agradecer al convenio ULA-CONICIT por el otorgamiento de la beca para la realización de este doctorado al igual que al DR. Santiago Esplugas, quien aceptó ser mi tutor y de quien he recibido amistad, confianza , conocimientos y toda su ayuda para llevar a feliz término esta tesis doctoral. Gracias por todo Santi.

Toda ésta invalorable experiencia ha sido posible por el compartir diario con mucha gente de gran calidad humana. No puedo olvidar mis primeros días de trabajo con Andreas. Los dias interminables y continuos de trabajo con Vitaliy y ya cerca del final con Florian.

To Dr. Gurol and her research's group in San Diego State University, especially to Melissa, who always gave me her help to make easier the difficulty of having to speak in another language. Thanks a lot for every thing.

En otras de mis andanzas en la búsqueda del conocimiento y de la experiencia requerida para asumir en el futuro con buena base la responsabilidad de seguir en el mundo de la investigación, tuve la oportunidad de compartir con el grupo del Dr. César Pulgarin, de la Escuela Politecnica Federal de Lausane, Suiza. De ellos solo puedo decir que se me metieron en el alma. Gracias Sandra, Víctor, Giovanna, Ricardo, Isabel, y por supuesto César, por toda la ayuda y la amistad que recibí de ustedes.

Antes de finalizar todo este periplo, también tuve la oportunidad de compartir y aprender de los amigos de la Plataforma Solar de Almería. A Sixto, Julián, Julia, Wolfgang, Agustín, Sonia y Antonio, para todos mi agradecimiento.

Ya habia advertido que seria largo, pero ya casi termino, solo que ahora viene un agradecimiento muy especial. Todo este andar de trabajo por estos centros de investigación, siempre tuvo como centro principal, la Universidad de Barcelona, y de ella, el Departamento de Ingeniería Química y Metalúrgica, donde por supuesto pasé la mayoria de estos 4 largos años. A todos sus profesores, gracias, y muy especialmente, Jaime Giménez, Carmen Sans, Carmen González, Esther Chamarro y David Curcó. También para el personal de este departamento de quien siempre he recibido el mejor de los tratos y debo resaltar de ellos al Sr. Antonio y al Sr. Somoza (quien ya lamentablemente no está entre

nosotros) personas que al inicio fueron de mucha ayuda y luego pasaron a ser mis amigos. Mi agradecimiento también a el resto de amigos que han estado todos estos años, y de alguna manera han contribuido para que los mismos sean mas llevaderos, me refiero a Marta, Esther, Alicia, Neus, Cristina, Nadia, Eva y Fares.

En medio de tantos nombres y momentos especiales, hay alguien para quien cualquier cosa que diga podría resultar poco. Alguno de ustedes pueden imaginarse a quien me refiero, y no puede ser otra que a mi amiga del alma, a la que por espacio de todos estos años siempre ha estado y de la que nunca podré olvidarme. Han sido tantos momentos compartidos, tanto trabajo juntos, tantas conversaciones y también de alguna discusión, como es lógico, pero ella siempre estuvo allí. No puede ser otra que mi amiga Sandra. Para tí, lo mejor de mis sentimientos para agradadecer todo lo que has hecho por mí.

Finalmente, hay gente que no ha estado en los laboratorios, pero si que han estado en mis dias, mis recuerdos y en mi vida diaria. Me refiero a mi familia, mi mamá, hermanas, sobrinos, quienes seguro habrian querido contribuir mas. Hay siempre sin embargo, alguién que se destaca, que da ese extra, que se entrega mas, y en este caso ha sido mi hermana Nina, a quien le agradezco infinitamente su amor, su compañía, su amistad y su solidaridad. Gracias por ser como eres.

No puedo dejar de agradecer a dos amigos que fueron fundamentales para mi estancia en esta hermosa ciudad, ellos son Victor y Ana, para ustedes también mi agradecimiento.

Quiero además agradecer a todos esos amigos que a pesar de la distancia, siempre han estado conmigo. A Miguel, Carmen, Luz, Carlos, J. Carlos, la flaca, Domingo, Cerrada, la familia Miranda y tantos otros, que no tendria espacio para nombralos.

Finalmente, mi más sentido agradecimiento al país que me vio nacer y de él, a ese pequeño pueblo, El Tocuyo, donde crecieron mis sueños, hoy, uno de ellos se hace realidad.

A todos, mil gracias.

Index

1.Introduction

1. Introduction

1.1. The problematic of water contamination

One of the characteristics that best defines today's society in what is understood as developed countries is the production of waste products. There is practically no human activity that does not produce waste products and in addition there is a direct relationship between the standard of living in a society or country and the amount of waste products produced. Approximately 23% of the world's population live in developed countries, consume 78% of the resources and produce 82% of the waste products (Blanco and Malato, 1996). In addition, it has to be pointed out that the volume of residual waste increases in an exceptional way with regards to a country's level of industrialisation. At present, there are some five million known substances registered, of which approximately 70,000 are widely used worldwide, and it is estimated that 1,000 new chemical substances are added to the list each year.

The need for sustainable growth is countered by the reality of demographic growth. Many countries are experiencing a period of non-sustainable growth, with very variable macroeconomic achievements in the various countries. Even in the case where some countries have achieved a beneficial macroeconomic progress, these achievements are not reflected in the standard of living and quality of life of large sections of the population. These large contrasts are reflected in the problems related to the rational management of water, which cannot be dealt with in a unilateral way, but by many different procedures.

A recent publication (Schertenleib and Gujer, 2000) describes in a generic form the problems that societies have had to face regarding water use as the society evolved. The countries with sustainable development have, one by one, confronted the problems related to biological contamination, with the levels of heavy metals, with the intensive use of nutrients, and with organic contaminants at very low levels. Water disinfections, the treatment of effluents before being discharged into water systems, the limitation and substitution of nitrates and phosphates in products that are used on a massive scale, and the development in analytical chemistry and in ecotoxicology are examples of some of the "tools" used to combat these problems. The result of its own harmonic evolution is shown in Figure 1.1. It must be noted that the time scale to resolve each problem as it arises, is always shorter.

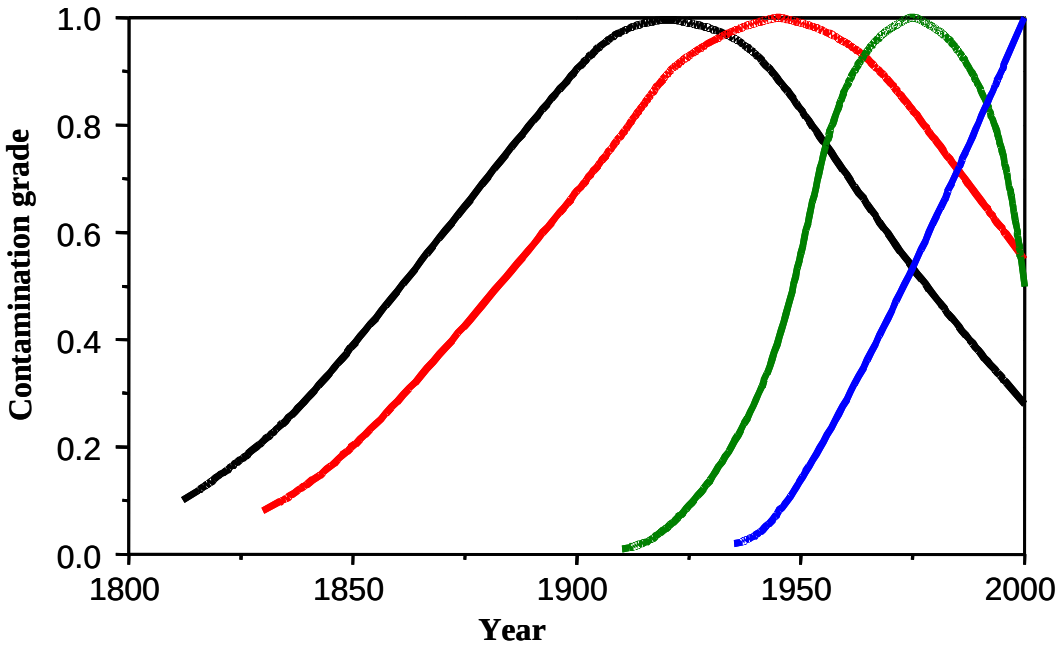

Figure 1.1. Line graph of the evolution of contamination levels (on an arbitrary scale) of natural waters in countries with sustainable development. From left to right the lines represent municipal faecal waste drainage, industrial effluents, nutrients and micro-pollutants. The environmental problems increase until a solution is found and then decrease.

In contrast, countries with non-sustainable development are represented in Figure 1.2. There is no doubt that many developing countries can be included in this category, or even in a more complicated situation with even more primitive stages of development. The problems derived from the toxicological effects of organic compounds, which are active at very low levels, must be resolved at the same time as water disinfection for rural communities. It is clear that innovative procedures are needed to deal with this wide range of problems, which vary notably in its application scale and the complexity of the problems (Blesa, 2001).

Up until relatively recently, the discharging of waste in the environment was the way of eliminating them, until the auto-purifying capacity of the environment was not sufficient. The permitted levels have been vastly exceeded, causing such environmental contamination that our natural resources cannot be used for certain uses and their characteristics have been altered. The main problem stems from waste coming from industry and agriculture, despite the fact that the population also plays an important role in environmental contamination.

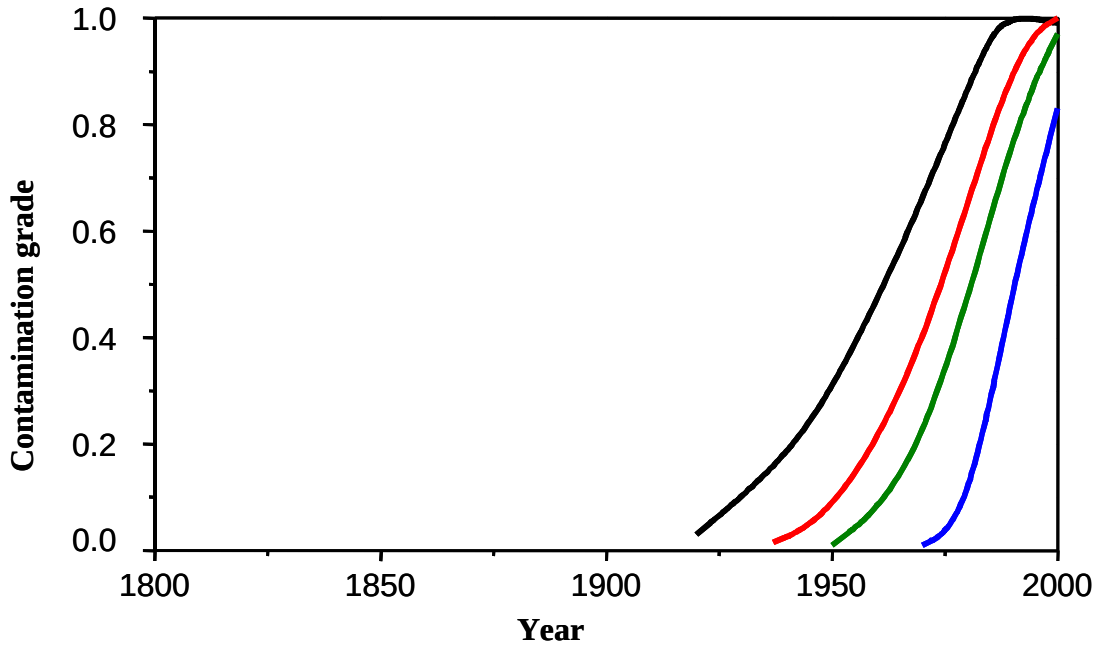

Figure 1.2. Line graph of the contamination levels (on an arbitrary scale) of the natural waters in non-sustainable developed countries. From left to right the lines represent municipal faecal waste drainage, industrial effluents, nutrients and micro-pollutants. The environmental problems increase without a solution being found to solve them.

Phenols, pesticides, fertilizers, detergents, and other chemical products are disposed of directly into the environment, without being treated, via discharging, controlled or uncontrolled and without a treatment strategy.

In this general context, is very clear that the strategy to continue in the search of solutions to this problem that every day presents a sensitive growth, mainly in the developing countries, it will be guided to two fundamental aspects:

- The development of appropriate methods for contaminated drinking, ground, and surfaces waters, and mainly
- The development of appropriate methods for wastewaters containing toxic or non-biodegradable compounds.

This thesis is focused in the second of the aspects. Dangerous and Toxic Waste is defined as "those solid, semi-liquid, and liquid materials, as well as those gaseous materials in recipients, which are the result of a process of production, transformation, use or consumption which are destined to be abandoned and whose composition contains some of the substances or materials that figure in the annex of Law 20/1986 of the 14th May,

"*Base for Dangerous and Toxic Residues"*, or in the successive revisions by the EU Committee, in such quantities or concentrations that represent a health risk to humans, natural resources and the environment and that need a treatment process or special elimination". The European Union made out a list of dangerous compounds, considered as contaminants, to which constantly new substances are added ("black list" of the E.U., see Table 1.1).

Among the before mentioned waste products, the most worrying, from an environmental point of view, are those so called non-biodegradable or persistent materials because in the case of not receiving a specific treatment necessary for their destruction or inertness, they can effect various sectors of the environment. From this, a series of very diverse and irreversible damages can result, ranging from the deterioration or disappearance of a determined environment to changes in the health of those individuals who live in that environment.

A large part of this type of residual waste is generated in an aqueous solution and, owing to its non-biodegradable nature, the biological treatment procedures (the most commonly used) are not effective, and unless there is an additional specific treatment, they end up being dumped in the environment. The presence of this type of pollutant in an aqueous dissolution is especially problematic as the residual waste cannot be stored indefinitely (as is the case with some solid waste) and it has the peculiarity that a small volume of water is able to contaminate much greater volumes of water. It must also be pointed out that a wide spectrum of compounds can transform themselves into potentially dangerous substances during the drinking water treatment process, particularly by chlorination, as is the case of the precursor compounds of the formation of chlorocarbons (Marhaba and Washington, 1998).

In general, the techniques available for the treatment of residues are very diverse. In some cases the residue is only made inert and it is later transferred to a controlled discharge, where it is stored safely. Another possibility is to transport the residues to an incineration plant. This process, in addition to needing a large consumption of energy to finish the process, has the problem of releasing intermediate toxins from mineralization into the atmosphere, which means that incineration is a cause for controversy. On the other hand, incineration is very expensive and usually involves long transport distances of the residues to a central installation (Steverson, 1991; Dempsey and Oppelt, 1993; Kakko *et al.*, 1995).

Table 1.1. Black list of chemicals substances selected by the E.U. (Harrinson, 1992)

Group	Included substances
Chloride Hydrocarbons	Aldrin, dieldrin, chlorobenzene, dichlorobenzene, chloronaphthalene, chloroprene, chloropropene, chlorotoluene, endosulfane, endrin, hexachlorobenzene, hexachlorobutadiene, hexachlorocyclo-hexane, hexachloroethane, PCBs, tetrachlorobenzene, trichlorobenzene.
Chlorophenol	Monochlorophenol, 2,4-dichlorophenol, 2-amino-4-chlorophenol, pentachlorophenol, 4-chloro-3-methylphenol, trichlorophenol.
Chloroanilines and nitrobenzenes	Monochloroanilines, 1-chloro-2,4-dinitrobenzene, dichloroaniline, 4-chloro-2-nitrobenzene, chloronitrobenzene, chloronitrotoluene, dichloronitrobenzene.
Policyclic Aromatic Hydrocarbons	Antracene, biphenyl, naphthalene, PAHs
Inorganic substances	Arsenic and its compounds, cadmium and its compounds, mercury and its compounds.
Solvents	Benzene, carbon tetrachloride, chloroform, dichloroethane, dichloroethylene, dichloromethane, dichloropropane, dichloropropanol, dichloropropene, ethylbenzene, toluene, tetrachloroethylene, trichloroethane, trichloroethylene.
Other	Benzidine, chloroacetic acid, chloroethanol, dibromomethane, dichlorobenzidine, dichloro-diisopropyl-ether, diethylamine, dimethylamine, epichlorhydrine, isopropylbenzene, tributylphosphate, trichlorotrifluoroethane, vinyl chloride, xilene.
Pesticides	Cyanide chloride, 2,4-dichlorophenoxyacetic acid and derivatives, 2,4,5-trichlorophenoxyacetic acid and derivatives, DDT, demeton, dichloroprope, dichlorvos, dimethoate, disulfoton, phenitrothion, phenthyon, linuron, malathion, MCPA, mecoprope, monolinuron, omethoate, parathion, phoxime, propanyl, pirazone, simacine, triazofos, trichlorofon, trifularin and derivatives.

In the present work, it has been deepened in the treatment of organic compound in aqueous solution by means of the use of advanced oxidation processes (AOP), in the search of their elimination or transformation in more biodegradable compound.

The experimental work has been divided into four chapters. First part (chapter 3) is focused on the kinetic study of Fenton process for what phenol has been taken as reference (model compound widely studied) and an aromatic non-biodegradable compound, such as nitrobenzene.

The second part (chapter 4) addresses to the optimisation of some treatment processes as photo-Fenton, H_2O_2/UV and Fe^{3+}/UV-vis using different sources of artificial light and sunlight. The experimental work of this chapter was divided into two parts. In the first one, experiments were performed at laboratory scale in University of Barcelona. In the second one, experiments in pilot plant were made in EPFL (Ecole Politechnique Federale de Lausanne, Switzerland) and at the Plataforma Solar de Almería, Spain.

Chapters 5 and 6 represent an application of the treatments methods used in chapter 4, in which their influence on the biodegradability of an organic chloride compound (DCDE) and of waters coming from the textile industry was studied. For this final part of the thesis, the experimental work was carried out in the University of San Diego (San Diego, USA) and at the EPFL (Lausanne, Switzerland), respectively.

1.2. Studied aqueous solutions

In this general context of the environmental problems caused by different kinds of pollutants, four different types of aqueous solutions containing organic compounds as phenol, nitrobenzene, DCDE and waters coming from the textile industry have been taken as model. The aim of the work was to make a deep study in the treatment of these compounds in water solution by means of the use of chemical oxidation processes in order to establish the best operating conditions to be applied.

Phenols have been widely used in many industrial processes, as synthesis intermediates or as raw materials in the manufacturing of pesticides, insecticides, wood preservatives, and so forth. Because of the great diversity of their origins, they have a great ubiquity and can be found not only in industrial wastewaters but also in soils and surface

and ground waters, as a consequence of their release in industrial effluents or improper waste disposal practices and accidental leakages (Benitez *et al*., 1997).

Aromatic nitro compounds are commonly used in the manufacture of pesticides, dyes and explosives, and are often detected in industrial effluents, in ambient freshwater, in ambient environments and in the atmosphere (Lipczynska-Kochany, 1992). Moreover, nitroaromatic hydrocarbons are naturally generated, as results of photochemical reactions produced in the atmosphere (in countries like Germany, Japan, Switzerland and USA nitrophenol and dinitrophenol have been detected in air and rain) (Alonso y del Pino, 1996 and reference herein).

Dichlorodiethylether (DCDE) is widely used in the US in the manufacture of pesticides and pharmaceuticals, as a solvent and cleaning fluid, as a constituent of paints and varnishes, and in the purifying of oils and gasoline (Toxnet, 2001).

Textile processing is one of the most important industries in the world and it employs a variety of chemicals, depending on the nature of the raw material and product. Some of these chemicals are different types of enzymes, detergents, dyes, acids, sodas and salts. The discharge of wastewaters that contains high concentration of reactive dyes is a well-known problem associated with dyestuff activities (Neppolian *et al*., 2001; Rodríguez *et al*., 2002).

The presence of these compounds in industrial wastewater and the discharge of textile waters, forces us to look for alternative processes to those well-known biological treatments, to achieve its effective elimination of the residual waters.

1.2.1. Environmental problems caused by phenolic compounds

At present, a large part of the pollution in the public water system is caused by industry (Blanco and Rodríguez, 1993). One particular case, which is important within these industrial effluents, is that of phenols. The word “phenols” includes phenol, C_6H_5OH, (taken as model compound in this study) and all its derivatives, i.e. those aromatic organic compounds that contain one or various hydroxyl groups. Therefore, although phenol is the compound that appears most frequently in liquid effluents, the presence of some of its derivatives, to be precise, ortho, meta and p-cresol, contribute notably to the toxicity of the effluents. Table 1.2 shows the physical properties of the four compounds: phenol, ortho, meta and p-cresol (Ullmann's, 1991).

Table 1.2. The physical properties of phenol, ortho, meta and p-cresol.

Properties	**o-cresol**	**m-cresol**	**p-cresol**	**phenol**
Melting point (^{o}C)	30.90	11.5	34.8	41
Boiling point (^{o}C)	191	202.7	201.9	182
Density d_4^{20} (solid) (g.cm^{-3})	1.047	-	1.034	1.071
Density d_4^{20} (liquid) (g.cm^{-3})	1.027	1.034	1.018	1.049
Density (vapor) (air = 1)	3.72	3.72	3.72	3.24
Vapor pressure (25^{o}C) (Pa)	33.3	14.7	14.7	47
Vapor pressure (60^{o}C) (Pa)	473	226	226	5300
Auto-inflammation Temp (^{o}C)	559	559	559	715
Solubility (25^{o}C) (%)	2.5	1.9	1.9	8.7
Molecular weight	108.14	108.14	108.14	94.11

The harmful characteristics of phenolic compounds lie in concentrations of parts per billion (García *et al.*, 1989), which are very inferior to toxic concentrations, and contribute a disagreeable smell and taste to chlorinated water. Normally, the taste cannot be detected in concentrations inferior of 0.1 to 0.01 ppb. Phenols are considered toxic for some aquatic life forms in concentrations superior to 50 ppb and the ingestion of one gram of phenol can have fatal consequences in humans. Its dangerousness lies in the effect that it has on the nervous system of living beings. In addition, they have a high oxygen demand, 2.4 mg O_2 per mg of phenol. Another additional effect is the capacity of phenols to combine with existing chlorine in drinking water, giving rise to chlorophenols, compounds that are even more toxic and difficult to eliminate.

Despite being high toxicity compounds, phenols have a wide range of uses:

- Plastics, resins and plasticizers: phenol in this type of industry is used above all in the production of plastics and phenol-formaldehyde resins. In addition cresols are used in the making of tricresyl phosphate, which is a plasticizer useful for cellulose acetate, nitrocellulose, ethanethiol cellulose and vinyl plastics.
- Preserving agent for wood, disinfectants and insecticides: creosote oil, a distillation obtained from the process of coal-making at high temperatures, is used for preserving wood in addition to being a source of cresylic acid and cresols used for disinfectants and insecticides.

- Vegetable hormones and detergents: phenol is used directly in the production of these types of compounds.
- Medicines: a clear example of a derivative of phenol is acetylsalicylic acid, a compound from which aspirin is obtained.
- Dyes, photography and explosives: these industries have many uses for phenol although the total consumption is not very high. Some aminophenols are used as dyes and photographic developers. Trinitrophenol, for example, is used as a dye and as an explosive.

In all these industries give rise to polluting phenolic effluents, which are much higher than the toxic levels. Table 1.3 shows phenol concentrations coming from different industries (García *et al.*, 1989).

Table 1.3. Phenols content in industrial waste

Industry	**Concentration of phenols ($mg.L^{-1}$)**
Coal mining	1000-2000
Lignite transformation	10000-15000
Gas production	4000
High ovens	4000
Petrochemicals	50-700
Benzene factory	50
Pharmaceuticals	1000
Oil refining	2000-20000

1.2.2. Environmental problems caused by aromatic nitro compounds

Taking into account that aromatics nitro compounds constitute a threat to human health and produce a public concern, several of them have been listed among the 130 priority pollutants given by the US EPA (United States Environmental Protection Agency) in the federal Clean Water Act (CWA), e.g. nitrobenzene (EPA, 2002). Recently, the US

EPA has also included them in a reduced list of drinking water contaminants to be investigated in the period 2001-2005 (Hayward, 1999).

Aromatic nitro compounds are commonly used in industrial processes (manufacture of pesticides, dyes and explosives) and as a consequence they appear as contaminants in every kind of water (especially in surface waters) and industrial wastewaters. This substances present a high toxicity, provoking serious health problems: blood dyscrasia, eyes and skin irritations, they affect the central nervous system, etc. Several studies have shown the presence of these substances in surface waters (Howard, 1989) and ground waters (Duguet *et al.*, 1989). One of the main ways of contamination of superficial wastewaters by nitroaromatic compounds are the residual industrial effluents. Table 1.4 shows the concentrations of some nitro compounds in industrials effluents (Howard, 1989).

Table 1.4. Concentration of nitroaromatic compounds in industrial effluents

Industry	Concentration of 2-nitrophenol ($\mu g.L^{-1}$)	Concentration of 4-nitrophenol ($\mu g.L^{-1}$)
Iron and steel manufacture	< 21	-
Foundries	20 - 40	-
Pharmaceuticals	< 10	-
Organic chemical manufacturing/plastics	< 130	< 190
Rubber processing	< 4,9	-
Textile mills	< 4,1	< 10
Coal mining	< 17	-
Metal finishing	72 - 320	< 10
Electrical/electronic components	75 - 320	22 - 35
Photographic equipment/supplies	19 - 32	< 57
Oil refining	1400	< 10

Nitrobenzene ($C_6H_5NO_2$, molecular weight 123.1) the most representative within nitroaromatics compounds, has been taken as one of the model compounds that has been included in this study. Nitrobenzene is readily soluble in most organic solvents and is

completely miscible with diethyl ether and benzene. It is a good solvent for aluminum chloride and is therefore used as solvent in Friedel-Craft reactions. It is only slightly soluble in water (0.19% at 20ºC; 0.8% at 80ºC). Some other physical properties of nitrobenzene are as follows (see Table 1.5).

Table 1.5. Physical properties of nitrobenzene (Ullmann's, 1991)

Physical property	Value
Melting point	5.85ºC
Boiling point at 101 kPa at 13 kPa at 0,13 kPa	 210.9ºC 139.9ºC 53.1ºC
Density $d_4^{1.5}$ (solid) $d_4^{15.5}$ (tech. spec.) d_4^{25}	 1.344 g.cm^{-3} 1.208 - 1.211 g.cm^{-3} 1.199 g.cm^{-3}
Vapor pressure (20ºC)	0.15 mm Hg
Viscosity (15ºC)	2.17x10^{-2} mPa.s
Surface tension (20ºC)	43.35 mN.m^{-1}
Dielectric constant (20ºC)	35.97
Specific heat (30ºC)	1.418 J.g^{-1}
Latent heat of fusion	94.1 J.g^{-1}
Latent heat of vaporization	331 J.g^{-1}
Flash point (closed cup)	88ºC

Nitrobenzene is released into the environment primarily from industrial uses but can also be formed in the atmosphere by the nitration of benzene, a common air pollutant. The largest sources of nitrobenzene release are from its manufacture and primary use as a chemical intermediate in the synthesis of aniline. Smaller amounts are also released from consumer products in which nitrobenzene is used as a solvent. The most familiar of these are metal and shoe polishes.

It can evaporate when exposed to air. Once in air, nitrobenzene breaks down to other chemicals. It dissolves when mixed with water. Most releases of nitrobenzene to the U.S. environment are to underground injection sites. In 1992, only a small percentage (6%) of environmental releases of nitrobenzene was to air. It can also evaporate slowly from water and soil exposed to air. Available information indicates that nitrobenzene is moderately toxic to aquatic life. Nitrobenzene may be stored in plants, but is not expected to accumulate in fish.

About the stability of nitrobenzene in water, it has been estimated that its half-life varies from one day for natural channels, as it has been confirmed by works carried out by Zoeteman (1980) in the Rhin river (Holland), and 3.8 days in an aerated lagoons (Davis *et al.*, 1983). Because it is a liquid that does not bind well to soil, nitrobenzene that makes its way into the ground can move through the ground and enter groundwater. In surface water, nitrobenzene was detected in only 0.4% of surface water stations and in 1.8% of reporting stations on industrial wastewaters. In Table 1.6, those industries in whose effluents nitrobenzene has been detected are indicated. Furthermore, the presence of nitrobenzene in municipal wastewaters in a concentration between 20 and 100 $\mu g.L^{-1}$ has been detected.

Table 1.6. Concentration of nitrobenzene in different industrial effluents

Industry	Average concentration ($\mu g.L^{-1}$)
Oil refining	7.7
Leather tanning	3.7
Nonferrous metals	47.7
Organics and plastics	3876.7
Pulp and paper	124.3
Auto and other laundries	40.4
Pesticides manufacture	16.3
Explosives	51.7
Organic chemicals	43.7
Inorganic chemicals	1995.3

As it has been commented before, aromatic nitro compounds have been included in the priority pollutants selected by the European union (see Table 1.1). Nevertheless, these compounds have been little studied, paying more attention to those compounds in whose composition halogens are present.

1.2.3. Environmental problems caused by DCDE

Dichlorodiethyl ether ($C_4H_8Cl_2O$, molecular weight 143.01) is a colorless liquid with chloroform-like odor that irritates the eyes and mucous membranes. It is occasionally detected as a constituent of municipal wastewater and is found often in surface waters. It is a chlorinated organic compound that has been used for decades in many industries associated with the manufacturing of solvents, oil and gasoline, pharmaceuticals, pesticides, textiles, paint and more.

In the petroleum industry is used as solvent and dewaxing agent. It is also used in the manufacture of oils, fats, napfthalenes, greases, pectin, waxes, gums, tars, resins, soaps, cellulose esters, varnish, lacquers, and finish removers. In the textile industry is used as scouring, wetting, cleansing, penetrating agent, and as a solvent in the dry cleaning industry.

In agriculture is used as soil fumigant, insecticide, and acaricide. Finally, in the pharmaceutical industry, it is used as a reagent for chemical synthesis during the manufacture of pharmaceuticals, rubber chemicals, resins, plasticizers and other chemicals (Ullmans's, 1991; Toxnet, 2001). Some physical properties of DCDE are shown in Table 1.7. It is low volatile and highly water-soluble. It travels quickly through groundwater since it does not adsorb easily to sediment (Toxnet, 2001).

DCDE is obtained as a byproduct in the production of ethylene chlorohydrin, where it collects in the distillation sump and is purified by vacuum distillation. DCDE is also produced by reaction of ethylene chlorohydrin with sulfuric acid at 90-100 ^oC or by saturation of an aqueous ethylene chlorohydrin solution with ethylene and chlorine below 85 ^oC. It is reactive, flammable, mutagenic and a probable carcinogen (NIOSH, 1995). When heated to decomposition, DCDE emits toxic fumes (Toxnet, 2001). Bioaccumulation in aquatic systems is low, and like many ethers, it is resistant to biodegradation (Toxnet, 2001). When water polluted with DCDE is intended for drinking purposes, a treatment process must be implemented to prevent public exposure. In fact, if ethyl ether is present in

the system, after chlorination, DCDE will be produced. Ingestion of contaminated water and inhalation of contaminated air are the two most common routes of general population exposure (Toxnet, 2001). A risk level of 0.3 μg per day has been set to minimize potential carcinogenic effects (Genium, 1993). Animal experiments have demonstrated that excessive levels of DCDE exposure can result in central nervous system depression, liver and kidney damage, and death (NIOSH, 1995). Due to its toxic properties, DCDE is on the Community Right to Know List and is regulated by the Resource Conservation and Recovery Act (RCRA) as well as the Comprehensive Environmental Response, Compensation, and Liability Act (CERCLA).

Table 1.7. Physical properties of DCDE (Ullmann's 1991)

Physical property	Value
Melting point	-50°C
Boiling point at 760 mmHg	178ºC
Density d_4^{20} (liquid)	1.219
Vapor pressure (20ºC)	0.4 mm Hg
Viscosity (25°C)	2.065 mPa.s
Surface tension (25°C)	41.8 $mN.m^{-1}$

1.2.4. Environmental problems caused by textile wastewater

Textile mills are major consumers of water and consequently one of the largest groups of industries causing intense water pollution. The extensive use of chemicals and water results in generation of large quantities of highly polluted wastewater. According to the U.S. EPA, about 1 to 2 million gallons of wastewater per day are generated by average dyeing facility in the US, reactive and direct dyeing generating most of the wastewater. Around 10^9 kg and more than 10,000 different synthetic dyes and pigments are produced annually worldwide and used extensively in dye and printing industries. Textile processing employs a variety of chemical, depending on the nature of the raw material and products. It is estimate that about 10 % are lost in industrial wastewater (Young and Yu, 1997). The

wastewater generated by the different production steps (i.e. sizing of fibers, scouring, desizing, bleaching, washing, mercerization, dyeing and finishing) has high pH and temperature. It also contains high concentration of organic matter, non-biodegradable matter, toxic substances, detergents and soaps, oil and grease, sulfide, sodas, and alkalinity. In addition, the high salt conditions (typically up to 100 g L^{-1} sodium chloride) of the reactive dyebaths result in high-salt wastewater, which further exacerbates both their treatment and disposal. The fate of these chemicals varies, ranging from 100% retention on the fabric to 100% discharge with the effluent. As a result, textile industry is confronted with the challenge of both color removal (for aesthetic reasons) and effluent salt content reduction. In addition, reactive dyes are highly water soluble and non-degradable under the typical aerobic conditions found in conventional, biological treatment system Neppolian *et al.*, 2001; Rodriguez *et al.*, 2002).

The contamination observed in textile wastewater is higher than the limits set by the National Environmental Quality Standards (NEQS) for all important wastewater parameters (see Table 1.8).

In general, the current practice in textile mills is to discharge the wastewater into the local environment without any treatment. This wastewater causes serious impacts on natural water bodies and land in the surrounding area. High values of COD and BOD, presence of particulate matter and sediments, and oil and grease in the effluents causes depletion of dissolved oxygen, which has an adverse effect on the marine ecological system. Effluent from mills also contains chromium, chemicals; effluents are dark in color, which increases the turbidity of water body. This in turn hampers the photosynthesis process, causing alteration in the habitat. Besides, the improper handling of hazardous chemical content in textile water has some serious impacts on the health and safety of workers. Contact with chemical puts them the high risk bracket for contracting skin diseases like chemical burns, irritation, ulcers, etc. and even respiratory problems (ETPI, 2003).

Table 1.8. Characteristic of Process Wastewater from a Textile Processing Unit (ETPI, 2003)

Parameter	Prevailing Range ($mg.L^{-1}$)	NEQS($mg.L^{-1}$)
BOD_5	120 - 440	80
COD	300 - 1100	150
TDS	200 - 5000	3500
TSS	50 - 120	150
pH	8 - 11	6 - 10
oil and grease	11 - 45	10
Cr	0.5 - 2.5	1.0

1.3. Methods for the removal of organic compounds in wastewater

The treatments processes of different types of effluents to be used must guarantee the elimination or recuperation of the pollutant in order to reach the strict authorized levels for the discharge of these effluents. The levels of pollutants allowed in discharge waters, are directly related with the type of present pollutant in the effluent.

In general, the elimination of organic pollutants in aqueous solution need one or various basic treatment techniques (Weber and Smith, 1986; Chuang *et al.*, 1992): chemical oxidation, air desorption, liquid-liquid extraction, adsorption, inverse osmosis, ultra-filtration and biological treatment. Depending on the present compound in solution the methods to use can be destructive as for example, chemical oxidation, incineration or degradation, which only allow the efficient elimination of the pollutant from an aqueous form; and the non-destructive methods, among which is liquid-liquid extraction and absorption, that allow the recuperation of the pollutant. On the other hand, the application of one or other of the methods depends on the concentration of the effluent. It is necessary to choose the most adequate method according to the characteristic of the concentration. Once again, it has to be chosen between those techniques, which are useful for high concentrations of pollutants, like incineration or some chemical oxidation methods, and those techniques for low concentrations of pollutants, for example adsorption, membrane techniques, and some chemical oxidation methods as well. The choice of one or other of

the methods basically depends on the cost of the process and other factors like the concentration and volume flow of the effluent to be treated.

The most widely used treatment methods of organic compounds are described next.

1.3.1. Incineration

The incineration is an useful method for small quantities of wastewater with high pollutant concentration. However, it presents the disadvantage of requiring big investments and having high energy cost as well. The incinerators normally used for this process are similar to those of sludge or industrial residues, and they can be horizontal, vertical or fluidized bed. A fundamental economic aspect in the incineration of organic solutions is the auxiliary fuel needed to maintain the combustion. The treatment of phenolic effluents by means of this method has been reported (Lanouette, 1977). For NB, DCED no references were found. In the case of textile activities, the incineration has been used in the treatment of sludge from textile wastewater and the ash is landfilled (Masselli *et al.*, 1970). The incineration can be also used to minimize the textile wastewater quantity and after other treatment processes could be applied.

1.3.2. Air stripping

Air stripping involves the transfer of volatile organics from liquid phase to the air phase by greatly increasing the air/water contact area. Typical aeration methods include packed towers, diffusers, trays, and spray aeration. It has the advantage that is more established and more widely understood technology than chemical oxidation. It can be accurately designed from theory and experience without the need for design tests. If air emissions are not regulated, air stripping is by far the simplest and cheapest solution for the removal of volatile compounds from water. The treatment of phenolic and nitro aromatic effluents by means of air stripping has not been reported. In the case of NB solutions, experiments to check the stripping effect demonstrate that the NB remains constant in solution. Taking into account that the DCDE is a volatile compound, air stripping can be thought as treatment method for this compound. However, air stripping has been used in the treatment of trichloroethylene (TCE), dichloromethane (DCM), 1,2-dichloroethylene (DCE), 1,2-dichloroethane (DCA), chlorobenzene (Cl-Bz), and dichloroethyl ether (DCEE) and the results showed that they could be removed easily from water solutions

except DCEE (Li *et al.*, 2000). In the case of textile wastewater, air stripping used as pretreatment resulted in high solvent removal (Kabdasli and Gurel, 2000).

1.3.3. Adsorption of organic compounds onto activated carbon

Carbon adsorption is an advanced wastewater treatment method used for the removal of recalcitrant organic compounds as well as residual amounts of inorganic compounds such as nitrogen, sulfides, and heavy metals. This is a separation method in which the contaminant is transferred from a water phase, where it is dissolved, to the surface of active carbon where is accumulated for its subsequent extraction or destruction. The adsorption onto activated carbon is widely used for wastewater treatment. Thus, it is used in the control of color and odors, in the removal of organic compounds or trihalomethanes precursors, to remove chlorine and in general to remove toxic compounds.

The adsorption of nitrobenzene (NB) and phenol onto activated carbon has been widely studied. Both (NB and phenol) showed to be well adsorbable compounds onto activated carbon but in low concentration (Cañizares *et al.*, 1999; Sacher *et al.*, 2001). This method has been also combined with other and a significant improvement has been obtained (Cañizares *et al.*, 1999). No reference about adsorption of DCDE by activated carbon has been found. Many studies have been found in the literature regarding the treatment of textile wastewater by means of activated carbon (Roy and Volesky, 1977; Lin and Lai, 2000; Yeh *et al.*, 2002). Most of them showed the high effectiveness of carbon activated adsorption process in the reduction of COD (Chemical Oxidation Demand) and color removal from textile wastewater.

1.3.4. Wet oxidation

In the wet oxidation processes, organic and inorganic compounds are oxidized in aqueous phase, with oxygen or air, at high pressure and high temperature conditions. The temperature depends on the nature of the compounds to degrade, however it oscillates between 150 and 350ºC. Pressure goes from 20 to 200 bar. COD removal ranges from 75 to 90% (Li *et al.*, 1991). The mechanism of wet oxidation has been deeply studied and seems to take place by means of a free radical process. Among the compounds that have been catalogued as readily oxidizable by means of wet oxidation are aliphatic, aliphatic chlorides and aromatic, which do not contain halogenated functional groups, such as

phenols or anilines. Compounds contain halogen and nitro functional groups have been found to be difficult to be degraded by this method (Scott, 1997). Experimental results indicate that over 90% removal of phenol or phenolic compounds can be achieved in the wet oxidation wastewater treatment. Besides activated sludge process combined with wet oxidation, if appropriately operated, is capable of drastically reducing the COD concentration of the high concentrated chemical wastewater to meet the safe discharge requirement (Lin and Chuang, 1994). For DCDE and textile wastewater treatment by means of wet oxidation process not reference were found.

1.3.5. Electrochemical oxidation

The use of electrochemical oxidation for the destruction of organic compounds in water solutions has been tried on bench and pilot plant scale (Mieluch *et al.*, 1975; Boudenne *et al.*, 1996; Brillas *et al.*, 1998b), but is not used commercially because of its high operating cost. One of the main advantages of the electrochemical processes is that electrons are given or consumed within the electrodes, supplying a clean reactant, which does not increase the number of chemical molecules involved in the process. Nevertheless, they present some disadvantages, as:

- The electrochemical treatment is expensive in comparison with other processes and the mechanism in water is rather complex
- The necessity of the effluent to be conductor, therefore in case that the stream to be treated does not present a good conductivity a salt should be added

The electrochemical oxidation of organic compounds is thermodynamically favored against the competitive reaction of oxygen production by oxidation of water. However, the kinetics of oxidation of water is much faster than the kinetics of oxidation of the organic compounds, among other reasons because of its higher concentration (Palau, 1998).

The mechanism of the electrochemical processes involves three stages: electrocoagulation, electroflotation and electrooxidation. (Prousek, 1996):

$$RH \xrightarrow{-e^-} RH^+ \quad (1.1)$$

$$RH^+ \xrightarrow{-H^+} R^\bullet \quad (1.2)$$

$$R^\bullet + R^\bullet \rightarrow R - R \quad (1.3)$$

The anodic oxidation is generally considered to be a direct technique, involving the direct transfer of an electron from the organic molecule to the electrode, thus generating a cationic radical. In the direct way, the fate of the cationic radical, the pH and the nature of the electrodes influence in a decisive manner on the formed products. The latter radical-radical combinations have been frequently observed.

Few studies have been found in the literature regarding the electrochemical oxidation of NB (Comminellis, 1994; Colucci *et al.*, 1999) and none for the DCDE. However, for phenol solutions many works recommend the use of this method for their treatment (Lanouette, 1977; Smith, and Watkinson, 1981; Comninellis and Pulgarin, 1993; Pulgarin *et al.*, 1994). Many articles have been published about the application of electrochemical process in industrial textile wastewater treatment as well. In many of them, the efficiency of this method for color removal has been proven (Lin and Peng, 1994; Vlyssides *et al.*, 1999, 2000; Zappi *et al.*, 2000; Gutierrez *et al.*, 2001). It has been also used in combination with coagulation to remove color, turbidity and COD (Lin and Cheng, 1997).

1.3.6. Photochemical processes

For the oxidation of organic pollutants, a series of researchers have proposed direct photooxidation with ultraviolet light (Petersen *et al.*, 1988). However, there are a number of limitations for its use. The first one being that the organic compound to be eliminated must absorb light in competition with other compounds of the effluent to be treated. The second one is that the organic compounds generate a wide variety of photochemical reactions that can produce products more complex for degradation. In addition, not all the radiation emitted by the source of radiation is fully exploited, only the radiation absorbed and only a part of this produces chemical changes which means that some reactions of photodegradation have very slow kinetics.

The addition of energy as radiation to a chemical compound is the principle of the photochemical processes. The molecules absorb this energy and reach excited states the enough time to be able to carry out chemical reactions.

A large amount of studies (Legrini *et al.*, 1993) dealt with the degradation of chemicals in water using the Hg emission at 253.7 nm produced by low-pressure mercury lamps. However, results showed that 253.7 nm irradiation alone could not be used as an

effective procedure for the removal of organics from water: it may be useful for the degradation of substituted aromatic, however it is totally inefficient for effective removal of chlorinated aliphatics. It should, however, be noted that low-pressure Hg lamps are quite efficient for water disinfections purposes. Medium and high-pressure lamps, with a broader emission spectrum, have been more frequently used for the degradation of contaminants. Medium-pressure Hg lamps emit particularly strongly in the spectral region between 254 and 400 nm and are not only effective in generating hydroxyl radicals from e.g. hydrogen peroxide or ozone, but also by causing electronic transitions in a large number of organic molecules.

In the photochemical reactions, hydroxyl radicals may be generated by water photolysis (Cervera and Esplugas, 1983):

$$H_2O \xrightarrow{h\nu} H^{\bullet} + OH^{\bullet} \qquad (1.4)$$

Photolysis involves the interaction of light with molecules to bring about their dissociation into fragments. This reaction is a poor source of radicals, and in the reaction medium large quantity of reaction intermediates that absorb part of the radiation are generated, which decreases considerably the photooxidation kinetics of the contaminants. That fact makes the process valid only for effluents with low concentration of pollutants.

The photochemical treatment, although partially solving the problem of the refractory compounds, has some negative aspects in its practical application, as the high cost of UV radiation production. Furthermore, not all the emitted radiation is used, only the absorbed radiation, and only a fraction of this radiation produces chemical changes. This fact makes that some photodegradation reactions have a very low yields and slow kinetics. To accelerate the process, other oxidants like hydrogen peroxide and/or ozone, metallic salts or semiconductors like TiO_2 can be added, giving rise to the so-called Advanced Oxidation Processes. Instead of UV lamps, solar light could be used as radiation energy to degrade some compounds.

No effect was observed during direct photolysis of NB with a 150-W mercury-xenon lamp in the study carried out by (Lipczynska-Kochany, 1992). With regard to phenol, DCDE, and textile wastewater no references were found.

1.3.7. Biological oxidation

Biological treatment, generally by means of activated sludge (Wiesmann and Putnaerglis, 1986; Givens *et al.*, 1991), in adequate conditions (Wu *et al.*, 1994) has unquestionable advantages for the destruction of organic compounds. However, many organic pollutants cannot be effectively eliminated by biological oxidation in the treatment of municipal or residual waters nor natural waters (Bishop *et al.*, 1968). Its application to the treatment of effluents with phenols, nitro aromatic, ether aliphatic compounds and textile waters is quite restricted because of the high toxicity inherent in these wastes, the need to adjust the pH to an adequate value and add food and oxygen in adequate quantities for the transforming microorganisms (González, 1993), as the viability of the process depends fundamentally on the health and activity of the latter. There are two kinds of processes in the biological treatment of biological compounds: aerobic and anaerobic (Eckenfelder *et al*., 1989; Wang, 1992). The aerobic processes are used more because of their efficiency and operational simplicity (Ruiz *et al.*, 1992). In the case of phenol solutions, for concentrations between 50 and 100 $mg.L^{-1}$, aerobic treatment process has been used successfully (Vian, 1982). NB has been found to be non-biodegradable at low concentration (Urano and Kato, 1986; Kameya *et al.*, 1995). For DCDE no reference was found. In the case of textile wastewaters taking into account that they have a low biodegradability, biological treatment combined with other treatments methods has been tested. The results showed that it could be a good solution in the treatment of this type of industrial wastewater (Pala, and Tokat, 2001). The coupled chemical and biological treatment system will be described in details in section 1.3.10.

1.3.8. Chemical oxidation

Oxidation, by definition, is a process by which electrons are transferred from one substance to another. This leads to a potential expressed in volts referred to a normalized hydrogen electrode. From this, oxidation potentials of the different compounds are obtained. Table 1.9 shows the potentials of the most commonly used oxidizers (Beltrán *et al.*, 1997; Munter *et al.*, 2001).

Table 1.9. Oxidation power of selected oxidizing species

Oxidation species	Oxidation power (V)
Fluorine	3.03
Hydroxyl radical	2.80
Atomic oxygen	2.42
Ozone	2.07
Hydrogen peroxide	1.77
Permanganate	1.67
Hypobromous acid	1.59
Chlorine dioxide	1.50
Hypochlorous acid	1.49
Hypoiodous acid	1.45
Chlorine	1.36
Bromide	1.09
Iodine	0.54

Chemical oxidation appears to be one of the solutions to be able to comply with the legislation with respect to discharge in a determined receptor medium. It can also be considered as an economically viable previous stage to a secondary treatment of biological oxidation for the destruction of non-biodegradable compounds, which inhibit the process. The optimization of the process (Akata and Gurol, 1992) arises in those conditions in which non-biodegradable material is eliminated, but with a minimum amount of oxidizer. That is to say, leading the oxidation to the formation of biodegradable compounds and not those of CO_2 and H_2O. It can be said that it is an appropriate technique for small loads of pollutants; load meaning the concentration of the pollutant multiplied by the volume of flow of the effluent to be treated. This would otherwise become an expensive technique, because of its large oxidizer consumption, and would have few possibilities in relation to other more appropriate techniques for greater loads, as could be the selective absorption of pollutants, when the concentration of the pollutant is high, or biological oxidation, for low concentrations.

In addition to the polluting load, for the chemical oxidation to be economically profitable, it has to bear in mind the concentration of this in the effluent. This operation is easier to apply in the destruction of compounds like phenol, nitrobenzene, DCDE, some colorants and its derivatives for concentrations between 100 and 500 mg L^{-1}. In the case of higher concentrations, other operations come into play like selective absorption or incineration, in the case that recuperation is not desired. For lower concentrations, there are techniques like absorption and biological oxidation.

In general it can be said that chemical oxidation shows good prospects for use in the elimination of non-biodegradable compounds in the following cases:

(a) For the treatment of high concentrations of the compound to be eliminated, without the interference of other possible compounds. For example, when incineration is not a viable alternative because the volume of flow of the effluent is great. Optimization is obtained because the reactant is consumed in attacking the desired compound. The existence of other compounds, which can oxidize, leads to a high level of consumption of the reactant.

(b) As a pretreatment of currents, to reduce toxicity by avoiding causing problems of inhibition in the biomass when being introduced in a biological treatment (activated sludge). Intermediate levels of oxidation are aimed at, with a reduced consumption of oxidizer, so that the effluent is in conditions to be biologically treated.

(c) As a final treatment for the adjustment of the effluent for the desired discharging conditions.

A reference parameter in case of using chemical oxidation as treatment process is the COD (see Fig.1.3). Only waters with relatively small COD contents (≤ 5 g.L^{-1}) can be suitably treated by means of these processes since higher COD contents would require the consumption of too large amounts of expensive reactants. In those cases, it would be more convenient to use wet oxidation or incineration: waste water with COD higher than 20 g.L^{-1} may undergo autothermic wet oxidation (Mishra *et al.*, 1995).

The chemical oxidation processes can be divided in two classes:

- Classical Chemical Treatments
- Advanced Oxidation Processes (AOPs)

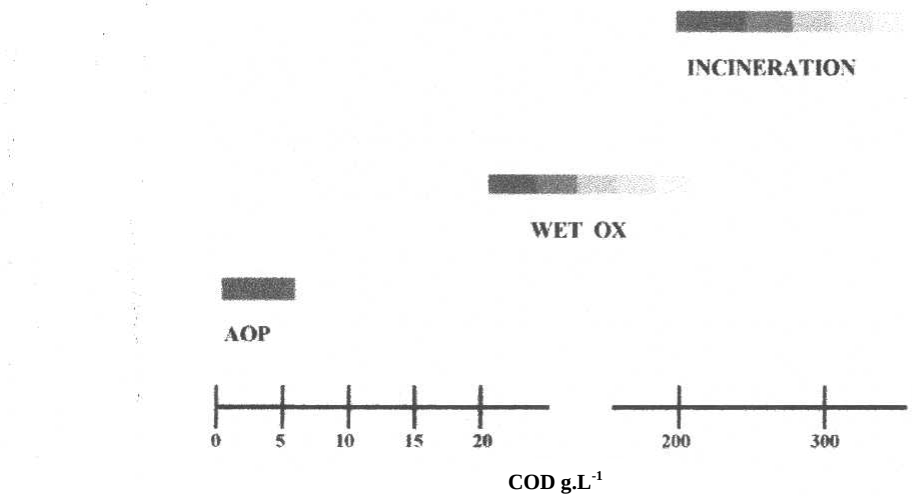

Figure 1.3. Suitability of water treatment technologies according to COD contents (Andreozzi *et al.*, 1999)

Classical Chemical Treatments

Classical chemical treatments consist generally on the addition of an oxidant agent to the water containing the contaminant to oxidize it. Among the most widely used it is possible to emphasize (Chamarro *et al.*, 1996):

- Chlorine: This is a good chemical oxidizer for water depuration because it destroys microorganisms. It is a strong and cheap oxidant, very simple to feed into the system and it is well known (Chamberlin and Griffin, 1952). Its main disadvantages are its little selectivity, that high amounts of chlorine are required and it usually produces carcinogenic organochloride by-products.

- Potassium permanganate: It has been an oxidizer extensively used in the treatment of water for decades. It can be introduced into the system as a solid or as a dissolution prepared *on site*. It is a strong but expensive oxidant, which works properly in a wide pH range. One of the disadvantages of the use of potassium permanganate as an oxidizer is the formation of magnesium dioxide throughout oxidation, which precipitate and has to be eliminated afterward by clarifying or filtration, both of which mean an extra cost.

- Oxygen: The reaction of organic compounds with oxygen does not take place in normal temperature and pressure conditions. Needed values of temperature and pressure are high to increase the oxidizing character of the oxygen in the reaction medium and to assure the liquid state of the effluent. It is a mild oxidant that requires large investments in installations. However, its low operating costs make the process attractive.

- Hydrogen peroxide: It is a multipurpose oxidant for many systems. It can be applied directly or with a catalyst. The catalyst normally used is ferrous sulphate (the so-called Fenton process, which will be presented below). Other iron salts can be used as well. Other metals can also be used as catalyst, for example, Al^{3+}, Cu^{2+}. Its basic advantages are:
  - It is one of the cheapest oxidizers that is normally used in residual waters.
  - It has high oxidizing power.
  - It is easy to handle.
  - It is water-soluble.
  - It does not produce toxins or color in byproducts.

  It can also been used in presence of ultraviolet radiation and the oxidation is based on the generation of hydroxyl radicals that will be considered an advanced oxidation process.

  An option to the adding of hydrogen peroxide to the reaction medium is its production *on site*. One production possibility is by electroreduction of the oxygen dissolved in the reaction medium (Sudoh *et al.*, 1986). This option is not used very much, because it is expensive and increases the complexity of the system.

- Ozone: It is a strong oxidant that presents the advantage of, as hydrogen peroxide and oxygen, not introducing "strange ions" in the medium. Ozone is effective in many applications, like the elimination of color, disinfection, elimination of smell and taste, elimination of magnesium and organic compounds (Sevener, 1990). In standard conditions of temperature and pressure it has a low solubility in water and is unstable (Whitby, 1989). It has an average life of a few minutes (Staehelin and Hoigné, 1982). Therefore, to have the

necessary quantity of ozone in the reaction medium a greater quantity has to be used.

Among the most common oxidizing agents, it is only surpassed in oxidant power by fluorine and hydroxyl radicals (see Table 1.9). Although included among the classical chemical treatments, the ozonation of dissolved compounds in water can constitute as well an AOP by itself, as hydroxyl radicals are generated from the decomposition of ozone, which is catalyzed by the hydroxyl ion or initiated by the presence of traces of other substances, like transition metal cations (Staehelin and Hoigné, 1982). As the pH increases, so does the rate of decomposition of ozone in water.

The major disadvantage of this oxidizer is that it has to be produced *on site* and needs installation in an ozone production system in the place of use. Therefore, the cost of this oxidizer is extremely high, and it must bear this in mind when deciding the most appropriate oxidizer for a given system. In addition, as it is a gas, a recuperation system has to be foreseen and that will make the obtaining system even more expensive (Benitez *et al.*, 1997).

Ozonation is used in many drinking water plants as a tertiary treatment and also for the oxidation of organic pollutants of industrial (paper mill industry) or agriculture (water polluted by pesticides) effluents. A lot of research has been carried out to investigate the kinetics of the ozonation reaction of various organic and inorganic compounds like carboxylic acids, phenols, amino acids, organometallic compounds, etc (Hoigné and Bader, 1983 and references herein). In the case of phenol, some studies have been made in order to establish a kinetic model to predict the magnitude of gas-liquid reaction between ozone and phenol. Contreras and co-workers (2001) studied the elimination of NB from aquoes solution by means of ozonation and enhanced ozonation. In the case of DCDE, the feasibility of enhancing biodegradability through the ozonation as pre-oxidation treatment was studied. With regard to textile wastewaters the ozonation has been found very efficient for decolorization of textile wastewaters (Balcioglu and Arslan, 2001; Ciardelli *et al.*, 2001; Sevimli and Kinaci, 2002). The ozone treatment may be enhanced by the addition of hydrogen peroxide. For this reason, a brief description of these combined systems will be presented.

Advanced Oxidation Processes (AOPs)

AOPs were defined by Glaze and et al. (1987) as near ambient temperature and pressure water treatment processes which involve the generation of highly reactive radicals (specially hydroxyl radicals) in sufficient quantity to effect water purification. These treatment processes are considered as very promising methods for the remediation of contaminated ground, surface, and wastewaters containing non-biodegradable organic pollutants. Hydroxyl radicals are extraordinarily reactive species that attack most of the organic molecules. The kinetics of reaction is generally first order with respect to the concentration of hydroxyl radicals and to the concentration of the species to be oxidized. Rate constants are usually in the range of $10^{8} - 10^{11}$ $L.mol^{-1}.s^{-1}$, whereas the concentration of hydroxyl radicals lays between 10^{-10} and 10^{-12} $mol.L^{-1}$, thus a pseudo-first order constant between 1 and 10^{-4} s^{-1} is obtained (Glaze and Kang, 1989). As it can be seen from Table 1.9, hydroxyl radicals are more powerful oxidants than the chemical agents used in traditional chemical processes.

Hydroxyl radicals are also characterized by a little selectivity of attack, attractive feature for an oxidant to be used in wastewater treatment. Several and different organic compounds are susceptible to be removed or degraded by means of hydroxyl radicals, as it is shown in Table 1.10. Nevertheless, some of the simplest organic compounds, such as acetic, maleic and oxalic acids, acetone or simple chloride derivatives as chloroform or tetrachloroethane, cannot be attacked by OH radicals (Bigda, 1995). Depending upon the nature of the organic species, two types of initial attacks are possible: the hydroxyl radical can abstract a hydrogen atom to form water, as with alkanes or alcohols, or it can add to the contaminant, as it is the case for olefins or aromatic compounds.

The attack by hydroxyl radical, in the presence of oxygen, initiates a complex cascade of oxidative reactions leading to mineralization. As a rule of thumb, the rate of destruction of a contaminant is approximately proportional to the rate constants for the contaminant with the hydroxyl radical. From Table 1.11 it can be seen that chlorinated alkenes treat most efficiently because the double bond is very susceptible to hydroxyl attack. Saturated molecules as mentioned before, have smaller rate constants and therefore are more difficult to oxidize.

Table 1.10. Oxidizable compouns by hydroxyl radicals (Bigda, 1995)

Compounds	
Acids	Formic, gluconic, lactic, malic, propionic, tartaric
Alcohols	Benzyl, *tert*-butyl, ethanol, ethylene glycol, glycerol, isopropanol, methanol, propenediol
Aldehydes	Acetaldehyde, benzaldehyde, formaldehyde, glyoxal, isobutyraldehyde, trichloroacetaldehyde
Aromatics	Benzene, chlorobenzene, chlorophenol, creosote, dichlorophenol, hydroquinone, p-nitrophenol, phenol, toluene, trichlorophenol, xylene, trinitrotoluene
Amines	Aniline, cyclic amines, diethylamine, dimethylformamide, EDTA, propanediamine, n-propylamine
Dyes	Anthraquinone, diazo, monoazo
Ethers	tetrahydrofuran
Ketones	Dihydroxyacetone, methyl ethyl ketone

Table 1.11. Reaction rate constant (k, L mol^{-1} s^{-1})

Compounds	**$OH^{\bullet}$**
Chlorinated alkenes	10^9 to 10^{11}
Phenols	10^9 to 10^{10}
N-containing organics	10^8 to 10^{10}
Aromatics	10^8 to 10^{10}
Ketones	10^9 to 10^{10}
Alcohols	10^8 to 10^9
Alkanes	10^6 to 10^9

The versatility of AOPs is also enhanced by the fact that they offer different ways of $HO^{\bullet}$ radicals production, thus allowing a better compliance with the specific treatment requirements. It has to be taken into account, though, that a suitable application of AOPs to wastewater treatment makes use of expensive reactants as hydrogen peroxide and/or ozone,

and therefore they should not replace, whenever possible, the more economic treatments as the biological degradation.

As hydroxyl radicals are so reactive and unstable, they must be continuously produced by means of photochemical or chemical reactions. The main processes of producing these radicals are described below. It is very difficult to make a classification of the advanced oxidation processes, for the diverse combinations that are presented among them. For this reason, they are presented in the way that has been considered more appropriate.

1.3.8.1. UV-based processes

As it has been commented previously, the slow kinetics achieved by photochemical reactions can be enhanced by the addition of hydrogen peroxide and/or ozone, metallic salts or semiconductors. The UV/oxidizer system involves direct excitation of the substrate due to the radiation with the subsequent oxidation reaction. Even so, there may be synergism between the oxidizer and the ultraviolet radiation, which causes the global effect to be different from the additive effect.

1.3.8.1.1. UV/O_3 process

The UV/O_3 system is an effective method for the oxidation and destruction of organic compounds in water. Basically, aqueous systems saturated with ozone are irradiated with UV light of 253.7 nm. The extinction coefficient of O_3 at 253.7 nm is 3300 $L.mol^{-1}.cm^{-1}$, much higher than that of H_2O_2 (18.6 $L.mol^{-1}.cm^{-1}$). The decay rate of ozone is about a factor of 1000 higher than that of H_2O_2 (Guittonneau *et al.*, 1991).

The AOP with UV radiation and ozone is initiated by the photolysis of ozone. The photodecomposition of ozone leads to two hydroxyl radicals, which do not act as they recombine producing hydrogen peroxide (Peyton and Glaze, 1988):

$$H_2O_2 + O_3 \xrightarrow{h\nu} 2\ HO^{\bullet} + O_2 \qquad (1.5)$$

$$2\ HO^{\bullet} \rightarrow H_2O_2 \qquad (1.6)$$

This system contains three components to produce OH radicals and/or to oxidize the pollutant for subsequent reactions: UV radiation, ozone and hydrogen peroxide.

Therefore, the reaction mechanism of O_3/H_2O_2 as well as the combination UV/H_2O_2 is of importance. Considering that hydrogen peroxide photolysis is very slow compared with the rate at which ozone is decomposed by HO_2^-, it seems that a neutral pH the second reaction is the main pathway.

Several authors have studied the efficiency of this process with different aromatic compounds. Gurol and Vatistas (1987) studied the photolytic ozonation of mixtures of phenol, p-cresol, 2,3-xylenol and catechol at acidic and neutral pH. Guittoneau et al. (1990) reported that the O_3/UV process was found to be more efficient than the UV/H_2O_2 system for the degradation of p-chloronitrobenzene. Some articles have been found as well in the literature regarding the degradation of NB by means of the O_3/UV process. Beltrán et al. (1998) have studied the effect of ozone feed rate, pH and hydroxyl radical scavengers in the removal of NB by this combination. Besides, Contreras et al. (2001) have studied the effect of pH and ozone in the oxidation of NB by this process. In the case of DCDE and textile wastewaters no references were found.

1.3.8.1.2. UV/O_3/H_2O_2 process

The addition of H_2O_2 to the UV/O_3 process accelerates decomposition of ozone resulting in increased rate of $HO^\bullet$ radicals generation. This is a very powerful method that allows a considerable reduction of the TOC. This process is the combination of the binary systems UV/O_3 and O_3/H_2O_2.

Mokrini et al. (1997) presented the degradation of phenol by means of this process at different pHs, establishing the optimal H_2O_2 amount. A 40% of TOC reduction was achieved by this method. Trapido et al. (2001) reported that the combination of ozone with UV radiation and hydrogen peroxide was found to be more effective for the degradation of nitrophenols than single ozonation or the binary combinations, increasing the reaction rate and decreasing the ozone consumption when using low pH values. Contreras et al. (2001) demonstrated that the addition of H_2O_2 to UV/O_3 system slightly improves the rate of TOC removal in solutions of nitrobenzene. With regards to DCDE and textile wastewaters no articles have been found in the literature about the oxidation of these compounds by means of this combined process.

1.3.8.1.3. Fe^{3+} / UV-vis process

Among the AOPs, the iron photo-assisted system Fe^{3+}/UV-vis, without addition of other electron acceptor than O_2 from air, has received special attention as a potential wastewater treatment process. The interesting point in such a system, compared to the photo-Fenton process is that no addition of hydrogen peroxide is needed. The excitation of $[Fe(OH)(H_2O)_5]^{2+}$, the dominant monomeric species of aqueous ferric ion in acidic solution, is known to yield $HO^{\bullet}$ (eq. 1.7 similar to 1.17) with a quantum yield of 0.075 at 360 nm (Benkelberg and Warneck, 1995).

$$Fe(OH)^{2+} \xrightarrow{h\nu} Fe^{2+} + HO^{\bullet} \qquad (1.7)$$

where $Fe(OH)^{2+}$ refers to $[Fe(OH)(H_2O)_5]^{2+}$.

This electron transfers process has been efficiently used to study the degradation of several organic pollutants in aqueous solution (Nansheng *et al.*, 1996; Brand *et al.*, 1997; Catastini *et al.*, 2001). Mazellier and Bolté (1999, 2001) used this process for the degradation of 4- and 3-chlorophenol in aqueous solution. The process was found to be an efficient photoinducer of these phenolic compounds. Regarding DCDE, NB, and textile wastewaters, no references were found.

1.3.8.1.4. UV/TiO_2 (Heterogeneous photocatalysis)

Over the last few years the tendency has been to carry out chemical oxidation in the presence of a catalyst that serves as a generator of hydroxyl radicals, and, therefore, the addition of an oxidizer in the medium is not necessary.

Heterogeneous photocatalytic process consists on utilizing the near UV radiation to photoexcite a semiconductor catalyst in the presence of oxygen. Under these circumstances oxidizing species, either bound hydroxyl radical or free holes, are generated. The process is heterogeneous because there are two active phases, solid and liquid. This process can also be carried out utilizing the near part of solar spectrum (wavelength shorter than 380 nm) what transforms it into a good option to be used at big scale (Malato *et al.*, 2002).

Many catalysts have been tested, although TiO_2 in the anatase form seems to possess the most interesting features, such as high stability, good performance and low cost (Andreozzi *et al.*, 1999). It presents the disadvantage of the catalyst separation from solution, as well as the fouling of the catalyst by the organic matter.

Minero et al. (1994) studied the photocatalytic degradation of NB on TiO_2 and ZnO, reporting that complete mineralization with TiO_2 was achieved. Mathew (1990) also reported that more than 90% of NB mineralization was achieved with TiO_2 and sunlight. Phenolic compounds have been successfully degraded by photocatalytic process (Giménez *et al.*, 1996; Curcó *et al*., 1999b; Minero, C. *et al*., 1993). Regarding DCDE, no references about the use of photocatalysis heterogeneous has been found. Few studies have been found in the literature regarding the photocalytic oxidation of textile wastewaters (Balcioglu and Arslan, 1999).

1.3.8.2. H_2O_2 -based processes

The most important advanced oxidation treatments based in the use of H_2O_2 are:

- H_2O_2/UV
- H_2O_2 /O_3 process and
- Fenton and photo-Fenton process.

1.3.8.2.1. H_2O_2 /UV process

This AOP process is explained extensively in chapter 4. Briefly, the H_2O_2/UV system involves the formation of $HO^{\cdot}$ radicals by hydrogen peroxide photolysis and subsequent propagation reactions. The mechanism most commonly accepted for the photolysis of H_2O_2 is the cleavage of the molecule into hydroxyl radicals:

$$H_2O_2 \xrightarrow{h\nu} 2\ HO^{\bullet} \quad \lambda \leq 400\ nm \qquad (1.8)$$

It presents the advantage compared when working with ozone that it provides a cheap and sure source of radicals, eliminating this way the problem of the handling of ozone. The major drawback of this process is that if the solution presents a strong absorbance this can compete with hydrogen peroxide for the radiation, thus cloudy waters or containing compounds absorbing UV radiation can present problems at being treated by this method.

The effectiveness of the UV/H_2O_2 system in the treatment of aromatic compounds such phenol and NB has been widely studied (e.g. García *et al.*, 1989 and Lipczynska-Kochany, 1992). However, in the case of DCDE, no reference was found. Alaton and Balcioglu (2002) show the effectiveness of H_2O_2/UV system as pretreatment or in combination with other advanced oxidation process in the treatment of textile wastewater.

1.3.8.2.2. H_2O_2/O_3 process

Addition of hydrogen peroxide to ozone offers another way to accelerate the decomposition of ozone, leading to the formation of OH radicals. Hydrogen peroxide in aqueous solution is partially dissociated in the hydroperoxide anion (HO_2^-), which reacts with ozone, decomposing this and giving rise to a series of chain reactions with the participation of hydroxyl radicals.

In the global reaction two ozone molecules produce two hydroxyl radicals (Glaze and Kang, 1989).

$$H_2O_2 + 2\,O_3 \rightarrow 2\,HO^{\bullet} + 3\,O_2 \qquad (1.9)$$

As this system does not depend on the UV radiation transmission to activate the ozone or hydrogen peroxide molecules, its greatest advantage is to be able to work with turbid waters without problems.

Balcioglu and Arslan (2001) studied the efficiency of ozonation and O_3/H_2O_2 of reactive dyes and textile dye-bath wastewater. They found a considerable improvement in COD and color removal rates at pH=11, which is normally the pH of textile wastewaters. With regards to phenol, NB and DCDE no references were found.

1.3.8.2.3. Fenton and photo-Fenton reaction

The Fenton reaction was discovered by H.J.Fenton in 1894 (Fenton, 1894). Forty years later the Haber-Weiss (1934) mechanism was postulated, which revealed that the effective oxidative agent in the Fenton reaction was the hydroxyl radical. Since then, some groups have tried to explain the whole mechanism (Walling, 1975; Sychev and Isak, 1995) that will be treated in details in the next two chapters. The Fenton reaction can be outlined as follows:

$$M^{n+} + H_2O_2 \rightarrow M^{(n+1)+} + HO^- + HO^{\bullet}$$

where M is a transition metal as Fe or Cu.

In the absence of light and complexing ligands other than water, the most accepted mechanism of H_2O_2 decomposition in acid homogeneous aqueous solution, involves the

formation of hydroxyperoxyl ($HO_2^{\bullet}/O_2^{-}$) and hydroxyl radicals $HO^{\bullet}$ (De Laat and Gallard, H., 1999; Gallard and De Laat, 2000).

The $HO^{\bullet}$ radical mentioned before, once in solution attacks almost every organic compound. The metal regeneration can follow different paths. For Fe^{2+}, the most accepted scheme is described in the following equations (Sychev and Isak, 1995).

$$Fe^{2+} + H_2O_2 \rightarrow Fe^{3+} + HO^- + HO^{\bullet} \quad (1.10)$$

$$Fe^{3+} + H_2O_2 \rightarrow Fe^{2+} + HO_2^{\bullet} + H^+ \quad (1.11)$$

$$Fe^{2+} + HO^{\bullet} \rightarrow Fe^{3+} + HO^- \quad (1.12)$$

$$HO^{\bullet} + H_2O_2 \rightarrow HO_2^{\bullet} + H_2O \quad (1.13)$$

$$Fe^{3+} + HO_2^{\bullet} \rightarrow Fe^{2+} + H^+ + O_2 \quad (1.14)$$

$$Fe^{3+} + O_2^{\bullet -} \rightarrow Fe^{2+} + O_2 \quad (1.15)$$

$$Fe^{2+} + HO_2^{\bullet} \rightarrow Fe^{+3} + HO_2^- \quad (1.16)$$

Fenton reaction rates are strongly increased by irradiation with UV/visible light (Ruppert *et al.*, 1993; Sun and Pignatello, 1993). During the reaction, Fe^{3+} ions are accumulated in the system and after Fe^{2+} ions are consumed, the reaction practically stops. Photochemical regeneration (eq 1.17) of ferrous ions (Fe^{2+}) by photoreduction of ferric ions (Fe^{3+}) is the proposed mechanism (Faust and Hoigné, 1990). The new generated ferrous ions reacts with H_2O_2 generating a second $HO^{\bullet}$ radical and ferric ion, and the cycle continues.

$$Fe^{3+} + H_2O \xrightarrow{h\nu} Fe^{2+} + HO^{\bullet} \quad (1.17)$$

Fenton and photo-Fenton reaction depend not only on H_2O_2 concentration and iron added, but also on the operating pH value as indicated in chapter 2. Both treatment processes will be described in detail in chapter 3 and 4.

Chamarro et al. (2001) used the Fenton process for the degradation of phenol, 4-chlorophenol, 2,4-dichlorophenol and nitrobenzene. The stoichiometric coefficient for the Fenton reaction was approximately 0.5 mol of organic compound/mol H_2O_2. The process was found to eliminate the toxic substances and increased the biodegradability of the treated water. Regarding DCDE, has been confirmed that DCDE's biodegradability can be enhanced by modified Fenton's reagent (Kaludjerski, 2001). Some works about textile

waters treatment by means of Fenton and photo-Fenton process have been published. Most of them showed their effectiveness for color removal and COD reduction (Balanosky *et al.*, 1999; Kang *et al.*, 2000; Perez *et al.*, 2002).

An improvement of photoassisted Fenton processes is the UV-vis/ferrioxalate/H_2O_2 system, which has been recently demonstrated to be more efficient than photo-Fenton for the abatement of organic pollutants (Zepp *et al.*, 1992; Safarzadeh-Amiri *et al.*, 1996).

Recently, two new electrochemical procedures for the detoxification of acidic waste waters, the so-called electro-Fenton and photoelectro-Fenton processes, where H_2O_2 is electrogenerated, have been developed and have shown their good efficiencies for the mineralization of aniline (Brillas *et al.*, 1998a), 4-chlorophenol (Brillas *et al.*, 1998b) and 2,4-D (Brillas *et al.*, 2000).

1.3.9. AOPs combined with biological treatments

Biological treatment of wastewater, groundwater, and aqueous hazardous wastes is often the most economical alternative when compared with other treatment options. The ability of a compound to undergo biological degradation is dependent on a variety of factors, such as concentration, chemical structure and substituents of the target compound. The pH or the presence of inhibitory compounds can also affect the biological degradation. Although many organic molecules are readily degraded, many other synthetic and naturally occurring organic molecules are biorecalcitrant (Adams *et al.*, 1997).

Several chemical processes, which use oxidizing agents such as ozone, hydrogen peroxide, etc. have been carried out to mineralize many synthetic organic chemicals. However, costs associated with chemical oxidation alone can often be prohibitive for wastewater treatment. A potentially viable solution is the integration of chemical and biological treatment processes as an economical means for treating biorecalcitrant organic chemicals in wastewater. The chemical process would be used as a pre-treatment in order to increase the biodegradability of the wastewater (Parra *et al*., 2000, 2002; Sarria *et al*., 2001). The oxidation of organic compounds in water with AOPs usually produces oxygenated organic products and low molecular weight acids that are more biodegradable (Gilbert, 1987; Heinzle *et al.*, 1995; Marco *et al.*, 1997; Ledakowicz, 1998). With the AOPs, toxic compounds would be removed until no inhibition due to its toxicity was there and/or non-biodegradable compounds turned into more biodegradable. This feature is

economically interesting, as investment and operating costs are much lower for a biological process than a chemical one: investments costs for biological processes range from 5 to 20 times less than chemical ones such as ozone or hydrogen peroxide, while treatment costs range from 3 to 10 times less (Scott and Ollis, 1996; Marco *et al.*, 1997).

In these combined processes, if we want to determine the variation of biodegradability as a function of the chemical reaction conditions (time of pre-treatment, concentration of the oxidizing agent, temperature, etc), a biodegradation test is required. Methods for measuring biodegradability in these systems have been proposed by a number of authors. BOD and BOD/COD or BOD/TOC are commonly used (Gilbert, 1987; Yu and Hu, 1994; Marco *et al.*, 1997; Chamarro *et al.*, 2001). Other biodegradability measures including substrate destruction, total organic carbon (TOC) evolution, oxygen uptake, EC_{50} toxicity measurements, cell growth counts and intracellular ATP levels also have been used (Scott and Ollis, 1995; Pulgarin *et al.*, 1999).

During the last decade, many studies focused in the use of advanced oxidation processes as pre-treatment step have increased. In this sense, it is proper to cite that the first coupled flow system was developed by Pulgarin et al. (1999). They showed the effectiveness of a coupling photochemical and biological treatment process in the mineralization of biorecalcitrant industrial pollutants (Pulgarin *et al.*, 1999; Parra *et al.*, 2000; Sarria *et al*., 2001)

Alaton and Balcioglu (2002) reported that ozonation and H_2O_2/UV as pretreatment of a textile wastewater were found to enhance the effectiveness of a subsequent biological treatment. Hu and Yu (1994) also reported that pre-ozonation of chlorophenolic compounds enhanced the effectiveness of a biological treatment. Lin and Peng (1994) reported that the combination of coagulation, electrochemical oxidation and activated sludge in the treatment of textile wastewater is highly competitive in comparison with the conventional treatment practiced in the textile industry. Besides this, Pala and Tokat (2002) outlined that due to the low biodegradability of the textile wastewaters and due to the not very efficient performed of the biological treatment in the color removal, it should be carried out in combination with activated carbon. No studies regarding the effect of Fenton and photo-Fenton process on the biodegradability of NB, DCDE, and textile solutions have been found in the literature.

2. Objectives

Nowadays, in those industries with aqueous effluents in which the concentration of recalcitrant organic compounds is important, an economical and technical solution has not been found in most cases yet. For this reason, the search for solutions of this problem is an interesting research topic.

Nitroaromatic, phenols, and chlorinated ethers constitute a risk to human health and produce a public concern, thus several of them have been listed among the 130 priority pollutants given by the US EPA in the Federal Clean Water Act (CWA), e.g. NB and phenol (EPA, visited in 2002).

Among nitroaromatic compounds, the US EPA has recently included nitrobenzene in a reduced list of drinking water contaminants to be investigated in the period 2001-2005 (Hayward, 1999). However, few articles have been found in the literature regarding the treatment of this compound by means of AOPs (Advanced Oxidation Processes), especially those based on the use of UV radiation and/or H_2O_2. Therefore an improved AOPs study are necessary to provide future successfully treatment of water contaminated with this compound. Moreover, taking into account that phenol is possibly the most widely organic compound studied in AOPs it was decided to use as model and to be compared with nitrobenzene treatment results. Regarding chlorinated ethers solvents, the 1996 Toxic Release Inventory for California indicates that e.g. DCDE exists in the discharge of various chemical and petrochemical companies in Southern California. Thus, the study of the removal of DCDE by means of an AOP (in this case, UV/H_2O_2) was performed as part of a project carried out in the Environmental Department of San Diego State University (CA, USA) and supported by the Water Environment Research Foundation (USA).

On the other hand, textile industries are major consumers of water and consequently one of the largest groups of industry causing intense waster pollution. The wastewater generated by the different production steps (i.e. sizing of fibers, scouring, desizing, bleaching, washing, mercerization, dyeing and finishing) contains high concentration of non-biodegradable matter, toxic substances, detergents and soaps, oil and grease, sulfide, sodas, and alkalinity. Following with the application of AOPs, the treatment of a wastewater from a textile industry by means of photo-Fenton process was carried out in the frame of a cooperation project between French Textile Institute and the Ecole Politechnique de Lausanne (Switzerland).

Accordingly, the general objective of this work was to study the effectiveness of the AOPs cited above in the degradation and mineralization of those organic pollutants (NB and phenol), as well as the influence of those processes in the biodegradability enhancement of a wastewater, e.g. containing DCDE and from a textile industry. For this latter objective, a general strategy focused on the application of a coupled chemical and biological treatment has been established to enhance the global removal degree.

The AOPs selected to carry out this study were:

- Fenton and photo-Fenton process
- UV/H_2O_2 system
- Fe^{3+}/UV-vis system

The work was divided in different sections with the following objectives:

- To study the effect of the Fenton process on the degradation rate of NB and phenol. The objective of this part was, after studying a wide range of experimental conditions to understand the mechanisms to propose a general empirical kinetic equation for the degradation of these compounds as a function of H_2O_2, Fe^{2+}, O_2, temperature, and its initial concentration.

- Following with the treatment of wastewaters containing NB and phenol, to study the mineralization of these solutions by means of different UV-based AOPs. Photo-Fenton, H_2O_2/UV, and Fe^{3+}/UV processes were studied in order to find the best experimental conditions for NB and phenol mineralization. Besides this, the influence of different sources of light was studied making special emphasis in the use of solar technology for water remediation. Kinetic intrinsic constants were estimated to be used as tool for the scaling-up of photo-reactors.

- To study the effect on the biodegradability enhancement of treated solutions of DCDE by means of AOPs. The goal of the study was not to chemically oxidize all organic matter to CO_2 and H_2O, but rather to convert DCDE into products that are readily biodegradable in conventional biological treatment plants. This part was carried out at the San Diego State University (CA, USA) and chosen AOP was UV/H_2O_2. The inhibition respiration rate caused by DCDE and its oxidation

byproducts was assessed by respirometric test by measuring the oxygen consumption.

- The development of a strategy to be applied in wastewater treatment, using as example waters produced in textile activities. Effluents produced in a textile industry located in the south of France were selected to evaluate a general strategy for the treatment of the different generated wastewaters. The aim of this study was to explore the possibility of using the photo-Fenton process as pre- or post-treatment to enhance the global removal performance. This study was performed at the EPFL in Lausanne (Switzerland) and in this case, the Zahn-Wellens test was used to follow the biodegradability of treated solution.

To achieve the experimental objectives, the following variables were chosen to be followed throughout the treatment:

- Concentration of target compounds
- pH
- Hydrogen peroxide concentration
- Total Organic Carbon (TOC)
- Chemical Oxygen Demand (COD)
- Biological Oxygen Demand (BOD)
- Oxygen consumption (Short-term and long-term respirometric test).

3. Removal of nitrobenzene and phenol by Fenton process. Kinetic model

3.1. Introduction

The oxidative decomposition and transformation of organic substrates by H_2O_2/Fe^{2+} (known as Fenton's reagent) has been known for nearly a century (Fenton, 1894). This method has the advantage that hydrogen peroxide, used as oxidant, is cheaper than other oxidants and it has also the advantage of using iron as catalyst. The iron is the second most abundant metal and the fourth most abundant element on earth. In water it is present as ferric or ferrous ions, which form complexes with water and hydroxyl ions depending on pH and the temperature. Fig.3.1, shows the percentage of Fe^{2+} and the species that appear together with it, in relation to the pH at 25°C and where is possible to see that up to a pH level around 8, Fe^{2+} exists in solution.

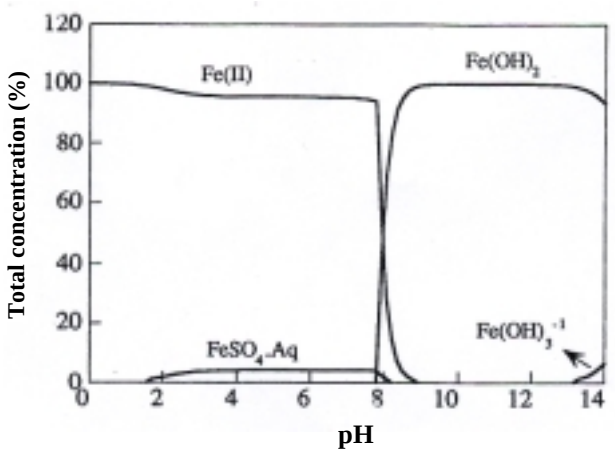

Figure 3.1. Proportion of Fe^{2+} and the species in equilibrium with it at 25°C.

From this, it can be concluded that Fe^{2+} in the Fenton system will be in this form and in solution. Fig.3.2 shows the concentration of Fe^{3+} in solution in relation to the pH at 25°C. This representation has been carried out for a pH of between 2 and 3.2 because this is the solubility limit. As it can be observed, the solubility of Fe^{3+} is very high for a pH lower than 2 and too small for a pH higher than 3.2. Therefore, in Fenton conditions the Fe^{3+} will be in solution if pH is maintained < 3.2.

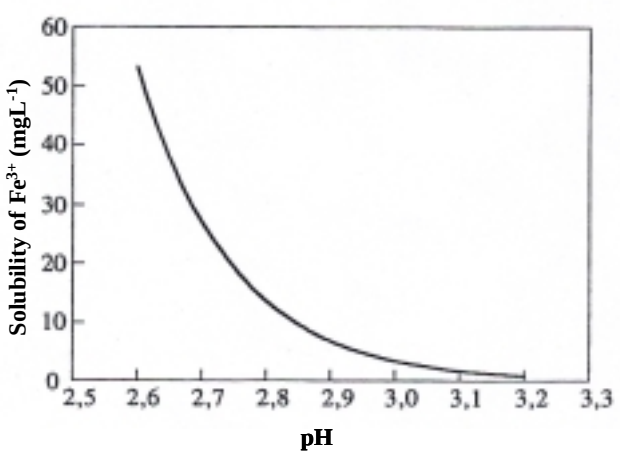

Figure 3.2. Concentration of Fe^{3+} in solution in relation to the pH at 25°C.

In Fig. 3.3 it can be also seen the proportion of Fe^{3+} species that are in equilibrium in relation to the pH (Safarzadeh-Amiri *et al.*, 1996)

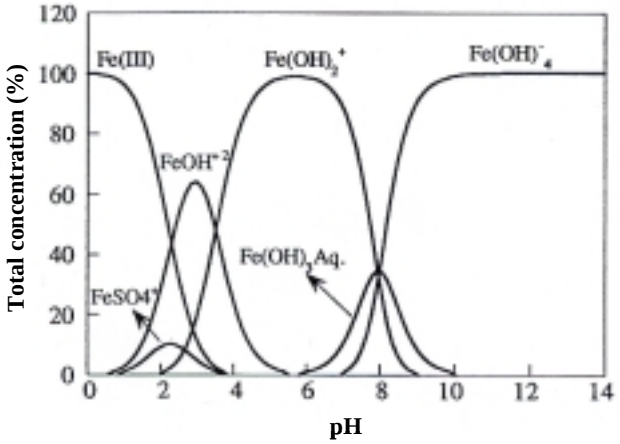

Figure 3.3. Proportion of Fe^{3+} and the existing species in equilibrium with it at 25°C

From this figure, the low solubility of Fe^{3+} and all its species can be seen at pH 3. At pH 3 the solubility of Fe^{3+} is around 4 $mg.L^{-1}$. According to Eisenhauer (1964), in spite of the low solubility of Fe^{3+} in presence of phenol in the reaction medium, ferric hydroxide does not precipitate throughout oxidation because it is transformed into Fe^{2+} due to the reaction of Fe^{3+} with some products of phenol oxidation. The commonly mentioned disadvantage of the Fenton method is the necessity to work at low pH (normally below 4),

because at higher pH ferric ions would begin to precipitate as hydroxide. In addition, by this process the maximum mineralization reached is around 40-60 %.

Although the Fenton reagent has been known for more than a century and shown to be a powerful oxidant, the mechanism of the Fenton reaction is still under intense and controversial discussion. Generation of $HO^{\cdot}$ radicals by the dark reaction of H_2O_2 with ferrous salt has been the subject of numerous studies during the last decade (Arnold *et al.*, 1995; Pignatello and Day, 1996; Chen and Pignatello, 1997; Hislop and Bolton, 1999). The oxidizing species generated in the Fenton's reaction have been discussed by many investigators but are still controversial (Walling, 1975; Stubbe and Kozarich, 1987; Bossmann *et al.*, 1998; MacFaul, 1998; Goldstein, 1999; Kremer, 1999). The recognition of the $HO^{\cdot}$ radical as the active intermediate is not yet universal and even doubts as to its very existence in the system have been raised (Bossmann *et al.*, 1998; Kremer, 1999). Bossmann and co. (1998) outlined clearly that recent thermodynamic calculations have demonstrated that outher-sphere electron-transfer reaction between Fe^{2+} and H_2O_2, as it is rationalized by the classic mechanism proposed by Haber and Weiss, cannot take place, because the formation of $H_2O_2^-$ by intermediates is not favored. In contrast, the formation of a hydrated Fe^{2+}- H_2O_2 complex is thermodynamically favored. However, in the main studies of the Fenton's reagent, it is generally considered that the reaction between H_2O_2 and Fe^{2+} in acidic aqueous medium (pH ≤ 3) produces $HO^{\bullet}$ radicals (eq.1.10) and can involve the steps presented below (eqs. 1.10 - 1.14, 1.16, 1.6). The rate constants are reported at 298 K for second-order reaction rate.

$Fe^{2+} + H_2O_2 \rightarrow Fe^{3+} + HO^- + HO^{\bullet}$	$k_1 = 63\ L.mol^{-1}s^{-1}$	(Gallard, 2000)	(1.10)
$Fe^{3+} + H_2O_2 \rightarrow Fe^{2+} + H^+ + HOO^{\bullet}$	$k_2 = 0.002\ L.mol^{-1}s^{-1}$	(Pignatello, 1992)	(1.11)
$Fe^{2+} + HO^{\bullet} \rightarrow Fe^{3+} + HO^-$	$k_3 = 3x10^8\ L.mol^{-1}s^{-1}$	(Haber, 1934)	(1.12)
$HO^{\bullet} + H_2O_2 \rightarrow HOO^{\bullet} + H_2O$	$k_4 = 2.7x10^7\ L.mol^{-1}s^{-1}$	(Butxon, 1988)	(1.13)
$Fe^{2+} + HO_2^{\bullet} \rightarrow Fe^{3+} + HOO^-$	$k_5 = 1.2x10^6\ L.mol^{-1}s^{-1}$	(Haber, 1934)	(1.16)
$Fe^{3+} + HO_2^{\bullet} \rightarrow Fe^{2+} + H^+ + O_2$	$k_6 = 2x10^3\ L.mol^{-1}s^{-1}$	(Hardwick, 1957)	(1.14)
$2\ HO^{\bullet} \rightarrow H_2O_2$	$k_7 = 5.2x10^9\ L.mol^{-1}s^{-1}$	(Sehested, 1968)	(1.6)

The hypothesis of Haber and Weiss (1934), that the Fenton reaction involves the formation of $HO^{\bullet}$ radicals has been proved by many techniques, including EPR spectroscopy. Although a considerable number of investigators, using the EPR spin-trapping technique, have found evidence for the formation of $HO^{\bullet}$ radicals from Fenton's reagent (Dixon and Norman, 1964; Rosen *et al.*, 2000), it has also been reported by others (Rahhal and Richter, 1988) that this species is not the only oxidizing intermediate, but also some type of high-valent iron-oxo intermediates (Groves and Watanabe, 1986; Kean *et al.*, 1987; Sychev and Isak, 1995; Bossmann *et al.*, 1998; Kremer, 1999). Using EPR spin-trapping, three types of oxidizing species (free $HO^{\cdot}$, bound $HO^{\cdot}$, and high-valence iron species, which is probably a ferryl ion, (Fe^{IV}) were detected by Yamazaki and Piette, 1991). In the present work, the principal oxidant is assumed to be $HO^{\bullet}$ radical, but others such as iron-oxo species cannot be ruled out.

A number of studies on the degradation of NB in aerated aqueous solutions by the Fenton's reagent have been reported (Lipczynska-Kochany, 1991, 1992). However in a system containing NB, H_2O_2, and Fe (II), the effects of temperature and initial concentrations of these components and dissolved oxygen, on the degradation rate of NB, have not been investigated in detail. In this context and taking into account that the NB is one of the most representative nitroaromatic compound, which is present in several wastewaters, a study on its chemical degradation by Fenton reagent was carried out. Besides, phenol has been also selected because it is the most typical and common model compound used in the application of different advanced oxidation processes as treatment method (Sadana and Katzer, 1974; Hashimoto *et al.*, 1979; Ohta *et al.*, 1980; Gurol and Vastistas, 1987; Kawaguchi, 1992; Serpone *et al.*, 1992; Litvintsev *et al.*, 1993; Lin and Chuang, 1994; Kannan, 1995; Benitez *et al.*, 1997; Vicente *et al.*, 2002). Therefore, the aim of this section was to determine some kinetic parameters in order to find a general kinetic equation for NB and phenol degradation by dark Fenton process.

3.2. Experimental

3.2.1. Reagents

In Table 3.1 all chemicals that were used in the experimentation are shown. All were used as received.

Table 3.1. List of chemicals used

Compound	*Formula*	*Vendor*	*Purity*
Acetronitrile	C_2H_3N	Merck	99.8%
Hydrogen peroxide	H_2O_2	Merck	30 wt.%
Iron sulphate heptahydrate	$FeSO_4 \cdot 7H_2O$	Panreac	98%
m-nitrophenol	$C_3H_5NO_2$	Merck	99%
Nitrobenzene	$C_3H_5NO_2$	Probus	99%
Nitrogen	N_2	AlphaGas	99.99%
o-nitrophenol	$C_3H_5NO_2$	Merck	99%
Oxygen	O_2	AlphaGas	99.99%
p-nitrophenol	$C_3H_5NO_2$	Merck	99%
Phenol	C_6H_6O	Merck	99%
Sodium hydrogen sulphite	$Na_2S_2O_3$	Panreac	40 w/v %

All solutions of NB, phenol, H_2O_2, and ferrous salt were prepared in millipore water (18 μS cm^{-1}) just before being used.

3.2.2. Experimental device and procedure (reactor A)

All experiments were conducted in a 1 L thermostated batch glass reactor (A) (Fig. 3.4), equipped with a magnetic stirrer, in the absence of light, and under air pressure about $1x10^5$ Pa ($[O_2]_o$ = 0.27 mmol.L^{-1}). Kinetic experiments of NB and phenol degradation were initiated by adding a known amount of H_2O_2 into the reactor, which contained the pollutant (NB or phenol) and $FeSO_4$ in water solutions under vigorous magnetic-stirring. The reactions were carried out in non-buffered conditions and pH values for all experiments decreased during the reaction from 3.5 to 2.5. In this range, values of the overall rate constants for the H_2O_2 decomposition by Fe^{2+} and Fe^{3+}, and consequently NB and phenol degradation rates, are relatively independents from pH within experimental

error (De Laat and Gallard, 1999; Hislop and Bolton, 1999). Samples were periodically withdrawn during kinetic experiments, quenched with sodium hydrogen sulphite solution 40% w/v to avoid further reactions, and used for analysis.

Figure 3.4. Reactor A

Some experiments were carried out bubbling oxygen and nitrogen into the solution, since 30 min before adding the corresponding amount of H_2O_2.

It is important to establish that the disappearance of NB and phenol in this batch reactor proceeds by the Fenton reaction, i.e. to exclude the possibility of vaporization of NB and phenol from water. In this sense, control experiments were carried out with prolonged heating (2 h) at 318 K, without Fenton's reagent. On the other hand, control experiments were conducted for sparged sampled. These experiments showed that absolutely no change is observed in NB and phenol initial concentration (HPLC analysis).

3.2.3. Analytical determinations

3.2.3.1. HPLC

To study the degradation of nitrobenzene and phenol, it is necessary to determine its concentration during time. The selected method has been the high performance liquid chromatography in reverse phase.

The liquid chromatograph used consists of:

- Waters degasser.
- Controller Waters 600.
- Autosampler Waters 717.
- Oven for columns and temperature controller Waters
- Photodiode array detector Waters 996.
- Millenium software.

The column presented the following characteristics:

- Packing: SPHERISORB ODS2
- Particle size: 5 μm
- Length: 25 cm
- Inner diameter: 0.46 cm.

The mobile phase used was a mixture acetonitrile:water:phosphoric acid (40:60:0.5%), isocratically delivered (constant composition and flow rate) by a pump at a flow rate of 1 $mL.min^{-1}$. The wavelength of the UV detector was selected from the absorption spectra of nitrobenzene and phenol. Maximum absorption of nitrobenzene and phenol were found to be 267.3 and 270 nm, respectively. Injected volume of each sample was 10 μL. Temperature was set at 25ºC. Under these conditions, retention time for nitrobenzene and phenol were 13.8 and 6 min, respectively. Integration was performed from the peaks area and the calibration was done by means of nitrobenzene and phenol standards.

Identification and quantification of some intermediates products from NB degradation has been also carried out by this method using similar conditions (see Fig. 3.5). *o*-, *m*-, and *p*-nitrophenols were detected at 282, 277, and 321 nm, respectively.

Under these conditions, the retention times of the compounds were as follow (min): 7.5 (*p*-nitrophenol), 7.8 (*m*-nitrophenol), 11.8 (*o*-nitrophenol).

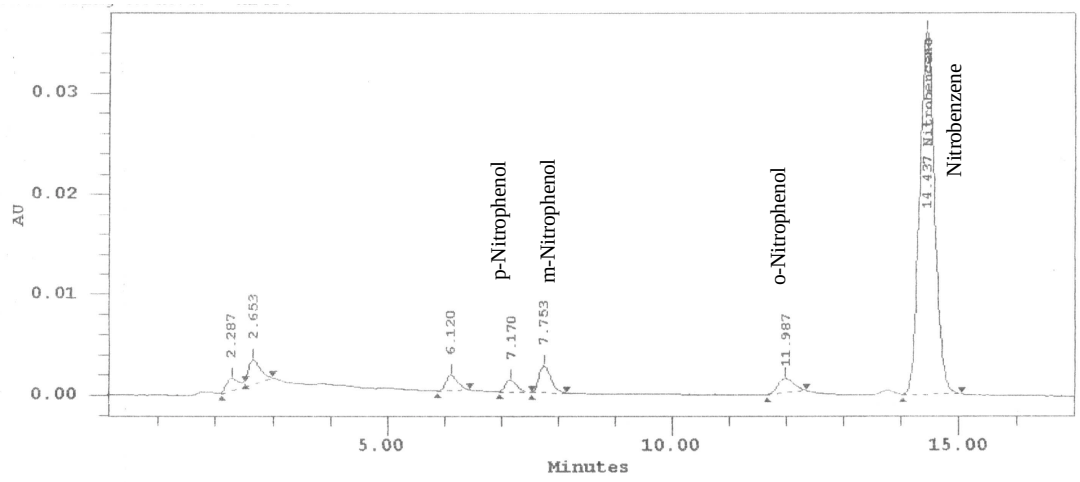

Figure 3.5. Chromatogram with some intermediates products identified after degradation of NB by Fenton process

3.2.3.2. pH

The pH measurements were carried out with a Crison GLP-22 pH-meter, calibrated with two buffer solutions of pH 4 and 7. The analysis was performed on line.

3.2.4. Range of experimental variables for NB and phenol degradation

Several series of experiments of NB and phenol degradation by "Fenton-like" reagent ($[H_2O_2]_o >> [Fe^{2+}]_o$) were conducted by varying the temperature (278-318 K) and the initial concentrations of H_2O_2, Fe^{2+}, NB or phenol and dissolved oxygen (0-1.4 mmol.L^{-1} in case of NB). Table 3.2 and 3.3 summarizes the values of these operating variables in a group of experiments for NB and phenol, respectively. The initial concentration of NB was tested from 0.37 to 2.46 mmol.L^{-1}. Hydrogen peroxide and Fe^{2+} concentration ranges were chosen addressing to reach the highest NB degradation

percentage in a time interval from 5 to 120 min. The $[H_2O_2]_o/[NB]_o$, $[H_2O_2]_o/[Fe^{2+}]_o$ and $[NB]_o/[Fe^{2+}]_o$ ratios varied from 2.1 to 32.3, 6.8 to 102.8 and 0.4 to 18.9, respectively.

Table. 3.2. Experimental conditions of the runs, first-order rate constants and initial oxidation rate of nitrobenzene

Exp N°	$[NB]_o$ (mmol.L^{-1})	$[H_2O_2]_o$ (mmol.L^{-1})	$[Fe^{2+}]_o$ (mmol.L^{-1})	T (K)	k_{obs} x10^3 (s^{-1})	R_D x 10^6 (L.mol^{-1}s^{-1}) eq.3.4	eq.3.12	Δ^a (%)
FN4	0.82	1.74	0.26	298	0.55	0.45	0.47	4.4
FN3	0.82	3.54	0.26	298	0.82	0.67	0.76	13.4
FN1	0.82	6.37	0.26	298	1.44	1.18	1.14	3.4
FN2	0.82	6.99	0.26	298	1.54	1.27	1.21	4.7
FN5	0.82	13.24	0.26	298	2.02	1.66	1.88	13.3
FN7	0.82	26.45	0.26	298	1.96	1.61	-	-
FN6	0.82	6.69	0.13	298	0.38	0.31	0.38	22.6
FN5	0.82	6.69	0.26	298	1.54	1.27	1.21	4.7
FN8	0.82	6.69	0.52	298	4.74	3.90	3.91	0.3
FN9	0.82	6.69	1.04	298	12.4	10.2	12.5	22.5
FN14	0.43	6.69	0.26	298	3.24	1.39	1.50	7.9
FN2	0.82	6.69	0.26	298	1.54	1.27	1.21	4.7
FN15	1.63	6.69	0.26	298	0.62	1.01	0.97	4.0
FN16	2.46	6.69	0.26	298	0.32	0.78	0.85	9.0
FN15[b]	0.82	6.69	0.26	298	1.72	1.41	1.21	14.2
FN1[c]	0.82	6.69	0.26	298	1.54	1.27	1.21	4.7
FN14[d]	0.82	6.69	0.26	298	1.51	1.51	1.21	2.4
FN12	0.82	6.69	0.26	278	0.20	0.16	0.21	31.3
FN10	0.82	6.69	0.26	288	0.66	0.54	0.53	1.9
FN2	0.82	6.69	0.26	298	1.54	1.27	1.21	4.7
FN11	0.82	6.69	0.26	308	3.18	2.61	2.65	1.5
FN13	0.82	6.69	0.26	318	5.03	4.13	5.52	33.7

$$\Delta^a = \frac{\left[R_D(\text{eq 11}) - R_D(\text{eq 18})\right]}{R_D(\text{eq 11}).} \text{x}100 .$$

[b]under nitrogen-saturated conditions ($[O_2]_o \cong 0$).
[c]under air-saturated conditions ($[O_2]_o \cong 0.27$ mmol.L^{-1}).
[d]under oxygen-saturated conditions ($[O_2]_o \cong 1.4$ mmol.L^{-1}).

Table 3.3. Experimental conditions of the runs, the pseudo-first-order rate constants and initial oxidation rate of phenol

Exp N°	$[Phenol]_o$ ($mmol.L^{-1}$)	$[H_2O_2]_o$ ($mmol.L^{-1}$)	$[Fe^{2+}]_o$ ($mmol.L^{-1}$)	T (K)	k_{obs} x10^3 (s^{-1})	R_D x 10^6 ($L.mol^{-1}.s^{-1}$) eq.3.14	eq.3.13	Δ^a (%)
FP1	1.06	2.45	0.054	298	1.40	1.41	1.69	19.9
FP4	1.06	1.07	0.054	298	0.71	0.75	0.71	5.3
FP5	1.06	5.34	0.054	298	4.53	4.82	3.68	23.7
FP6	1.06	10.67	0.054	298	6.17	6.56	7.46	13.7
FP1	1.06	2.45	0.054	298	1.40	1.41	1.69	19.9
FP2	1.06	2.45	0.132	298	3.96	4.12	4.00	2.9
FP3	1.06	2.45	0.261	298	6.52	6.68	7.73	15.7
FP5	1.06	2.45	0.054	298	1.53	1.63	1.67	1.8
FP10	2.10	2.45	0.054	298	1.35	2.84	3.19	12.3
FP11	0.53	2.45	0.054	298	7.33	3.89	4.27	9.8
FP12	3.37	2.45	0.054	298	0.79	2.67	2.88	7.9
FP13	1.13	2.45	0.054	298	2.98	3.39	3.63	7.1
FP7	1.06	2.45	0.054	298	1.53	1.54	1.69	9.7
FP8	1.06	2.45	0.054	303	2.75	2.76	2.11	26.3
FP9	1.06	2.45	0.054	318	6.68	6.93	5.88	15.2
FP14	1.06	2.45	0.054	288	1.38	1.40	1.65	19.0

$$\Delta^a = \frac{\left[R_D(\text{eq 21}) - R_D(\text{eq 20})\right]}{R_D(\text{eq 11})} \text{x} 100$$

In the same way that in the case of the experiments with NB, H_2O_2 and Fe^{2+} concentration ranges were chosen addressing to reach the highest phenol degradation percentage in the range from 5 to 60 min. The $[H_2O_2]_o/[phenol]_o$, $[H_2O_2]_o/[Fe^{2+}]_o$ and $[phenol]_o/[Fe^{2+}]_o$, ratios varied from 1.0 to 10.1, 19.8 to 40.9 and 2.1 to 12.9, respectively. The time of degradation for the phenol is sensibly smaller than the degradation time for NB. This fact could be explained taking into account that the effectiveness of a given treatment process depends strongly on the nature of the substrate, at least for organic compounds. In the case of phenol, the OH is electro-donating substituent and therefore, the electrophilic substitution by $HO^{\bullet}$ radical is favored. By the contrary, in the case of NB, the NO_2 electron accepting substituents the electrophilic substitution by $HO^{\bullet}$ radical is unfavorable.

3.3. Results and discussion for NB degradation

3.3.1. Intermediates in the degradation of NB

To clarify the reaction pathways for NB after the dark Fenton reaction, the identification of reaction products by HPLC was carried out (see Fig. 3.5). Identification and quantification of nitrophenols as reaction intermediates suggests that the degradation of NB by the Fenton process takes place by reaction with $HO^{\bullet}$ radical, which is assumed to be the main oxidant. Reaction of NB with $HO^{\cdot}$ radicals to form $HO^{\bullet}$-NB adducts (nitrohydroxy-cyclohexadienyl radicals) has a significantly high rate constant (eq.3.1).

$$HO^{\bullet} + NB \rightarrow o\text{-}, m\text{-}, \textit{and } p\textit{-isomeric } HO^{\bullet}\text{-NB } \textit{adducts} \qquad (3.1)$$

$$k_8 = 3x10^9 \text{ L.mol}^{-1}\text{s}^{-1} \text{ (Adams, 1965)}$$

It is worth mentioning, that hydroxy-cyclohexadienyl radicals have been observed by UV and EPR methods in the reaction of benzene with $HO^{\bullet}$ radicals (Walling, 1975). When the reaction is run in presence of oxygen, the $HO^{\bullet}$-NB adducts formed react preferably with dissolved oxygen (Kunai *et al.*, 1986; Bohn and Zetzsch, 1999), rather than $HO^{\bullet}/HOO^{\bullet}$ radicals or Fe^{2+}/Fe^{3+} ions due to their very low steady-state concentration, thus producing nitrophenols and $HOO^{\bullet}$ radicals (reaction 3.2).

$$o\text{-}, m\text{-}, and\ p\text{-}isomeric\ HO^{\bullet}\text{-NB}\ adducts + O_2 \rightarrow o\text{-}, m\text{-}, and\ p\text{-nitrophenols} + HOO^{\bullet} \quad (3.2)$$

In absence of oxygen, the HO·-NB adducts formed react preferably with Fe^{2+} or Fe^{3+} (Koltoff and Medalia, 1949) leading eventually to the formation of isomeric nitrophenols as reaction intermediates. Fig. 3.6 shows an example to visualize the conversion of NB in isomers of nitrophenols. In this figure is observed that a maximum of nitrophenol isomers was reached during the first 10 minutes of reaction. Afterwards, these concentrations were decreasing until total disappearance of these isomers. Something that is worthwhile to highlight, is that in all the carried out experiments where these isomers were quantified, their total elimination took place at the same time that the NB.

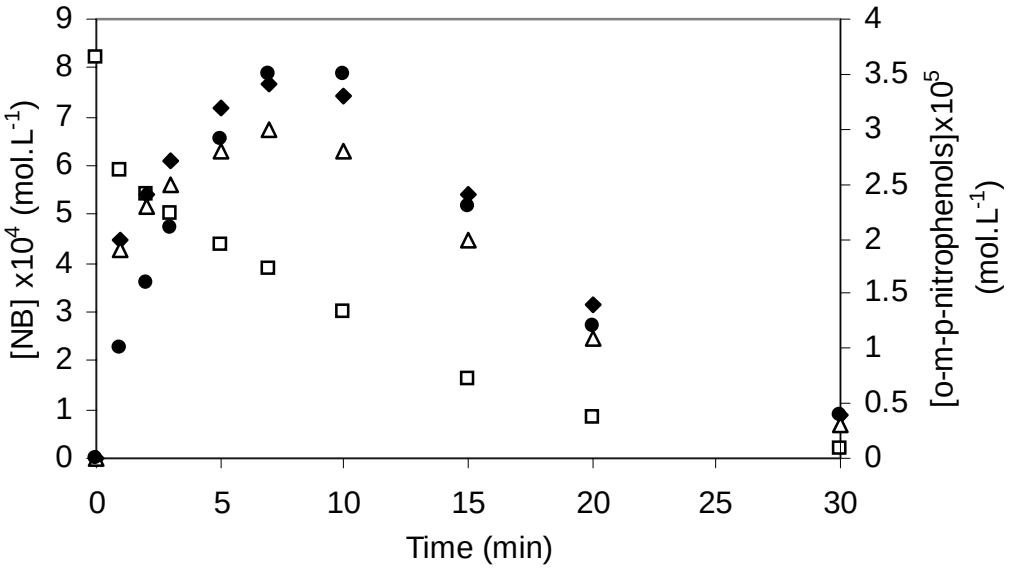

Figure 3.6. Formation and elimination of nitrophenol isomers in the degradation of NB by Fenton process. $[NB]_o$ = 0.82 mmol.L^{-1}, $[H_2O_2]_o$ = 26.45 mmol.L^{-1}, $[Fe^{2+}]_o$ = 0.26 mmol.L^{-1}. (□) NB, (•) o-nitophenol, (♦) p-nitrophenol, (Δ) m-nitrophenol.

When conversion of NB was 15-25% ratios of the *o*-, *m*-, and *p*-isomers were 1 : 1.2 - 3.8 : 1.4 - 2.7. At high conversion of NB (80-90%) ratios of the *o*-, *m*-, and *p*-isomers were found to be 1 : 0.6 – 1.0 : 0.8 – 1.2. As it can be seen, formation of *o*-isomer is increased at higher conversion of NB, which can be expected if the *o*-nitrophenol degradation rate is lower than *m*- and *p*-isomers. In fact, it has been shown by Lipczynska-

Kochany (1991) that *o*-nitrophenol degradation rate is lower than that of *p*-nitrophenol. Besides, it has been found that *o*-nitrophenol degradation rate is lower than that of *m*-nitrophenol under the same experimental conditions.

Comparison of isomeric ratios can be used to verify if the $HO^{\bullet}$ radical is the attacking species in different chemical systems. The isomeric distribution of nitrophenols formed during the degradation of NB by Fenton reagent, photolysis and radiolysis are presented in Table 3.4. These ratios reflect the extent of the attack by the $HO^{\bullet}$ radical at different positions of the aromatic ring and go in agreement with the expected for a very reactive homolytic reagent with some electrophilic character. As it can be seen in Table 3.4, the ratio of the *o*-, *m*-, and *p*-isomers is practically the same under the different degradating methods. This fact supports the hypothesis of generation of $HO^{\bullet}$ radicals in the Fenton reaction. A mass balance within the NB converted and nitrophenols isomers formed was also made in order to reinforce the idea about the generation of $HO^{\bullet}$ radical in the Fenton reaction. From this mass balance is proven that 30% of NB is converted in nitrophenols isomers after 1 min of Fenton reaction (see Fig. 3.6). This can also be corroborated in each one of the experiments presented in Table 3.2.

Table 3.4. The isomeric distribution of nitrophenols formed during the action of Fenton reagent, photolysis, and radiolysis on the aqueous solutions of nitrobenzene

Source of attacking species	Ratio of o-,m-, and p-isomers	Reference
Fenton reagent [a]	1 : 1.3 – 2.8 : 1.4 – 2.7	This work
Fenton reagent [b]	1 : 0.6 – 1.0 : 0.8 – 1.2	This work
Fenton reagent	1 : 1.3 : 1.9	Norman and Radda, 1962
Fenton reagent	1 : 0.8 : 1.8	Loebl *et al.*, 1949
Photolysis [c]	1 : 0.6 : 0.7	Lipczynska-Kochany and Bolton, 1992
Radiolysis		
pH= 2	1 : 0.9 : 1.0	Loebl *et al.*, 1949
pH= 6	1 : 1.0 : 1.0	Loebl *et al.*, 1949
Radiolysis (pH= 5.5)		
Air	1 : 0.6 : 0.7	Matthews and Sangster, 1967
Nitrogen	1 : 0.7 : 1.8	Matthews and Sangster, 1967

[a]conversion of NB (15-25%). [b]conversion of NB (80-90%). [c]in presence of H_2O_2.

3.3.2. Estimation of initial operating ratios in Fenton process

As it has been demonstrated in the previous section, $HO^{\bullet}$ radical can be considered as the main oxidant species in this process. In this sense, taking into account the mechanisms proposed by Haber and Weiss described in section 3.1, initial operating $[compound]_o/[H_2O_2]_o$, $[compound]_o/[Fe^{2+}]_o$ and $[H_2O_2]_o/[Fe^{2+}]$ ratios were determined. Hydroxyl radicals react with organic compounds according to eq. 3.1. However, it could also participate in the competition reaction described by eqs.1.12, 1.13 and 1.6. Therefore, it is very important to choose the adequate operating conditions in order to favor the reaction between $HO^{\bullet}$ with the organic compounds (eq. 3.1), avoiding those secondary reactions, which would consume hydroxyl radicals. In the case of NB, under these conditions and being eq. 3.1 the main way for the decay of $HO^{\bullet}$ radicals in comparison with eq. 1.13, i.e. $(k_8/k_4)>10$, the following molar ratio was obtained:

$$[NB]_o/[H_2O_2]_o>10\ k_4/k_8 \quad \Rightarrow \quad [NB]_o/[H_2O_2]_o>0.016$$

In a same way it was obtained that,

$$[NB]_o/[Fe^{2+}]_o>10\ k_3/k_8 \Rightarrow \quad [NB]_o/[Fe^{2+}]_o>0.17$$

From these ratios, the values for $[H_2O_2]/[Fe^{2+}] > 11$ were obtained. This means that H_2O_2 will be in excess.

These ratios were considered to select the range of H_2O_2 and Fe^{2+} concentration used in the experimental part (see section 3.2.4).

3.3.3. Degradation of NB by Fenton reagent. Kinetic study

The linear regression analysis of the data representing NB concentration versus reaction time indicates that in a first approach, the oxidation reaction (3.1) can be described by a pseudo-first-order kinetics with respect to NB concentration (eq. 3.3)**.**

$$\mathrm{Ln}\left(\frac{[NB]}{[NB]_o}\right) = -k_{obs}\ t \qquad (3.3)$$

where k_{obs} represents the pseudo-first-order rate constant. In this case, a plot of Ln $([NB]/[NB]_o)$ versus time in every experiment must lead to a straight line whose slope is k_{obs}. For example, Fig. 3.7 shows this plot for some experiments where the temperature and initial concentration of H_2O_2, NB, and dissolved oxygen were fixed and

Fe^{2+}concentration was varied. As it can be seen, points lie satisfactory in straight lines with correlation coefficients greater than 0.92.

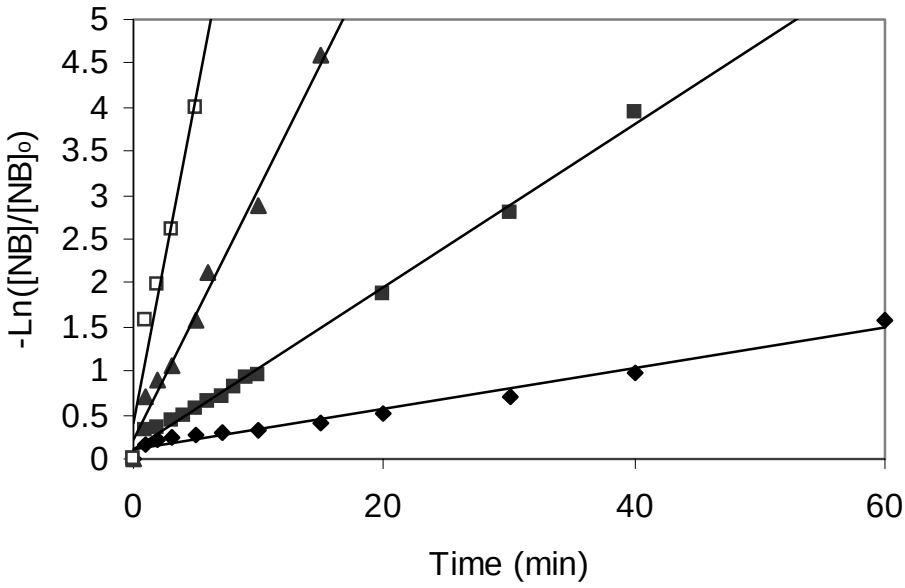

Figure 3.7. Effect of initial concentration of Fe^{2+} on the degradation of NB. First-order plots for NB degradation at pH ≅ 3.0 by Fenton reagent: $[NB]_o$ = 0.82 mmol.L^{-1}, $[H_2O_2]_o$ = 6.99 mmol.L^{-1}, $[Fe^{2+}]_o$ = (♦) 0.13 mmol.L^{-1}, (■) 0.26 mmol.L^{-1}, (▲) 0.52 mmol.L^{-1}, (□) 1.04 mmol.L^{-1}, 298 K.

It is worth noting that the k_{obs} values (Table 3.2) were calculated from experimental data covering 76-99% removal of NB. In experiments carried out in duplicate, k_{obs} varied less than 10%. All these results support the pseudo-first-order kinetics.

Nitrobenzene degradation rates (R_D) were calculated by eq. 3.4 (Table 3.2)

$$R_D = -\frac{d[NB]}{dt} = k_{obs}[NB]_o \qquad (3.4)$$

Careful analysis of our reaction conditions for NB degradation taking into account the reaction mechanism proposed by Walling (1975) for Fe^{2+} with H_2O_2 (eqs. 1.6, 1.10-1.14 and 1.16), shows why it is a "Fenton-like" process. The rate constant for the reaction of ferrous ions with H_2O_2 is high (k_1 = 63 L.$mol^{-1}s^{-1}$ at 298 K) (De Laat and Gallard, 1999) and therefore Fe^{2+} oxidizes to Fe^{3+} in a few seconds in excess of H_2O_2 (Table 3.2, 6.8 ≤

$[H_2O_2]_o/[Fe^{2+}]_o \leq 102.8$). If Fe^{2+} oxidation is a pseudo-first-order process, the time required for the conversion of 99% of Fe^{2+} to Fe^{3+} can be calculated by eq. 3.5

$$t_{99} = Ln\left(\frac{100}{k_1[H_2O_2]_o}\right) \quad (3.5)$$

and was found to be 2.6 – 46 s. Therefore, the NB degradation by Fenton's reagent performed in this study (at $[H_2O_2]_o >> [Fe^{2+}]_o$) is simply a Fe^{3+}/H_2O_2 catalyzed process. The Fenton's reagent with excess of H_2O_2 with respect to Fe^{2+} is known as a "Fenton-like" reagent (Pignatello, 1992). It is worth noting that some publications describe the degradation of NB by Fenton's reagent (Lipczynska-Kochany, 1991, 1992) although they were actually proceeding by a "Fenton-like" process.

3.3.4. Steady-state radical concentration

If a steady-state $HO^{\bullet}$ radical concentration ($[HO^{\cdot}]_{ss}$) is assumed, $[HO^{\cdot}]_{ss}$ value in such system can be estimated by eq. 3.6

$$[HO^{\bullet}]_{ss} = \frac{k_{obs}}{k_7} \quad (3.6)$$

The steady-state $HO^{\bullet}$ radical concentration occurs only when H_2O_2 concentration is relatively constant during the experiment. Furthermore, the $[HO^{\cdot}]_{ss}$ concentration is governed by both its formation rate, dependent on H_2O_2 and $[Fe^{2+}]_o$, and scavenging rate. In this study, H_2O_2 complete decomposition time (t_d) in the Fenton reaction could be estimated by eq. 3.7 (assuming that $[Fe^{3+}] \cong [Fe^{2+}]_o$ and the limiting step for this process is reaction 1.11.

$$t_d = \left(\frac{1}{(k_d\ [Fe^{2+}]_o)}\right) \quad (3.7)$$

where k_d is the second-order rate constant for the overall rate of decomposition of $[H_2O_2]_o$ by Fe^{3+}, k_d which was found to be equal to 0.47 $L.mol^{-1}s^{-1}$ at 298 K and pH 3.0 (De Laat and Gallard, 1999). Calculations by eq. 3.7 showed that the H_2O_2 concentration did not significantly change even up to complete degradation of NB, which can be

expected for a Fenton process. For example, for run FN5 H_2O_2 complete decomposition time was found to be 136 min with the rate constant (k_{obs}) determined within a 60 min interval. In this case, the H_2O_2 was decomposed less than 45%, i. e., more than 55% of H_2O_2 is present in the solution after complete degradation of NB. It can be concluded that the decrease in the H_2O_2 initial concentration did not have a significant effect on the $HO^{\bullet}$ radical steady-state concentration. Furthermore, the linearity of the $Ln([NB]/[NB]_o)$ against time plot for all runs (e.g., Fig. 3.7), give evidence of a $HO^{\bullet}$ radical steady-state concentration. $[HO^{\cdot}]_{ss}$ values were calculated by eq. 3.13 and found to be very low (10^{-14} – 10^{-12} mol.L^{-1}) which is in agreement to the data reported for the oxidation of antrazine (~10^{-13} mol.L^{-1}) by Fenton's reagent Fe^{3+}/H_2O_2 (Gallard and De Laat, 2000). $[HO^{\cdot}]_{ss}$ values were calculated assuming that the rate production of $HO^{\bullet}$ radicals in the Fenton process (limiting step, reaction 1.11) is equal to the decay rate of the radicals by reaction with NB (reaction 3.1).

The iron dynamics can be extremely complex in the Fenton reaction because of a shift from Fe^{2+} to Fe^{3+} along with precipitation of the iron ions as amorphnous oxyhydroxides. This iron speciation changes can affect the $HO^{\bullet}$ radical generation stoichiometry. As a result, these systems cannot be considered as being in steady-state. Given that all the experiments were carried out at pH ≅ 3.0 and with $[H_2O_2]_o >> [Fe^{2+}]_o$, no iron precipitates were observed.

Several references are available concerning H_2O_2 loss and $HO^{\bullet}$ production in the reaction of H_2O_2 with iron salts and oxides (Lin and Gurol, 1998; Lindsey and Tarr, 2000). The formation of $HO^{\cdot}$ radicals in pure water was studied using chemical probes (benzoic acid and 1-propanol), finding linear increase with H_2O_2 concentration (Lindsey and Tarr, 2000). In this study, the steady-state $HO^{\bullet}$ radical concentration also showed a linear dependence on the H_2O_2 initial concentration (eq. 3.8),

$$[HO^{\bullet}]_{ss} = 4.30\text{x}10^{-11}[H_2O_2]_o + 1.48\text{x}10^{-13} \quad (3.8)$$

with Fe^{2+} and NB constant concentrations at 298 K.

3.3.5. Effect of H_2O_2 initial concentration

Hydrogen peroxide is considered the limiting reagent in the Fenton process. Therefore, its effect on the R_D has been studied and can be observed in runs FN1-FN5 and FN7, with Fe^{2+} and NB constant concentrations (Table 3.2, Fig. 3.8 and Fig.3.9). Initially, it can be expected that as the molar ratio of H_2O_2 to pollutant is increased, more $HO^{\bullet}$ radicals are available to attack the aromatic structure and therefore the degradation reaction rate should increase.

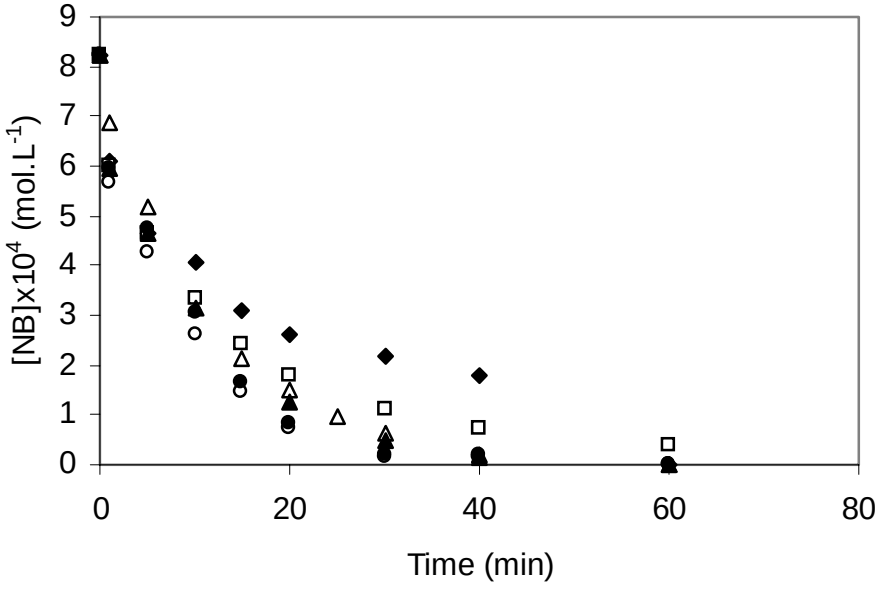

Figure 3.8. Effect of initial concentration of H_2O_2 on the degradation of NB by Fenton reagent: $[NB]_o$= 0.82 mmol.L^{-1}, $[Fe^{2+}]_o$ = 0.26 mmol.L^{-1}, $[H_2O_2]$ = (♦) 1.74 mmol.L^{-1}, (□) 3.54 mmol.L^{-1}, (Δ) 6.37 mmol.L^{-1}, (▲) 6.99 mmol.L^{-1}, (○) 13.24 mmol.L^{-1}, (●) 26.45, 298 K.

In the present case, this rate increment is obtained for H_2O_2 initial concentration in the range 1.74 - 13.24 mmol.L^{-1} (the continuous line does not mean any fitting but only a way of showing the tendency). However, higher H_2O_2 concentrations (H_2O_2 > 13.24 mmol.L^{-1}, run FN7) lead to the saturation in the NB removal rate. It suggests that NB degradation rate becomes insensitive to H_2O_2 concentration when H_2O_2 to NB molar ratio is higher than 16 (Fig. 3.9).

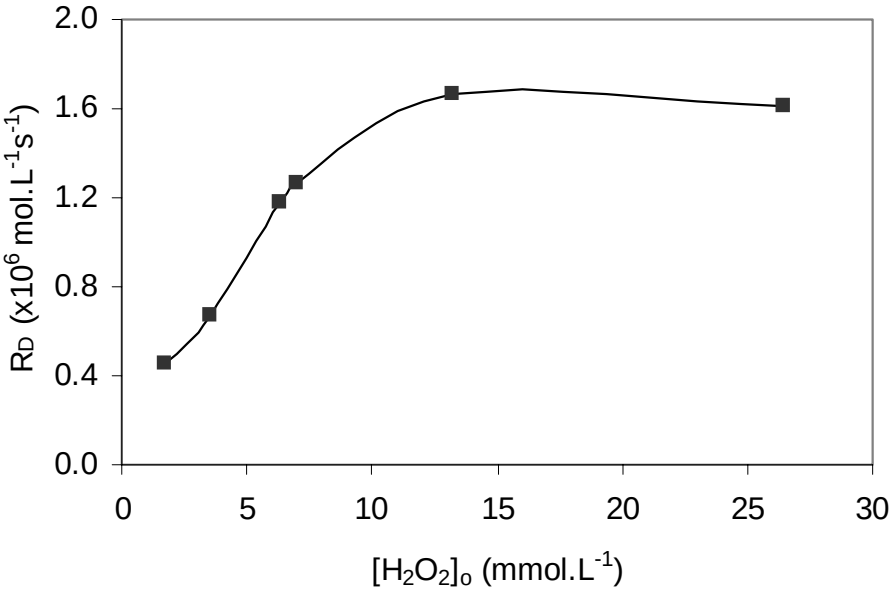

Figure 3.9. Effect of $[H_2O_2]_o$ on the degradation rate of NB. $[NB]_o$ = 0.82 mmol.L^{-1}, $[Fe^{2+}]_o$ = 0.26 mmol.L^{-1}, pH ≅ 3.0, 298 K.

At high H_2O_2 concentration it becomes the main way for $HO^{\bullet}$ radical decay according to reaction 3.4. Therefore, the effect of a high H_2O_2 concentration can be attributed to the fact that it is competing with NB (eq.3.1) for $HO^{\bullet}$ radicals (eq.1.13), thus decreasing their steady-state concentration and NB oxidation rate.

Rate order for H_2O_2 ($[H_2O_2]_o$ < 13.24 mmol.L^{-1}) was determined to be 0.68, from a Log (R_D) against Log $[H_2O_2]_o$ plot.

3.3.6. Effect of Fe^{2+} initial concentration

The Fe^{2+} effect is illustrated in Fig. 3.10, where the variation of NB concentration (in mol.L^{-1}) versus time is represented. As it can be seen in this figure, the initial concentration of Fe^{2+} (runs FN2, FN6, FN8, and FN9 in Table 3.2) shows a significant influence on NB degradation rate.

At constant H_2O_2 and NB concentrations, R_D increases as does Fe^{2+} concentration (see Fig. 3.10 and 3.11). Given that $[H_2O_2] >> [Fe^{2+}]$, the metallic ion is consumed during the first seconds (2.6 - 46 s, see above) and leads to a fast production of $HO^{\bullet}$ radicals and consequently to a rapid NB degradation. After a few seconds, reaction 2 becomes the

limiting step, which regenerates Fe^{2+} ions. Hydroxyl radical formation from this reaction becomes very slow and NB degradation is proceeding by "Fenton-like" reagent.

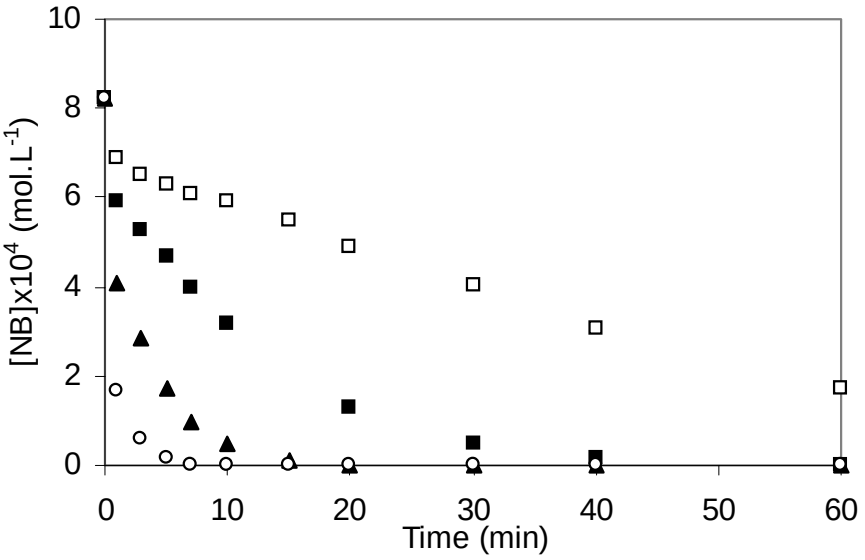

Figure 3.10. Effect of initial concentration of Fe^{2+} on the degradation of NB by Fenton reagent: $[NB]_o$ = 0.82 mmol.L^{-1}, $[H_2O_2]_o$ = 6.99 mmol.L^{-1}, $[Fe^{2+}]_o$ = (□) 0.13 mmol.L^{-1}, (■) 0.26 mmol.L^{-1}, (▲) 0.52 mmol.L^{-1}, (○) 1.04 mmol.L^{-1}, 298 K.

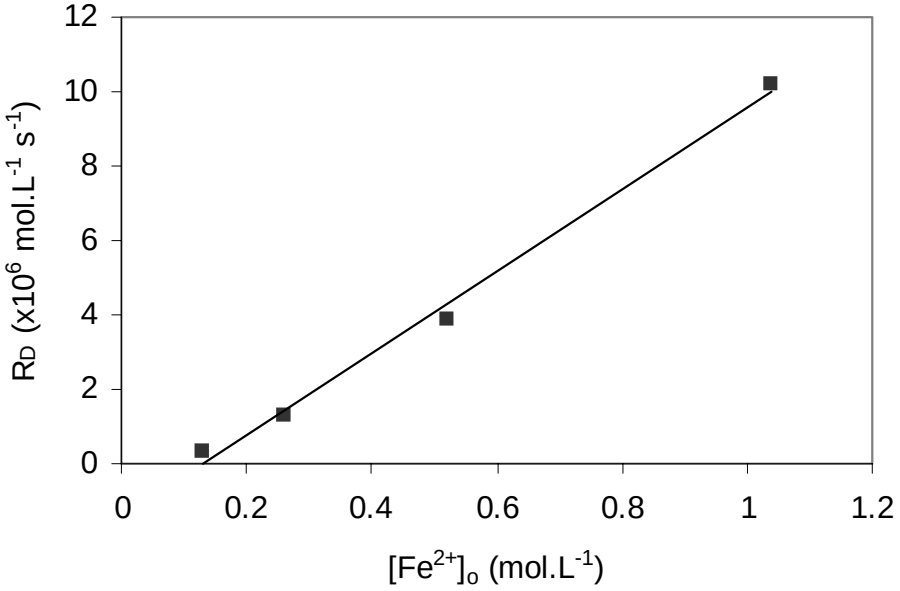

Figure 3.11. Effect of $[Fe^{2+}]_o$ on the degradation rate of NB. $[NB]_o$ = 0.82 mmol.L^{-1}, $[H_2O_2]_o$ = 6.69 mmol.L^{-1}, pH ≅ 3.0, 298 K.

The rate of H_2O_2 decomposition by Fe^{3+} has been extensively studied. Many kinetic models derived from hypothetical mechanisms have been tested (Barb et al., 1951; Walling *et al.*, 1974; Kremer and Stein, 1977; De Laat and Gallard, 1999; Gallard *et al.*, 1999; Gallard and De Laat, 2000).

Recently, De Laat et al. (1999) demonstrated that the rate of H_2O_2 decomposition by Fe^{3+} could be very accurately predicted by a kinetic model which takes into account the rapid formation and slower decomposition of Fe^{3+}-hydroperoxy complexes ($Fe^{3+}(HO_2)^+$ and $Fe^{3+}(OH)(HO_2)^+$). For $5 < [H_2O_2]_o/[Fe^{3+}]_o < 500$, a second-order kinetic law describes the H_2O_2 decomposition initial rate (eq. 3.9)

$$-\frac{d[H_2O_2]_o}{dt} = k_d[H_2O_2]_o[Fe^{3+}]_o \qquad (3.9)$$

where k_d is the second-order rate constant for the overall rate. The k_d value was found to be 0.47 $L.mol^{-1}s^{-1}$ at 298 K and pH = 3.0 (De Laat and Gallard, 1999). Hydroxyl radicals generation rate constant (eq. 1.10) is more than two orders of magnitude higher than the rate constant of H_2O_2 decomposition by Fe^{3+}. Therefore, after a few seconds the latter reaction becomes the limiting step.

Rate order for Fe^{2+} ($[Fe^{2+}]_o < 1.04$ $mmol.L^{-1}$) was determined to be 1.67, from a Log (R_D) against Log$[Fe^{2+}]_o$ plot.

3.3.7. Effect of NB initial concentration

Nitrobenzene initial concentration effect can be observed in runs FN2 and FN14-FN16, at H_2O_2 and Fe^{2+} constant concentrations (Table 3.2, Fig.3.12 and 3.13).

Degradation rate values showed non-linear dependence on NB initial concentration (Fig. 3.13) and is somewhat decreased when its concentration is increased.

If it is assumed, that $HO^\bullet$ radicals production rate is equal to their decay rate by reaction with NB (eq.3.1), i.e., $k_d[Fe^{3+}][H_2O_2]_o = k_{obs}[NB]_o$ there must be a linear dependence of k_{obs} *vs* $1/[NB]_o$ (eq. 3.10). In other words, k_{obs} value will be inversely proportional to the NB initial concentration while all other parameters are kept constant (eq. 3.10).

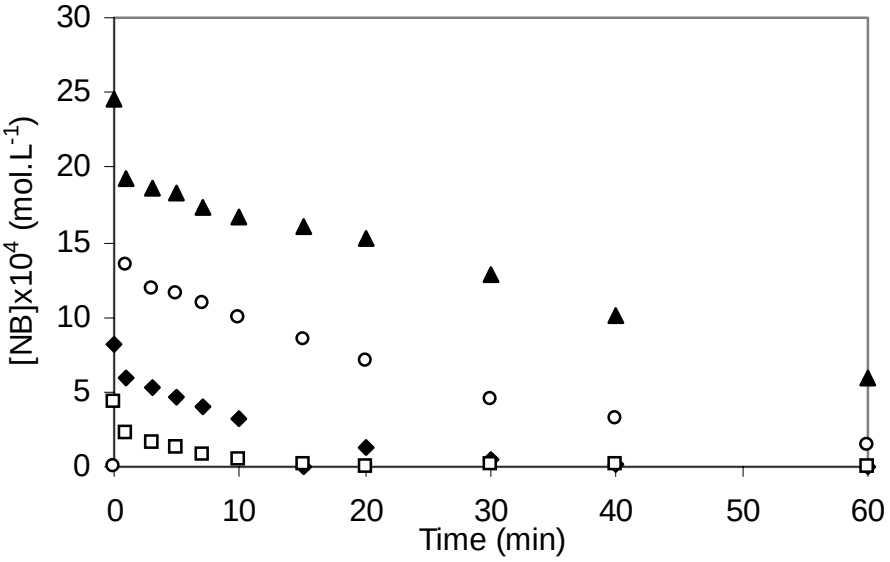

Figure 3.12. Effect of NB initial concentration on the degradation of NB by Fenton reagent: $[H_2O_2]_o$= 6.99mmol.L^{-1}, $[Fe^{2+}]_o$ = 0.26 mmol.L^{-1}, $[NB]_o$ = (▲) 2.46 mmol.L^{-1}, (○) 1.63 mmol.L^{-1}, (♦) 0.82 mmol.L^{-1}, (▫) 0.43 mmol.L^{-1}, 298 K.

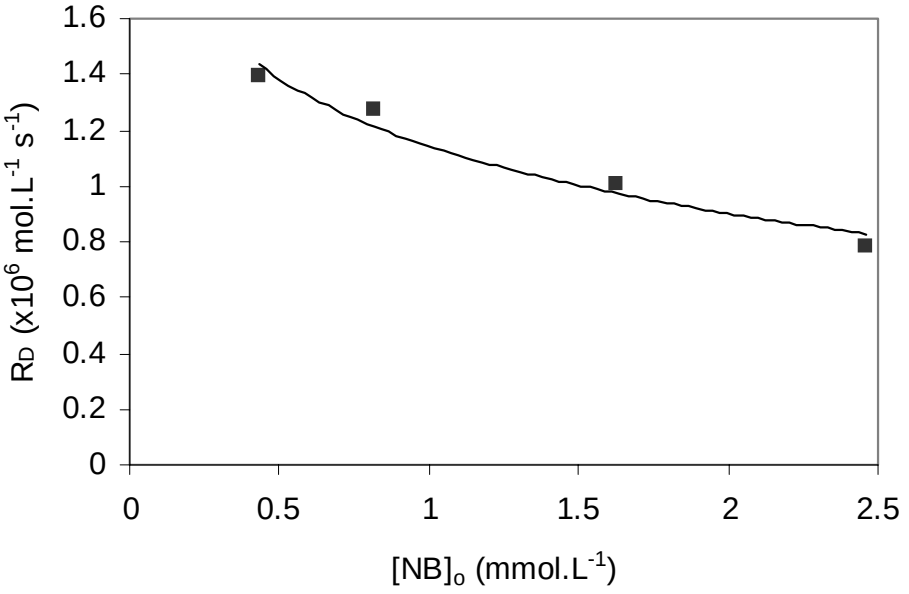

Figure 3.13. Effect of $[NB]_o$ on the degradation rate of NB. $[Fe^{2+}]_o$ = 0.26 mmol.L^{-1}, $[H_2O_2]_o$ = 6.69 mmol.L^{-1}, pH ≅ 3.0, 298 K.

$$k_{obs} = \frac{k_d[Fe^{3+}][H_2O_2]_o}{[NB]_o} \qquad (3.10)$$

Figure 3.13 shows the regression analysis for eq. 17 giving a slope (k_d[Fe(III)][H_2O_2]$_o$) of 1.5x10^{-6} mol.L^{-1}s^{-1}. Taking [Fe^{3+}] ≅ [Fe^{2+}]$_o$ = 0.26 mmol.L^{-1} and [H_2O_2]$_o$ = 6.99 mmol.L^{-1} (Table 3.2) it was calculated k_d = 0.83 (mol.L^{-1})$^{-1}$ s^{-1} at 298 K. In the previous work performed by De Laat and Gallard (1999) the second-order overall rate constant for H_2O_2 decomposition was found to be 0.47 L.mol^{-1}s^{-1} at 298 K and pH = 3.0

Rate order for NB was determined to be -0.32, from a Log (R_D) against Log[NB]$_o$ plot. Since k_{obs} is inversely proportional to NB initial concentration (Fig. 3.14), this species degradation rate should be concentration independent (eq. 3.10), i.e. NB degradation rate order should be zero. The deviation from zero with such unusual order (-0.32) can arise as a result of several successive steps of different stoichiometries interacting in the reaction of H_2O_2 with Fe^{2+} in presence of NB.

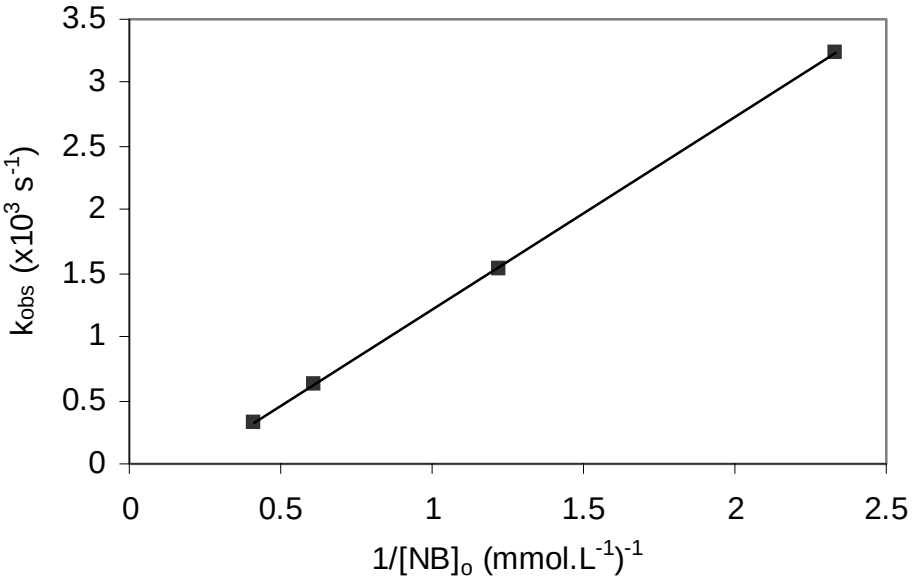

Figure 3.14. Plots k_{obs} vs 1/[NB]$_o$.[Fe^{+2}]$_o$ = 0.26 mmol.L^{-1}, [H_2O_2]$_o$ = 6.69 mmol.L^{-1}, pH ≅ 3.0, 298 K.

3.3.8. Effect of O_2 initial concentration

It has been observed that dissolved oxygen ($0 < [O_2]_o < 1.4$ mmol.L^{-1}) has a very weak effect on NB degradation rate (Table 3.2 and Fig. 3.15).

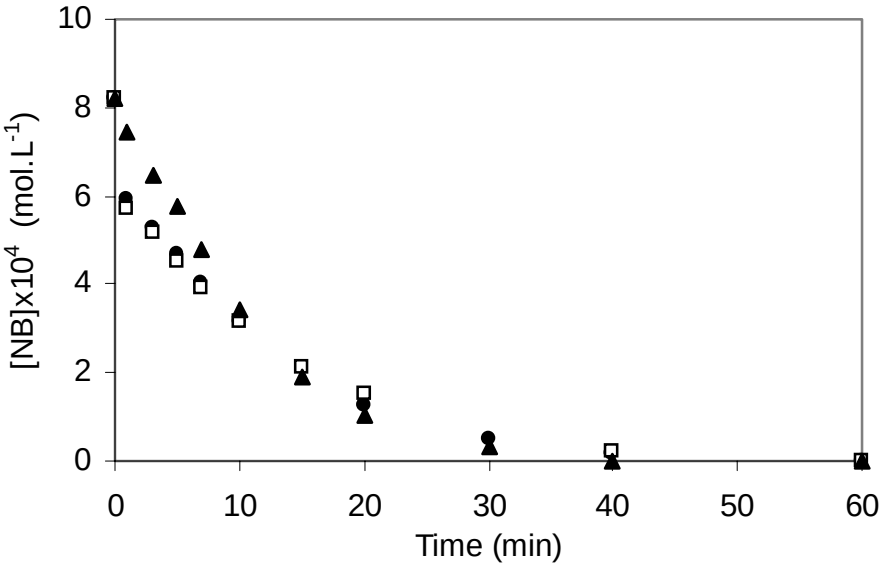

Figure 3.15. Effect of $[O_2]_o$ on the degradation of NB by Fenton reagent: $[NB]_o = 0.82$ mmol.L^{-1}, $[H_2O_2]_o = 6.99$ mmol.L^{-1}, $[Fe^{2+}]_o = 0.26$ mmol.L^{-1}, pH ≅ 3.0, 298K , (•) without bubling O_2 , (□) bubling O_2, (▲) bubling N_2

When oxygen is replaced by nitrogen, NB degradation rate suffers a decrease of about 12%, which is close to the precision in the determination of k_{obs}. With this slight influence, the rate order for molecular oxygen will be zero. These data may indicate that organic radicals R$^{\cdot}$ and ROO$^{\cdot}$ do not affect HO$^{\bullet}$ radical steady-state concentration and oxygen is probably not involved in the first step of NB oxidation mediated by hydroxyl radical. Thus, the oxygen effect may not be apparent when observing NB loss by Fenton process. It may be involved in subsequent steps, i.e., further reactions of the intermediate organic radicals. For example, HO$^{\bullet}$-NB adducts reacts faster with oxygen than with HO$^{\bullet}$ or HOO$^{\bullet}$ radicals producing nitrophenols by reaction (3.2) in presence of dissolved oxygen. In absence of oxygen, the HO$^{\bullet}$-NB adducts or organic radicals resulting from secondary reactions may either dimerize or react with Fe^{2+} or Fe^{3+} (Walling, 1975;

Bandara *et al.*, 1997). The reaction of $HO^{\bullet}$-NB adducts with Fe^{2+} or Fe^{3+} may also lead to formation of isomeric nitrophenols. In addition, other hydroquinone/quinone type intermediate by-products can be oxidized or reduced by Fe^{2+} or Fe^{3+} and in the absence of molecular oxygen, these reactions may have a significant effect on the overall rate of formation and distribution of final products (Kolthoff and Medalia, 1949; Kunai *et al.*, 1986; Bohn and Zetzsch, 1999). This aspect of the effect of oxygen was not studied in this work.

It is worth noting that the pH in all the experiments decreased during the reaction going from 3.5 to 2.5, i. e., the reactions proceeded in acidic medium. At such pH values, Fe^{2+} cannot rapidly be oxidized to Fe^{3+} by molecular oxygen. Indeed in reports done by Lin and co. (1999), no significant effect of dissolved oxygen on H_2O_2 decomposition rate was observed in the heterogeneous catalytic reaction with granular size goethite (α-FeOOH) particles in aqueous solution under various experimental conditions.

3.3.9. Effect of the temperature

Degradation of NB was carried out at five different temperatures (from 278 to 318K) (Table 3.2, runs FN2 and FN10-FN13).

As it can be expected (Fig. 3.16), the temperature exerts a strong effect on NB degradation rate, which is increased at high temperature due to an increment in the first-order rate constant.

The data exhibiting an Arrhenius type behaviour with an activation energy of 59.7 kJ mol^{-1} (eq. 3.11) was calculated from the usual Lg (R_D) vs 1/T (Fig. 3.17)

$$R_D = 3.2 \times 10^4 \exp\left(-\frac{59.7}{RT}\right) \qquad (3.11)$$

It is interesting to note that the activation energy is somewhat higher than those measured for ferrous ion catalyzed decomposition of H_2O_2 in different media (sulphuric or perchloric acid): 39.5 and 40.8 $kJ.mol^{-1}$ (Hardwick, 1957).

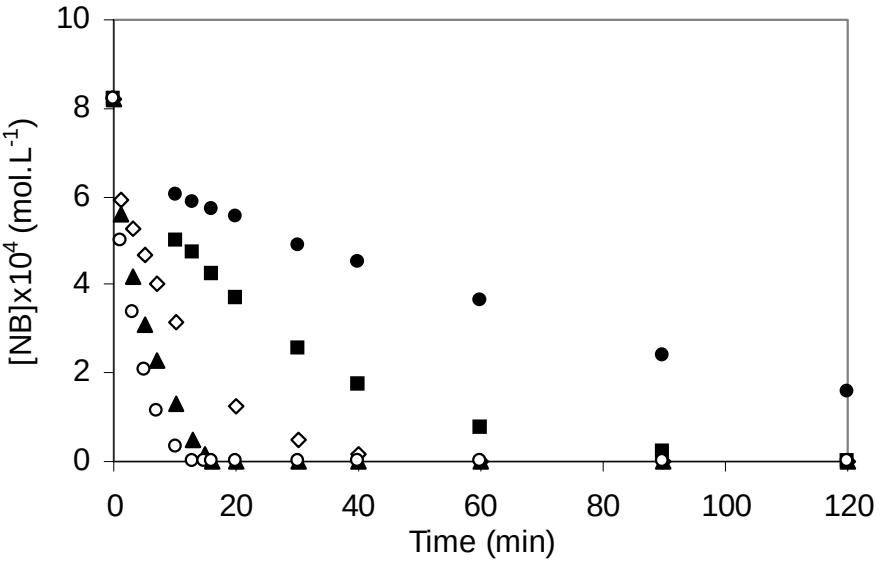

Figure 3.16. Effect of the temperature on the degradation rate of NB by Fenton reagent: $[H_2O_2]_o$ = 6.99 mmol.L^{-1}, $[Fe^{2+}]_o$ = 0.26 mmol.L^{-1}, (●) T = 278 K, (■) T = 288 K, (◇) T = 298 K, (▲) T= 308 K, (○)T= 318 K.

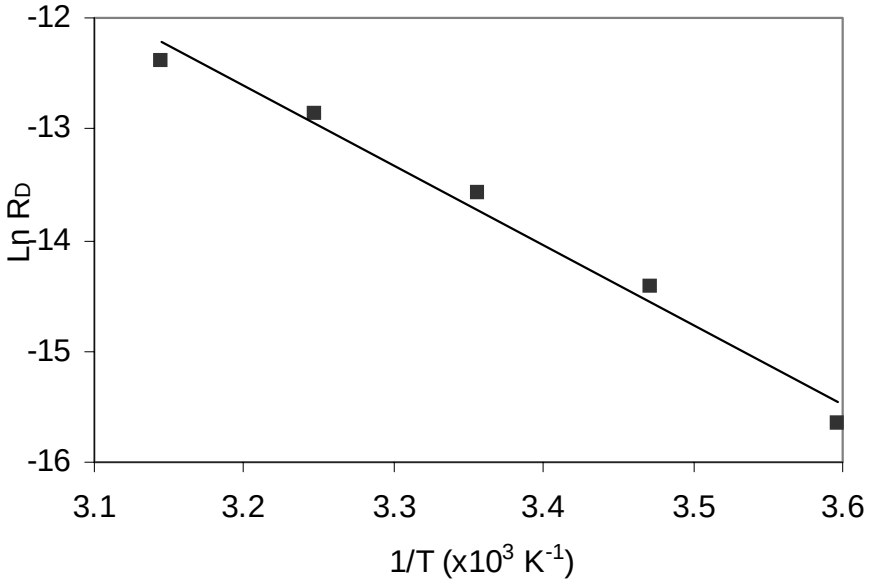

Figure. 3.17. Plot of Ln R_D vs 1/T for the degradation of NB. $[NB]_o$ = 0.82 mmol.L$^{-1,}$ $[Fe^{2+}]_o$ = 0.26 mmol.L^{-1}, $[H_2O_2]_o$ = 6.69 mmol.L^{-1}, pH ≅ 3.0.

3.3.10. Rate equation for the degradation of NB

Rate equation can be expressed in a simple way, as

$$R_D = A\,[H_2O_2]_o^a\,[Fe^{2+}]_o^b\,[NB]_o^c\,[O_2]_o^d\,e^{(-Ea/RT)}$$

where E_a is NB degradation activation energy (59.7 $kJmol^{-1}$). The exponents a = 0.68, b = 1.67, c = -0.32, and d = 0 represent H_2O_2, Fe^{2+}, NB, and molecular oxygen reaction orders, respectively. The coefficient A can be calculated on the basis of experimental NB degradation rate (eq 3.4, Table 3.2) at the determined temperature and H_2O_2, Fe^{2+} and NB initial concentrations. This coefficient was determined to be $1.05x10^{11}$, as an average value from 19 experiments (Table 3.2). Giving all these parameters, the rate equation for NB degradation under Fenton reagent becomes

$$R_D = 1.05 \times 10^{11}[H_2O_2]_o^{0.68}[Fe^{2+}]_o^{1.67}\,[NB]_o^{-0.32}e^{(-59.7/RT)} \qquad (3.12)$$

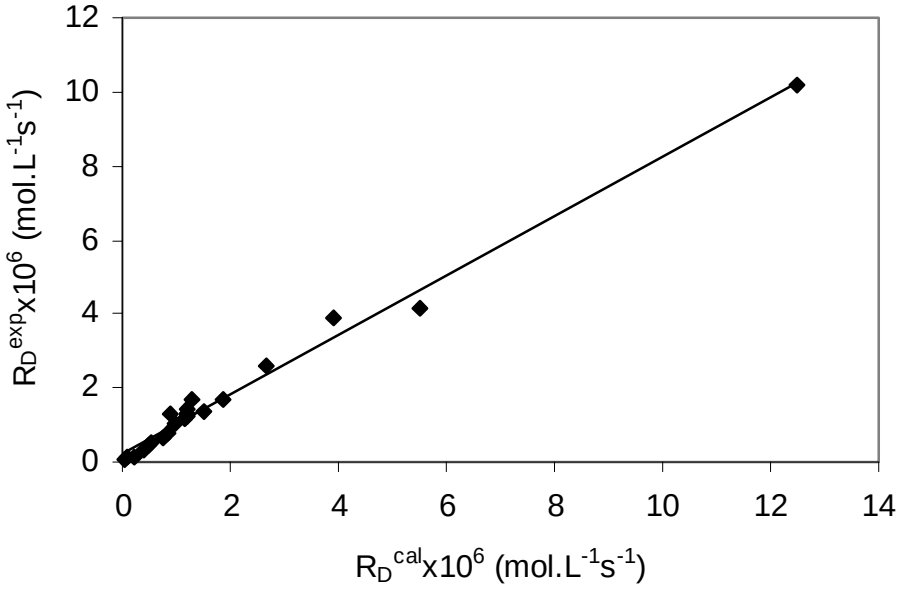

Figure 3.18. Plot of the R_D values determined by eq. 3.4 (R_D^{exp}) and calculated by eq. 3.12 (R_D^{cal}).

The degradation rates of NB calculated by eq. 3.12 are presented in Table 3.2 together with the experimental ones calculated by eq. 3.4. As shown in Table 3.2 and Fig. 3.18 there is a good agreement between experimental and calculated degradation rates. The plot of the initial rate of NB oxidation calculated by eq. 3.12 vs. the one determined from experiment by eq. 3.4 gave a slope of 0.8. Thus, empirical eq. 3.12 may be used for the prediction of NB degradation rate with sufficient precision (ca. 13.4%) under a wide range of experimental conditions: pH ≅ 3.0; 278-318 K; $1.5 < [H_2O_2]_o < 26.5$ mmol.L^{-1}; $0.04 < [Fe^{2+}]_o < 1.1$ mmol.L^{-1}; $0.3 < [NB]_o < 3.5$ mmol.L^{-1}; $0 < [O_2]_o < 1.4$ mmol.L^{-1}.

3.4. Results and discussion for phenol degradation

3.4.1. Degradation of phenol by Fenton reagent. Kinetic studies

A kinetic study was also performed for phenol aqueous solution. However, in this study some parameters that were considered in the case of NB were not studied. This is the case of the effect of oxygen because a little influence in the case of NB was observed. Besides this, some parameters were not studied as carefully as in the case of the nitrobenzene, because the idea was only to compare the obtained results. It is important to point out that in this section the details of the calculations are not presented because the same procedure described in the previous section has been used.

The initial degradation rate for phenol can be described by a first-order kinetics with respect to phenol concentration according to eq. 3.3, where k_{obs} represents again the pseudo-first-order rate constant. A plot of Ln ([Phenol]/[Phenol]$_o$) versus time in every experiment must lead to a straight line whose slope is k_{obs}.

For example, Fig. 3.19 shows this plot for experiments where the temperature and initial concentration of H_2O_2, Fe^{+2} and dissolved oxygen were constants and phenol concentration was varied. As it can be seen, points lie satisfactory in straight lines with correlation coefficients greater than 0.95.

It is worth noting that the k_{obs} values (Table 3.3) were calculated from experimental data covering 50-99% removal of phenol.

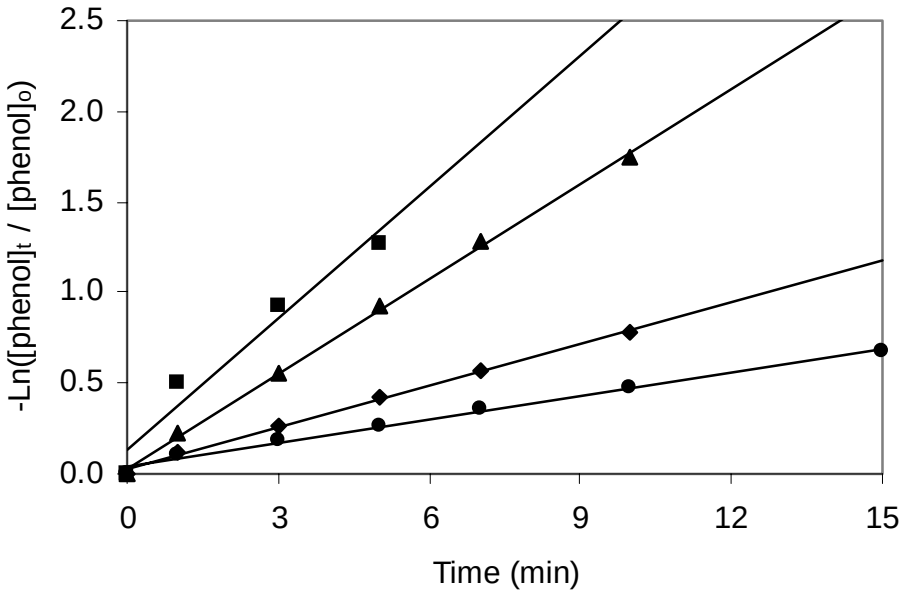

Figure 3.19. First-order plots for the oxidation of phenol: $[Fe^{2+}]_o$ = 0.054 mmol.L^{-1}, $[H_2O_2]_o$ = 5.33 mmol.L^{-1}, $[Phenol]_o$ = (■) 0.53 mmol.L ^{1}, (▲) 1.14 mmol.L^{-1}, (◆) 2.10 mmol.L^{-1} , (●) 3.38 mmol.L^{-1}, 298 K.

3.4.2. Effect of H_2O_2 initial concentration

A significant enhancement of degradation efficiency was verified when the H_2O_2 concentration was increased from 0 to 5.34 mmol.L^{-1} (Table 3.3 and Fig. 3.20). However, at higher concentration ($[H_2O_2]_o$ > 5.34 mmol.L^{-1}, run FP6 the degradation rate is negatively affected. Values of phenol degradation rate as function of the initial H_2O_2 concentration are also show in Table 3.3.

Rate order for H_2O_2 ($[H_2O_2]_o$ < 5.34 was determined to be 1.02, from a Log (R_D) against $[H_2O_2]_o$ plot.

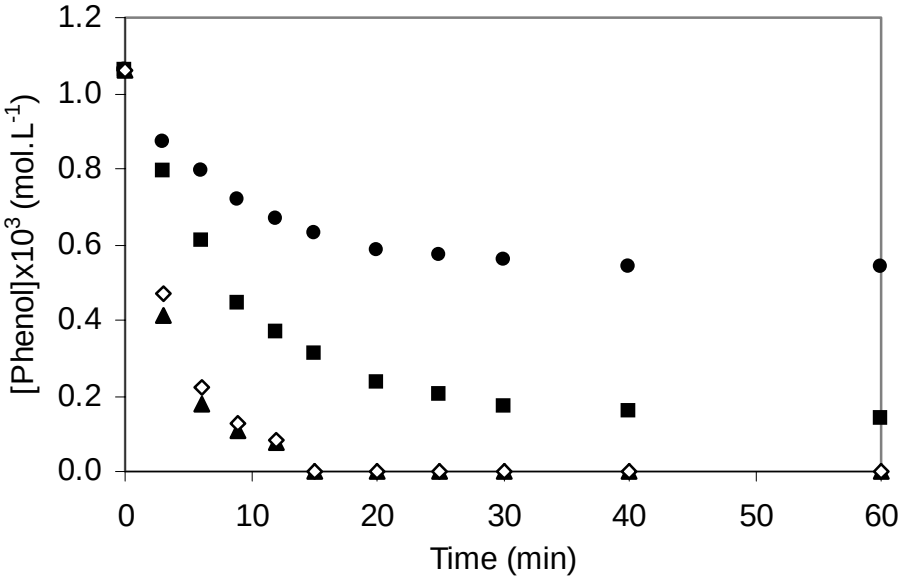

Figure 3.20. Effect of initial concentration of H_2O_2 on the degradation of phenol by Fenton reagent: $[phenol]_o$= 1.06 mmol.L^{-1}, $[Fe^{2+}]_o$= 0.054 mmol.L^{-1}, $[H_2O_2]$= (•) 1.06 mmol.L^{-1}, (■) 2.45 mmol.L^{-1}, (▲) 5.34 mmol.L^{-1}, (◇) 10.67 mmol.L^{-1}, 298 K.

3.4.3. Effect of Fe^{2+} initial concentration

The Fe^{2+} effect is shown in Fig.3.21, where the variation of phenol versus time is represented. As it can be seen in this figure, the initial Fe^{2+} concentration (runs FP1-FP3 in Table 3.3) showed a significant influence on the phenol degradation rate. Once again, after a few seconds, reaction 1.11 becomes the limiting step, which generate Fe^{2+}ions. Hydroxyl radical formation from this reaction, becomes very slow and phenol degradation proceeded by "Fenton-like" reagent.

Similar procedure was used to determine the rate order with respect to Fe^{2+} ($[Fe^{2+}]_o$ < 0.26 mmol.L^{-1}) being its value equal to 0.96.

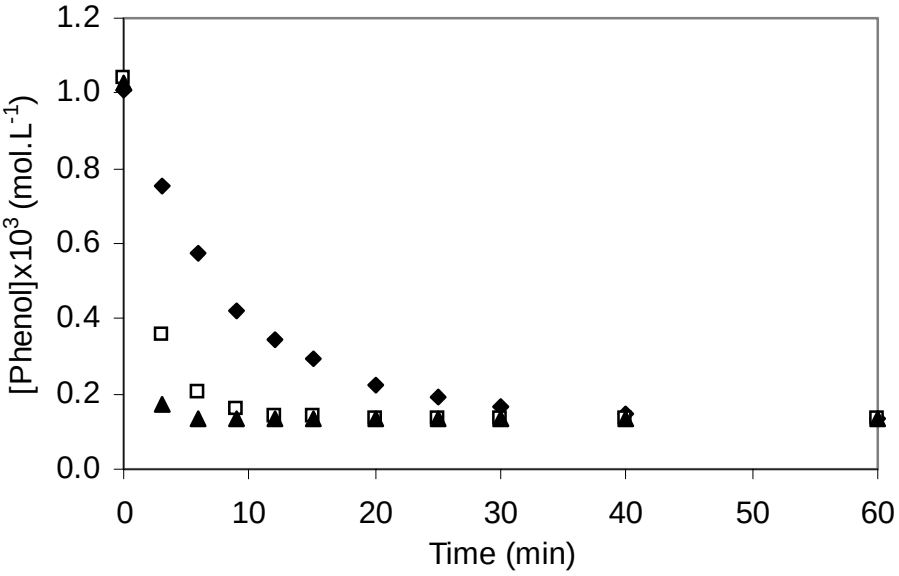

Figure 3.21. Effect of initial concentration of Fe^{2+} on the degradation of phenol by Fenton reagent: $[phenol]_o$ = 1.06 $mmol.L^{-1}$, $[H_2O_2]_o$ = 2.45 $mmol.L^{-1}$, $[Fe^{2+}]_o$ = (◆) 0.054 $mmol.L^{-1}$, (□) 0.13 $mmol.L^{-1}$, (▲) 0.26 $mmol.L^{-1}$, 298 K.

3.4.4. Effect of phenol initial concentration

Phenol concentration effect can be observed in runs (FP10-FP13) at H_2O_2 and Fe^{2+} constant concentrations (Table 3.3 and Fig.3.22). Degradation rate value, showed non-linear dependence on phenol initial concentration and is somewhat decreased when its concentration is increased.

Rate order for phenol was determined to be -0.21, from a $\mathrm{Log}\left(R_D\right)$ against $\mathrm{Log}[NB]_o$ plot.

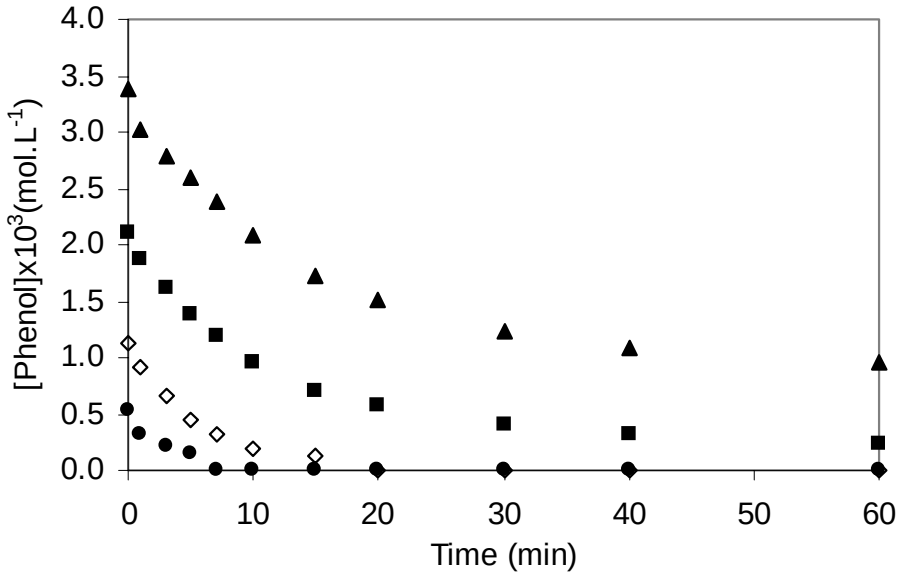

Figure 3.22. Effect of initial concentration of phenol on the degradation of phenol by Fenton reagent: $[H_2O_2]_o$ = 2.45 mmol.L^{-1}, $[Fe^{2+}]_o$ = 0.054 mmol.L^{-1}, $[phenol]_o$ = (▲) 3.38 mmol.L^{-1}, (■) 2.10 mmol.L^{-1}, (◇) 1.14 mmol.L^{-1}, (●) 0.53 mmol.L^{-1}, 298 K.

3.4.5. Effect of the temperature

The degradation of phenol at three different temperatures runs FP7-FP10 and FP14 (288-318 K) was carried out. The temperature showed a strong effect on the degradation rate of phenol (Table 3.3 and Fig. 3.23) and the data exhibiting an Arrhenius type behavior with an activation energy of 47.7 kJ.mol^{-1} (eq. 3.11) was calculated from the usual Log (R_D) vs 1/T (Fig. 3.24).

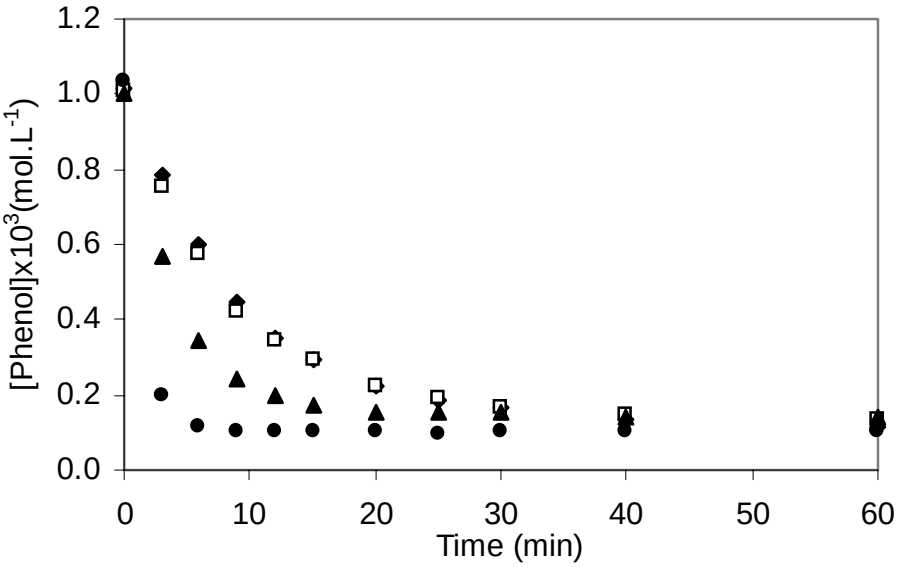

Figure 3.23. Effect of the temperature on the degradation rate of phenol by Fenton reagent: $[H_2O_2]_o$ = 2.45 mmol.L^{-1}, $[Fe^{2+}]_o$ = 0.054 mmol.L^{-1}, (♦)[T]=288 K, (□) T= 298 K, (▲)T= 303 K, (●)T= 318 K.

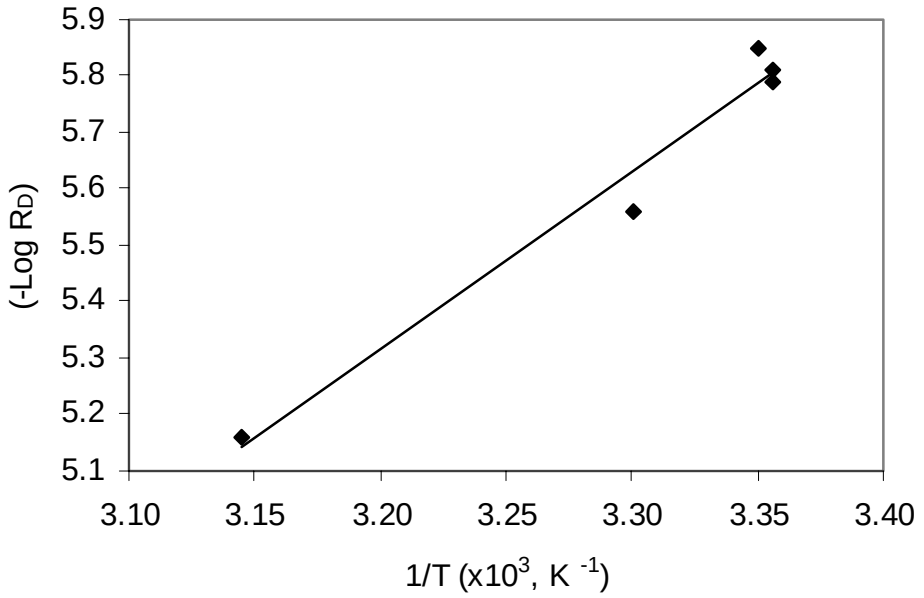

Figure 3.24. Plot of -Log R_D vs 1/T for the degradation of phenol. $[Phenol]_o$ = 1.02 mmol.L^{-1}, $[Fe^{2+}]_o$ = 0.054 mmol.L^{-1}, $[H_2O_2]_o$ = 2.45 mmol.L^{-1}.

It is interesting to note that the activation energy is comparable with those measured for the reaction of ferrous ion catalyzed decomposition of H_2O_2 in different medium ($kJ.mol^{-1}$): 39.5 and 40.8 (Hardwick, 1957)

3.4.6. Rate equation for the degradation of phenol

The rate equation for the degradation of phenol has been developed in the same way that the rate equation for NB. In this sense, the eq.3.12 for the degradation of phenol is:

$$R_D = 5.78 \times 10^8 [H_2O_2]_o^{1.02} [Fe^{2+}]_o^{0.96} [phenol]_o^{-0.21} e^{(-47.7/RT)} \quad (3.13)$$

where E_a is phenol degradation activation energy (47.7 $kJmol^{-1}$). The exponents a = 1.02, b = 0.26, c = -0.21, represent H_2O_2, Fe^{2+}, and phenol orders, respectively. The coefficient A can be calculated on the basis of experimental phenol degradation rate that was calculated by eq. 3.14 (Table 3.3) at the determined temperature and H_2O_2, Fe^{2+} and phenol initial concentrations.

$$R_D = -\frac{d[phenol]}{dt} = k_{obs} [phenol]_o \quad (3.14)$$

This coefficient was determined to be 5.78×10^8, as an average value from 14 experiments (Table 3.3).

The degradation rates of phenol calculated by eq. 3.13 are presented in Table 3.3 together with the experimental ones calculated by eq. 3.14. As shown in Table 3.3 and Fig.3.25 there is a good agreement within a range of 2-24% (average error to be about 12%) experimental and calculated degradation rates. Besides this, the plot of initial rate of the oxidation of phenol that was calculated by eq. 3.13 vs. the one determined from experiments by eq.3.14 (Table 3.3 and Fig. 3.25) gave a slope of 1.004. This value indicates on the possibility to make use of the eq.3.13 for the prediction of the initial phenol oxidation rate by Fenton reagent under the planned experimental work.

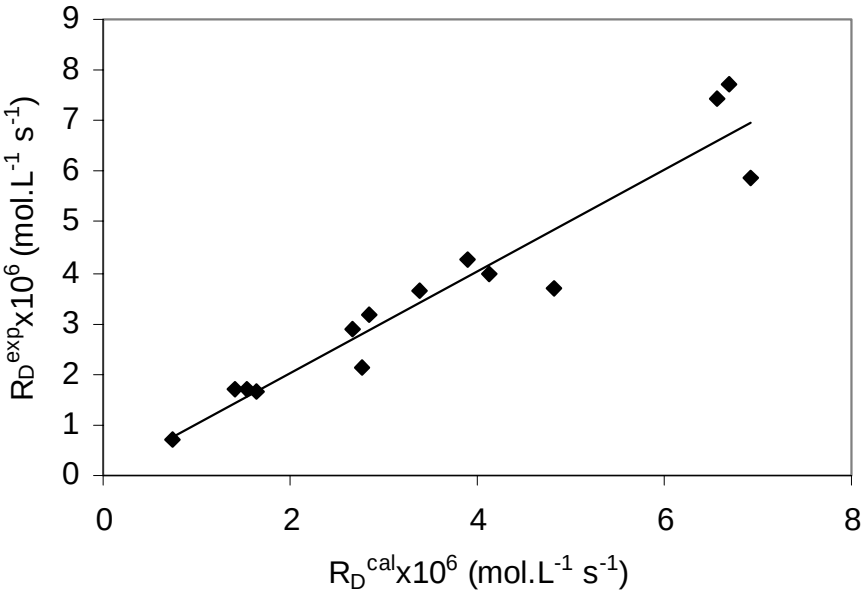

Figure 3.25. Plots of the R_D values determined by eq. 3.14 (R_D^{exp}) and calculated by eq. 3.13 (R_D^{cal})

4. UV-based processes for removal of NB and phenol. Photo-Fenton, UV/H_2O_2, and Fe^{3+}/UV

4.1. Introduction

As commented in the Introduction chapter, the photo-Fenton and UV/H_2O_2 systems are widely known AOPs and are in practical use (Stanislav and Sedlak, 1992; Ruppert *et al.*, 1993; Liao and Gurol, 1995; De Laat *et al.*, 1999; Esplugas *et al.*, 2002). More recently, the homogeneous Fe^{3+}/UV system has been also presented as an alternative photochemical method for the treatment of organic pollutants (Mazellier and Bolté, 1997; Catastini *et al.*, 2002).

UV light-based processes have been successfully utilized for the destruction of nitroaromatic and phenolic compounds in water (Lipczynska-Kochany, 1992; Lipczynska-Kochany *et al.*, 1995; Beltran *et al.*, 1998; Benitez *et al.*, 2000; Fernando *et al.*, 2002). However, a detailed study on the influence of the type of light has not yet been performed.

In this context, three different photochemical treatment processes (photo-Fenton, H_2O_2/UV and Fe^{3+}/UV) in homogeneous phase have been selected and a detailed study was made to test their effectiveness in the treatment of phenol and NB in water solution. Three sources of artificial UV/visible light in three different devices were tested.

Due to its low costs and keeping in mind its growing use in the photocalytic processes of waters detoxifications (Malato *et al.*, 2002), solar radiation was also tested using a parabolic collector (PC) and two compound parabolic collectors (CPC). The major part of the study using solar radiation has been made in a qualitative way, representing the first steps in our laboratory in this area. All these reactors are described and shown in the experimental section.

For the development of effective wastewater treatment methods, complete mineralization of the pollutant to harmless end products (CO_2 + H_2O) is important and, taking into account that the degradation reaction for phenol and NB by photo-Fenton process is very fast, monitoring of total organic carbon (TOC), one of the most important parameters in wastewater analysis was made instead of following the concentration of organic compounds under study.

The results obtained by each treatment method applied in this chapter are presented in separated sections according to the source of light used. In this sense, the use of artificial UV-visible light corresponds to the first part and the use of solar light to the second one.

Finally, experiments presented in this chapter were carried out in three different locations. All experiments at laboratory scale (reactors B, C, D and E), both with artificial light and with solar light, were performed at the University of Barcelona. The experiments at pilot plant scale were carried out at the Ecole Politechnique Federal de Lausanne (Lausanne, Switzerland) and the Plataforma Solar de Almería (PSA) (Almería, Spain).

4.2. Fundamental aspects of the processes under study

4.2.1. Photo-Fenton process

The basic chemistry, as well as applications of Fe^{2+}/H_2O_2 and Fe^{3+}/H_2O_2 system for hazardous waste treatment, have been already described in chapter 1 and 3. Briefly, other details about this process will be described. Ferrous ion combined with hydrogen peroxide (Fenton's reagent) reacts stoichiometrically to give $HO^{\bullet}$ according to:

$$Fe^{2+} + H_2O_2 \rightarrow Fe^{3+} + OH^- + HO^{\bullet} \qquad (1.10)$$

In the dark, the reaction is retarded after complete conversion of Fe^{2+} to Fe^{3+}. Nowadays, it is known that the oxidizing power of the Fenton system can be greatly enhanced by irradiation with UV or UV-visible light (Pignatello, 1992; Legrini *et al.*, 1993; Pignatello and Sun, 1993; Ruppert *et al.*, 1993). This effectiveness has been proven with the total mineralization of many organic compounds in aqueous solution (Lipczynska-Kochany, 1991; Pignatello and Sun, 1993). The reason for the positive effect of irradiation on the degradation rate include the photo-reduction of Fe^{3+} to Fe^{2+} ions, which produce new $HO^{\bullet}$ radicals with H_2O_2 (eq. 1.11) according to the following mechanism

$$Fe^{3+} + H_2O \xrightarrow{h\nu} Fe^{2+} + HO^{\bullet} + H^+ \qquad (1.17)$$

$$H_2O_2 \xrightarrow{h\nu} 2HO^{\bullet} \qquad (\lambda < 400 \text{ nm}) \qquad (1.8)$$

There are more equations (as shown in chapter 1 and 3) involved in the mechanism of hydroxyl radical generation, but the above cited are the most significant. The main compounds absorbing light in the Fenton system are ferric ion complexes, e.g.

$[Fe^{3+}(OH)^{-}]^{2+}$ and $[Fe^{3+}(RCO_2)^{-}]^{2+}$, which produce additional Fe^{+2} by following (eqs. 4.1 and 4.2) photo-induced, ligand-to-metal charge-transfer reactions (Sagawe *et al.*, 2001)

$$[Fe^{3+}(OH)^{-}]^{2+} \rightarrow Fe^{2+} + HO^{\bullet} \quad (\lambda < \text{ca. } 450) \qquad (4.1)$$

$$[Fe^{3+}(RCO_2)^{-}]^{2+} \rightarrow Fe^{2+} + CO_2 + R^{\bullet} \quad (\lambda < \text{ca. } 500 \text{ nm}) \qquad (4.2)$$

Additionally, eq.4.1 yields $HO^{\cdot}$ radicals, while eq.4.2 results in a reduction of the total organic carbon (TOC) content of the system due to the decarboxylation of organic-acid intermediates. It is very important to note that both reactions form the ferrous ions required for the Fenton reaction (eq.1.11). The overall degradation rate of organic compounds is considerably increased in the photo-Fenton process, even at lower concentration of iron salts present in the system (Chen and Pignatello, 1997). Although in the photo-Fenton process, the energy requirement is reduced and it is highly effective in the treatment of phenol and NB solutions, its application would not completely replace a more economical treatment, such as biological degradation, when possible. Thus, the photo-Fenton process as well as other oxidation processes could be used for pretreatment of recalcitrant compounds in order to improve treatment efficiency and assure their biocompatibility. For this pretreatment, sunlight may be applied, thereby reducing energy costs and favoring the environment. As already mentioned in the case of dark-Fenton process, the main disadvantage of the photo-Fenton method is the necessity to work at low pH (normally below 4), because at higher pH ferric ions would begin to precipitate as hydroxide. Furthermore, depending on the iron concentration used, it has to be removed after the treatment in agreement with the regulation established for wastewater discharge. The possibility to reuse the precipitate formed is still under study, therefore, is not discarded their reuse in a future.

4.2.2. H_2O_2/UV process

Other way of generating hydroxyl radicals in the reaction medium and not impaired by the pH is the photolysis of hydrogen peroxide with ultraviolet radiation. Thus, since the sixties, numerous researchers have used the H_2O_2/UV process to oxidize various organic substances in water. Recently, commercial units employing this process have been developed for on-site oxidation of organic contaminants in groundwater. The success of

this process has been generally attributed to the stoichiometric formation of hydroxyl radicals ($HO^{\bullet}$) by photolytic decomposition of H_2O_2. Early investigations of hydrogen peroxide photolysis (Hunt and Taube, 1952; Baxendale and Wilson, 1957; Volman and Chen, 1959; Sehested *et al.*, 1968) as well as a more recent study (Bielsky *et al.*, 1985) have indicated that the following radical chain reactions occur in hydrogen peroxide solution in pure water with UV-light irradiation.

Initiation: (primary photolysis of H_2O_2 or HO_2^-)

$$H_2O_2 / HO_2^- \xrightarrow{h\nu} 2HO^{\bullet} \qquad (4.3)$$

Propagation:

$$H_2O_2 / HO_2^- + HO^{\bullet} \rightarrow HO_2^{\bullet}/O_2^- + H_2O \qquad (4.4)$$

$$HO_2^{\bullet} + H_2O_2 \rightarrow HO^{\bullet} + H_2O + O_2 \qquad (4.5)$$

Termination:

$$HO^{\bullet} + HO^{\bullet} \rightarrow H_2O_2 \qquad (4.6)$$

$$HO^{\bullet} + HO_2^{\bullet} / O_2^- \rightarrow H_2O/OH^- + O_2 \qquad (4.7)$$

$$HO_2^{\bullet} + HO_2^{\bullet} / O_2^- \rightarrow H_2O_2 / HO_2^- + O_2^{\bullet} \qquad (4.8)$$

The overall quantum yield (ϕ_T) of hydrogen peroxide in this reaction chain is 1 at the UV-light wavelength of 254 nm, while the primary quantum yield (ϕ_P) of the primary photolysis reaction of hydrogen peroxide (eq.4.3) at the same wavelength is 0.5.

There are two types of ultraviolet lamps on the market that produce efficiently this photolytic decomposition. The main characteristic of these lamps is basically their band or wavelength emission within the ultraviolet range. Fig. 4.1 shows different bands of the electromagnetic spectra (Froelich, 1992), which indicates the position of ultraviolet radiation and its types. This figure shows that these ultraviolet lamps emit wavelengths between 100 and 400nm, and two types are usually used in this kind of systems (Legrini *et al.*, 1993). The polychromatic lamps emit a wavelength range of between 180 and 400nm, and the monochromatic lamps emit at 254 nm.

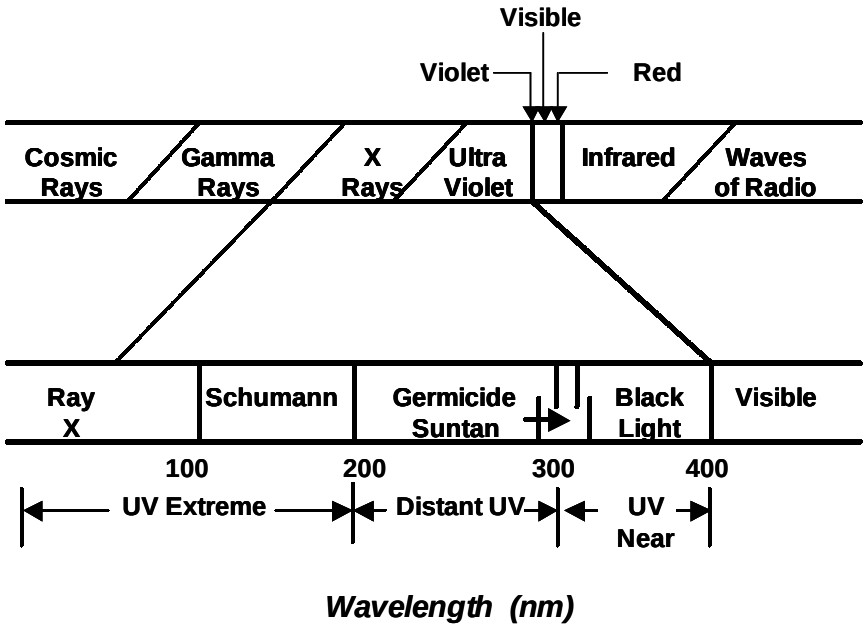

Figure 4.1. Electromagnetic spectrum and enlargement of the ultraviolet field

Although better results are obtained with the polychromatic lamps (Froelich, 1992), the monochromatic lamps are more effective when aromatic organic compounds are the ones to be eliminated (Sundstrom *et al.*, 1989; Guittonneau *et al.*, 1990; Rupper *et al.*, 1994). Many studies with promising results for the elimination of this type of compounds with monochromatic lamps and hydrogen peroxide have been carried out (Mansour, 1985; Ku and Ho, 1990). Polychromatic lamps (Karametaxas *et al.*, 1995) are less selective than the monochromatic ones, and therefore better when there are many different kinds of organic compounds and in not very high concentrations in the effluent to be treated (Malaiyandi *et al.*, 1980; Froelich, 1992).

In this study one monochromatic and two polychromatic lamps were used. The characteristics of these lamps are described in the experimental section.

Reaction mechanism in presence of organic compounds

Glaze et al.. (1995) and Liao and Gurol (1995) proposed different oxidation mechanisms of an organic compound with hydrogen peroxide. Both carried out experiments with monochromatic ultraviolet radiation lamps, which emitted radiation at

254 nm. According to Glaze, the photolysis of hydrogen peroxide is expressed in the following way:

$$H_2O_2 \xrightarrow{h\nu} 2\,HO^{\bullet} \quad (1.8)$$

The splitting of hydrogen peroxide into hydroxyl radicals due to ultraviolet radiation can be expressed as:

$$-\left[\frac{d[H_2O_2]}{dt}\right] = \phi_{H_2O_2} I_o (1 - \exp(-A_t)) \quad (4.9)$$

where:

$\phi_{H_2O_2}$ = the primary quantum yield for the photolysis of H_2O_2 with a value of 0.5 mol H_2O_2. Einstein^{-1}

I_o = monochromatic ultraviolet incident radiation (Einteins.L^{-1}.s^{-1})

A_t = total absorbance of the effluent

In the case of hydrogen peroxide, the absorbance can be expressed by the following expression:

$$A_t = 2.303\, b\, \varepsilon_{H_2O_2} [H_2O_2] \quad (4.10)$$

where:

$\varepsilon_{H_2O_2}$ = the absorbency of hydrogen peroxide at 254 nm, with a value of 19.6 L.mol^{-1}cm^{-1} according to Liao, (1995)

b = the length of the optic way (cm)

Bearing in mind the aforementioned definitions, eq. 4.9 can be reordered giving rise to the following (Liao and Gurol, 1995):

$$-\left[\frac{d[H_2O_2]}{dt}\right] = (2.303\, \phi_{H_2O_2}\, b\, I_o \eta)\, [H_2O_2] \quad (4.11)$$

where,

$$\eta = \frac{1\text{-}10^{-e_{H_2O_2} b [H_2O_2]}}{2.303 \varepsilon_{H_2O_2}\, b\, [H_2O_2]} \quad (4.12)$$

For sufficiently low concentrations of hydrogen peroxide, the value η is approximately 1, and therefore the decomposition of hydrogen peroxide by photolysis is the following:

$$-\left[\frac{d[H_2O_2]}{dt}\right] = (2.303\ \phi_{H_2O_2}\ \varepsilon\ b\ I_o)\ [H_2O_2] \qquad (4.13)$$

The aforementioned expression indicated the formation rate of hydroxyl radicals as a consequence of the direct action of ultraviolet radiation. However, hydroxyl radicals are susceptible to react with other species in solution, and of course, with the organic compounds to be eliminated. Among the most representative reactions, it can be cited the following (Guittonneau *et al.*, 1990; Froelich, 1992; Liao and Gurol, 1995):

$$HO^{\bullet} + H_2O_2 \rightarrow O_2^{\bullet -} + H_2O + H^+ \qquad (4.14)$$

$$HO^{\bullet} + HO_2^- \rightarrow O_2^{\bullet -} + HO^- + H^+ \qquad (4.15)$$

$$HO^{\bullet} + HO_2^{\bullet} \rightarrow H_2O + O_2 \qquad (4.16)$$

$$HO^{\bullet} + O_2^- \rightarrow HO^- + O_2 \qquad (4.17)$$

$$HO^{\bullet} + RH \rightarrow RH_{oxi.} \qquad (4.18)$$

$$O_2^{\bullet -} + H_2O_2 \rightarrow HO^{\bullet} + HO^- + O_2 \qquad (4.19)$$

$$HO_2^{\bullet} + HO_2^{\bullet} \rightarrow H_2O_2 + O_2 \qquad (4.20)$$

From these reactions and by means of complex mathematical expressions, Glaze and co. calculated the concentration of the $HO^{\bullet}$ and $O_2^{\bullet -}$ radicals and the species that form part of the oxidation as reactant. In addition to Glaze et al. (1995), proposed a mechanism to explain the oxidation of an organic compound in the presence of hydrogen peroxide.

4.2.3. Fe^{3+}/UV process

Iron is one of the most abundant elements on earth. Many classes of iron metal, compounds, and mixtures are extensively used in industrial production and daily life. It is therefore important the development of environment-friendly iron catalyst with high efficiency and less energy, which is one of the essential goals of Green Chemistry. In this sense, the same as the case of the Fenton process, the iron photo-assisted system Fe^{3+}/light, without addition of other electron acceptor than O_2 from air, has been received special attention as a potential wastewater treatment process. Hydroxyl radicals formed upon

excitation of Fe^{3+} alone can provide an efficient and less expensive treatment method in comparison with photo-Fenton and H_2O_2/UV processes (Mazellier *et al.*, 1997). For this reason, the photo-oxidation of organic compounds in aqueous solutions containing Fe^{3+}- hydroxy complexes with UV-light radiation has been investigated extensively. At acidic pH (2.5-5), $Fe(OH)^{2+}$ is the dominant photoreactive species. The oxidant was believed to be hydroxyl radical produced from the photolysis of Fe^{3+}- OH complexes (Faust and Hoigné, 1990), according to eq. (1.7):

$$Fe(OH)^{2+} \xrightarrow{h\nu} Fe^{2+} + HO^{\bullet} \qquad (1.7)$$

as the quantum yield of $Fe(OH)^{2+}$ is much higher than the other species. Besides, there are other reactions where $HO^{\bullet}$ radicals can also be formed and Fe^{2+} is involved (Feng and Nansheng, 2000)

$$Fe^{2+} + O_2 \rightarrow Fe^{3+} + O^{2-} \qquad (4.21)$$

$$2O^{2-} + 2H^{+} \rightarrow H_2O_2 + O_2 \qquad (4.22)$$

$$Fe^{2+} + H_2O_2 \rightarrow Fe^{3+} + HO^{\bullet} + OH^{-} \qquad (4.23)$$

Some interesting quantum yields for eq. 1.7 may be found in the bibliography. In this context, useful quantum yields for hydroxyl radical production at wavelengths 313 nm (ϕ = 0.14) and 365 nm (ϕ = 0.07) have been reported (Mazellier *et al.*, 1997). According to the reaction, hydroxyl radicals production will end when all the Fe^{3+}extinguishes, and in consequence, the simultaneous reoxidation of the Fe^{2+} formed in the reaction into Fe^{3+} by an oxidant (i.e., oxygen better than hydrogen peroxide) confers an interesting catalytic aspect to the process. A model to describe the reaction involved is shown in Fig. 4.2. (Catastini *et al.*, 2002).

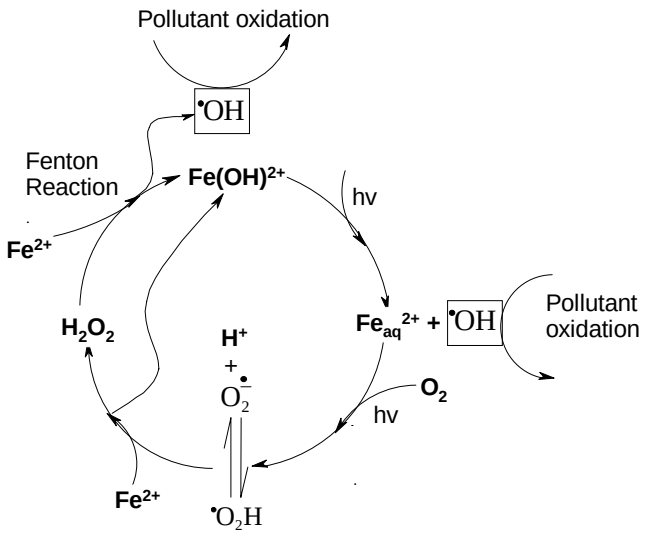

Figure 4.2. Model of iron photoassisted system

The case of using H_2O_2 as oxidant constitutes the typical Fenton process. The disappearance extension may be enlarged because iron ions may give complexes with the photodegradation compounds formed, which can be able to be degraded by the UV radiation. The use of Fe^{3+} in presence of light represents an economical alternative in comparison with the photo-Fenton process, which needs the use of H_2O_2.

4.3. Solar radiation as source of light

Solar radiation and in particular its ultraviolet component**,** is considered of interest being the existence of ultraviolet radiation the key of some heterogeneous and homogeneous photocatalytic processes, such as TiO_2/UV and H_2O_2/Fe^{2+}/UV-vis or H_2O_2/Fe^{3+}/UV-vis system (photo-Fenton). The use of solar light as source of radiation in the photo-Fenton and Fe^{3+}/UV-vis system has been studied, taking as reference the recent development of solar technology in water detoxification by means of heterogeneous photocalysis (TiO_2/UV) (Bahnemann *et al.*, 1994; Malato, 1999; Blanco and Malato, 2001). In this sense, this section describes the power of sunlight as source of energy, as well as the basic factors related to the photocatalytic technology and its application. In addition, it outlines the basic principles related to the solar spectrum and especially to the

solar UV radiation since this part of the solar spectrum is the most important one for driving chemical processes and the main features of the collectors used for wastewater detoxification.

All the energy coming from that huge reactor, the Sun, from which the earth receives $1.7x10^{14}$kW, means $1.5x10^{18}$ kWh per year, approximately 28000 times the consumption of all the world in that period (Malato, 1999).

The radiation in the exterior of the atmosphere has a wavelength between 0.2μm and 50μm, which is reduced in an interval between 0.3 μm and 3 μm when reaching the surface, due to the absorption of part of it by different atmospheric components (ozone, oxygen, carbon dioxide, aerosols, steam, clouds). The solar radiation that reaches the ground level without being absorbed or scattered, is called direct radiation; the radiation, which has been dispersed but reaches the ground level is called diffuse radiation and the addition of both is called global radiation (see Fig.4.3). In general, the direct component of global radiation in cloudy days is minimum and the diffuse component is maximum, producing the opposite situation in clear days.

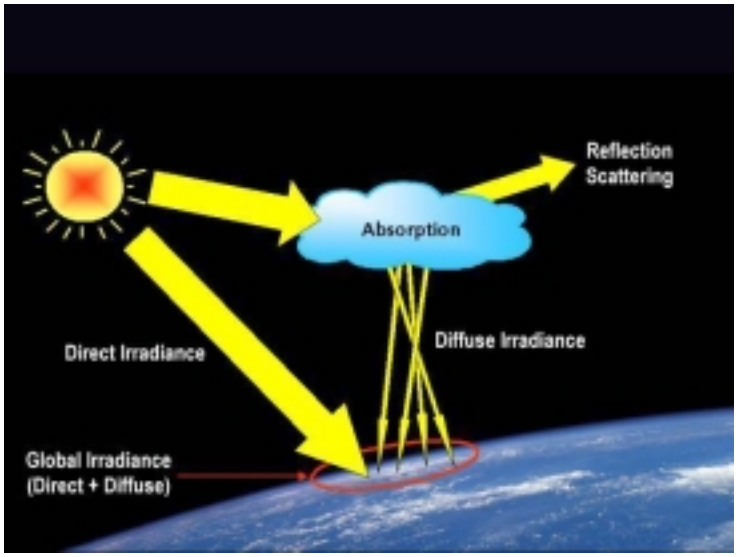

Figure 4.3. Direct and diffuse radiation

Fig. 4.34 shows the standard spectrum (ASTM, 1987a) of the direct solar radiation on the ground level on a clear day, reflecting the substances, which absorb part of the radiation and their absorption wavelength (Iqbal, 1983). The dotted line corresponds to the

extraterrestrial radiation in the same interval of wavelength. It is clearly seen the scarce part of the solar spectrum that can be used in the photochemical process under study but, as the energy source is so cheap and abundant, even under these limitations it is interesting to use it (Wilkins and Blake, 1994).

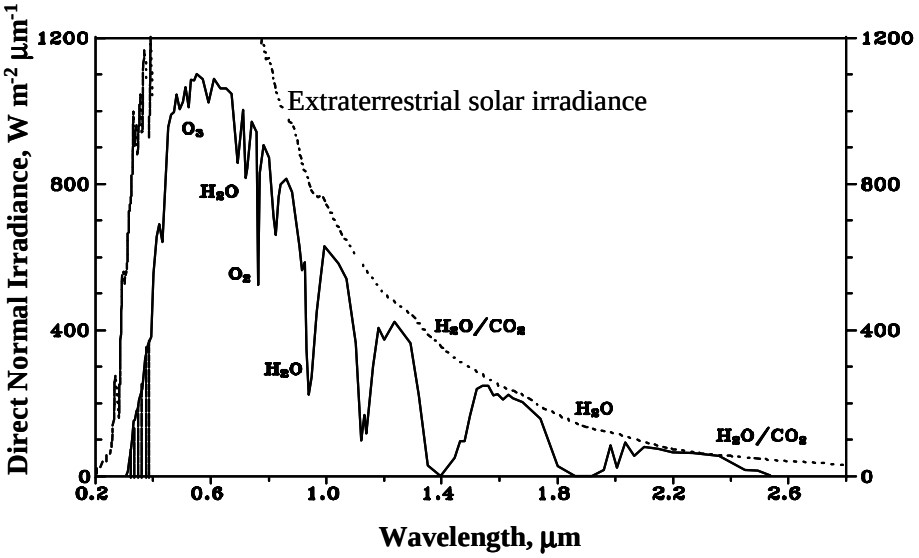

Figure 4.4. Effect of atmospheric components on solar spectrum

UV radiation is, as explained above, a very small part of the solar spectrum. The measurements carried out have demonstrated that the UV part of the solar spectrum represents between 3.5% and 8% of the total (Hulstrom *et al.*, 1985), although this relation can change for a determined location between cloudy and clear days. The percentage of global UV radiation (direct + diffuse), with regard to the global, generally increases when the atmospheric transmitivity decreases, due mainly to clouds, but also to aerosols and dust (Mehos and Turchi, 1992). In fact, the average percentage of UV with respect to total radiation on cloudy days is up to two percent points higher than values on clear days.

The two spectra shown in Fig. 4.5 correspond to the standard (ASTM, 1987b) for the UV range of the solar spectrum. The smallest of them refers to direct UV (radiation without scattering) and its value reaches 22 W m^{-2} between 300 and 400 nm, the biggest corresponds to the global UV (direct + diffuse) and its value is 46 W m^{-2}. These two values give an idea of the energy coming from the sun that is available for the photochemical

reactions that use UV-vis solar radiation just up to 520 nm. In any case, the UV radiation values vary from one location to another, and obviously, at different hours of the day and in different seasons, making necessary to know these data for any particular location in real time.

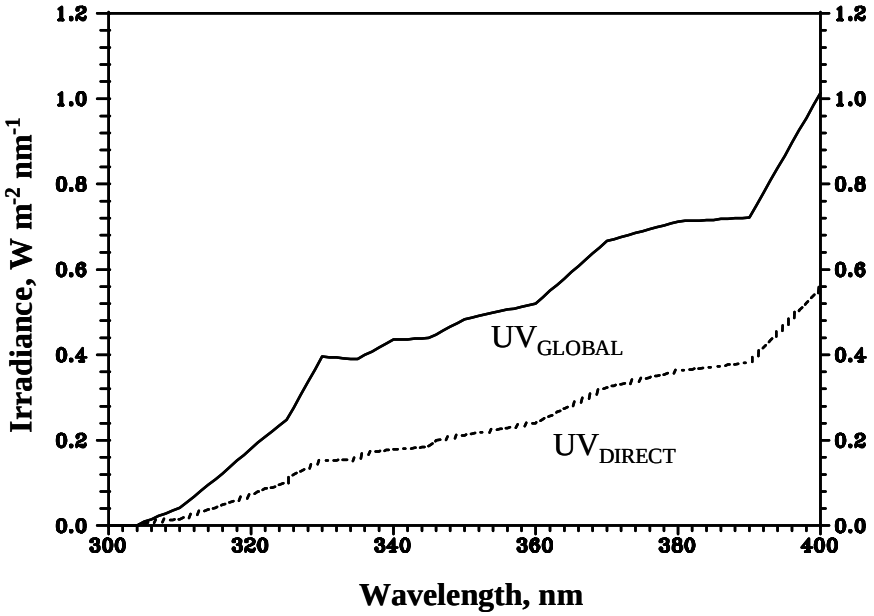

Figure 4.5. Ultraviolet spectrum on the earth surface (standard ASTM)

4.3.1. Solar collectors

Traditionally, the different solar collector systems have been classified depending on the concentration level attained with them (relationship between the collecting surface and the surface where the final result is produced), which is directly related with the system working temperature. According to this criteria, there are three type of collectors:

I. No concentration or low temperature, up to 150º C
II. Medium concentration or medium temperature, from 150º C to 400º C
III. High concentration and high temperature, over 400º C.

This classification is performed from a traditional point of view, considering only the thermal efficiency of the solar collectors. However, what is important in photocatalysis is not only the amount of radiation collected, but its wavelength.

Non-concentrating solar collectors (Fig. 4.6) are static, without any solar tracking device. They are usually a flat plate, in many cases aiming to the sun with a determined tilt, depending on the geographic situation. Their main advantage is the reduced cost and, for many applications, the collected radiation is sufficient.

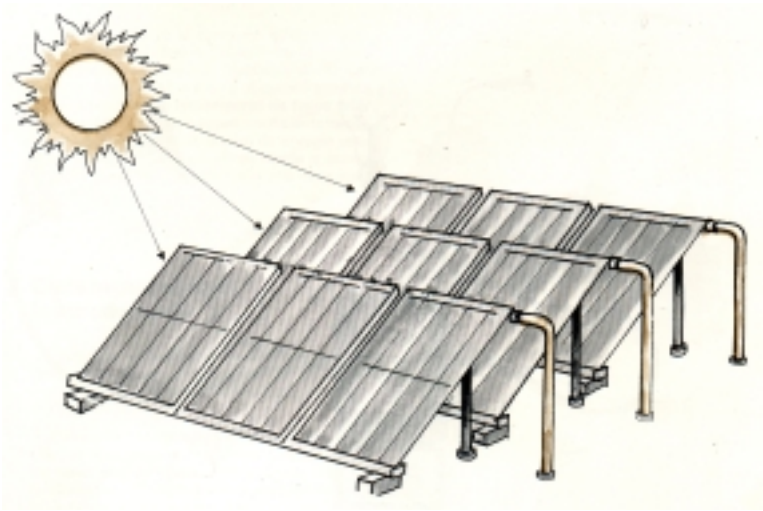

Figure 4.6. Non-concentrating solar collectors for domestic heat water application.

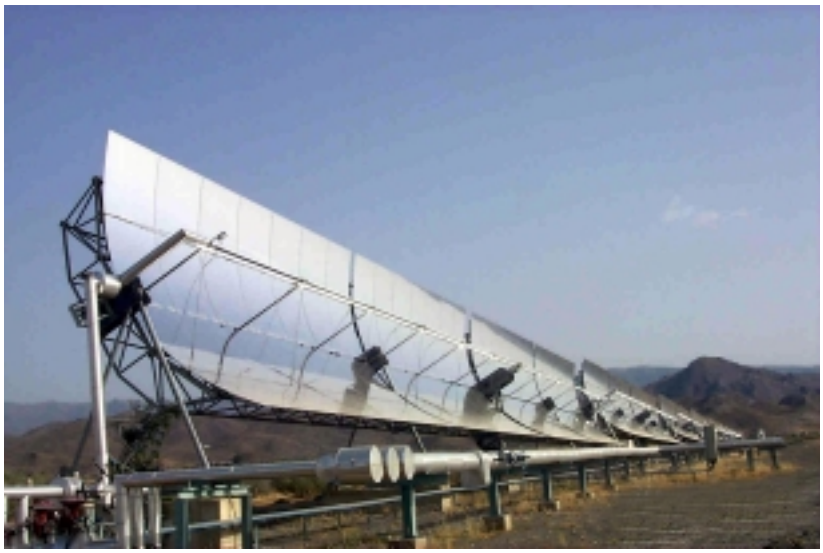

Figure. 4.7. Medium-concentring solar collectors. PTC type (PSA, Spain)

Medium concentration solar collectors concentrate the sunlight between 5 and 50 times. Parabolic Trough Collectors (PTC) and collectors with Fresnel lenses are within this group. The first ones have a parabolic reflecting surface (Fig. 4.7), which concentrates the radiation on a tubular receiver located in the focus of the parabola. They can be of one axis tracking, either azimuth (East-West movement around one axis North-South oriented) or elevation (North-South movement around one axis East-West oriented), or two tracking axis (azimuth + elevation) as the Helioman collector shown in the next section.

High concentration collectors have a focal point instead of a linear one and are based on a paraboloid with solar tracking. Parabolic dishes and solar furnaces are among them (Fig. 4.8). Typical concentration ratios are in the range of 100 to 10000 requiring optimal precision elements.

The specific hardward needed for solar photocatalitic applications has a lot in common with those used for thermal applications. As a result, photocatalytic system and reactors have followed conventional solar thermal collector designs, such as parabolic troughs and non-concentrating collectors (Turchi and Ollis, 1990; Anderson *et al.*, 1991; Minero *et al.*, 1993).

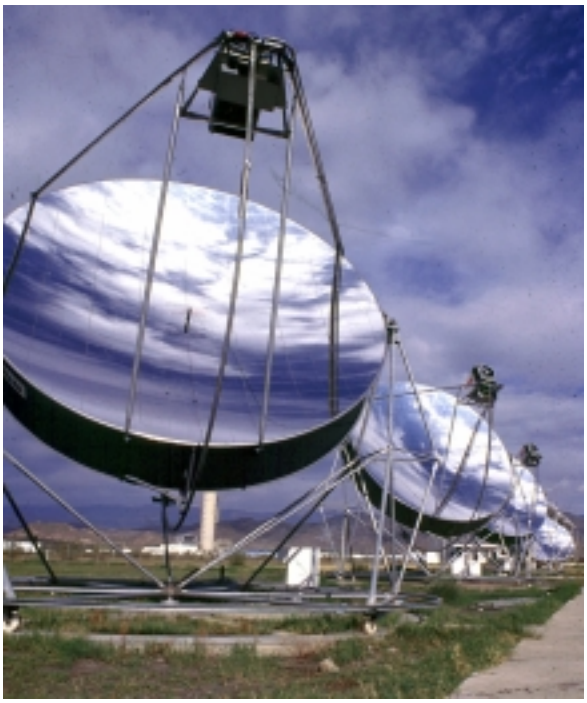

Figure 4.8. High concentrating solar collector. Parabolic dish solar collector (PSA, Spain)

The first engineering-scale outdoor reactor for solar detoxification was developed by Sandia National Laboratory (USA) at the end of the eighties. A parabolic-trough solar thermal collector was simply modified by replacing the absorber/glazing-tube combination with a Pyrex tube through which contaminated water could flow. Since then, many different concepts with a wide variety of designs have been proposed and develop all over the world, in a continuous effort to improve performance and to reduce the cost of solar detoxification system (Malato *et al.*, 2002).

One of the most important reactor-design issues is the decision between concentrating or non-concentrating collector systems. Concentrating systems present the advantage of much smaller reactor-tube area, which could mean a shorter circuit in which to confine, control and handle the contaminate water to be treated. If concentrating collector system has to be used, an improving alternative, from both economical and engineering points of view, would be the use of high-quality ultraviolet-light-trasmitting reactors.

4.3.1.1. Parabolic Trough Collectors

The first engineering-scale solar photochemical facility for water detoxification was developed in 1989 by Sandia National Laboratories (USA) using one-axis PTC. The second one was developed by Plataforma Solar de Almería (PSA), Spain in 1992 using two-axis PTC (see Fig.4.9) Both facilities are considerably large pilot plants (hundreds of square meters of collecting surface) and can be considered the first step toward the industrialization of photochemical processes.

One-axis tracking PTC has been demonstrated to be the most economically advantageous for solar thermal applications. However, two-axis tracking PTC are the better suited for photocatalysis research purpose, since they allow the exact calculation of the radiation hitting the photoreactor (Minero *et al*., 1996; Curco *et al*., 1996a; Malato, 1999). This feature permits comparison of experiments carried out in such large photoreactors with those performed at laboratory-scale, where the calculation of incident radiation is simple (Gimenez *et al.*, 1996; Curco *et al.*, 1996b). Nevertheless, concentrating reactors have two important disadvantages compared to non-concentrating ones. The first one is that they cannot concentrate (i.e use) diffuse solar radiation. This fact is irrelevant for solar thermal applications because diffuse radiation is just a small fraction of the total

solar radiation. However, this disadvantage becomes important in solar TiO_2-photocatalytic and photo-Fenton detoxification as it uses only the UV fraction of the solar spectrum from which as much as 50 percent can be diffuse, since it is not absorbed by water vapor (Romero *et al.*, 1999). This percentage can be even higher in very humid location or during cloudy or partly cloudy periods. In this sense, efficiency of non-concentrating solar collectors can be noticeably higher, as they can take advantage of both direct and diffuse UV radiation. The second disadvantage of concentrating collectors is their complexity, cost and maintenance requirements. As a consequence of these disadvantage, the present state-of-the art favors the use of non-concentrating reactors for solar photocatalytic applications.

Figure 4.9. Two-axis tracking Parabolic Trough Collector (PTC)

4.3.1.2. Compound Parabolic Collectors (CPC_s)

Compound parabolic collectors are a very interesting cross between through concentrators and one-sun system and are one of the best options for solar phototocatalytic applications. These collectors have been found to provide the best optics for low-concentrating system. CPCs are static collectors with a reflective surface describing an

involute around a cylindrical reactor tube; it can be designed with a CR=1 (or near one), thus having the advantages of both PTCs and one-sun collectors (Curco *et al.*, 1996a; Gimenez *et al.*, 1999).

Thanks to the reflector design, almost all the UV radiation arriving at the CPC aperture area (not only direct, but also diffuse) can be collected being available for the process in the reactor. The UV light reflected by the CPC is distributed around the back of the tubular photreactor and as a result most of the reactor tube circumference is illuminated. However, due to the ratio of CPC aperture to tube diameter, no single point on the tube receives more than one sun of UV light. The incident light is then very similar to that of a one-sun photoreactor and, as in the case of flat-plate collectors, maximum annual efficiency is obtained at the same collector angle inclination as the local latitude (Blanco *et al.*, 2000). Performance is very close to that of the simple tubular photoreactor, but only about 1/3 of the reactor tube material is required. As in a parabolic through, the water is more easily piped and distributed than in many one-sun designs. All these factors contribute to excellent CPC-collector performance in solar photocatalytic applications (Malato *et al.*, 1997; Blanco *et al.*, 1999; Ajona and Vidal, 2000; Malato *et al.*, 2000a, 2000b).

Figure 4.10. Detail of a collector CPC where the configuration of the tubes reactors is observed

Compound parabolic concentrator reflectors are usually made of polished aluminium and the structure can be a simple photoreactor support frame with connecting tubing (Figure 4.10). Since this type of reflector is considerably less expensive than tubing, their use is more cost-effective compared to deploying non-concentrating tubular photoreactors that do not use reflectors. The advantages of using tubing for the active photoreactors area is still preserved in CPCs.

4.4. Experimental

4.4.1. Reagents

In Table 4.1 all chemicals that were used in the experimentation are shown. All were used as received.

Table 4.1. List of chemicals used

Compound	*Formula*	*Vendor*	*Purity*
Acetronitrile	C_2H_3N	Merck	99.8%
Ferric chloride	$FeCl_3$	Probus	98%
Hydrogen peroxide	H_2O_2	Merck	30 wt.%
Iron sulphate heptahydrate	$FeSO_4 \cdot 7H_2O$	Panreac	98%
Nitrobenzene	$C_3H_5NO_2$	Probus	99%
Nitrogen	N_2	AlphaGas	99.99%
Oxygen	O_2	AlphaGas	99.99%
Phenol	C_6H_6O	Merck	99%
Sodium hydrogen sulphite	$Na_2S_2O_3$	Panreac	40 w/v %
Zinc iodide	Zn I_2	Merck	99.8%

Millipore water (18μS cm^{-1}) was used in the cases of reactor B, C, D and E. In the case of reactor F, water coming from the municipal aqueduct (Lausanne, Switzerland) and in reactor G distilled water from the PSA desalination plant (evaporation by multi-effect system using solar energy, conductivity < 10 μS.cm^{-1}, organic carbon < 0.5 mg.L^{-1}).

4.4.2. Experimental device and procedure

Experiments using artificial and natural sunlight radiation were carried out in six different devices. The first group of three photo-reactors that use artificial light is formed by a tubular photo-reactor (reactor B), an annular reactor (reactor C), and solarbox with a tubular reactor inside (reactor D). The second one, three devices using solar radiation: a photo-reactor mounted in the axis of a parabolic collector (reactor E), and two photo-reactors mounted in the axis of CPC collectors at a pilot scale (reactors F and G). The systems were operated in batch mode, and the aqueous solutions of phenol and NB were continuously re-circulated through the reactors. The photo-reactors were always charged

with aqueous solution of phenol or NB and sulfuric acid was added for adjustment of the pH to the range between 2.7 and 3.0. With regard to photo-Fenton experiments, the beginning of the experiment corresponded to the addition of hydrogen peroxide and simultaneously start of irradiation. In the case of H_2O_2/UV and Fe^{3+}/UV, the beginning of the experiments corresponded to the start of irradiation. At various intervals, samples of the reaction solution were withdrawn from the reactor during the mineralization experiments. The samples were tested for H_2O_2 consumption and were used for TOC and HPLC analysis after being quenched with sodium hydrogen sulphite solution, in order to avoid further reactions.

4.4.2.1. Tubular Reactor (reactor B)

Experiments for the three treatment processes under study (see Table 4.2) were conducted in a recirculating tubular photo-reactor, which is shown in Fig. 4.11 and Fig. 4.12. The photo-reactor capacity is 5 L. It is equipped with four "germicides" low-pressure mercury lamps, placed parallel to its axis. These lamps emit radiation basically at 253.7 nm and they are cooled by air. The nominal power is 15 W each one. The reaction zone consists of a cylindrical quartz tube, 100 cm in longitude, with an exterior diameter of 2.2 cm and an interior diameter 1.85 cm. The reaction volume is 269 cm^3. It is mounted within a quartz tube with a longitude of 48 cm, exterior diameter of 5.4 cm and interior diameter of 5.0 cm. Air circulates in the tubular space between the two tubes. The exit zone was designed to maintain a constant level by means of a spillway. Before coming out experiments, actinometry experiments based on the photochemical decomposition of oxalic acid in the presence of uranyl ion (Volman and Seed, 1964; Heidt *et al.*, 1979) were performed to determine the flux of radiation entering the reactor. It was found that the flux of radiation entering the reactor was 24.99 $\mu Einstein.s^{-1}$ at 253.7 nm (see Appendix). Because NB is highly absorbent at 253.7 nm (see Fig. 4.46), the 253.7 nm photon flow absorbed per unit of reaction volume (sometimes defined as volumetric intensity) is 92.55 $\mu Einstein.s^{-1}L^{-1}$. Phenol is less absorbent than NB, but at 253.7 nm it absorbs lightly (see Fig. 4.35). Therefore, the photon flow absorbed per unit of reaction volume at 253.7 in the case of phenol is 69.70 $\mu Einstein.s^{-1}L^{-1}$.

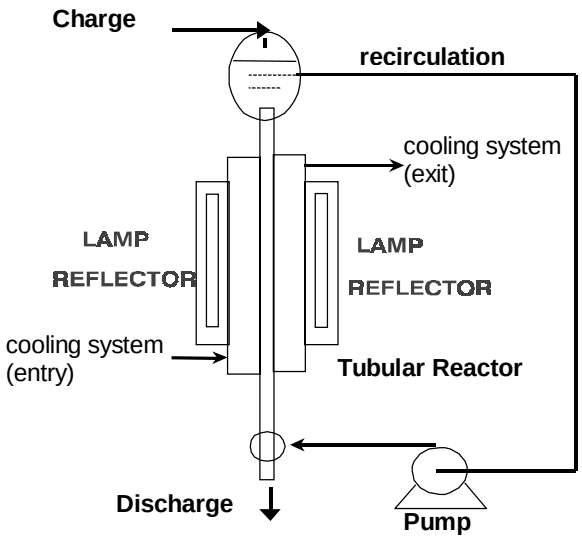

Figure 4.11. Installation scheme of Reactor B

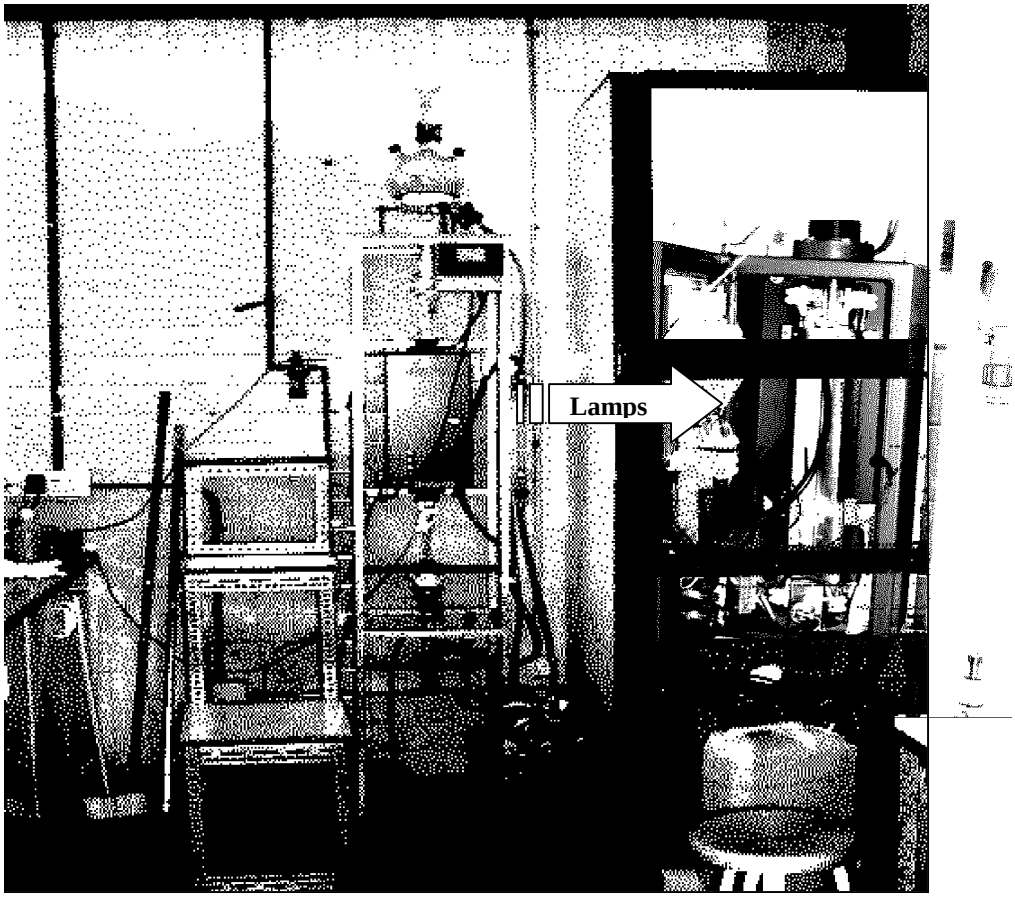

Figure 4.12. Reactor B

The reactor was always charged with 2.5 L of an aqueous NB or phenol solution. All the experiments were carried out in a batch operation at room temperature, with a recirculation flow rate of 100 $L.h^{-1}$.

4.4.2.2. Annular Reactor (reactor C)

A number of experiments were conducted in a jacketed thermostated 1.5 L glass photoreactor (see Fig. 4.13 and Fig. 4.14). It is equipped with a 4-W black (ARC-P04/23 04W, F4T5BLB Layrton) lamp, placed inside of the reactor. This lamp emits radiation between 300-400 nm. Magnetic stirring was used to keep the solution homogeneously. The temperature of the reactor was controlled by circulating water from an external thermostatic bath (Haake C-40). All experiments were carried out at 25^{o}C. Actinometric experiments based on the photochemical decomposition of oxalic acid in the presence of uranyl ion were also performed. It was found that the flux of radiation entering the reactor was 0.83 μEinstein.s^{-1} at 360 nm (see Appendix). The photon flow absorbed per unit of reaction volume at 360 nm are 0.37 μEinstein.s^{-1} L^{-1} and 0.11 μEinstein.$s^{-1}L^{-1}$ for NB and phenol, respectively.

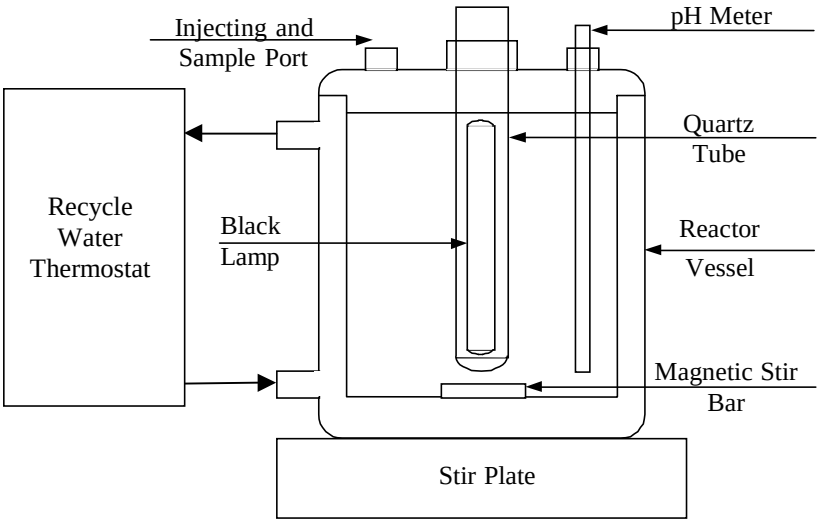

Figure 4.13. Installation scheme of Reactor C

Figure 4.14. Reactor C

4.4.2.3. Solarbox (reactor D)

A number of experiments were also carried out in a quartz tubular reactor inside of a solarbox (see Fig. 4.15 and Fig. 4.16). The solarbox is a commercial solar simulator from COFOMEGRA (Milano, Italy). The assembly is quite simple. The inner surface of the solarbox is a parabolic reflector installed at the bottom and providing an effective reflecting surface of 0.054 m^2. This reflector concentrates the emitted radiation of the lamp within the focus. The focus is localized at the center of the tubular reactor, through which the solutions are led inside the solarbox. The quartz reactor is a cylinder providing a length of 26 cm with an inner diameter of 2.1 cm and outer diameter of 2.5 cm. The reactor volume is 90 cm^3. The source of radiation is a 1500-W Xenon lamp (Philips, XOP 15-OF, 290 nm < λ < 560 nm). The 1.5 L volume is treated at a recirculation flow rate of 100 $L.h^{-1}$. The reactor volume is 90 cm^3 and the reactor temperature was controlled by circulating water from a thermostatic bath (Haake C-40).

The photon flow entering the reactor and absorbed by the reaction medium within the wavelength range 300 nm < λ < 400 has been calculated using a Microsoft Excel spreadsheet and its value was 2.17×10^{-6} Einstein s^{-1} (see details in Appendix).

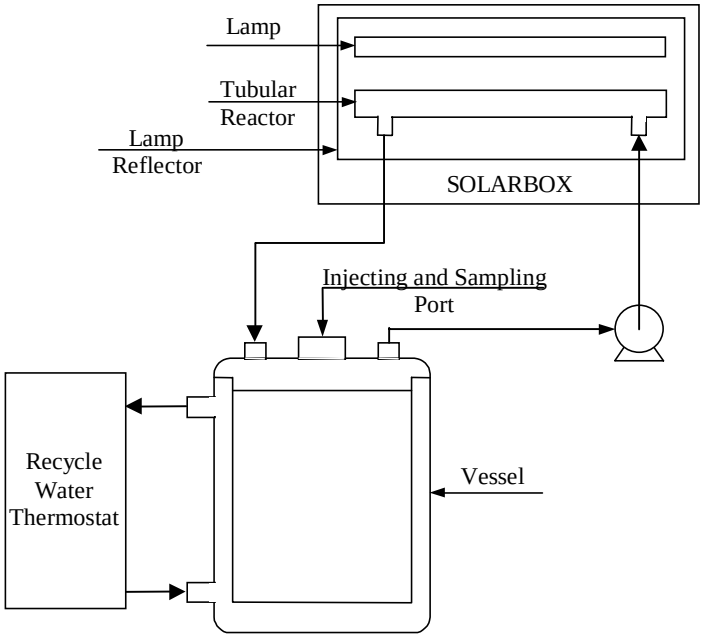

Figure 4.15. Installation scheme of Reactor D

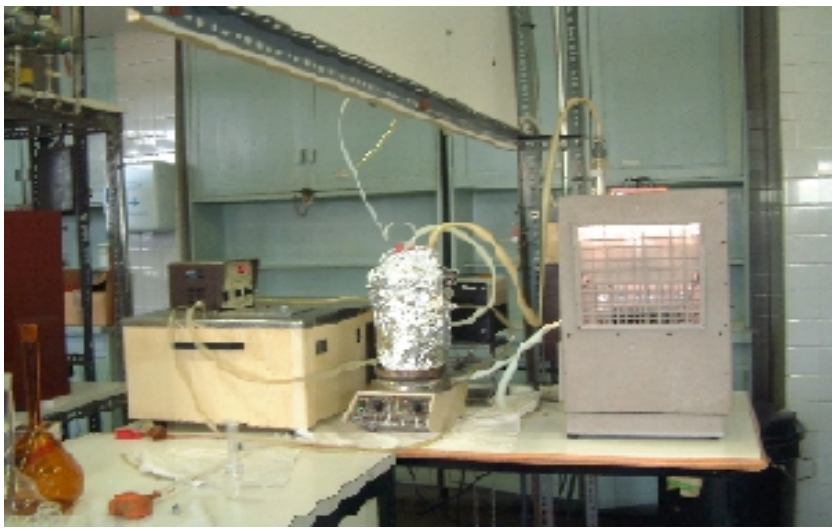

Figure 4.16. Reactor D

4.4.2.4. Parabolic collector (reactor E)

This prototype was designed based on a parabolic concentrator (PTC) photoreactor. This kind of medium-concentrating solar collector concentrates sunlight between 5 and 50 times, and usually requires continuous tracking of the sun's movement (Blanco and Malato, 1992). In our case, this was done manually. The solution goes through a tubular reactor placed in the focus of a parabolic reflector. The cylindrical reactor strongly resembles the reactor used in the Solarbox (see Fig. 4.17).

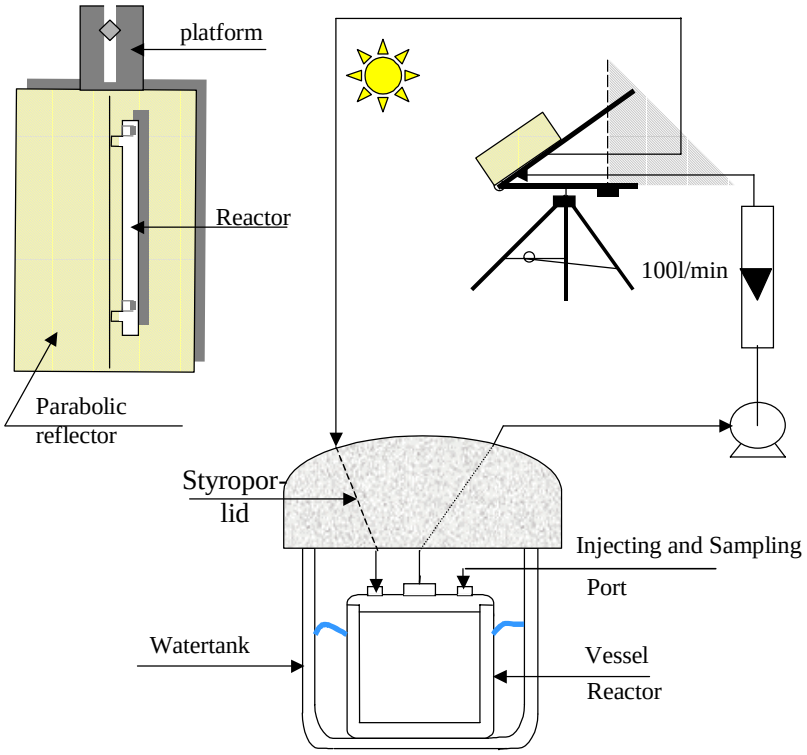

Figure 4.17. Installation scheme of Reactor E

It also has a length of 26 cm and a diameter of 2.1 cm. The dimensions of the reflector are 32 cm x 54.5 cm (0.174 m^2), whereby, for design reasons, only half of the surface (0.087 m^2) can be considered reflecting in so far as surface supplying the process with photons. Again, the treated volume is 1.5 L at a recirculation flow rate of 100 $L.h^{-1}$ and reactor volume is 90 cm^3 (Fig.4.17).

As with the Solarbox, a perfect parabolic form of the reflector surface was assumed. Therefore, the same assumptions can be made: rays enter into the tube and are

concentrated onto the focus. In all experiments performed in this reactor, the incident radiation was not quantified.

4.4.2.5. CPC 1 (reactor F)

A Compound Parabolic Collector (CPC) installed at the Swiss Federal Institute of Technology (EPFL) in Lausanne-Switzerland was used in order to test the technical feasibility of this technology in the treatment of organic compound at field pilot scale (Fig. 4.18). The configuration of CPC is the same one that of the reactor constructed at the Plataforma Solar de Almería (PSA) (Malato *et al.*, 2001). The CPC has 3 modules (collector surface, 3.08 m^2, photoreactor volume 22 L and total reactor volume 100 L) whereas one module consists of 8 tubes (1.03 m^2 each) connected in series and mounted on a fixed platform 40^o tilted (local latitude). The three modules are connected in series with water directly flowing through them at 20 L min^{-1}, leading finally to a recirculation tank. A centrifugal pump then returns water to the collectors. At the beginning of the experiments, with collectors covered, all the chemicals are added to the tank and mixed until homogenization. The cover is then removed and samples are collected at predetermined times.

Figure 4.18. Reactor F

The incident solar radiation was measured by means of a global UV radiometer (KIPP & ZONEN, model CUV3), mounted on a platform tilted 40^{o} (same angle as the CPC). The evaluation of this parameter is widely described in section 4.4.3.6.

4.4.2.6. CPC 2 (reactor G)

A Compound Parabolic Collector (CPC) installed at the Plataforma Solar de Almería (PSA) has been also used (Fig. 4.19 and Fig. 4.20). The current CPC field configuration consists of 4 modules (collector surface 5.93 m^2, photoreactor volume 72 L, photoreactor inner diameter 48 mm, total plant volume 190 L) connected in series and mounted on a fixed platform inclined 37^{o} (local latitude). The 4 modules are connected in series as well with water directly flowing through them, leading finally to a recirculating tank. A centrifugal pump then returns the water to the collectors. The water flows (3.7 m^3.h^{-1}) directly from one module to the other and finally to a reservoir tank (52 L).

Figure 4.19. Reactor G

The piping and valves (87 L) between the reactor and the tank are black HDPE (High Density Polyethylene), material chosen because it is strongly resistant to chemicals,

weather-proof and opaque, in order to avoid any photochemical effect outside of the collectors. In the same way that in the CPC located in Lausanne, at the beginning of the experiments, with collectors covered, all the chemicals were added to the tank and mixed until homogenization. The cover is then removed and samples are collected at the predetermined times. This plant has been operating since 1994. The schematic configuration of the system is shown in Fig. 4.20.

The incident solar radiation was also measured by means of a global UV radiometer (KIPP & ZONEN, model CUV3), mounted on a platform tilted 37^{o} (same angle as the CPC).

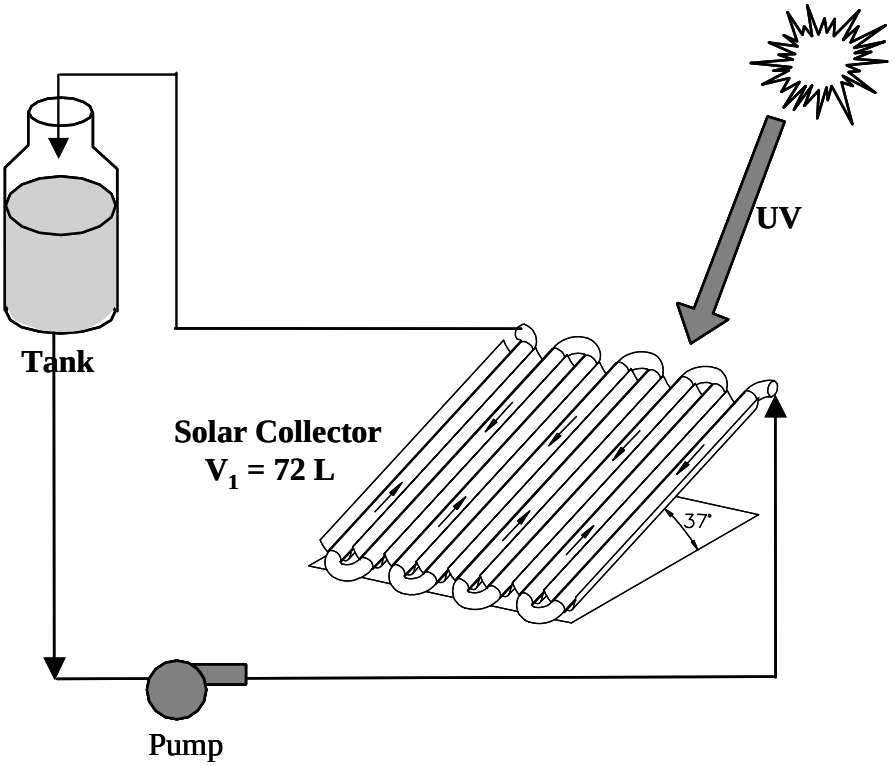

Figure 4.20. Installation scheme of Reactor G

4.4.3. Analytical determinations

4.4.3.1. Actinometry

This is a common method to determine the intensity of a radiation source. In the present case, the actinometric system used is the photochemical decomposition of oxalic acid in presence of uranyl nitrate (Volman and Seed, 1964; Heidt *et al*., 1979; Vicente and Esplugas, 1983). The decomposition reaction of oxalic acid, in a pH range of between 3 and 7, and a conversion of oxalic acid lower than 20% is the following:

$$(UO_2)^{2+} + H_2O_2 \xrightarrow{hv} (UO_2)^{2+} + CO_2 + CO + H_2O \qquad (4.24)$$

By the knowledge of the actinometer and the lamp characteristics, the radiation intensity can be calculated. This method will be deeper presented in appendix.

4.4.3.2. Total Organic Carbon (TOC)

To determine the quantity of organically bound carbon, the organic molecules must be broken down to single carbon units and converted to a single molecular form that can be measured quantitatively. TOC methods utilize heat and oxygen, ultraviolet irradiation, chemical oxidants, or combinations of these oxidants to convert organic carbon to carbon dioxide (CO_2).

In the present work, TOC has been determined by the combustion method and analyzing the resultant CO_2 with a Dohrmann DC-190 TOC analyzer for experiments carried out in Barcelona University and a Shimadzu-5050A TOC analyzer for experiments carried out in the EPFL and the PSA. Both instruments were equipped with an automatic sample injector and they were calibrated with standard solutions (100 $mgC.L^{-1}$ of potassium hydrogen phthalate). Samples were acidified at pH lower than 3 and aerated with oxygen to keep the solution free of atmospheric CO_2.

4.4.3.3. HPLC

In some experiments carried out at laboratory scale in University of Barcelona , phenol and NB concentration was followed by means of HPLC, already described in chapter 3.

4.4.3.4. Hydrogen peroxide

Concentrations of H_2O_2 were determined and monitored by Merk Merkoquant, Quantofix (Macherey-Nagel) peroxide analytical test strip and by iodimetric titration in the case of the experiments performed in Almería according to the following procedure:
Prepare a starch solution by heating a few spatulas in a 250 mL Erlenmeyer flask. Put "x" mL of sample (e.g. 25 mL) + 25 mL 0.2N KI + 20 mL 2N H_2SO_4 in a closed bottle. Add a few drops of stark solution as an indicator. After 30 min titrated with 0.1N $Na_2S_2O_3$ (24.82 g/L) $\Rightarrow$ where "y" is the volume of consumed $Na_2S_2O_3$. Concentration of hydrogen peroxide would be calculated as follows:

$$H_2O_2\ [mg/L] = 1700 * y/x$$

$$H_2O_2\ [mol/L] = 1/20 * y/x$$

Remarks

The solution is pitch dark in most cases. Add the starch solution after the solution has become noticeably brighter. After the addition the solution becomes blue black again and is titrated till there is no color. If the flask stands for a while after the end point, the solution will again darken since the iodide is reoxidized by air/oxygen.

Modifications and control checks of the initial method

Zinc iodide-starch solution ready for use has been utilized as indicator. 10 drops have been added to the sample. The 30-minutes analysis has been performed in a closed bottle and in the dark. 25 mL of sample have been always used. The sample has proceeded from phenol photo-Fenton experiments diluted 1/100 or 1/25 as function of the hydrogen peroxide concentration used in the experiment (20g.L^{-1} or 5 g.L^{-1}). Few mL of 0.1N $Na_2S_2O_3$ are spent if this dilution is applied. This dilution factor has been applied to the previous calculations.

In presence of Fe

The presence of iron could affect the determination of hydrogen peroxide. Different tests were made with higher Fe concentration than the usual in the photo-Fenton experiments (5 mmol.L^{-1} or 1 mmol.L^{-1} diluted 1/100 or 1/25, as function of the hydrogen peroxide concentration).

4.4.3.5. pH measurement

The pH measurements were carried out with a Crison GLP-22 pH-meter, calibrated with two buffer solutions of pH 4 and 7. In all these experiments the analysis was not performed on line, but after each sample withdrawal.

4.4.3.6. Evaluation of solar radiation

Solar radiation is an essential parameter for the correct evaluation of data obtained from experiments in a solar water decontamination pilot plant. A global UV radiometer (KIPP & ZONEN, model CUV3), mounted on a platform tilted 40^o (same angle as the CPC reactor located in Laussane, Switzerland) and 37^o (same angle as the CPC reactor located in Almería, Spain). The sensors provide data in terms of global and direct UV solar energy power incident per unit area, $W_{UV}.m^{-2}$ ($UV_{G-D,n}$) respectively. Solar-UV power varies during experiments, especially when clouds are passing by. This gives an estimation of the energy reaching any surface in the same position with regards to the sun. It may be assumed that the average solar UV (300-400 nm) on a perfectly sunny day in June for 2 hours around noon is about 45 $W_{UV}.m^{-2}$.

With eq. 4.25, combination of data from several days experiments and their comparison with other photocatalytic experiments are possible:

$$Q_{UV,n} = Q_{UV,n-1} + \Delta t_n \ \overline{UV}_{G,n} \frac{A_{CPC}}{V_{TOT}} \qquad (4.25)$$

where t_n is the experimental time for each sample (min). $UV_{G,n}$ is the average UV during Δt_n, A_{CPC} is the collector surface, V_{TOT} is the total plant volume and $Q_{UV,n}$ is the accumulated energy (per unit of volume, $kJ.L^{-1}$) incident on the reactor for each sample taken during the experiment. For the CPC reactor located in Lausanne, $A_{CPC} = 3.08\ m^2$ and $V_{TOT} = 100$ L. In the cases of CPC reactor located in the PSA, $A_{CPC} = 5.93\ m^2$ and $V_{TOT} = 190$ L.

Consequently, when $Q_{UV,n}$ is used, the reaction rate could be expressed in terms of mg per kJ of UV incident on the illuminated photoreactor surface.

4.5. Range of experimental variables for phenol and NB experiments

Several series of the experiments of phenol and NB mineralization by photo-Fenton, H_2O_2/UV-vis and Fe^{3+}/UV-vis were carried out using different sources of artificial and solar light. All experimental conditions are summarized in Tables 4.2, 4.3, 4.4, 4.5 and 4.6. Two initial concentration of phenol and NB were tested, 1.14 and 5.68 mmol.L^{-1}. The effect of Fe^{2+}, Fe^{3+} and H_2O_2 concentration was studied. The concentration ranges were chosen addressing to reach the highest mineralization percentage. In this sense, Fe^{2+} and Fe^{3+} concentration ranged between 0.054 and 2.15 mmol.L^{-1} and for H_2O_2 concentration, between 5.33 and 106.7 mmol.L^{-1}. Otherwise, the effect of oxygen on the mineralization rate of phenol was studied using for these experiments only the reactor B. The chosen environmental conditions for the realization of the experiments in reactor E were only sunny days. In tables 4.3 and 4.6 the specific date and time of the day when each experiment was made is shown. In table 4.4, the experimental conditions for the experiments carried out in the CPC collector reactors are shown. CPC reactors were used only for experiments with phenol as model compound. The working temperature in the case of photo-reactors that use artificial light was around 25^oC and in some cases it was controlled by means of a thermostated bath. In the case of photo-reactors with solar radiation the temperature was not controlled and a variation between 25 and 35^oC was observed. Regarding photo-Fenton and iron photo-assisted system (Fe^{3+}/UV-vis), pH was always adjusted close to 3 by means of sulfuric acid. For H_2O_2/UV-vis process, the pH was not adjusted and the system evolved freely. Other specific experimental conditions are also described in the experimental section.

It is important to point out that due to the extension of the experimental part, the effect that all these parameters have on the selected processes were studied only with phenol. Some of them, considering that their effect could be similar, were not studied for NB.

Table 4.2. Experimental conditions of the runs for phenol experiments in photo-reactors with artificial light

Exp. N°	Reactor used	$[Phenol]_o$ ($mmol.L^{-1}$)	$[H_2O_2]_o$ ($mmol.L^{-1}$)	Fe^{2+} / Fe^{3+} ($mmol.L^{-1}$)	Process used
Ph1	Reactor B	1.14	5.33	0.054	DarkFenton+UV
Ph2	Reactor B	1.14	5.33	0.107	DarkFenton+UV
Ph3	Reactor B	1.14	5.33	1.07	DarkFenton+UV
Ph4	Reactor B	1.14	21.30	1.07	DarkFenton+UV
Ph5	Reactor B	1.14	21.30	1.07	$Fe^{2+}/H_2O_2/UV$
Ph6	Reactor B	1.14	21.30	0.00	H_2O_2/UV
Ph7	Reactor B	1.14	0.00	1.07	Fe^{3+}/UV
Ph8	Reactor B	1.14	21.30	1.07	DarkFenton+UV
Ph9	Reactor B	1.14	21.30	1.07	$Fe^{3+}/H_2O_2/UV$
Ph10	Reactor B	1.14	21.30	0.00	H_2O_2/UV
Ph11	Reactor B	1.14	0.00	0.00	UV
Ph12	Reactor B	5.68	21.30	1.07	$Fe^{3+}/H_2O_2/UV$
Ph13	Reactor B	1.14	21.30	1.07	$Fe^{3+}/H_2O_2/UV+O_2$
Ph14	Reactor B	5.68	42.60	1.07	$Fe^{3+}/H_2O_2/UV$
Ph15	Reactor B	5.68	42.60	1.07	$Fe^{3+}/H_2O_2/UV+O_2$
Ph16	Reactor B	5.68	85.30	1.07	$Fe^{3+}/H_2O_2/UV$
Ph17	Reactor B	5.68	106.7	1.07	$Fe^{3+}/H_2O_2/UV$
Ph18	Reactor B	5.68	64.00	1.07	$Fe^{3+}/H_2O_2/UV$
Ph19	Reactor C	1.14	21.30	1.07	$Fe^{3+}/H_2O_2/UV$
Ph20	Reactor C	1.14	0.00	1.07	Fe^{3+}/UV
Ph21	Reactor C	1.14	21.30	0.00	H_2O_2/UV
Ph22	Reactor C	1.14	21.30	1.07	Fe^{3+}/H_2O_2
Ph23	Reactor D	1.14	0.00	0.00	UV
Ph24	Reactor D	1.14	21.30	1.07	$Fe^{3+}/H_2O_2/UV$
Ph25	Reactor D	1.14	0.00	1.07	Fe^{3+}/UV
Ph26	Reactor D	1.14	21.30	0.00	H_2O_2/UV
Ph27	Reactor D	1.14	32.00	1.07	$Fe^{3+}/H_2O_2/UV$
Ph28	Reactor D	1.14	21.30	1.07	$Fe^{2+}/H_2O_2/UV$

Table 4.3. Experimental conditions of the runs for Phenol experiments in Reactor E using solar radiation

Exp. N^{o}	Date of Exp.	Time of radiation (h)	$[H_2O_2]_o$ (mmol.L^{-1})	Fe^{2+} / Fe^{3+} (mmol.L^{-1})	Process used
Ph29	06/08/01	3:00-6:00	0.00	0.00	UV
Ph30	06/11/01	10:20-12:50	21.30	1.07	$Fe^{2+}/H_2O_2/UV$
Ph31	06/11/01	14:20-15:00	21.30	1.07	$Fe^{2+}/H_2O_2/UV$
Ph32	06/18/01	12:50-14:50	35.60	1.07	$Fe^{2+}/H_2O_2/UV$
Ph33	06/19/01	10:30-11:30	21.30	1.07	$Fe^{2+}/H_2O_2/UV$
Ph34	06/19/01	14:15-15:05	21.30	0.54	$Fe^{2+}/H_2O_2/UV$
Ph35	06/21/01	11:10-13:10	21.30	0.00	H_2O_2/UV
Ph36	06/25/01	12:18-15:48	21.30	0.00	H_2O_2/UV
Ph37	06/26/01	10:10-13:50	10.66	0.00	H_2O_2/UV
Ph38	06/26/01	15:35-18:35	0.00	1.07	Fe^{3+}/UV
Ph39	06/27/01	11:50-14:50	0.00	2.15	Fe^{3+}/UV
Ph40	06/27/01	15:48-16:48	10.66	1.07	$Fe^{2+}/H_2O_2/UV$
Ph41	06/28/01	12:08-13:08	21.30	1.07	$Fe^{3+}/H_2O_2/UV$
Ph42	06/28/01	14:02-15:02	21.30	0.54	$Fe^{3+}/H_2O_2/UV$
Ph43	06/28/01	14:45-17:45	0.00	2.15	Fe^{3+}/UV
Ph44	07/21/01	10:38-13:38	42.60	0.00	H_2O_2/UV
Ph45	07/21/01	14:09-14:49	21.30	0.54	$Fe^{2+}/H_2O_2/UV$
Ph46	07/21/01	15:28-16:28	21.30	0.54	$Fe^{3+}/H_2O_2/UV$
Ph47	07/22/01	12:00-13:00	42.60	1.07	$Fe^{3+}/H_2O_2/UV$
Ph48	07/22/01	13:36-14:36	10.66	1.07	$Fe^{3+}/H_2O_2/UV$
Ph49	07/22/01	15:10-16:10	21.30	2.15	$Fe^{3+}/H_2O_2/UV$

Table 4.4. Experimental conditions of the runs for Phenol experiments in Reactors F and G using solar radiation

Exp. N^0	Date of Exp.	Time of radiation (h)	$[H_2O_2]_0$ (mmol.L^{-1})	Fe^{2+} / Fe^{3+} (mmol.L^{-1})	Process used
Ph50	07/17/01	10:00-15:15	21.30	0.00	H_2O_2/UV
Ph51	07/21/01	10:45-16:45	21.30	0.00	H_2O_2/UV
Ph52	07/22/01	11:30-16:30	42.60	0.00	H_2O_2/UV
Ph53	07/23/01	11:15-16:15	0.00	1.07	Fe^{3+}/UV
Ph54	07/24/01	11:00-16:00	0.00	0.54	Fe^{3+}/UV
Ph55	07/25/01	11:15-16:15	0.00	0.54	Fe^{3+}/UV
Ph56	07/26/01	11:00-16:00	0.00	1.07	Fe^{3+}/UV
Ph57	07/30/01	11:15-13:45	21.30	0.54	Fe^{3+}/H_2O_2/UV
Ph58	07/31/01	11:00-14:00	42.60	0.54	Fe^{3+}/H_2O_2/UV
Ph59	08/01/01	10:00-11:30	21.30	1.07	Fe^{3+}/H_2O_2/UV
Ph60	08/03/01	11:00-13:00	21.30	1.07	Fe^{3+}/H_2O_2/UV
Ph61	08/05/01	11:00-13:00	21.30	0.54	Fe^{3+}/H_2O_2
Ph62	08/07/01	11:00-13:00	54.41	1.07	Fe^{3+}/H_2O_2/UV
Ph63	08/11/01	11:00-13:00	73.53	1.07	Fe^{3+}/H_2O_2/UV
Ph64	10/23/02	10:00-1:00	21.30	1.07	Fe^{3+}/H_2O_2/UV
Ph65	10/24/02	10:00-1:00	21.30	0.54	Fe^{3+}/H_2O_2/UV
Ph66	10/28/02	10:00-1:00	21.30	0.27	Fe^{3+}/H_2O_2/UV

Table 4.5. Experimental conditions of the runs for NB experiments in photo-reactors with artificial light

Exp. N^{o}	Reactor used	NB (mmol.L^{-1})	$[H_2O_2]_o$ (mmol.L^{-1})	Fe^{2+} / Fe^{3+} (mmol.L^{-1})	Process used
NB1	Reactor B	1.14	0.00	0.00	UV
NB2	Reactor B	1.14	0.00	1.07	Fe^{3+}/UV
NB3	Reactor B	1.14	21.30	0.00	H_2O_2/UV
NB4	Reactor B	1.14	21.30	1.07	Fe^{3+}/H_2O_2/UV
NB5	Reactor B	1.14	42.60	1.07	Fe^{3+}/H_2O_2/UV
NB6	Reactor B	1.14	42.60	1.067	Fe^{2+}/H_2O_2/UV
NB7	Reactor B	5.68	85.36	1.07	Fe^{3+}/H_2O_2/UV
NB8	Reactor B	5.68	85.36	1.07	Fe^{3+}/H_2O_2/UV+O_2
NB9	Reactor B	5.68	0.00	0.00	UV
NB10	Reactor B	5.68	85.36	0.00	H_2O_2/UV
NB11	Reactor B	5.68	0.00	1.07	Fe^{3+}/UV
NB12	Reactor D	1.14	0.00	0.00	UV
NB13	Reactor D	1.14	21.30	1.07	Fe^{3+}/H_2O_2/UV
NB14	Reactor D	1.14	0.00	1.07	Fe^{3+}/UV
NB15	Reactor D	1.14	21.30	0.00	H_2O_2/UV
NB16	Reactor D	1.14	21.30	1.07	Fe^{2+}/H_2O_2/UV

Table 4.6. Experimental conditions of the runs for NB experiments in Reactor E using solar radiation

Exp. N°	Date of Exp.	Time of radiation (h)	$[H_2O_2]_0$ (mmol.L^{-1})	Fe^{2+} / Fe^{3+} (mmol.L^{-1})	Process used
NB17	07/03/01	15:00-18:00	0.00	0.00	UV
NB18	07/04/01	13:00-15:00	21.30	1.07	$Fe^{2+}/H_2O_2/UV$
NB19	07/05/01	10:00-11:00	10.60	1.07	$Fe^{2+}/H_2O_2/UV$
NB20	07/05/01	12:00-13:00	21.30	1.07	$Fe^{2+}/H_2O_2/UV$
NB21	07/05/01	14:00-15:00	42.60	1.07	$Fe^{2+}/H_2O_2/UV$
NB22	07/10/01	13:00-15:00	0.00	1.07	Fe^{2+}/UV
NB23	07/10/01	16:00-8:00	0.00	1.07	Fe^{3+}/UV
NB24	07/11/01	11:00-14:00	10.60	0.00	H_2O_2/UV
NB25	07/17/01	13:00-16:00	21.30	0.00	H_2O_2/UV
NB26	07/20/01	14:00-15:00	21.30	0.54	Fe^{3+}/UV
NB27	07/20/01	16:00-17:00	21.30	2.14	$Fe^{2+}/H_2O_2/UV$
NB28	07/23/01	10:00-11:00	21.30	0.54	$Fe^{3+}/H_2O_2/UV$
NB29	07/23/01	12:00-13:00	21.30	1.07	$Fe^{3+}/H_2O_2/UV$
NB30	07/23/01	13:00-14:00	42.60	2.14	$Fe^{3+}/H_2O_2/UV$
NB31	07/23/01	15:00-16:00	10.60	1.07	$Fe^{3+}/H_2O_2/UV$
NB32	07/23/01	16:00-17:00	42.60	1.07	$Fe^{3+}/H_2O_2/UV$
NB33	07/27/01	10:00-11:00	21.30	2.14	$Fe^{2+}/H_2O_2/UV$
NB34	07/27/01	12:00-15:00	0.00	0.00	UV
NB35	07/30/01	13:00-15:00	0.00	0.00	UV

4.6. Results and discussion for phenol mineralization

The influence of different sources of light in the mineralization of phenol was studied. As it was mentioned before, phenol was selected taking into account that it is a well known compound used as model in different studies, and on the other hand it is a very difficult compound to degrade via photolysis in comparison with others compounds as NB studied in this research. This difference between both compounds will allow knowing the influence of the light on the photochemical processes under study. It is important to point out that most of the experiments performed in this chapter were carried out in duplicate or triplicate (see Tables 4.2 – 4.6) in order to ensure the reproducibility of these results.

4.6.1. Direct photolysis of phenol by means of artificial and solar radiation

Several experiments (Ph11, Ph30, Ph23 and Ph29, Table 4.2 and 4.3) were made as a blank experiment in order to know the influence of artificial and solar radiation on the mineralization rate of the phenol solution without catalyst. Fig. 4.21 shows the effect of the different types of light: UV 254 nm (reactor B), UV 360 nm (reactor C), Xenon light (solarbox) 300-560 nm (reactor D) and solar light (reactor E) on direct photolysis of phenol solutions. In Table 4.7 the obtained results for direct photolysis are summarized.

Table 4.7. Mineralization of phenol by means of direct photolysis after 2 hours of irradiation.

Irradiation Source	UV (253.7 nm) Gemicide Lamp (15W)	UV(300-400nm) Black lamp (4W)	UV(300-560nm) Xenon lamp (1500W)	UV-vis Sunlight
Mineralization (TOC %)	12	2	2	2.8

These results indicate that there was no mineralization in the cases of reactors C, D and E. The best results were reached in reactor B, where four 15 W mercury lamps (253.7 nm) were installed. This is in agreement with the results obtained by several authors (Sundstrom *et al.*, 1989; Guittonneau *et al.*, 1990; Rupper *et al.*, 1994). Therefore, direct

photolysis of phenol solutions at the tested conditions is not a very effective method for mineralization. In a same way it is not an effective method for its degradation, because the yield obtained was also very low.

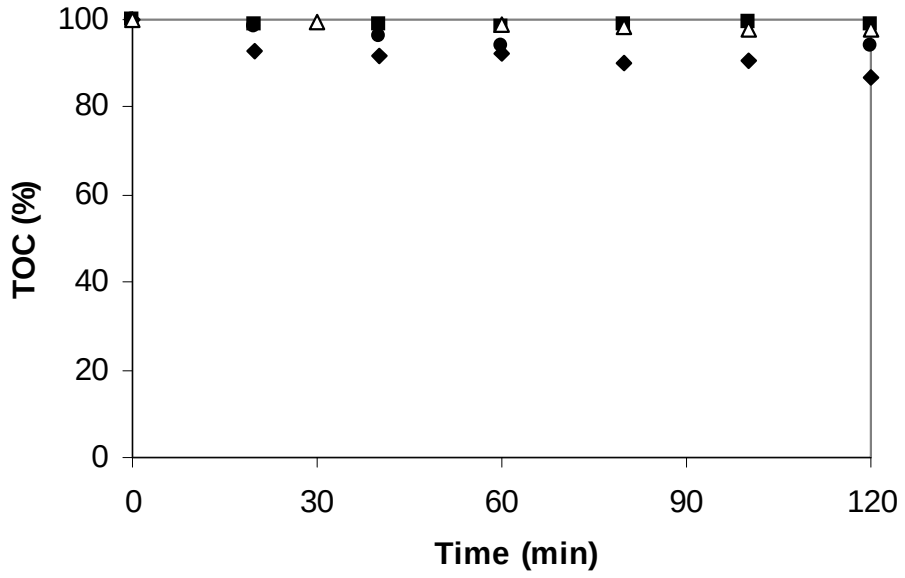

Figure 4.21. Effect of direct photolysis on the mineralization of phenol. $[phenol]_o$= 1.14 mmol.L^{-1} (■) Reactor D, (Δ) Reactor E, (●) Reactor C, (♦) Reactor B.

4.6.2. Photo-Fenton using artificial light

The effectiveness of photo-Fenton process in the mineralization of aromatic organic compounds in aqueous solutions is well-known (Lipczynska-Kochany, 1992; Li and Comfort, 1998; Bauer *et al.*, 1999). However, a complementary study, using three different sources of artificial light has been made in order to check the effect of the radiation source in this photocatalytic homogeneous process.

As it can be observed in Fig. 4.22, a very high degree of TOC reduction (more than 80 % in 1 hour irradiation) was obtained in reactors B and D. In reactor C, 60 % of TOC was eliminated in 1 h (Table 4.2, Ph9, Ph14, and Ph24). These results are in agreement with both the photon flux entering the reactor and the emitting wavelength in each case. In this sense, the best results were achieved in reactor B, where 100 % of mineralization was

obtained. This could also be explained by the effectiveness of the ultraviolet radiation (254 nm) in the photolysis of the H_2O_2 to produce hydroxyl radicals (see eq. 4.3). In the three experiments performed in three different reactors (Fig. 4.22), the main part of the TOC reduction takes place during the first 20 minutes when most of H_2O_2 is consumed, producing most of the hydroxyl radicals.

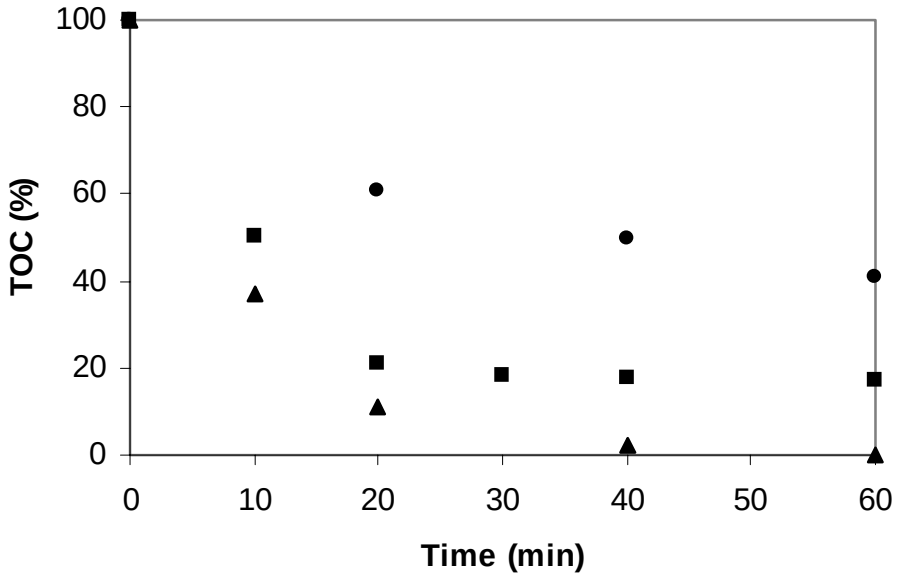

Figure 4.22. Photo-Fenton mineralization of phenol using different sources of light. $[phenol]_o$= 1.14 mmol.L^{-1}, $[Fe^{3+}]_o$ = 1.07 mmol.L^{-1}, $[H_2O_2]_o$ = 21.30 mmol.L^{-1}, T = 298 K.(●) Reactor C, (■) Reactor D, (▲) Reactor B.

4.6.2.1. Effect of the use of Fe^{2+} or Fe^{3+} in the photo-Fenton process

In order to study the influence of the most important parameters in the photo Fenton process, reactor B was chosen as model reactor, taking into account the previous results and in order to reduce the number of experiments. Traditionally, the Fenton process is carried out in presence of Fe^{2+} ($FeSO_4$) as catalyst. However, the mineralization step appears to be driven by Fe^{3+}-catalyzed processes, especially in presence of light (Pignatello, 1992). For this reason, preliminary experiments to know the influence of using Fe^{2+} or Fe^{3+} were carried out. As it can be seen in Fig. 4.23 (Ph5 and Ph9, Table 4.2) a similar mineralization degree was obtained using both Fe^{2+} ($FeSO_4$) and Fe^{3+}($FeCl_3$).

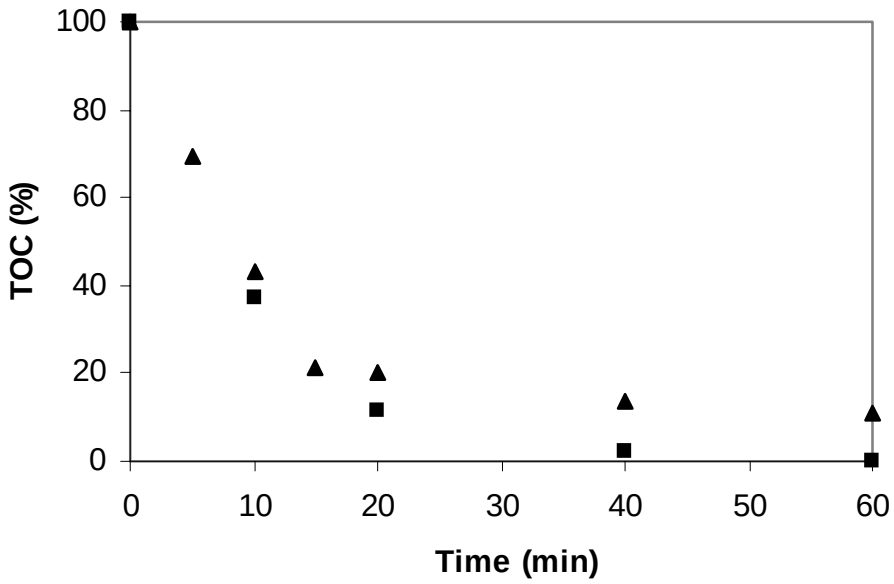

Figure 4.23. Effect of Fe^{2+} and Fe^{3+} on the photo - Fenton mineralization of phenol in Reactor B. $[phenol]_o$= 1.14 mmol.L^{-1}, $[H_2O_2]$ = 21.30 mmol.L^{-1}, T = 298K. (▲) $[Fe^{2+}]$ = 1.07 mmol.L^{-1}, (■) $[Fe^{3+}]$ = 1.07 mmol.L^{-1}.

Therefore, the use of one or another ion seems not to be important under the studied conditions. Related to that, another aspect that should be considered is the anion of the used salt. In this sense, the influence of different anions normally present in natural water and wastewater has been widely studied (Pignatello, 1992; Lipczynska-Kochany *et al.*, 1995). These studies showed that Cl^-, SO_4^{2-}, HPO_4^{2-} and HCO_3^- anions delayed the Fenton reaction. This retard is attributed to their scavenging power of hydroxyl radicals. This effect is particularly strong for bicarbonate and phosphate ions. Consequently, their presence is unfavorable in Fenton reagent. However, the scavenging effect of phosphate and bicarbonate anions on the degradation of organic pollutants by means of the Fenton process may be somewhat reduced by the necessity of the application of this technique at moderately low pH.

In light of the experimental results, where an important difference of the used iron ion is not observed besides the fact that mineralization appears to be driven by Fe^{3+}-catalyzed processes, Fe^{3+} has been selected as catalyst to be used in most of the photo-Fenton experiments.

4.6.2.2. Effect of H_2O_2 initial concentration

In the photo-Fenton process the limiting reagent is H_2O_2. However, as it has been demonstrated before in the dark-Fenton process, an excess of this reagent does not mean a continuous increase in the mineralization and degradation rate of the treated solution. In this sense, a series of experiments was also carried out in order to study the effect of initial concentration of H_2O_2 on the mineralization rate of a phenol solution in reactor B.

The experimental data obtained for phenol mineralization can be fitted according to a pseudo-first-order reaction (eq. 4.26):

$$\frac{-d(TOC)}{dt} = k(TOC)_o \tag{4.26}$$

where k is the first-order reaction rate constant (eq.4.27). The integration leads to

$$-\ln\left(\frac{TOC}{TOC_o}\right) = kt \tag{4.27}$$

From the plot Ln(TOC/TOC_o) versus t (time of irradiation), the first-order reaction rate constant (the slope) was calculated and used to study the effect of different concentration of H_2O_2 and Fe^{3+}.

As shown in Fig. 4.24 (Ph12, Ph14 and Ph16-Ph18, Table 4.2) a significant enhancement of the mineralization efficiency was observed when the H_2O_2 concentration was increased from 0 to 64.06 $mmol.L^{-1}$ (the continuous line does not mean any fitting but only a way of showing the tendency).

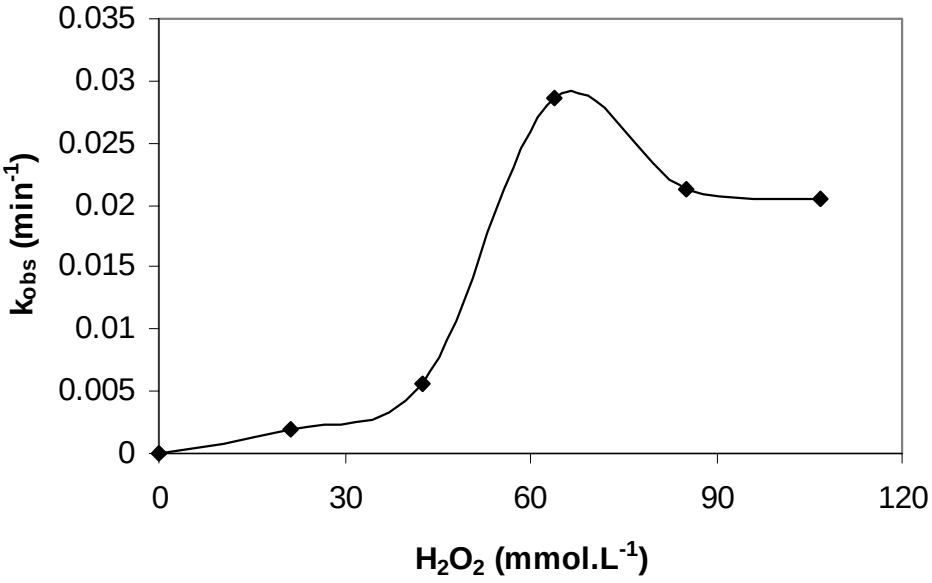

Figure 4.24. The initial rate constant of photo-Fenton mineralization using different [H_2O_2] concentration in reactor B. [phenol]$_o$= 5.69 mmol.L^{-1}, [Fe^{3+}] = 1.07 mmol.L^{-1}, T = 298 K.

Above this H_2O_2 concentration, the oxidation rate seems to be negatively affected by the increase of H_2O_2 up to106.7 mmol.L^{-1}. This is probably due to both the auto-decomposition of H_2O_2 into oxygen and water (eq.4.28) and the scavenging effect of hydroxyl radicals by H_2O_2 (eq. 4.29) as follows:

$$2H_2O_2 \rightarrow 2H_2O + O_2 \quad (4.28)$$

$$HO^{\bullet} + H_2O_2 \rightarrow HOO^{\bullet} + H_2O \quad (4.29)$$

Excess of H_2O_2 will react with $HO^{\bullet}$ competing with organic pollutants and consequently reducing the efficiency of the treatment.

The percentage of mineralization is shown in Fig. 4.25. As it can be observed, the mineralization reached above 64.06 mmol.L^{-1} of H_2O_2 is smaller than the one achieved at this concentration (Ph16 and Ph17, Table 4.2). Therefore, 64.06 mmol.L^{-1} seemed to be the optimal concentration of H_2O_2 for mineralization of phenol at the experimental conditions.

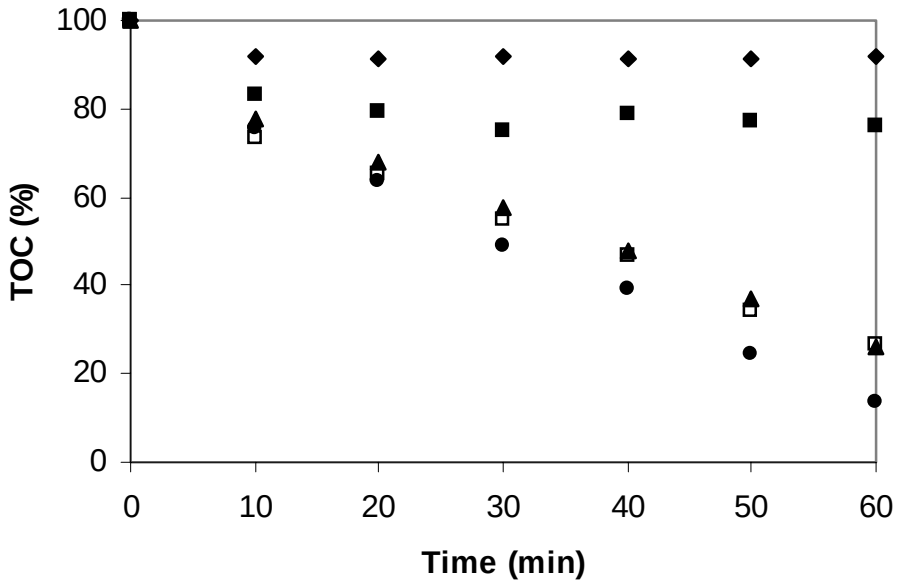

Figure 4.25. Photo-Fenton mineralization using different H_2O_2 concentrations. $[phenol]_o$ = 5.69 mmol.L^{-1}, [Fe^{3+}] = 1.07 mmol.L^{-1}, T = 298K. (♦)[H_2O_2]= 21.30 mmol.L^{-1}, (■)[H_2O_2]= 42.6 mmol.L^{-1}, (▲)[H_2O_2] = 106.7 mmol.L^{-1}, (□) [H_2O_2] = 85.3 mmol.L^{-1}, (•)[H_2O_2] = 64.0 mmol.L^{-1}.

4.6.2.3. Effect of O_2 concentration

The effect of bubbling oxygen into the reactor was also studied. It is important to keep in mind that the reactor B, where all these experiments were performed, was open to the atmosphere. Thus, it is not possible to know if the oxygen concentration during the experiment provided by dissolved oxygen and by the decomposition of H_2O_2 is enough for the mineralization of the compound. In this sense, several experiments were carried out with and without bubbling oxygen through the solution using two different concentration of phenol (1.07 and 5.69 mmol.L^{-1}) at the same concentration of H_2O_2 , Fe^{3+} and room temperature.

In Fig. 4.26 experiments Ph9, Ph13, Ph14 and Ph15 were represented. In the case of experiment Ph9 (without bubbling O_2) and Ph13 (bubbling O_2), similar mineralization degree was obtained. This means that oxygen concentration to reach 100 % of mineralization at the working conditions (Ph9 and Ph13) was sufficient when phenol concentration was low (1.07 mmol.L^{-1}).

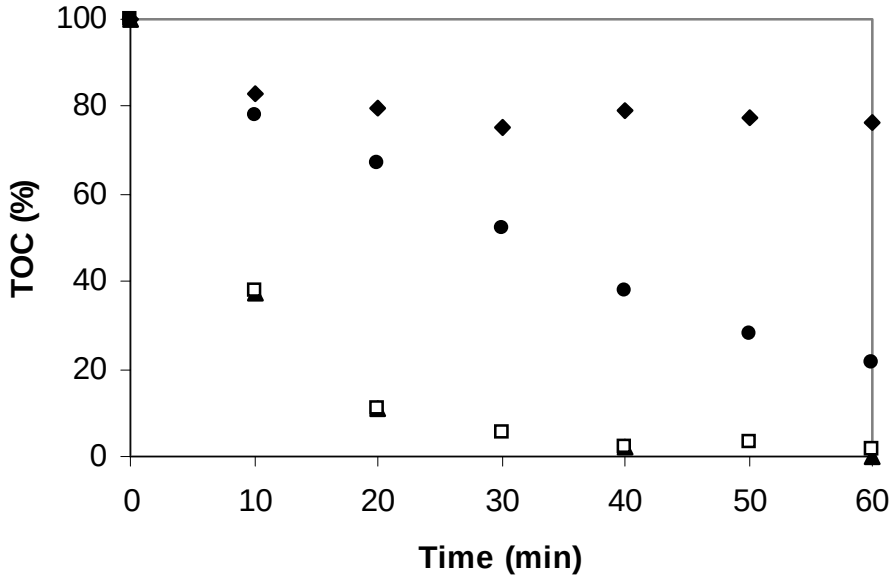

Figure 4.26. Effect of bubbling O_2 in the photo-Fenton mineralization of phenol. [Fe^{3+}] = 1.07 mmol.L^{-1}, T = 298K. (♦) Ph14, (●) Ph15, (□) Ph9, (▲) Ph13.

However, in the case of experiments Ph14 (without bubbling O_2) and Ph15 (bubbling O_2) when phenol concentration was 5.69 mmol.L^{-1}, the reached mineralization degree was significantly different. In those cases, the percentage of TOC eliminated was 80 % and 24 %, respectively. These differences can be explained keeping in mind two important elements. The first one is that the excess of oxygen in the reaction medium avoids the auto-decomposition of H_2O_2 in H_2O and O_2 according to eq. 4.28. It means that more H_2O_2 can produce $HO^{\bullet}$ through equation (1.8). The second one may be attributed to the high concentration of phenol, needing more oxygen for its mineralization.

4.6.3. Dark-Fenton combined with UV artificial radiation

Some experiments (Ph1-Ph4 and Ph8, Table 4.2) were also carried out in reactor B, where the Fenton reaction in the dark was followed by a period of irradiation. The aim of these experiments was to compare them with the photo-Fenton process. In Fig. 4.27 the combined experiment (dark + UV) and the photo-Fenton process are presented. The reaction time in the dark was sufficiently long (60 min) in order to guarantee that all Fe^{2+}

was converted to Fe^{3+}. The maximum TOC reduction took place during the first 10 min. Afterwards, a plateau was reached and after 60 min the irradiation was applied. The rate constant of the second (illuminated) step was estimated in order to compare with the photo-Fenton process and was 0.101 min^{-1}. The initial rate constant for the photo-Fenton process was 0.0798 min^{-1}. An important difference is not observed even when the first step of reaction was carried out in the dark in comparison to when the reaction took place in presence of UV from the beginning. However, the final degree of mineralization was higher when the photo-Fenton process was used since the beginning (100% in 60 minutes of treatment), as the involved reactions in presence of light take place throughout all the treatment time. These results confirm that the mineralization power of the Fenton system is greatly enhanced by irradiation with UV. It is very important to note that in the combined process a plateau was reached after 80% of mineralization and the reaction began to advance very slowly, while the photo-Fenton process proceed until total mineralization. Concluding, it is not worthy to carry out this process in two stages, but taking profit of the synergistic use of the light from the beginning of the process.

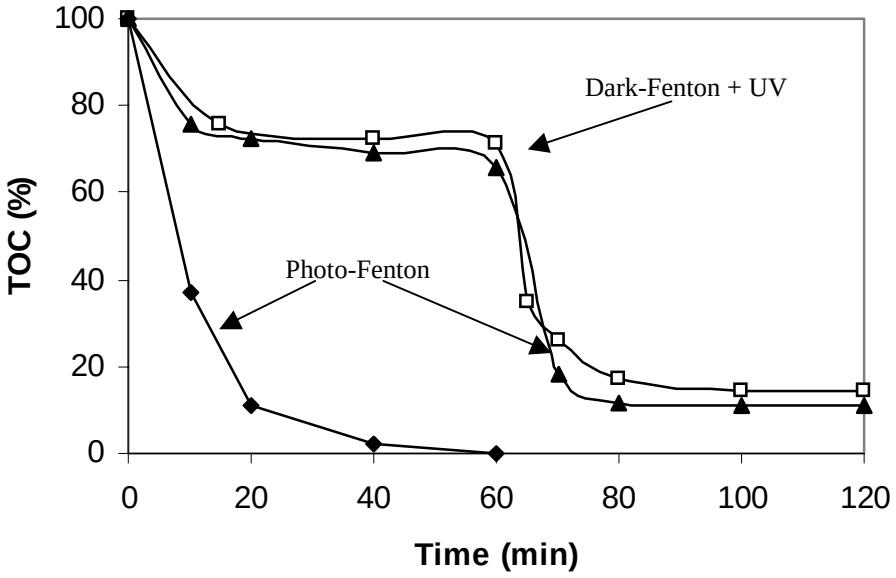

Figure 4.27. Effect of irradiation on the photo-Fenton mineralization in Reactor B. $[phenol]_o$ = 1.14 $mmol.L^{-1}$, $[Fe^{3+}]$ = 1.07 $mmol.L^{-1}$, $[H_2O_2]$ = 21.30 $mmol.L^{-1}$, T = 298K.(□,▲) Ph4, Ph8 (the irradiation period started after 60 min).(◆) Ph5 (with irradiation from the beginning).

4.6.4. Photo-Fenton process using solar radiation

As it has been mentioned before en section 4.6.2, the photo-Fenton process was very effective in the mineralization of many organic compounds in aqueous solution. However, one problem of this treatment process is the electrical energy demand of UV-lamps. In addition, the photo-reactor design at big scale is also expensive and difficult to operate. Therefore, the total costs of a photo-Fenton process using artificial light are usually high. In this context, the use of solar light would dramatically decrease the cost of the process, thus, providing a major step towards industrials applications (Blanco *et al.*, 1999; Krutzler and Bauer, 1999). The use of solar light is possible for photocatalytic processes, such as photo-Fenton and TiO_2/UV.

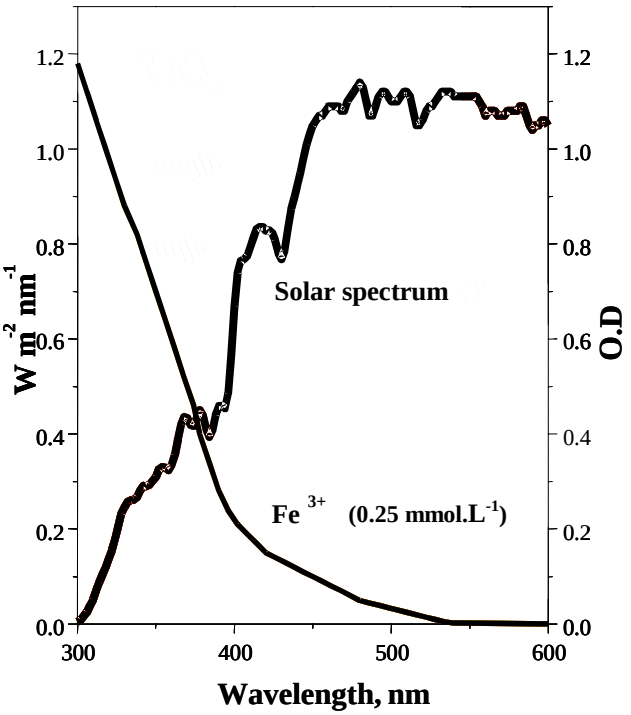

Figure 4.28. PSA typical solar spectrum compared to the optical density (O.D., optical path length 1 cm) of a $Fe_2(SO_4)_3$ solution (0.25 mmol.L^{-1} as Fe^{3+}).

The sensitivity of photo-Fenton process to light up to wavelengths of 520 nm can be observed in Fig 4.28. Light penetration is deep and the contact between pollutant and the oxidizing agent is intimate, because of the homogeneous phase.

4.6.4.1. Photo-Fenton process in Reactor E

In this context, the solar radiation has been tested as source of radiation in reactor E, a prototype that tried to simulate an Helioman (PTC) but without the sun track, which was designed in our lab to perform a preliminary study about the effectiveness of the solar radiation in this photocatalytic process. These experiments represented the first step of our laboratory in the use of the solar energy as radiation source.

The influence of solar radiation at the same experimental conditions (Table 4.3) during sunny days was studied. In Fig. 4.29, three experiments performed in two days at different times of the day are presented and the results showed a similar trend (Ph30, Ph31, Ph33, Table 4.3).

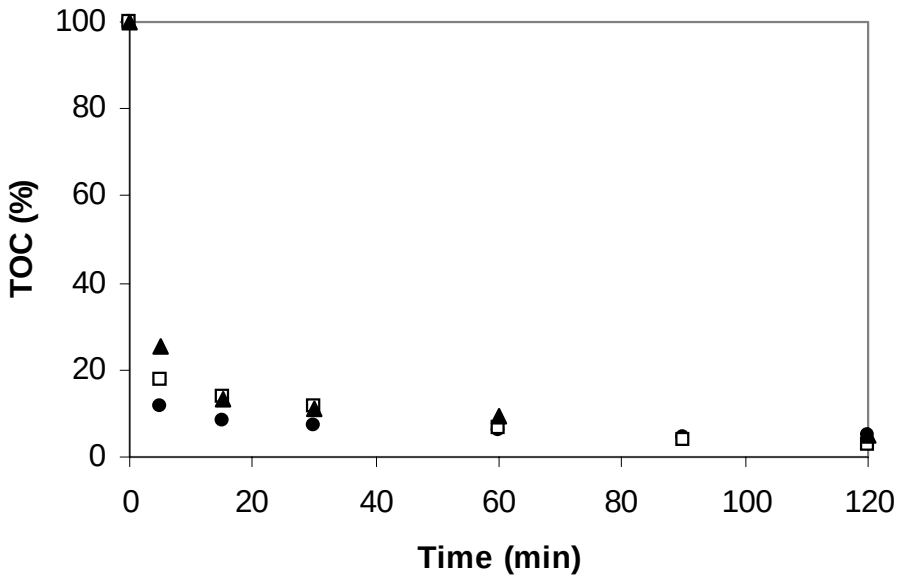

Figure 4.29. Photo-Fenton mineralization process at different irradiation time. $[phenol]_o$= 1.14 mmol.L^{-1}, $[Fe^{3+}]_o$ = 1.07 mmol.L^{-1}, $[H_2O_2]$ = 21.30 mmol.L^{-1}, T = 298 K. (▲) Ph33, (□) Ph31, (●) Ph30.

A plateau was reached after 90% of mineralization and the reaction began to advance very slowly. That happened because there was not enough hydrogen peroxide in the reaction medium, as commented before. Almost total mineralization was achieved after 1 hour of phototreatment. These results, in spite of the limitations in the reception of the

radiation of the designed reactor, are a good qualitative demonstration of the effectiveness of the solar light in the Fenton process.

The optimal concentration of Fe^{3+} and H_2O_2 are the key factor of this process and need to be determined to find out the values at which maximum efficiency is obtained. Therefore, H_2O_2 and Fe^{3+} concentrations were optimized for mineralization of phenol solution using the reactor E. The experimental conditions determined in this reactor will be used as reference to operate the CPCs. For this reason, and bearing in mind that it is a laboratory scale prototype, the solar radiation was not quantified in these preliminary experiments. Again, mineralization rate is described assuming a first-order kinetics, as shown in section 4.6.2.2.

4.6.4.1.1. Effect of Fe^{3+}

To further elucidate the role of Fe^{3+} concentration on the mineralization of the phenol solution, a series of experiments, varying the concentration of iron and keeping fixed the other parameters, were carried out. Fig. 4.30 (Ph41, Ph42, and Ph49, Table 4.3) shows that a high mineralization rate was obtained with Fe^{3+} concentration in the range (0.54-1.067 $mmol.L^{-1}$). In all cases, this concentration of Fe^{3+} was selected to continue the phototreatment during ca.60 min and reach around 95% of mineralization by using 21.3 $mmol.L^{-1}$ of H_2O_2 concentration. According to these results, the iron concentration recommended is around 0.5 $mmol.L^{-1}$. This will contribute to a smaller formation of iron precipitate, one of the main disadvantages of this process.

4.6.4.1.2. Effect of H_2O_2

As shown in Fig. 4.31 (Ph41, Ph47 and Ph48, Table 4.3) a significant enhancement of mineralization efficiency was verified when the H_2O_2 concentration was increased from 0 to 21.22 $mmol.L^{-1}$. Mineralization rate increased with H_2O_2 concentration, which is explained by the effect of the additional produced $HO^{\bullet}$ radicals. However, above a certain concentration (21.30 $mmol.L^{-1}$) the constant rate levels off and sometimes is negatively affected (as it was the case of the example shown in section 4.6.2.2) by the progressive increase of the hydrogen peroxide concentration. Therefore, an excess of H_2O_2 will react with $HO^{\bullet}$ competing with organic pollutants and consequently reducing the efficiency in

the treatment. Again, the continuous line does not mean any fitting, but only a way of pointing out the trend for the effect of Fe^{3+} and H_2O_2 in the mineralization of phenol.

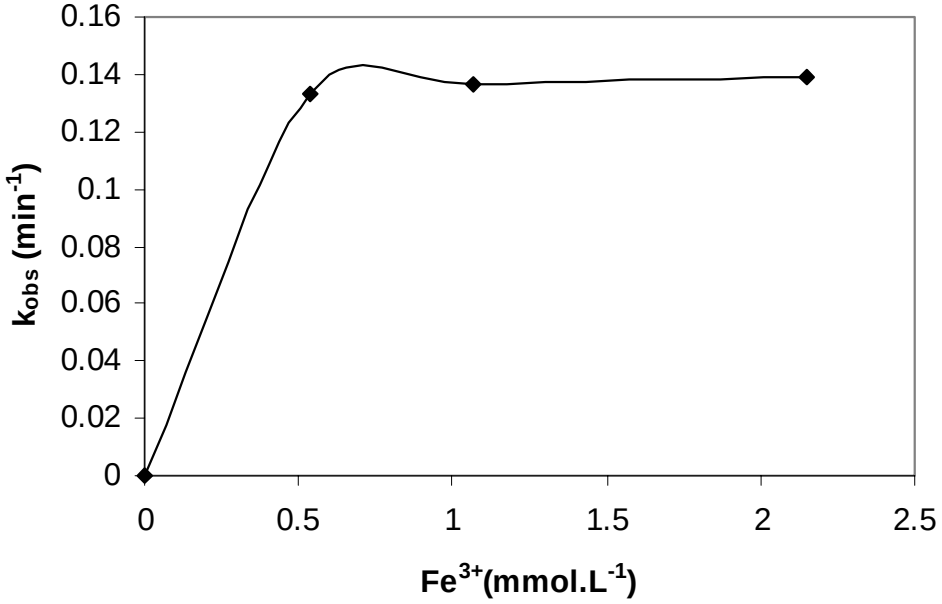

Figure 4.30. The initial rate constant of photo-Fenton mineralization at different Fe^{3+} concentrations in reactor E. $[phenol]_o$= 1.14 $mmol.L^{-1}$, $[H_2O_2]$ = 21.30 $mmol.L^{-1}$

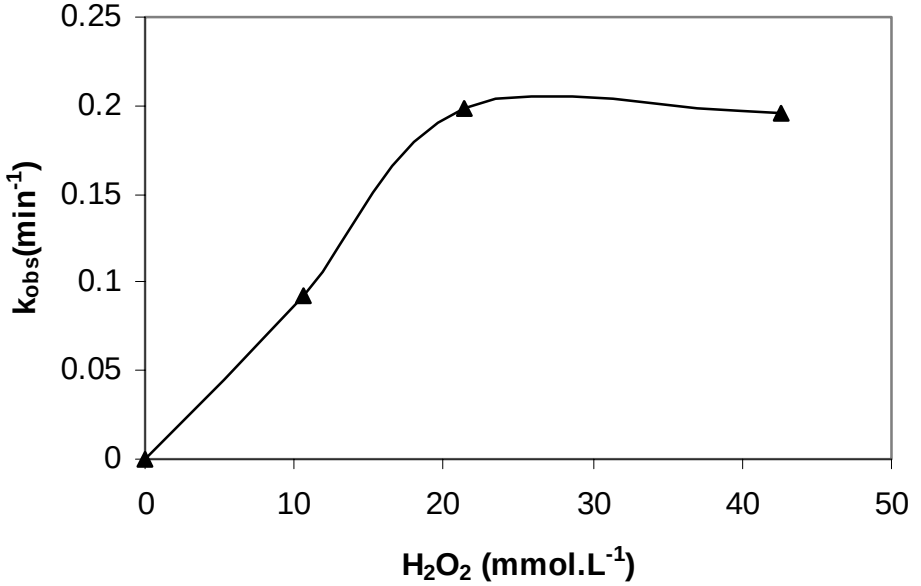

Figure 4.31. The initial rate constant of photo-Fenton mineralization at different $[H_2O_2]$ concentration in reactor E. $[phenol]_o$= 1.14 $mmol.L^{-1}$, $[Fe^{3+}]$ = 1.07 $mmol.L^{-1}$

4.6.4.2. Photo-Fenton process in the CPCs (reactors F and G)

After setting the working conditions (Fe^{3+} and H_2O_2 concentrations) with the lab-scale parabolic collector (reactor E), some photo-Fenton experiments (Ph50-Ph56, Table 4.4) were also carried out using two CPC collectors at pilot scale, reactors F (100L) and G (190L), located in Laussane (Switzerland) and in Almería (Spain), respectively. In those cases, the radiation was quantified and the mineralization was related to the solar energy consumed. In all the range of Fe^{3+} concentration tested in reactor E, H_2O_2 consumption was very fast. Bearing in mind this fact, a lower concentration of Fe^{3+} (0.27 mmol.L^{-1}) was also tested in reactor G.

Firstly, results achieved with reactor G are presented. Fig. 4.32 shows the mineralization achieved related to accumulate energy per unit of volume (Q) calculated according to eq. 4.25 described in section 4.4.3.6. Although that a high mineralization rate was obtained with Fe^{3+} concentration in the range under study (0.27-1.07 mmol.L^{-1}), the best results was reached when the minor Fe^{3+} concentration (0.27 mmol.L^{-1}) was used. In this case, the mineralization achieved was 100% in 2 hours. In the case of major concentrations of Fe^{3+}, keeping the H_2O_2 concentration constant, the mineralization reached was 94 % and 98% in two hours for 1.07 and 0.54 mmol.L^{-1} of Fe^{3+}, respectively. In spite of also getting a high mineralization degree at these iron concentrations, the idea is to use the smallest amount of iron in order to avoid problems with their necessary elimination. The European Community directives allow 2 mg L^{-1} of iron in treated water to be discharged directly into the environment and 20 mg L^{-1} to be discharged into municipal biological treatment plant (EEC, 1992) . Nevertheless, iron could be reutilized after precipitation like iron hydroxide. The recycling of iron sludge has not only the advantage of avoiding its disposal but also of saving chemical cost for iron salt. Previous work showed that the repeated use of iron sludge has no negative consequences on his catalytic activity (Renner *et al.*, 2000).

In Fig. 4.33 the initial rate constant of the treated phenol solution at different Fe^{3+} concentration is also shown.

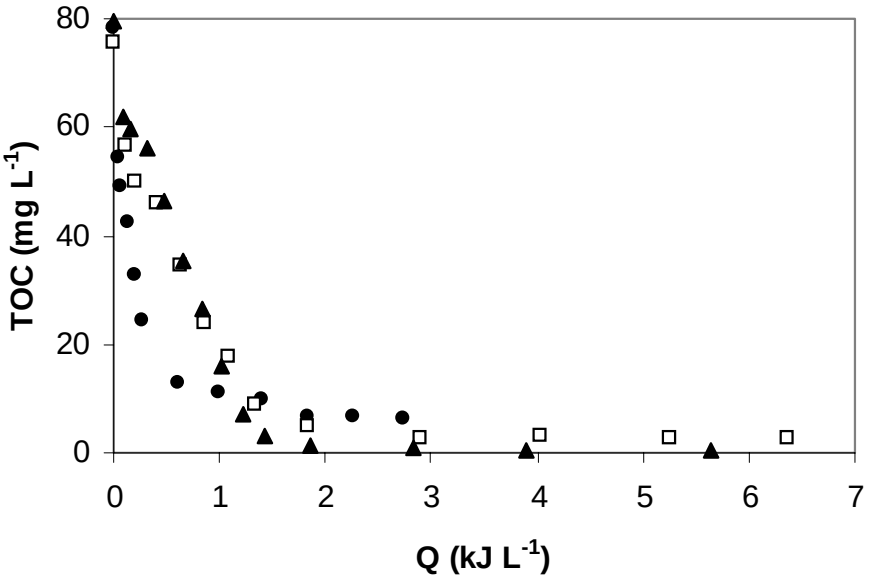

Figure 4.32. Photo-Fenton mineralization at different Fe^{3+} concentrations related to accumulated energy per unit volume. $[phenol]_o$= 1.14 $mmol.L^{-1}$, $[H_2O_2]$ = 21.30 $mmol.L^{-1}$.(•) $[Fe^{3+}]$ = 1.067 $mmol.L^{-1}$, (□) $[Fe^{3+}]$ = 0.54 $mmol.L^{-1}$, (▲) $[Fe^{3+}]$ =0.27 $mmol.L^{-1}$.

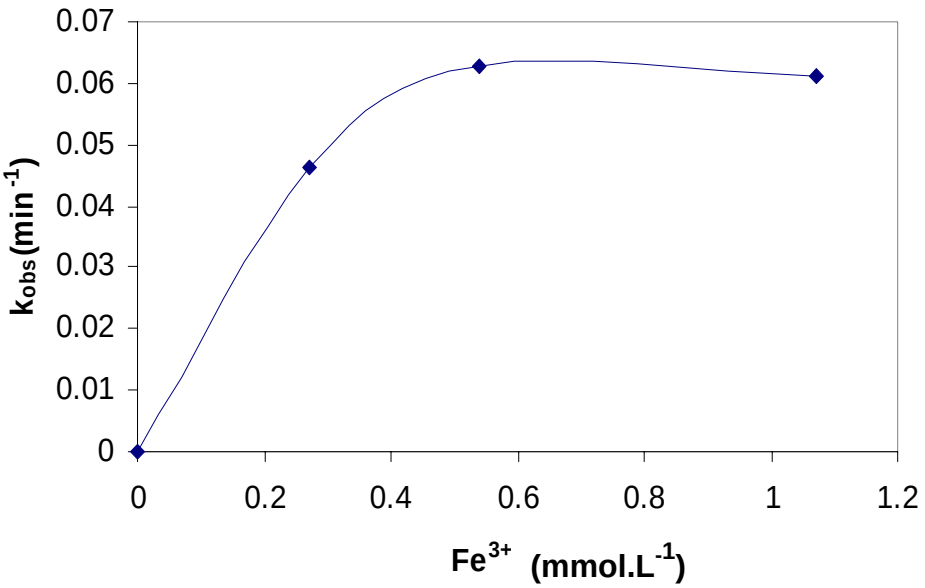

Figure 4.33. The initial rate constant of photo-Fenton mineralization of phenol at different Fe^{3+} concentrations in reactor G. $[phenol]_o$ = 1.14 $mmol.L^{-1}$, $[H_2O_2]$ = 21.30 $mmol.L^{-1}$

As it can be seen in this figure, a significant enhancement of mineralization efficiency was verified when the Fe^{3+}concentration was increased from 0.27 to 0.54 $mmol.L^{-1}$. Above this concentration, the mineralization rate is insensitive to this effect as has been already shown in most of the cases under study.

The consumption of H_2O_2 in these experiments was followed using the iodimetric titration method. As it can be observed in Fig. 4.34, the hydrogen peroxide consumed depends on the Fe^{3+} concentration and it was present in solution until total mineralization of the carbon content (see Fig. 4.35). In light of these results and those presented in Fig. 4.32, seems that with lower Fe^{3+} concentration (and then, lower hydroxyl radical production), hydrogen peroxide is not consumed by reaction with those radicals but only by reaction with iron and light. The idea is then to consume the peroxide slowly, obtaining a higher mineralization.

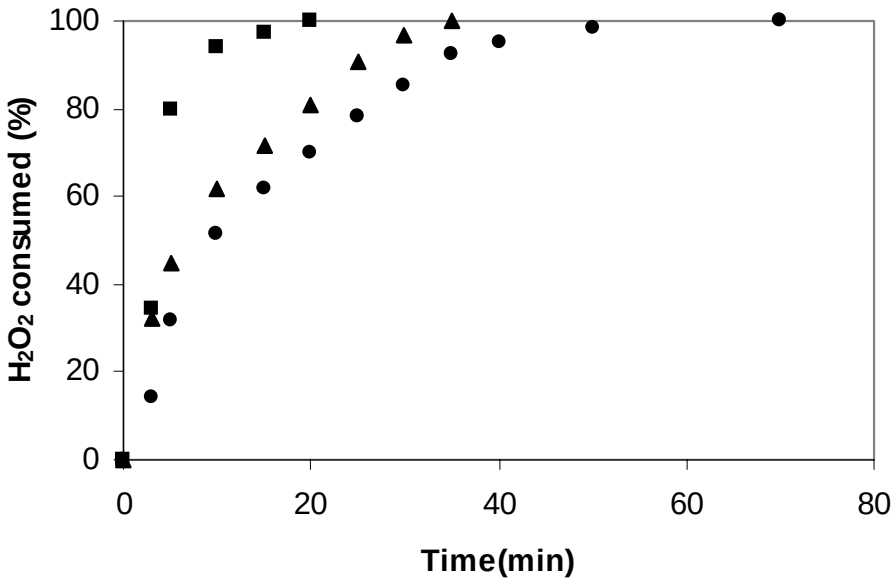

Figure 4.34. Hydrogen peroxide consumed at different Fe^{3+} concentrations in reactor G. $[phenol]_o$=1.14 mmol.L-1, $[H_2O_2]$ = 21.30 $mmol.L^{-1}$. (■) $[Fe^{3+}]$ = 1.067 $mmol.L^{-1}$, (▲) $[Fe^{3+}]$ = 0.54 $mmol.L^{-1}$, (•) $[Fe^{3+}]$ = 0.27 $mmol.L^{-1}$

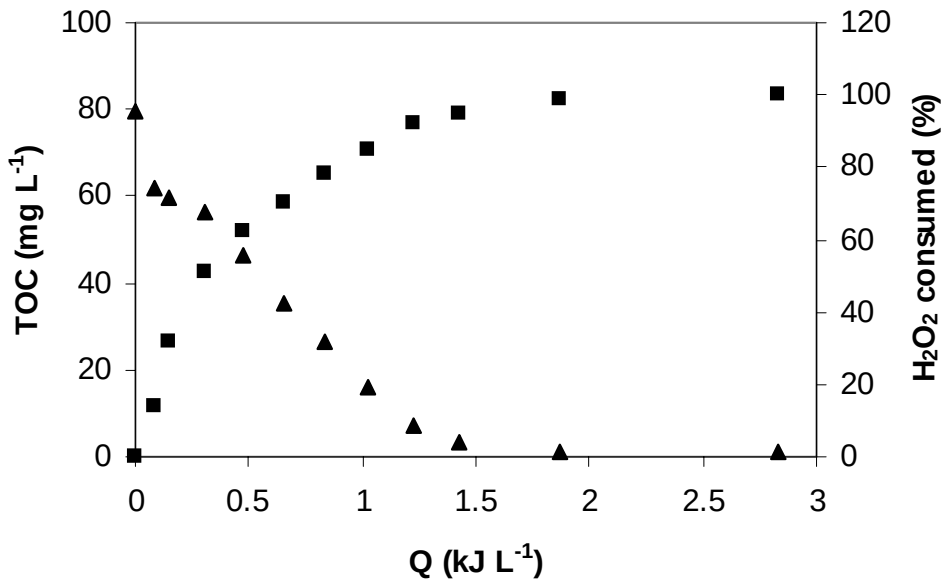

Figure 4.35. Photo-Fenton mineralization and hydrogen peroxide consumed related to accumulated energy per unit volume. $[phenol]_o$ = 1.14 mmol.L^{-1}, $[Fe^{3+}]$ = 0.27 mmol.L^{-1}, $[H_2O_2]$ = 21.30 mmol.L^{-1}

Finally, a comparative study between both CPC reactors (G and F) has also been made. This part of the study focuses on the comparison of performance of two CPC solar collectors, with regard to the mineralization of phenol via photo-Fenton process. The same experimental conditions (same concentration of H_2O_2 and two concentrations of Fe^{3+} (0.54 and 1.07 mmol.L^{-1})) were used in order to evaluate the efficiency of both solar reactors (see Fig.4.36). A higher TOC reduction (94 and 98 %) is reached in the reactor G in comparison with the 60% obtained in reactor F. This is an important fact to point up, as using the same experimental conditions and apparently the same kind of reactors, different experimental results were achieved showing a dissimilar efficiency. Several factors could account for this difference. First of all, the recirculation flow rate is three times higher in the case of reactor G than in reactor F, allowing a better mixing of the solution. Secondly, the ratio of irradiated volume per total volume is 0.38 and 0.24 for reactors G and F, respectively. Thus, the effectiveness would be higher for reactor G. And finally, the presence of oxygen is determinant for mineralization of the target compounds, as was already demonstrated in section 4.6.2.3. In this sense a high recirculation flow, besides improving the mixing, allows a better oxygenation of the mixture in the tank and therefore

the consumption of H_2O_2 product of its dissociation according to eq. 4.28 would be avoided.

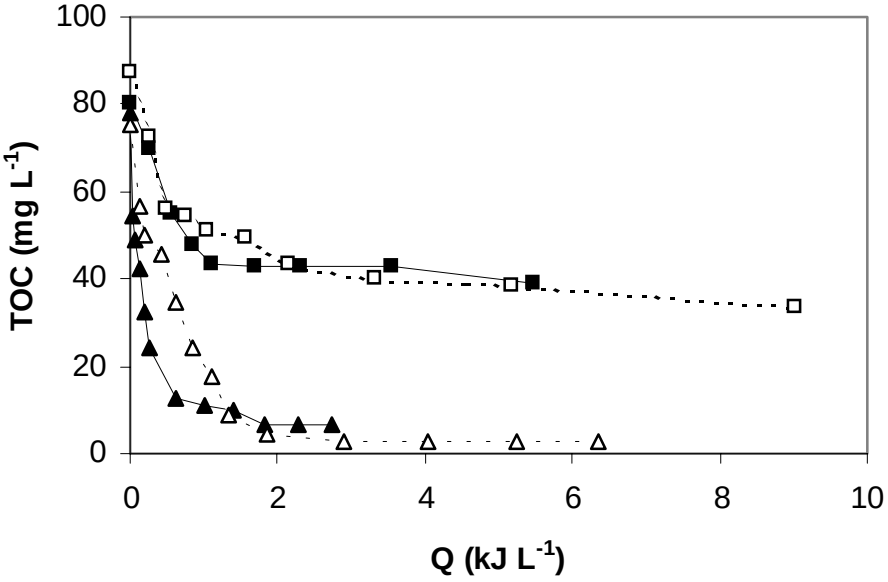

Figure 4.36. Evolution of mineralization rate as function of accumulated energy per unit volume in reactors F and G. $[phenol]_o$=1.14 mmol.L^{-1}, $[H_2O_2]$ = 21.30 mmol.L^{-1}. (■,▲)$[Fe^{3+}]$ = 1.067 mmol.L^{-1}, (□,△) $[Fe^{3+}]$ = 0.54 mmol.L^{-1}.

Thus, in reactor G the H_2O_2 consumption was slower and could be used for hydroxyl radical production, therefore for phenol mineralization. As it can be seen in Fig. 4.36, reaction in system F seems to stop after a 60% of mineralization degree coinciding with exhaustion of the hydrogen peroxide, while in reactor G the presence of hydrogen peroxide was detected until total mineralization. These factors should be taken into account when designing this type of reactors.

Fig. 4.37 shows the linear relation between $-Ln(TOC/TOC_o)$ and Q_{UV} for the phenol mineralization in both reactors. In both cases, the kinetics of phenol mineralization are of apparent first order, with rate constants equal to 4.40 and 0.58 L.kJ^{-1} for the CPC located in Almería and the CPC located in Lausanne, respectively.

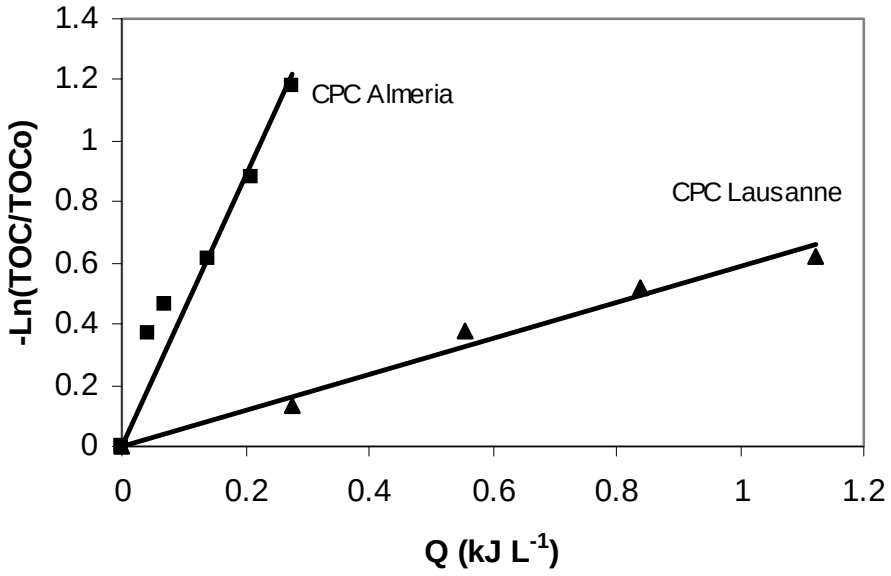

Figure 4.37. Linear transform of the kinetic curves of phenol mineralization in CPC reactors. $[phenol]_o$ = 1.14 mmol.L^{-1}, $[H_2O_2]$ = 21.30 mmol.L^{-1}. $[Fe^{3+}]$ = 1.067 mmol.L^{-1}

4.6.4.3. Estimation of intrinsic kinetic constant for photo-Fenton process in reactors D and G

The estimation of global experimental kinetic constants has been widely performed in most of the photo-Fenton works by assuming a first order or second order kinetics. However, in this work it is desired to estimate the individual contribution of both steps, the dark and illuminated one, on the photo-Fenton system. The estimation of these constants could be very helpful in the scale-up of these reactors. With this objective in mind, those intrinsic constants were calculated in two scales: at lab scale in a solarbox (reactor D) and at pilot plant in the CPC reactor (reactor G), to establish a comparison for this process at different scale. The following assumptions were made:

- The mineralization kinetics follows a first order (eq. 4.30), being k_{exp} the global experimental kinetic constant:

$$\frac{d(C_{TOC})}{dt} = - k_{exp}\ C_{TOC} \qquad (4.30)$$

- Hydroxyl radical production changes according to the two steps present in the photo-Fenton process. In the dark step they will be produced by reaction (1.10) described in chapter 1. On the contrary, in the reaction in presence of light the $HO^{\bullet}$ radicals are produced both by the reaction in the darkness and by reactions in presence of light (see reactions 1.17 and 1.8). Thus, it is assumed that:

$$V_{total} \frac{d(C_{TOC})}{dt} = - k_{dark} V_{total} C_{TOC} - k'_{illuminated} V_{illuminated} C_{TOC} \quad (4.31)$$

and dividing both sides by the total volume,

$$\frac{d(C_{TOC})}{dt} = - \left(k_{dark} + k'_{illuminated} \frac{V_{illuminated}}{V_{total}} \right) C_{TOC} \quad (4.32)$$

In addition, $k_{illuminated}$ (intrinsic kinetic constant of the illuminated step) could be considered non-proportional to the photon flux absorbed per unit volume, in order to extend its application to any system. Thus, eq. 4.32 can be rewritten as:

$$\frac{d(C_{TOC})}{dt} = - \left(k_{dark} + k_{illuminated} \frac{W_{abs}}{V_{illuminated}} \frac{V_{illuminated}}{V_{total}} \right) C_{TOC} \quad (4.33)$$

and

$$k_{exp} = k_{dark} + k_{illuminated} \frac{W_{abs}}{V_{total}} \quad (4.34)$$

being W_{abs} the absorbed radiation by the *absorbing* species in the reaction medium.

From eq. 4.34, $k_{illuminated}$ can be calculated according to the following expression:

$$k_{illuminated} = \frac{k_{exp} - k_{dark}}{W_{abs}} V_{total} \quad (4.35)$$

Taking into account the complexity in terms of reaction species during photo-Fenton process, W_{abs} has been estimated by considering Fe^{3+} as the main absorbing species in the reaction medium. It is important to point out that the studied compound

(phenol) disappears during the first minutes of photo-Fenton reaction. Therefore, it could not be considered among the species that would absorb the light. Besides this, hydrogen peroxide absorption has been considered negligible in comparison to Fe^{3+}, as it absorbs very little in the used range of wavelength. It is also certain that iron is not present in the reaction medium only as Fe^{3+}, but in other forms as well. However, as a first approach, it has been considered that all the iron is present as Fe^{3+}, in order to estimate a value of this constant. Other important aspect is the range of wavelengths considered to estimate the absorbed radiation by the reaction medium. In this sense, a range between 300-400 nm has been selected, taking into account that it is in this range where Fe^{3+} absorbance is more important and, on the other hand, this is the radiation band captured by the radiometer installed in the CPC. Further details about the calculation of the radiation absorbed (W_{abs}) in reactors D and G are shown in the appendix.

Thus, global kinetic constants have been calculated for experiments carried out in reactors D and G at the same working conditions, i.e. phenol, H_2O_2, and Fe^{3+} concentrations (Ph24 and Ph64, Tables 4.2 and 4.4). From these experiments, the linear regression analysis of the data representing Ln (TOC/TOC_o) versus time showed a straight line, whose slopes (k_{exp}) were equal to 0.0749 min^{-1} and 0.0602 min^{-1} for the solarbox and the CPC, respectively. Regarding the kinetic constant in the darkness, it was calculated for a Fenton experiment performed at the same working conditions, such as Ph22 (see Table 4.2). From linear regression analysis of the data representing Ln (TOC/TOC_o) versus time of this experiment, the slope k_{dark} was found to be equal to 0.0156 min^{-1}, with a correlation coefficient higher than 0.98. This value will be used in both reactors, as the dark-Fenton process depends only on the pollutant, H_2O_2, and Fe^{3+} concentration.

According to eq. 4.35, the intrinsic illuminated kinetic constant for the photo-Fenton process carried out in the solarbox and in the CPC reactor, can be calculated as follows:

$$(k_{illuminated})_{solarbox} = \frac{(0.0794\ min^{-1} - 0.0156\ min^{-1})/60\ s}{3.16 \times 10^{-7}\ Einstein\ s^{-1}}\ 1.5\ L = 5.04 \times 10^{-3}\ \mu Einstein^{-1}\ L$$

$$(k_{illuminated})_{cpc} = \frac{(0.0602\ min^{-1} - 0.0156\ min^{-1})/60\ s}{3.44 \times 10^{-5}\ Einstein\ s^{-1}}\ 190\ L = 4.10 \times 10^{-3}\ \mu Einstein^{-1}\ L$$

In light of these results, taking into account that the values of intrinsic kinetic constants calculated for both reactors are very similar (difference is smaller than 20%), it may be deduced that the assumption that these constants are not proportional to the photon flux absorbed per volume unit has been corroborated. The values of these intrinsic kinetic constants are independent of the source of light and therefore they could be used in the scaling-up of a photo-reactor.

4.6.5. H_2O_2/UV-vis process

4.6.5.1. H_2O_2/UV-vis process with artificial light

Some experiments (Table 4.2) were carried out in order to study the effectiveness of the H_2O_2/UV system in presence of different sources of artificial light. As it has been aforementioned in the fundamental aspects about this process, the hydrogen peroxide absorbs very little at wavelengths longer than 300 nm and, although it increases steadily at shorter wavelengths, its molar absorption coefficient at 254 nm is only 18.7 L mol^{-1} cm^{-1} (Carter *et al.*, 2000). For this reason, a low-pressure monochromatic mercury lamp was used for H_2O_2 photolysis. However, besides using a monochromatic lamp at 253.7 nm (reactor B), two lamp were also used: a polychromatic black lamp emitting at 300-400 nm installed in reactor C and a polychromatic lamp, 300-560 nm, installed in reactor D. As it can be observed in Fig. 4.38 (Ph10, Ph19, and Ph26, Table 4.1) the high effectiveness of UV radiation at 253.7 nm (reactor B) is confirmed, as 80% of mineralization was obtained in two hours.

The degree of mineralization obtained in the cases of reactor C (300-400 nm) and reactor D (300-560 nm) was 2 and 15 % in 2 hours respectively. These results confirm the fact that the peroxide absorbs very weakly above 300 nm. It is important to take into account that in spite of the low percentage (15%) of mineralization obtained when the solarbox was used, the use of the solar light as radiation source is not completely discarded, if one keeps in mind that the objective is sometimes only the degradation of the primary compound. Thus, it could be used as pretreatment step.

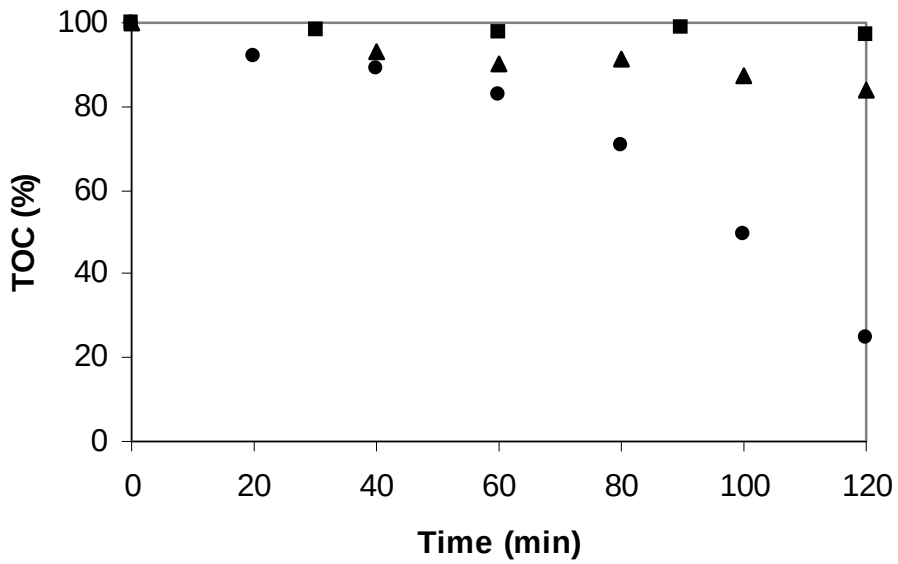

Figure 4.38. Effect of different irradiation sources on the mineralization of phenol by means H_2O_2/UV system. $[phenol]_o$ = 1.14 mmol.L^{-1}, $[Fe^{3+}]$ = 1.07 mmol.L^{-1}, $[H_2O_2]$ = 21.30 mmol.L^{-1}, T = 298 K. (■) Reactor C, (▲) Reactor D, (●) Reactor B.

4.6.5.2. H_2O_2/UV-vis process with solar light

Taking into account the results obtained in the previous section when the solarbox (reactor D) was used, some experiments (Table 4.3) were carried in reactor E in order to study the effectiveness of the H_2O_2/UV-vis system in presence of natural solar light. In spite of the weak hydrogen peroxide absorbance above 300 nm but considering that in the reactor E quartz tube has been also used to avoid filtering the little existent solar radiation in the range of 285-320 nm, a group of experiments at different H_2O_2 concentrations were performed. In Fig.4.39 the absorption spectrum of H_2O_2 and the solar emission spectrum (ASTM) are represented. Hydrogen peroxide absorption and the solar emission between 300-320 nm have been enlarged in order to be able to observe the H_2O_2 absorbance even above 300 nm (see insert in Fig. 4.39).

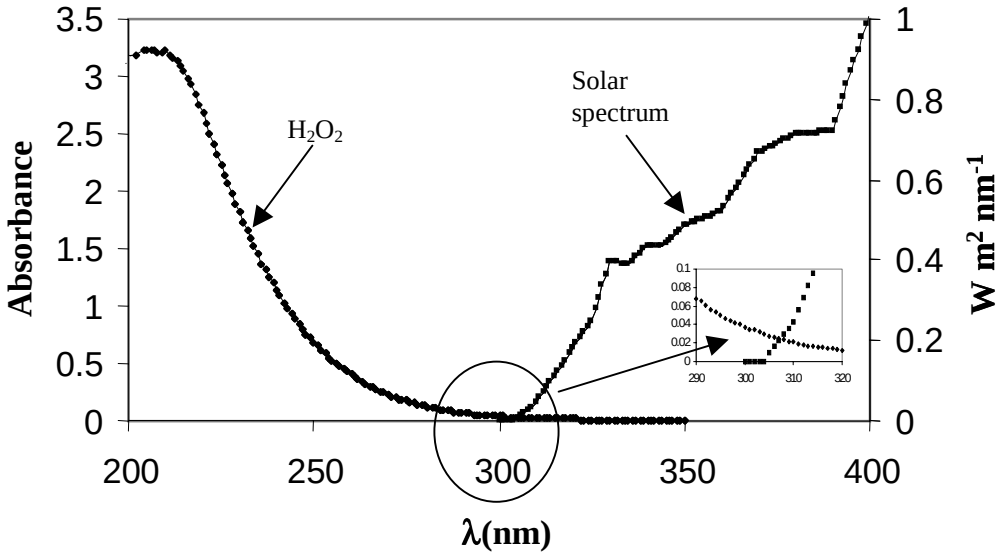

Figure 4.39. UV-vis absortion spectra for H_2O_2 (21.30 mmol.L^{-1}) and sunlight. (O.D., optical path length 1 cm).

The absorbance of solar radiation above 300 nm by a H_2O_2 solution is very small. However, sometimes depending on the amount of UV solar radiation (UV_A+UV_B), this can be enough to cause the H_2O_2 photolysis and in consequence the hydroxyl radical production. This will also depend on the used concentration of H_2O_2, as it will be observed in the experimental results.

In Fig. 4.40 (Ph35, Ph37, and Ph38, Table 4.3), the mineralization of phenol solution by means of H_2O_2/UV-vis system is shown. A high mineralization is reached at higher H_2O_2 concentration, which could be explained by its higher concentration and therefore higher absorbance of the solar light. This fact increases the production of hydroxyl radicals and therefore, the mineralization grade also increases. However, under a certain concentration (21.30 mmol.L^{-1}) the mineralization grade remained constant and even it would be possible to be negatively affected, as it has been happened in previous cases.

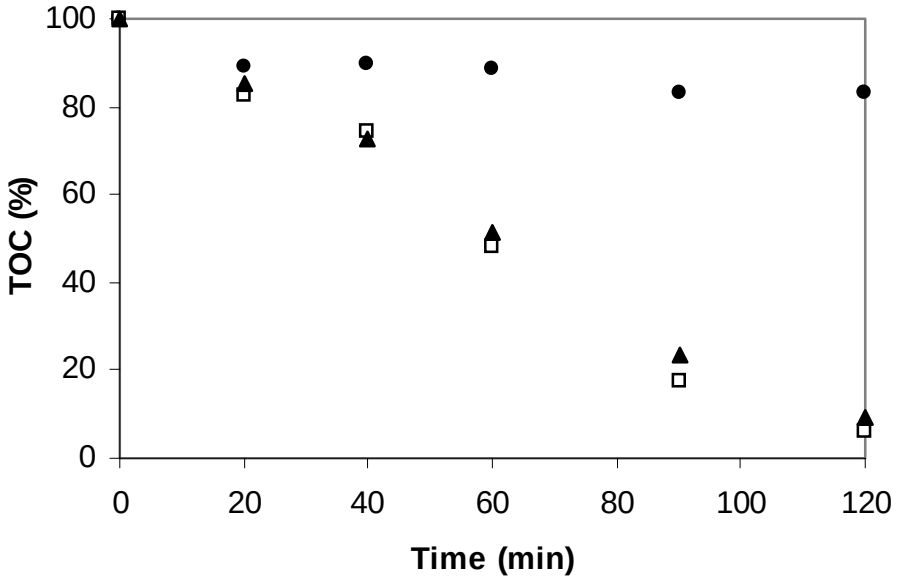

Figure 4.40. Effect of H_2O_2 concentration on the mineralization of phenol by means H_2O_2/UV-vis system. $[phenol]_o$= 1.14 mmol.L^{-1}, T = 298 K. (•) $[H_2O_2]$ = 10.66 mmol.L^{-1}, (□) $[H_2O_2]$ = 21.30 mmol.L^{-1}, (▲) $[H_2O_2]$ = 42.60 mmol.L^{-1}

Although these results are very satisfactory, it is necessary to keep in mind that probably better ones could be obtained in less time using iron as catalyst. In addition, it is necessary to remember that this prototype of CP reactor has been made using quartz tube. However, for industrial and pilot plant scale this kind of tube is not recommended because its very expensive cost in comparison with Pyrex and PTFE (Teflon) tubes. The quartz tube is also a type of tube of difficult handling and the easiness of breaking. In Fig. 4.41 UV-vis absorption spectra of quartz and Pyrex tube is shown. With these spectra it is most clear to see the big influence of the material in this process. The tube of Pyrex almost filters the whole radiation below 350 nm that is the range where H_2O_2 would absorb. This can be confirmed with experiments performed in reactor F, with Pyrex tubes (see Table 4.4) in order to test this treatment method in the CPC solar collector. As it was expected, Fig. 4.42 shows very poor mineralization rate (10%) in 5 hours of treatment. However, the degradation rate of phenol was about 90%.

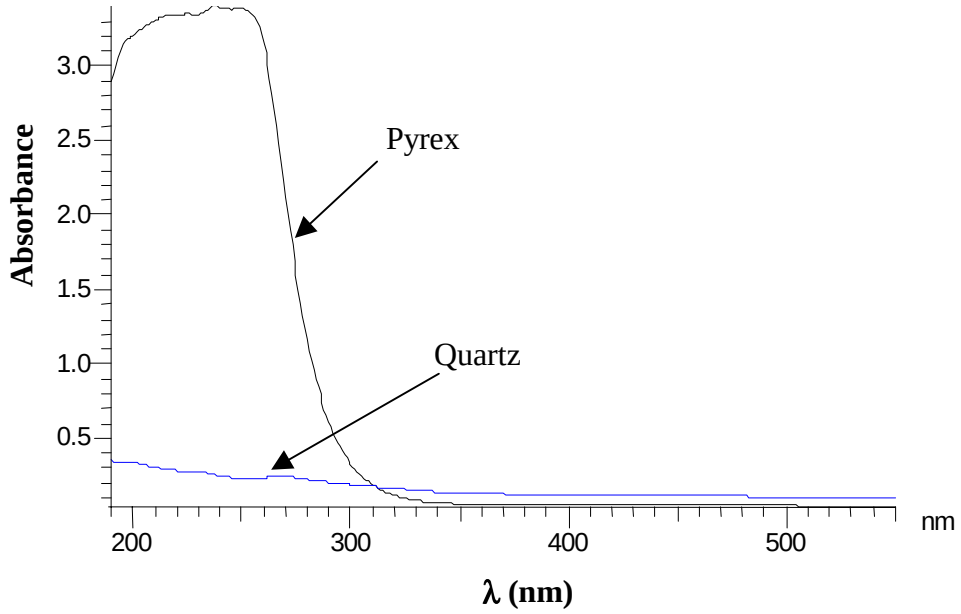

Figure 4.41. UV-vis absorption spectra of quartz and Pyrex tubes. (O.D., optical path length 1 cm)

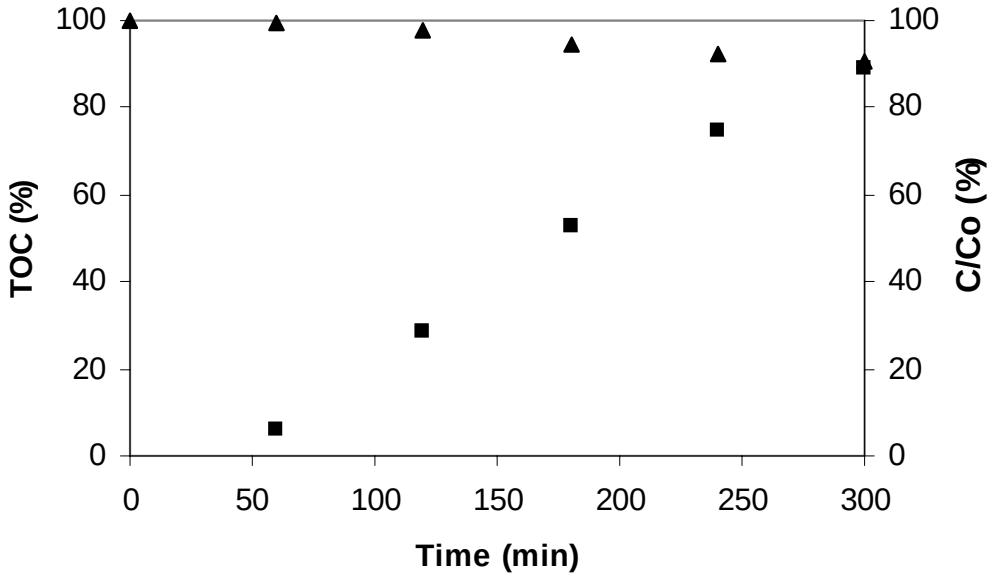

Figure 4.42. Effect of solar irradiation on the mineralization and degradation of phenol by means H_2O_2/UV-vis system in reactor F $[phenol]_o$ = 1.14 mmol.L^{-1}, $[H_2O_2]$ = 21.30 mmol.L^{-1}. (▲) Mineralization (%), (■) Degradation (%)

Thus, even at unfavorable conditions, a high degradation rate was obtained. It is important to stand out that this degradation is achieved when only 10 % of H_2O_2 was consumed. This means that hydrogen peroxide photolysis did not happen and therefore this is the reason for which those poor results were obtained.

4.6.6. Fe^{3+}/UV-vis process

4.6.6.1. Fe^{3+}/UV-vis process with artificial light

This process has been proposed as an alternative to the use of photo-Fenton process, taking into account that hydroxyl radicals can be produced according to eq.1.18 in a more economical way, since it is not necessary the use of H_2O_2. In this sense, some experiments to study the influence of different sources of light in presence of Fe^{3+} in the mineralization of phenol in aqueous solution were performed. Fig. 4.43 shows the effect of the different types of light: UV 254 nm (reactor B), UV 360 nm (reactor C), and Xenon light (solarbox) 300-560 nm (reactor D) on the mineralization of phenol solutions by means of the Fe^{3+}/UV-vis system. The experimental conditions correspond to experiments Ph7, Ph20 and Ph28 (see Table 4.2).

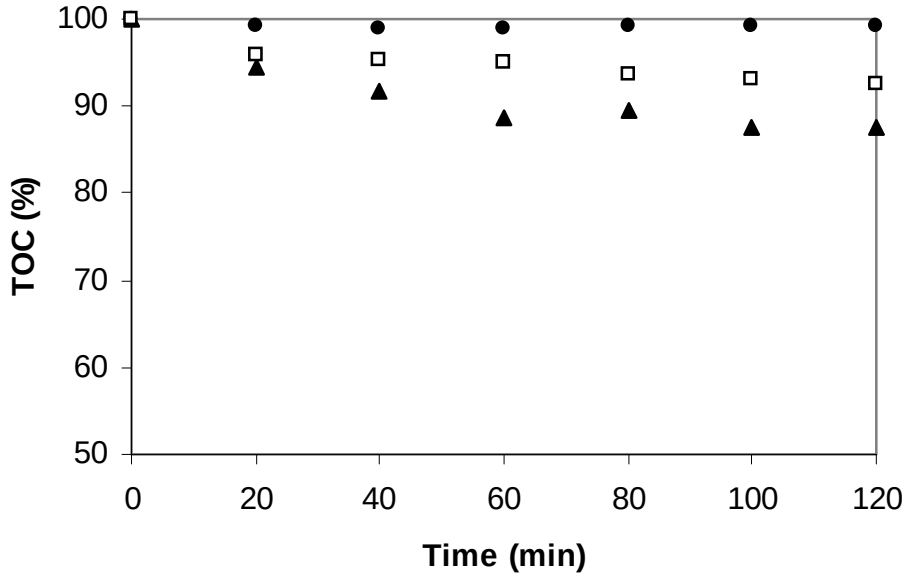

Figure 4.43. Mineralization of phenol solution by means Fe^{3+}/UV-vis artificial light process. $[phenol]_o$ = 1.14 mmol.L^{-1}, $[Fe^{3+}]$ = 1.07 mmol.L^{-1}, 298K. (•) Reactor C, (□) Reactor D, (▲) Reactor B

The degree of mineralization obtained was 0, 7 and 12 % in reactor D, C and B, respectively, after 120 minutes of treatment. Results from experiments carried out in reactor C could be considered surprising, taking into account that iron absorbs strongly in this band of emission of the lamp used by this reactor where the iron absorbs strongly. However, these results are in agreement with the photon-flux entering the reactor, which in this case was smaller as the nominal power of the lamp was also lower (4W). On the contrary, in the other reactors the mineralization reached was 7 and 12 % in reactor D and B in two hours, respectively. This means that the Fe^{3+}/UV-vis process is not very effective if the objective is to obtain the mineralization of phenol solution at the tested conditions. For this reason, the degradation of phenol was also followed by HPLC (Ph7) and 50 % of phenol was eliminated in 2 hours. These values are comparable to those obtained by other research groups with other organic compounds, mainly taking into account that the time of treatment is relatively short (Brand *et al.*, 1997; Mazellier and Bolte, 1997). This leaves open the possibility to use this method when the objective is the elimination of the initial compound in order e.g. to increase its biodegradability.

4.6.6.2. Fe^{3+}/UV-vis process with solar light

Some experiments (Ph38, Ph39, and Ph43, Table 4.3) were carried out in order to study the effectiveness of the Fe^{3+}/UVvis system in reactor E using sunlight. When the pollutant does not absorb the solar light, photo-induced degradation processes appear to be of considerable interest**.** It is just the case of phenol, as it can be seen in Fig. 4.44. As shown in this figure, phenol presents a UV absorption spectrum with a maximum at 270 nm. No absorption is present above 300 nm. It is worth noting that under this experimental condition, no mineralization of phenol solution was observed when the irradiation was carried out in the absence of Fe^{3+} (see section 4.6.1, direct photolysis).

In Fig. 4.45 (Ph38, and Ph39, Table 4.3) the mineralization of phenol solution at different concentrations of Fe^{3+} are presented. The achieved mineralization was close to 10%. Although these results do not represent an important mineralization degree, they come to confirm the higher effectiveness of the treatment process related to direct photolysis. In these experiments the degradation rate of phenol was not followed. However, taking as references the previous results it is possible to affirm that the degradation of phenol should be close to 50 % in 2 hours (see section 4.6.6.1). For

prolonged irradiation time, it could be expected to get a major mineralization and therefore a higher degradation of phenol. In this figure it is also observed that for both Fe^{3+} concentration (1.067 and 2.16 $mmol.L^{-1}$) the same mineralization rate was reached.

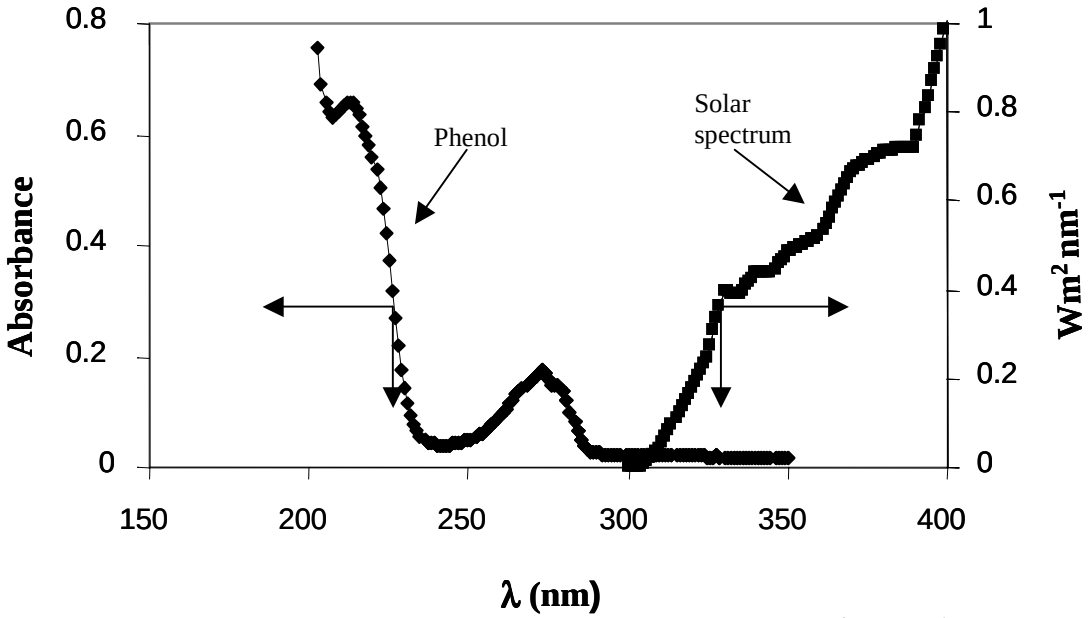

Figure 4.44. UV-vis absorption spectra of phenol (1.5×10^{-4} $mol.L^{-1}$) and sunlight (O.D.=1 cm)

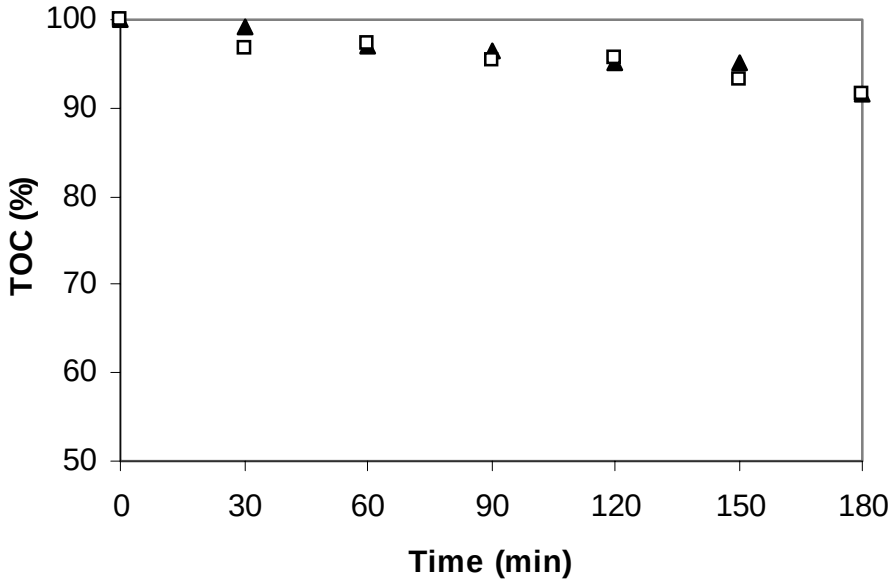

Figure 4.45. Mineralization of phenol solution by means Fe^{3+}/UV-vis solar light process in reactor E. $[phenol]_o$= 1.14 $mmol.L^{-1}$, (▲) $[Fe^{3+}]$ = 1.07 $mmol.L^{-1}$, (□) $[Fe^{3+}]$ = 2.15 $mmol.L^{-1}$

4.6.7. Summary of results with phenol solutions

Due to the diversity of obtained results in previous sections, the more relevant of them are presented in Table 4.8. The three studied processes and some experimental conditions taking into account the used reactor are shown with a brief comment for each one.

Table 4.8. Summary of phenol results

Process	Reactor	Source of light (nm)	Studied parameters	Maximum TOC removal (%)	Figures	Comments
Direct photolysis	B C D E	254 300-400 300-520 Sunlight	Effect of incident light	12 Negligible Negligible Negligible	4.21	*It is not recommended for phenol treatment*
Photo Fenton	B C D E F G	254 300-400 300-520 Sunlight Sunlight Sunlight	Effect of incident light $[H_2O_2]$,$[Fe^{3+}]$ $[Fe^{2+}]$, $[O_2]$	100 80 60 100 60 98	4.22 4.29 4.32 4.36	*It is a very effective treatment method. Sunlight represents a very good alternative source of light.*
Photo Fenton + O_2	B	254	Effect of O_2 content	80 (bubbling O_2) 24 (without O_2)	4.26	*A marked difference is observed when O_2 is bubbling.*
Fenton + UV	B	254	Fenton combined with UV	90	4.27	*Photo-Fenton process could be carried out in two steps.*
H_2O_2/UV	B C D E	254 300-400 300-520 Sunlight	Effect of incident light $[H_2O_2]$	80 Negligible 15 90	4.38 4.40	*Very efficient at UV (254). Good results with sunlight but using quartz tube.*
Fe^{3+}/UV	B C D E	254 300-400 300-520 Sunlight	Effect of incident light $[Fe^{3+}]$	12 Negligible 7 10	4.43 4.45	*It is recommended for phenol degradation but no for mineralization.*

4.7. Results and discussion for NB mineralization

The influence of different sources of light in the mineralization of NB was also studied. However, some parameters that have been widely studied for phenol mineralization were not studied for NB, as it was considered that the effect that they have on the mineralization rate of this compound should be the same. NB experiments were performed with the fundamental objective of applying the processes (direct photolysis, photo-Fenton, H_2O_2/UV and Fe^{3+}) before described on another compound with a marked difference in terms of light absorption. Taking into account that NB is an aromatic compound that absorbs the light, results obtained by the combined processes used will be shown in comparison with direct photolysis.

In Fig. 4.46 the absorption spectra of phenol and NB are shown. The peaks of NB and phenol maximum absorption are reached at 263 and 273 nm, respectively. These spectra have been carried out at the same concentration (15 $mg.L^{-1}$) and the absorption properties of these compounds are certainly different. Therefore, it is reasonable to presume that their behavior in presence of light should be different.

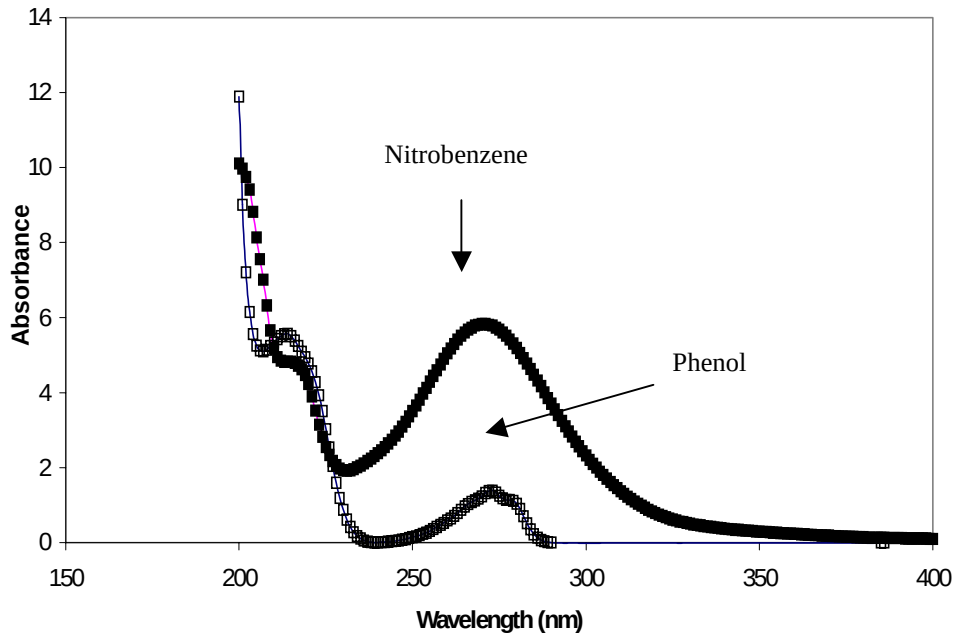

Figure 4.46. UV absorption spectra of phenol and NB (1.5×10^{-4} $mol.L^{-1}$) (O.D.=1 cm)

4.7.1. Direct photolysis of NB by means of artificial and solar radiation.

Several experiments (NB1, NB9, NB12, NB17, NB34, and NB35, Tables 4.5 and 4.6) to study the effectiveness of direct photolysis in the mineralization of NB were carried out. Fig. 4.47 (NB1, NB12, and NB17) shows the effect of three different types of light: UV 254 nm (reactor B), UV-vis 300-520 nm (reactor D) and solar light (reactor E).

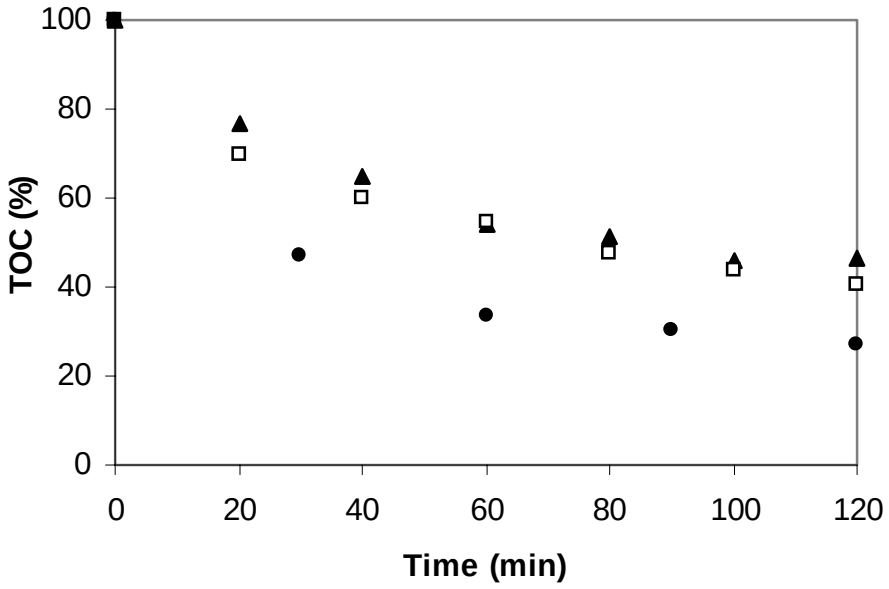

Figure 4.47. Effect of direct photolysis on the mineralization of NB. $[NB]_o$= 1.14 mmol.L^{-1}. (▲) Reactor B, (□) Reactor D, (●) Reactor E

By direct illumination of the aqueous solutions, organic radicals are generated for the photolysis of the substrates. These radical intermediates are subsequently trapped by dissolved molecular oxygen and lead, via peroxyl radicals ($ROO^{\cdot}$), to an enhancement of the overall degradation process. Moreover, the absorption spectrum of the aqueous solutions of NB extends into the lower-energetic UV region of the solar spectrum (UV-A, see Fig. 4.46). Since the parameter μ (see appendix, Table A.6) is directly proportional to the absorption characteristics, NB is able to perform a remarkable absorption of photons up to 400 nm. It is obvious that even high wavelengths (> 250 nm) contribute to the total absorption of NB in a notable manner. Consequently, photoalteration processes of the NB molecules can occur. This fact could help to explain the high effectiveness of direct

photolysis in the mineralization of NB solutions. In Table 4.9 the obtained results for direct photolysis are summarized.

Table 4.9. Mineralization of NB by means of direct photolysis after 2 hours of irradiation

Irradiation Source	UV (253.7 nm) Gemicide lamp (15W)	UV(300-560nm) Xenon lamp (1500W)	UV-vis Sunlight
Mineralization (TOC %)	54	60	73

The best results were reached in a parabolic collector (reactor E). As the dimensions of the reactor used in the solarbox (reactor D) and in the solar experiments (reactor E) are the same, and the radiation spectrum was similar, it is possible to compare the results of the solarbox and the solar light. TOC reduction was greater in the solar reactor, because the absorbed photon flow per unit of reaction volume was higher.

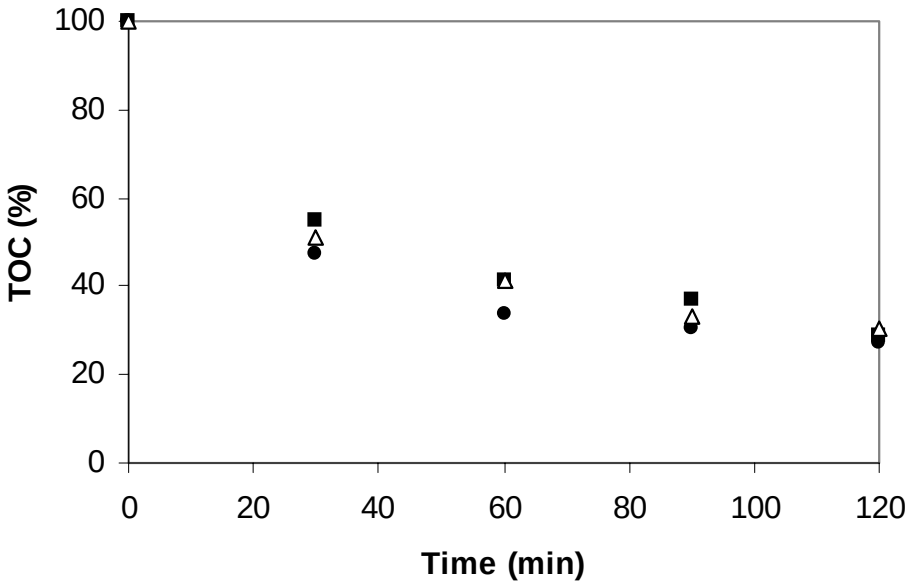

Figure 4.48. Effect of direct photolysis on the mineralization of NB in reactor E. $[NB]_o$ = 1.14 mmol.L^{-1}. (■) NB 34, (△) NB 35, (●) NB 17

In order to assure about these results, photolysis experiments in reactor E were made in triplicate at different dates and different time of the day (NB 17, NB 34, and NB 35, Table 4.6). Fig. 4.48 shows that the mineralization rate in all these cases had a similar tendency. The mineralization degree achieved in these experiments was around 70 % in 2 hours. This fact would confirm that direct photolysis of NB by means of the use of solar light is an effective method for its elimination from aqueous solution.

4.7.2. Photo-Fenton process in presence of artificial and sunlight

The effectiveness of the photo-Fenton as treatment process has been already shown. As it can be observed in Fig. 4.49 a very high degree of TOC reduction (nearly 96%) is obtained in the solar reactor in only 40 minutes of irradiation, when the initial concentrations of Fe^{3+} and H_2O_2 were 1.067 mmol.L^{-1} and 21.3 mmol.L^{-1}. For long irradiation times, the best results were obtained when using sunlight, but the differences in TOC reduction are very small when compared to UV radiation (254 nm). However, especially at initial times, solar light (80% TOC reduction in 20 minutes) is more effective than UV light (50% TOC reduction in 20 minutes). This behavior can be explained by the fact that Fe^{3+} is converted to $Fe(OH)^{2+}$ in aqueous solution. This complex absorbs notably in the range above 300 nm, which leads to a remarkable production of hydroxyl radicals according to eq. 1.18. In spite of the good obtained results when direct photolysis was used, by means of the photo-Fenton process 100% of mineralization rate could be reach in less than one hour. It has to be taken into account, though, that H_2O_2 needs to be used, therefore increasing the treatment costs.

In the same way that in the case of phenol, the key parameters in the photo-treatment of NB were determined. In this sense, optimum values for H_2O_2 and Fe^{3+} were found and they were 21.3 and 0.54 mmol.L^{-1}, respectively. In the case of H_2O_2, the mineralization rate was negatively affected by the progressive increase of H_2O_2 up to 21.3 mmol.L^{-1}.

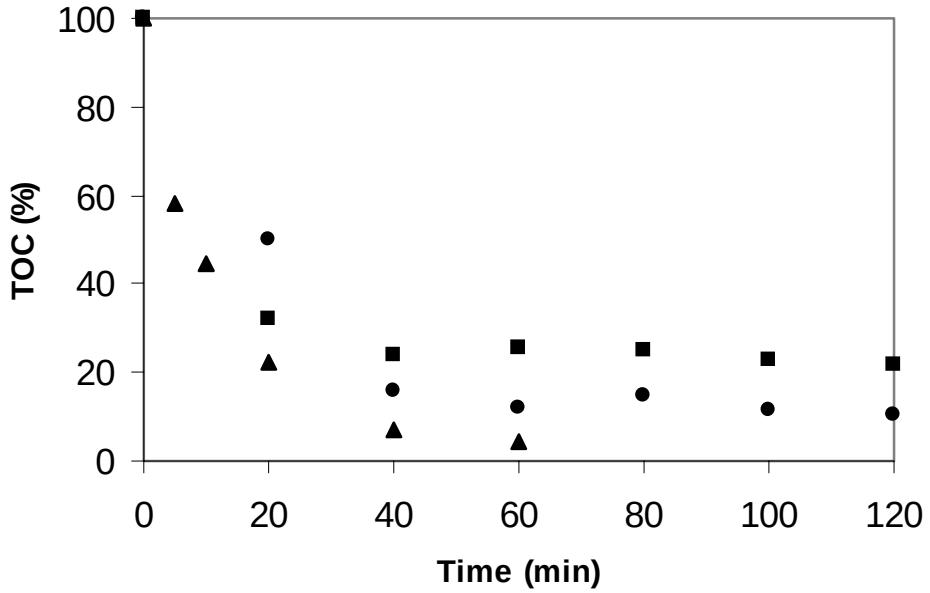

Figure 4.49. Photo-Fenton mineralization of NB using different sources of light. $[NB]_o$ = 1.14 mmol.L^{-1}, $[Fe^{3+}]_o$ = 1.07 mmol.L^{-1}, $[H_2O_2]$ = 21.30 mmol.L^{-1}, (■) Reactor D, (●) Reactor B,(▲) Reactor E

4.7.3. H_2O_2/UV-vis artificial and solar light process

Some experiments (NB3, NB10, NB15, NB24, and NB25, Tables 4.5 and 4.6) were carried out in order to study the effectiveness of H_2O_2/UV-vis in presence of different sources of light in the mineralization of NB in aqueous solution. In Fig. 4.50 the effect of direct photolysis and H_2O_2/UV processes on the mineralization of NB are represented (NB3 and NB1, Table 4.5).

Both experiments were made in reactor B with UV lamps at 253.7 nm. As it has been already demonstrated, the H_2O_2/UV system at this wavelength showed a high effectiveness in the mineralization of phenol solution. However, in the case of NB, the obtained mineralization by means of this process is only 30 %, whereas by direct photolysis it was higher than 50 %. This means that an inhibition effect took place by the competition for the impacting photons between H_2O_2 and NB, that is a very strong light absorbent. In this concrete case, it is very clear that the presence of H_2O_2 in the reaction medium is unfavorable to the mineralization rate.

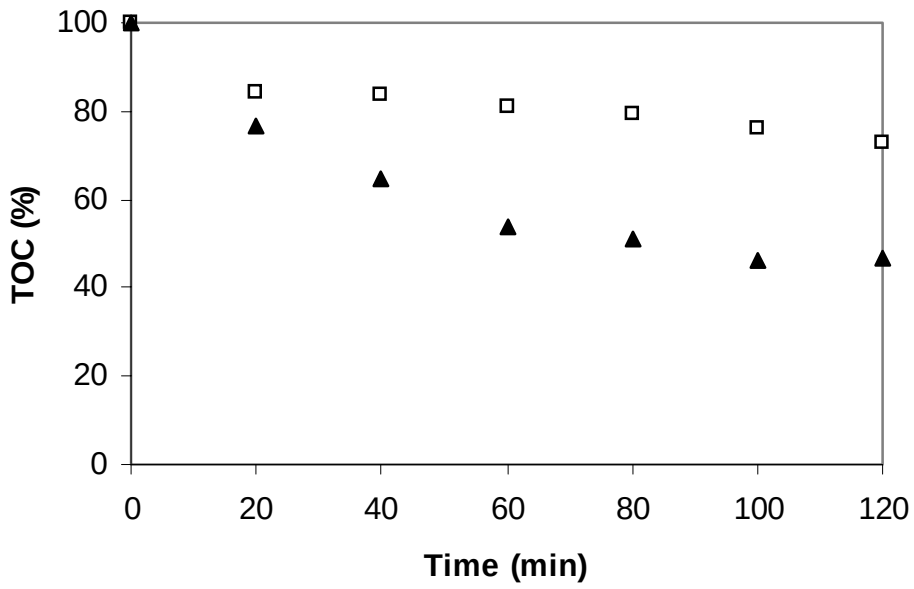

Figure 4.50. Effect of direct photolysis and H_2O_2-UV system on the mineralization rate of NB in reactor B. $[NB]_o$= 1.14 mmol.L^{-1} $[H_2O_2]$ = 21.30 mmol.L^{-1}. (□) H_2O_2/UV system, (▲) direct photolysis

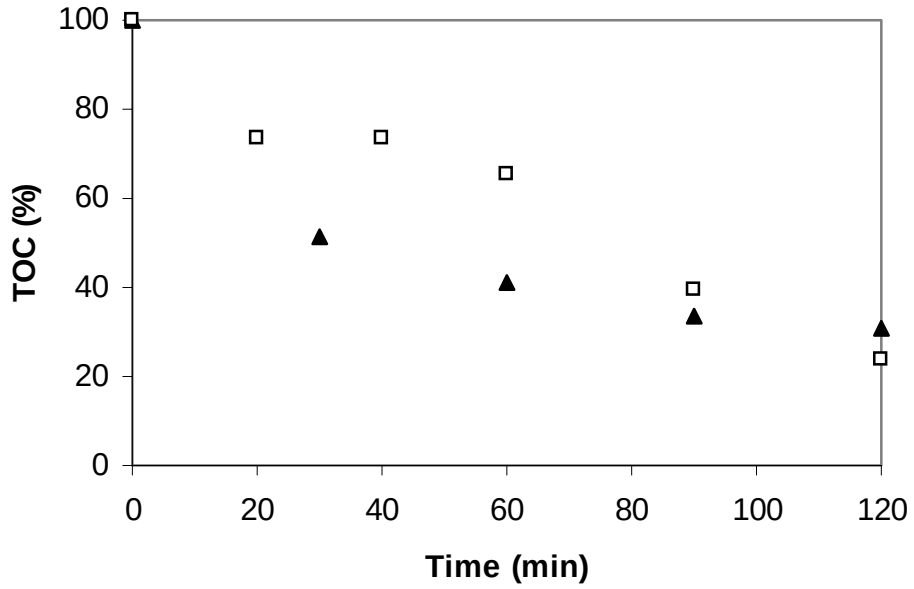

Figure 4.51. Effect of direct photolysis and H_2O_2-UV-vis system on the mineralization rate of NB in reactor E. $[NB]_o$= 1.14 mmol.L^{-1} $[H_2O_2]$ = 21.30 mmol.L^{-1}. (□) H_2O_2/UV system, (▲) direct photolysis.

This study was also made using solar light (see Fig. 4.51). Although hydrogen peroxide does not show good absorption properties in the UV-vis range, total absorption is remarkable due to the relatively high amounts of H_2O_2 in the solution, which results in a kind of competition as it has already been pointed out in the previous case. Therefore, an inhibition effect is also observed but in this case it showed to be more important in the first reaction step. At the end, the mineralization rates of photolysis and H_2O_2-UV-vis system achieved were similar.

4.7.4. Fe^{3+}/UV-vis artificial and solar light process

Experiments were performed using artificial and sunlight in order to test the effectiveness of iron photo-assisted process in the mineralization of NB in aqueous solution (NB2, NB11, NB14, NB23, and NB26, Tables 4.5 and 4.6). In Fig. 4.52 the effect of direct photolysis and Fe^{3+}/UV processes on the mineralization of NB are represented (NB1 and NB2, Table 4.5). Both experiments were carried out in reactor B with UV lamps at 253.7 nm. The results indicated that within 2 h, the mineralization of NB was 30 and 56% by means of iron photo-assisted process and direct photolyis, respectively. This means that the presence of iron in the medium acts as inhibitor of the reaction. These results are not surprising since this process is recommended for the case of pollutants that do not absorb the light, like phenol. As in the case of the UV/H_2O_2 system, an inhibition effect took place by the competition for the impacting photons between Fe^{3+} and NB.

In the case of sunlight, this inhibition effect was much less important, as it can be observed in Fig. 4.53.

These results come to confirm that the iron photo-assisted process works well in presence of compounds that do not absorb the light, in such a way that is better to carry out the treatment via direct photolysis.

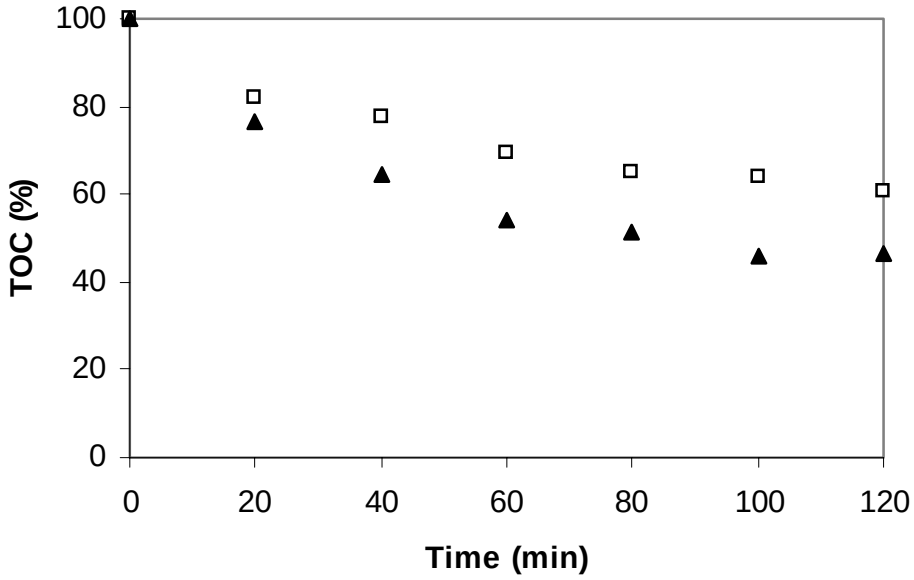

Figure 4.52. Effect of direct photolysis and Fe^{3+}/UV system on the mineralization rate of NB in reactor B. $[NB]_o$ = 1.14 mol.L ^{1} $[Fe^{3+}]$ = 1.07 mmol.L^{-1}. (□) Fe^{3+}/UV system, (▲) direct photolysis

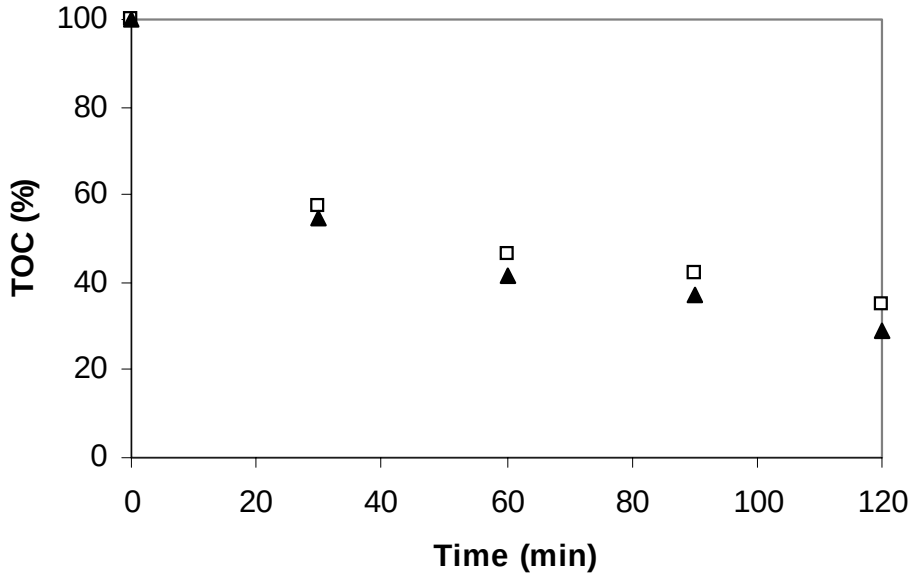

Figure 4.53. Effect of direct photolysis and Fe^{3+}/UV-vis system on the mineralization rate of NB in reactor E. $[NB]_o$= 1.14 mmol.L^{-1}. $[Fe^{3+}]$ = 1.07 mmol.L^{-1}. (□) Fe^{3+}/UV system, (▲) direct photolysis.

4.7.5 Summary of results with NB solutions

In Table 4.10, the main experimental results for NB treatment by means direct photolysis, photo-Fenton, H_2O_2/UV-vis, and Fe^{3+}/UV-vis are summarized. All the studied processes and some experimental conditions taking into account the used reactor are shown making a brief comment for each one.

Table 4.10. Summary of NB results

Process	Reactor	Source of light (nm)	Studied parameters	Maximum TOC removal (%)	Figures	Comments
Direct photolysis	B D E	254 300-520 Sunlight	Effect of incident light	54 60 70	4.47	*It could be recommended for NB treatment.*
Photo Fenton	B D E	254 300-520 Sunlight	Effect of incident light $[H_2O_2]$,$[Fe^{3+}]$	90 70 96	4.49	*It is very effective. Sunlight is a very good alternative source of light.*
H_2O_2/UV	B E	254 Sunlight	Effect of incident light $[H_2O_2]$	30 70	4.50 4.51	*Good results with sunlight but using quartz tube.*
Fe^{3+}/UV	B E	254 Sunlight	Effect of incident light $[Fe^{3+}]$	30 70	4.52 4.53	*It is not recommended for NB treatment.*

4.8.Comparison of the results for phenol and NB mineralization

In this section a comparison between the results obtained for mineralization of phenol and NB in aqueous solution by means of direct photolysis and photo-Fenton is presented. In order to avoid recurrences, H_2O_2/UV-vis and Fe^{3+}/UV-vis were not compared by considering that their differences would be marked by the light absorption properties of each compound and the presence of donating/acceptor groups in each molecule, thus these parameters are analyzed only in the cases of direct photolysis and photo-Fenton process. It

is important to stand out that this comparison was made taking into account the treatment process and the irradiation source used. In this sense, a group of experiments have been selected to show clearly the influence of the treated compounds in the obtained results.

4.8.1. Direct photolysis

Fig. 4.54 shows the effect of three different types of light: UV 254 nm (reactor B), UV-vis 300-520 nm (reactor D) and solar light (reactor E) in the mineralization rate of phenol and NB.

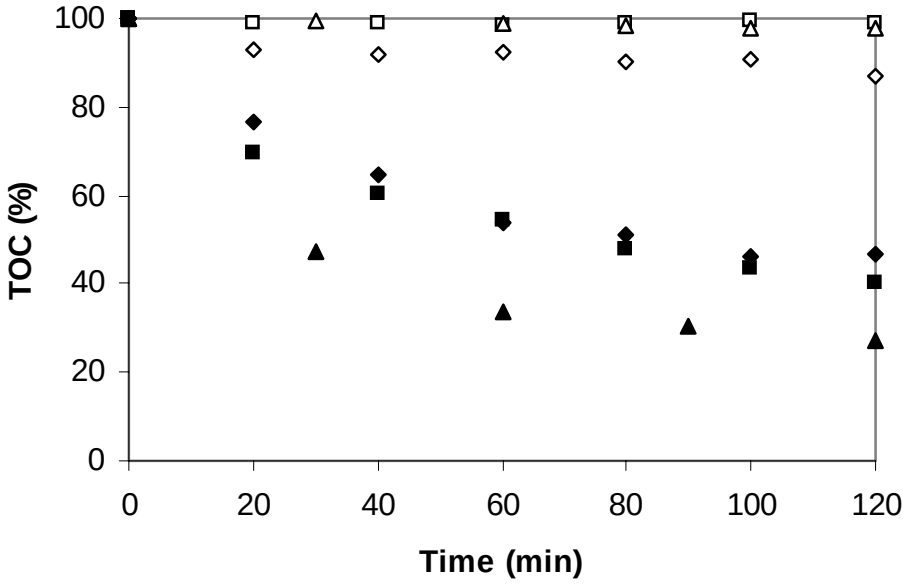

Figure 4.54. Effect of direct photolysis on the mineralization of phenol and NB. [phenol] = 1.14 mmol.L^{-1}, $[NB]_o$= 1.14 mmol.L ^{1}, [phenol] = (△,□,◊); [NB] = (▲,+,♦). (△,▲) Reactor E, (+,□) Reactor D, (◊,♦) Reactor B.

While for phenol the maximum mineralization degree for the different irradiation sources used was 12 %, for NB it was 70%. This difference is closely related with what already commented, i.e. the capacity of NB to absorb the light (see Fig. 4.54). Therefore, in all the processes where the radiation is used, it is necessary to know the behavior of the treated compounds in presence of light. That will give an idea of the contribution of direct photolysis in the photochemical process selected as alternative in the treatment of organic compounds.

4.8.2. Photo-Fenton

As it has been commented before, this treatment process is very effective in the treatment of organic compounds. In Fig. 4.55 the mineralization rates by means of photo-Fenton process in reactor B (254 nm) are presented. In the case of phenol, total mineralization (100%) was reached in 40 minutes and 90 % for NB in 1 h.

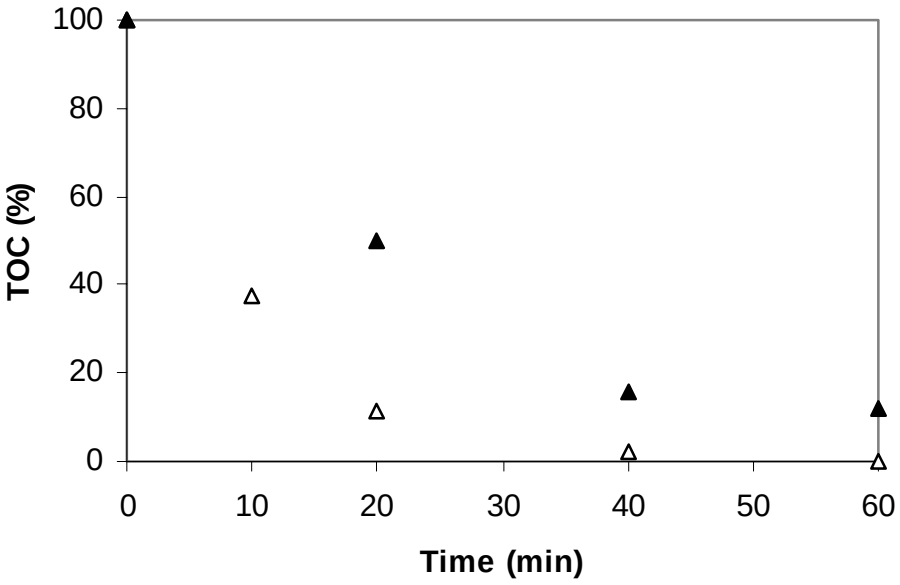

Figure 4.55. Photo-Fenton mineralization of phenol and NB in reactor B. [phenol] = 1.14 mmol.L^{-1}, $[NB]_o$ = 1.14 mmol.L^{-1}, $[Fe^{3+}]_o$ = 1.07 mmol.L^{-1}, $[H_2O_2]$ = 21.30 mmol.L^{-1}.[phenol] = (△); [NB] = (▲)

The difference in the kinetics of mineralization of both compounds could be explained taking into account that the main pathway of the degradation of organic compounds is based on hydroxyl radical attack (generated by means of the photo-Fenton process or by hydrolysis of hydrogen peroxide in presence of UV), which is an electrophilic substitution. Therefore, the effectiveness of a given treatment process depends strongly on the nature of the substrate. In this sense, as it has been already commented in section 3.2.4, in the case of phenol the OH, electro-donating substituent, favors the electrophilic substitution by $HO^{\bullet}$ radical. On the contrary, in the case of NB, the presence of NO_2, electron-accepting substituent, is unfavorable for the eletrophilic substitution. Thus, the $HO^{\bullet}$ radicals produced by means of photo-Fenton process would attack more

easily phenol than NB. Besides this, in presence of UV (254 nm) NB competes with H_2O_2 for the absorption of radiation, therefore the contribution of radicals by means of this reaction would be smaller.

When sunlight was used, the difference in the kinetics of mineralization between phenol and NB by means of photo-Fenton process was much smaller (see Fig. 4.56).

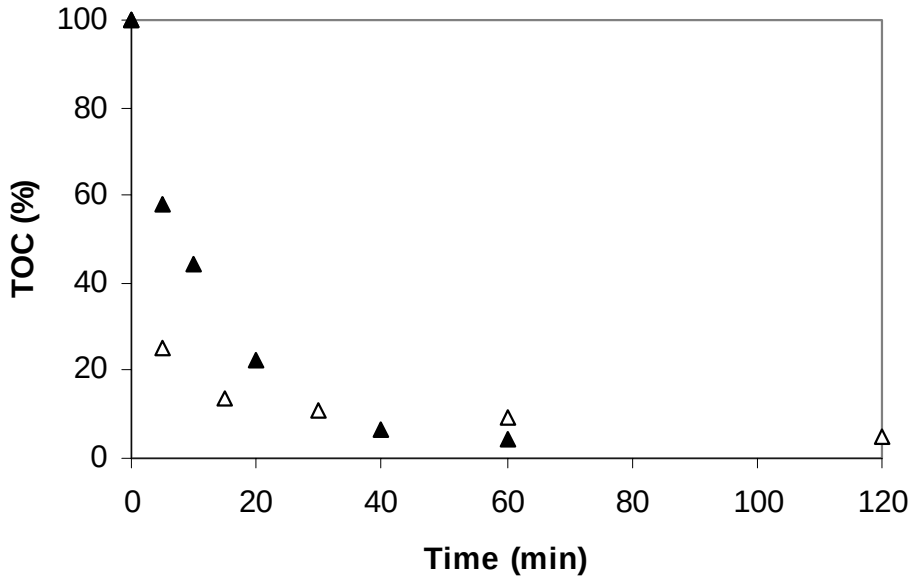

Figure 4.56. Photo-Fenton mineralization ofphenol and NB in reactor E. [phenol]= 1.14 mmol.L^{-1}, $[NB]_o$= 1.14 mmol.L^{-1}, $[Fe^{3+}]_o$ =1.07 mmol.L^{-1}, $[H_2O_2]$ = 21.99 mmol.L^{-1},[phenol] = (∆); [NB] = (▲)

The weak H_2O_2 absorbance within the solar spectrum could account for this, implying that there will not be competition of hydrogen peroxide with NB for the photons entering the reactor and therefore, the direct photolysis of NB is favored. Furthermore, at these wavelengths the improvement by the higher absorption of the iron present contributes to a higher production of hydroxyl radicals, thus kinetics of both NB and phenol is faster in presence of solar light than with 254-UV radiation.

5. Biodegradability enhancement of DCDE in aqueous solution by means of H_2O_2 /UV process

5.1. Introduction

As it has been already mentioned in the general introduction of this thesis, the objective of this chapter is to examine the effectiveness of H_2O_2/UV system in the biodegradability enhancement of dichlorodiethyl ether (DCDE). The fundaments about H_2O_2/UV process were described extensively in chapter 4. DCDE is a non-biodegradable compound (Lewis, 1991; Kaludjerski, 2001) widely used as a solvent throughout the world, and it has been regulated in the USA as a "priority and toxic pollutant" due to its mutagenicity and probable carcinogenecity at a risk level of 0.3 $\mu gr.day^{-1}$ (Fisher, 2000).

The pre-oxidation of recalcitrant organic compounds combined with biological oxidation is a real challenge in order to achieve a widely use of the advanced oxidation processes that are normally limited by the high costs required for its application. In this sense, all the studies directed in this field are of a lot of interest. For this reason, and keeping in mind the effectiveness of the methods that have been used for the treatment of organic compounds (phenol and NB) in chapter 4, the H_2O_2/UV process has been selected as pre-oxidation method of DCDE.

The goal of the study was not to chemically oxidize all organic matter to CO_2 and H_2O, but rather to convert DCDE into products that are readily biodegradable in conventional biological treatment plants. Coupling chemical oxidation and biological process may allow the removal of the target pollutants by using minimum amounts of usually expensive chemical oxidants, followed by a relatively inexpensive, and often already existing biological process, such as activated sludge (Scott and Ollis, 1995; Pulgarin *et al.*, 1999, Parra *et al*, 2000).

The biodegradability of untreated and treated solutions of recalcitrant compounds has been traditionally measured by the Biological Oxygen Demand (BOD) in which a fraction of the solution is diluted by distilled water, and then subjected to a five days test, during which oxygen is consumed by the seed microorganisms. The extent of oxygen uptake within this period was used to evaluate the biodegradability of the compound. Obviously, possible toxicity of the parent compound or the oxidation intermediates to the microorganisms could not be assessed properly because of extensive dilutions. Furthermore, very few of the earlier studies provided rate information on the biodegradation of the oxidation products. Hence, the need for development of a

methodology that can provide fundamental information and better insight into the process of integrated chemical oxidation/biodegradation is clear.

This research attempted to provide this methodology first by oxidizing the model chemical, DCDE, at various levels, and then subjecting the solutions preoxidized at inhibition respiration test and different levels to three different biodegradability tests using activated sludge culture.

The inhibition respiration rate caused by DCDE and its oxidation byproducts was assessed by respirometric test by measuring the oxygen consumption described in experimental section. The rate and extent of biodegradability of the oxidized DCDE solutions was also assessed by short-term and long-term respirometric tests and/or carbon dioxide production as a function of time. The extent of organic matter mineralization during biodegradation was measured through a third test (mid-term) over a 6-hour period by monitoring the COD and TOC of the test solutions. Furthermore, in this study, the responses of acclimated and non-acclimated cultures to non-oxidized DCDE were compared.

5.2. Experimental

5.2.1. Reagents

Table 5.1 shows all the reagents used in the experimentation. All were analytical grade and were used as received.

Table 5.1. List of chemicals used

Compound	*Formula*	*Vendor*	*Purity*
Acetic acid	CH_3COOH	J.T.Baker	99.6%
Ammonium chloride	NH_4Cl	Mallinckrodt	99.99%
Boric acid	H_3BO_3	EM Science	99.5%
Butyric acid	C_3H_7COOH	Alfa Aesar	99%
Calcium chloride	$CaCl_2$	Aldrich	98%
Catalase	-	Sigma	2,390 units/mg
Dibasic potassium phosphate	K_2HPO_4	J.T.Baker	100.4%
Dichlorodiethyl ether	DCDE	Sigma-Aldrich	99%
Ethanol	C_2H_6OH	Aldrich	99.5%

Compound	*Formula*	*Vendor*	*Purity*
Ferric chloride	$FeCl_3$	Aldrich	97%
Glucose	$C_6H_{12}O_6$	Aldrich	100%
Glutamic acid, monosodium salt	$C_5H_8NO_4Na$ x H_20	Acros	99%
Hydrogen peroxide	H_2O_2	Aldrich	30 wt.%
Magnesium sulfate	$MgSO_4$	Aldrich	99%
Manganese sulfate monohydrate	$MnSO_4 \cdot H_2O$	Aldrich	98%
Monobasic sodium phosphate	NaH_2PO_4	Aldrich	99%
Monobasic potassium phosphate	KH_2PO_4	Acros	99%
Potassium chloride	KCl	Aldrich	99%
Potassium dichromate	$K_2Cr_2O_7$	Mallinckrodt	99.9%
Potassium hydrogen phthalate	2-(HO_2C) $C_6H_4CO_2K$	Mallinckrodt	99.95%
Propionic acid	$CH_3CH_2CO_2H$	Alfa Aesar	99%
Silver sulfate	Ag_2SO_4	Mallinckrodt	99.95%
Sodium hydroxide	NaOH	J.T. Baker	98.7%
Sodium chloride	NaCl	Fisher	99.9%
Sulfuric acid	H_2SO_4	J.T. Baker	96.4%
Zinc sulfate	$ZnSO_4$	J.T. Baker	100.7

5.2.2. Experimental device and procedure for chemical oxidation experiments

The UV/H_2O_2 oxidation studies were conducted in an installation based on a 4 L quartz reaction vessel. The circulation of solution by using a peristaltic pump ensures the mixing. The rate of circulation was set at 200 mL.min^{-1}. The cylindrical quartz reaction vessel (diameter of 140 mm and a height of 260 mm) was placed inside a Rayonet Photochemical Reactor (see Fig. 5.1, reactor H), equipped with 8 low-pressure mercury vapor UV (253.7 nm) lamps surrounding the reaction vessel. For each test, the reaction vessel was filled with three liters of DCDE solution (200 mg.L^{-1}), connected to the circulating pump and exposed to UV light. Before the experiments were carried out, actinometry experiments based on the photochemical decomposition of H_2O_2 were performed. Decomposition of H_2O_2 was measured by gas chomatography at various irradiation times to calculate the power of the lamps. The total flux of radiation entering to the reactor was 5.37 x 10^{-6} μEinstein.s^{-1}.

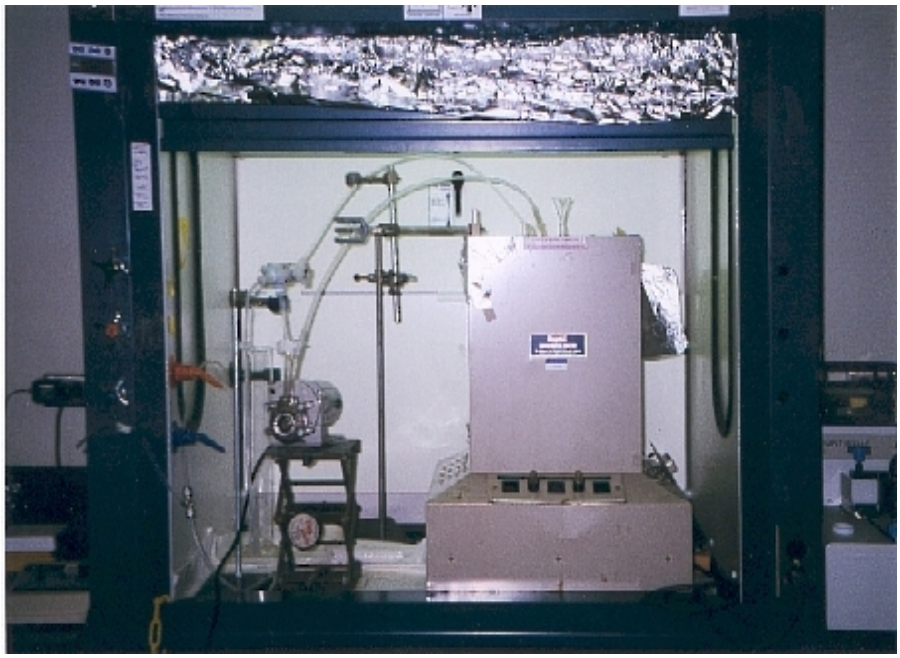

Figure 5.1. Reactor H

Samples from the reaction vessel were withdrawn for analysis utilizing the three-way control valve on the Teflon circulation tubing. Catalase was used to quench any remaining H_2O_2 prior to the biodegradability studies. Specific levels of oxidation were achieved by determining the H_2O_2 addition and UV exposure time required to bring DCDE down to the concentration that corresponded to the desired level of oxidation.

5.2.3. Biological reactors

Heterogeneous microbial populations used in this study were grown in the laboratory in two 5 L stirrer tank reactors, both operated in semi-batch mode (see Fig. 5.2). The original biomass was obtained from the return line of the activated sludge reactor (RAS) in the North City Reclamation Plant, San Diego, CA. The mixed liquor suspended solid concentration in the reactor (MLSS) was adjusted to and maintained at 3,200 $mg.L^{-1}$. The biomass was fed with a mixture of filtered primary effluent and chemical oxygen demand (COD) supplement solution to adjust the strength of the feed to 1,500 $mg.L^{-1}$ as COD. The COD supplement solution was prepared using the modified recipe of Henze (1992) and this solution contained per liter of distilled water:

- 2.5 mL acetic acid
- 2.5 mL butyric acid
- 2.0 mL propionic acid
- 1.0 mL ethanol
- 3.75 g glucose
- 5.0 g glutamic acid monosodium salt
- 80 g dibasic potassium phosphate
- 40 g monobasic potassium phosphate

The primary effluent was collected once a week from the same plant, and the COD supplement solution was prepared in the laboratory. The mixture of filtered primary effluent and COD supplement solution was added to the reactors daily at a volume of 4 liters.

Figure 5.2. Biological reactors. B: Non-acclimated culture; A: Acclimated culture

Upon arrival at the San Diego State University (SDSU) laboratories, the primary effluent was filtered through a high porosity filter paper and then through a glass-fiber filter paper with a pore size of 0.45 μm. The filtrate was refrigerated to slow down the

biodegradation of the organic compounds. Prior to its use, the COD concentration of the primary effluent was measured by the Closed Reflux, Colorimetric method (Standard Methods, 1995). The strength of the feed was adjusted to 1,500 $mg.L^{-1}$ as COD by mixing a predetermined amount of primary effluent with the predetermined amount of the COD supplement solution. Twice daily, 2 L of the supernatant were withdrawn from the reactors to maintain the desired liquid and solid residence times. The operating parameters of the reactors consisted of sludge residence time of 5 days, food to microorganisms ratio (F/M ratio) of 0.375 day^{-1} and a hydraulic residence time (HRT) of 1.25 days. The reactors were aerated with compressed air (1 $Lmin^{-1}$), which maintained about 4 $mg.L^{-1}$ of dissolved oxygen at ambient temperature (22°C ± 2). Once a week, one liter from each reactor was replaced by fresh RAS from the same plant in order to maintain a diverse microbial community. Prior to experimentation, non-acclimated cultures were grown in our laboratories for at least 2 weeks. Also, in order to acclimate the microorganisms, one of the two reactors was fed with 0.4 $mg.L^{-1}$ of DCDE in addition to the mixture of the primary effluent and the COD supplement solution for at least 4 weeks before the experiments were conducted.

5.2.4. Biomass harvesting

A standardized biomass harvesting protocol was used for each experiment. One liter of the biomass was withdrawn from the reactors and the biomass was harvested by centrifugation at 3,500 rpm for 15 minutes. Supernatant was discarded and the solids were resuspended in one liter of mineral salt solution (MSS). Ten milliliters of the suspension were filtered through a glass fiber filter; after the filter was dried for two hours at 105 degrees Celsius, suspended solid concentration was determined. The mineral salt solution was used to avoid osmotic shock to the microorganisms and it contained per liter of distilled water:

- 20 mg ammonium chloride
- 0.03 mg ammonium molybdate
- 0.06 mg boric acid
- 27.5 mg calcium chloride
- 86 mg dibasic potassium phosphate
- 217.5 mg monobasic potassium phosphate

- 26.2 mg monobasic sodium phosphate
- 0.25 mg ferric chloride
- 22.5 mg magnesium sulfate
- 0.04 mg manganese sulfate
- 0.04 mg zinc sulfate

The biomass concentration was adjusted with MSS to yield 2000 $mg.L^{-1}$ as MLSS.

5.2.5. Experimental device and procedure for inhibition study

A modified version of the Organization of Economic Cooperation (OECD) Method 209 (OECD, 1981) was used to monitor respiration rates and quantify inhibition caused by DCDE and its oxidation byproducts. Six samples were poured into biological oxygen demand (BOD) bottles and continuously stirred with Teflon- coated magnetic stir bars. Dissolved oxygen (DO) probes (Orion, Model #97-08) were fitted securely with plastic inserts through the openings of the BOD bottles so no air could enter or escape. The plastic inserts came with the DO probe equipment and they are designed specifically to fit the DO probe and a standard BOD bottle (see Fig 5.3). Cables from the DO probes led to a data acquisition board (IO Tech, Model DynaRes-8U) that transferred data for dissolved oxygen concentrations to a personal computer. Prior to each experiment, DO probes were calibrated at their zero point and for air concentration (approximately 6.5 $mg.L^{-1}$) using designated dials on the probes.

The biomass concentration was adjusted to 2000 $mg.L^{-1}$ as suspended solids with MSS after harvesting and placed in 60 mL aliquots to each BOD bottle so that in the final volume of 300 ml the concentration was consistent at 400 $mg.L^{-1}$ as suspended solids. In addition, in each experiment, one BOD bottle was used to measure the endogenous respiration that means only biomass without any substrate. Two additional bottles were used to measure the exogenous respiration using a biogenic substrate (acetate) and three more to measure inhibited exogenous respiration (acetate plus inhibitor). The endogenous respiration rate was calculated from the measurement of oxygen depletion over time by activated sludge in its “resting state”. Since the microorganisms at this stage are without food, they are not very active. Hence, their oxygen demand is minimal. The exogenous respiration rate was calculated from the rate of oxygen depletion in the presence of a

readily biodegradable substance. Since the microorganisms are actively biodegrading the substrate, their oxygen demand is high and the concentration of dissolved oxygen in a closed system drops dramatically. In these studies, acetate was used as a readily biodegradable substance. Lastly, inhibited exogenous respiration rate represents the decrease in the rate of oxygen consumption over time in a system with microorganisms and acetate in the presence of a potentially inhibitory compound or combination of compounds.

Figure 5.3. Dissolved Oxygen probes

To check the inhibition of DCDE four experiments were performed using solutions with UV/H_2O_2–treated DCDE after 25, 50, 75 and 100% oxidation. The initial concentration of DCDE solution prior to oxidation was approximately 200 $mg.L^{-1}$ for all experiments. The level of oxidation achieved was within 5% of the desired level. Test samples were capped prior to the inhibition studies to avoid volatilization of DCDE. All experiments were performed for acclimated and non-acclimated culture.

5.2.6. Experimental device and procedure for biodegradation experiments

As it has been already commented in the introduction, the biodegradation studies were conducted by using three different tests, whose fundaments and its application form are explained next.

5.2.6.1. Short-term test.

The short-term biodegradation test involved the measurement of biomass respiration rate by oxygen probes for a period of 30 minutes. This test was conducted using DCDE over a wide concentration range while keeping the biomass concentration constant at 400 mg L^{-1} as suspended solids. This concentration of microorganisms was chosen to yield a significant oxygen decrease within 30 minutes of experimentation, thereby allowing accurate measurement of respiration rates. A modification of the (OECD) Method 209 (OECD, 1981) was also followed as the experimental protocol for the short-term tests. The method was based on the measurement of endogenous and exogenous respiration rates with dissolved oxygen (DO) probes. The experiments were conducted in the same experimental devices used for inhibition test (see Fig. 5.3).

The short-term biodegradation tests were performed with both non-acclimated and acclimated microorganisms. For this method the biomass concentration was also adjusted to 2000 $mg.L^{-1}$ as suspended solids with MSS after harvesting and placed in 60 mL aliquots to each BOD bottle so that in the final volume of 300 mL the concentration was consistent at 400 $mg.L^{-1}$ as suspended solids. Samples of oxidized DCDE solutions were then added to the BOD bottles in different dilutions and the volumes were made up to 300 mL with distilled water. Yeast extract (0.15 $mg.L^{-1}$) was added to each BOD bottle before starting the experiments to provide the necessary macronutrient for the microorganisms. The oxidized solutions of DCDE and a non-oxidized DCDE solution containing 200 $mg.L^{-1}$ of DCDE were tested in triplicate. The duration of the experiments were kept at 30 minutes in order to prevent further acclimation of microorganisms as well as prevent complete depletion of oxygen. Using DO probes attached to a highly sensitive data acquisition system allowed the collection of data at a very high speed: one data point per second per bottle. The respiration rate of the microorganisms in each bottle was determined by measuring the oxygen concentration as a function of time, and by calculating the corresponding slopes using Microsoft Excel spreadsheet.

The endogenous rate of respiration of microorganisms was obtained by running a control experiment with microorganisms alone. The net exogenous respiration rates for DCDE solutions were obtained by subtracting the endogenous rate from the observed exogenous respiration rates. The net exogenous respiration rates that are directly proportional to the substrate removal rate were substituted in the Monod equation to

$$-\frac{dS}{dt} = \mu = \frac{\mu_{max} \cdot S}{S + K_s} \quad (5.1)$$

determine the specific substrate removal rate constants:

Where,

μ = specific growth rate

μ_{max} = maximum specific growth rate

S = substrate concentration

K_s = half-saturation constant

The constants, μ_{max} and K_S were determined through non-linear curve fitting. The calculations of kinetic constants and statistical significance tests were performed by using Sigma Plot software for the 95% confidence level. Comparison of the kinetic constants obtained for the oxidized samples and the non-oxidized samples allowed the assessment of the extent of improvement of biodegradation.

5.2.6.2. Long-term test

The long-term respirometric experiments were conducted over a period up to 14 days to obtain information on biodegradability and toxicity of the by-products of oxidation and of the parent compound. These data allowed us to see if prolonged exposure would prompt microorganisms to develop the necessary enzymes for degradation of DCDE and/or the oxidation by-products, or would result in toxicity and killing of the microorganisms.

A ten channel Micro Oxymax Respirometer (Columbus Instruments International Corporation, Columbus, OH), equipped with oxygen and carbon dioxide sensors and a computer interface, was used to assess the improvement in the biodegradability of DCDE after 0, 25, 50, 75 and 100% oxidation of DCDE by H_2O_2/UV system (see Fig.5.4). The respirometric technique involved placing the oxidized or non-oxidized solutions with microbial inocula into sealed 250 mL bottles and continuously measuring oxygen consumption and the production of carbon dioxide by the bacteria as they grow under batch conditions while degrading the substrate.

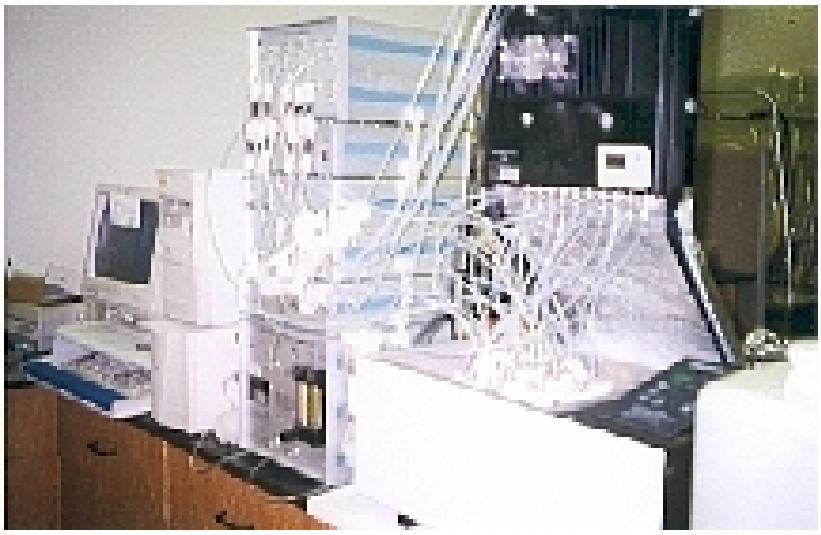

Figure 5.4. Micro Oxymax Respirometer

The respirometer was used for continuous measurement of oxygen and carbon dioxide in the gas phase up to 14 days. The process involved automatic gas withdrawal from the test chambers, which was pumped through the gas sensors and then returned to the test chambers. The percent oxygen and carbon dioxide gas levels of the test chamber environment were measured every 3 hours and the changes in the levels were used to compute oxygen consumption and carbon dioxide production. Micro Oxymax software stored the data obtained during the experimental period directly to a hard disc.

Respirometric studies were conducted with acclimated and non-acclimated cultures of microorganisms harvested from the activated sludge reactors as before. The appropriate amount of biomass was placed into the respirometer bottles to result in 400 $mg.L^{-1}$ of biomass as suspended solids along with the oxidized solutions diluted by 50%. The bottles were capped and the experiments started. All the tests were run in duplicates.

The experiments included three levels of controls, each with duplicates: 1) Test with no microorganisms (no mo), 2) Test with microorganisms and 100 $mg.L^{-1}$ of non-oxidized DCDE (no oxidation), and 3) Test with microorganisms alone (endogenous).

5.2.6.3. Mid-term test

These experiments were designed to present data in terms of degradation of the biodegradable organic matter, as measured by the changes in TOC and COD content of the solutions as a function of time. The total amount of oxidation by-products that were biodegradable within 6 hours was then determined and compared among different treatments. Six hours was used as the time span because 1) the rate of biodegradation as measured by COD or TOC change leveled off beyond 6 hours, and 2) 6 hours is a typical hydraulic residence time in wastewater treatment plants.

The amount of TOC and COD due to the parent compound (DCDE) was subtracted from the total measured concentrations of TOC and COD, and the remaining amounts of TOC and COD were attributed to the oxidation products. The theoretical chemical oxygen demand of 1 mg of DCDE is 160/143 = 1.12 mg. Hence, the COD contributed by the oxidation products, i.e., "the non-parent COD" was estimated as follows: npCOD = (Total COD – $1.123C_{DCDE}$). Non-parent TOC for this purpose was defined as the TOC contributed by the chemical oxidation products, and it was estimated by subtracting the TOC attributable to DCDE from the total TOC, i.e., non-parent TOC = npTOC = total TOC – $0.34C_{DCDE}$, where total TOC is the measured TOC value, C_{DCDE} is the measured concentration of DCDE, and 0.34 is the theoretical amount of TOC per mg of DCDE.

A different experimental system was set up to conduct the mid-term biodegradation tests. These experiments were conducted in duplicates in 1-L glass bottles open to the atmosphere (see Fig 5.5). Air was supplied with glass diffusers with a flow rate of 1.65 $L.min^{-1}$. The concentration of microorganisms, measured as mixed liquor suspended solids (MLSS), was adjusted to 400 $mg.L^{-1}$, with dilution of all samples by 50% once DCDE solution was added.

The mid-term experiments were performed using 100% oxidized DCDE by H_2O_2/UV either acclimated or non-acclimated cultures. Over 24 hours, samples (20 mL) were withdrawn every 1.5 hours, filtered directly into 20 mL vials through 0.2 μm pore filter papers, and the filtrate immediately analyzed for DCDE concentration. The remaining filtrate was acidified with H_2SO_4 and stored at 4°C. The measurements of suspended solids, COD and TOC were performed within 24 hours.

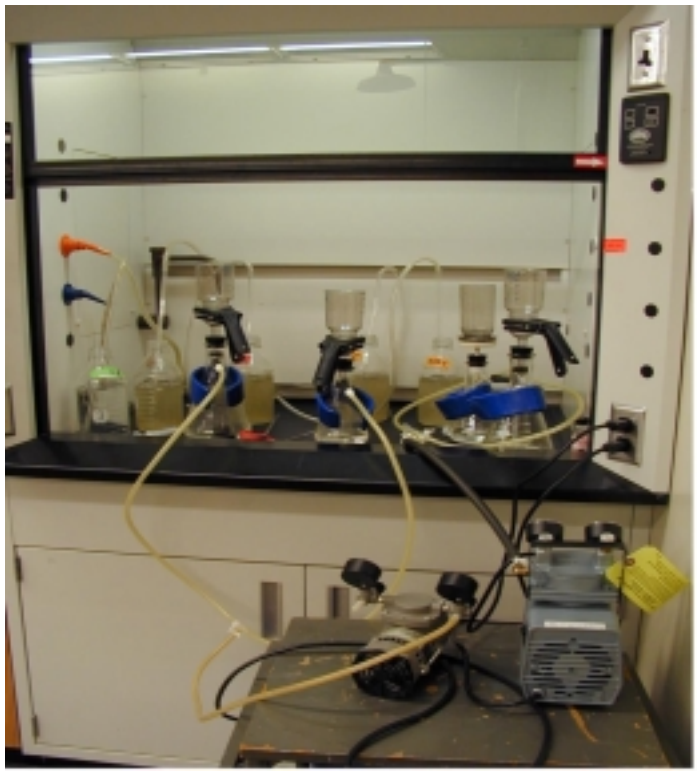

Figure 5.5. Experimental device for Mid-term test

5.2.7. Analytical determinations

In order to maintain accuracy and consistency during inhibition and toxicity studies, standard analytical methods were established. Measurements of DCDE concentration, detection of residual H_2O_2 and COD concentration were all critical factors. These factors were carefully monitored by the following methods.

5.2.7.1. DCDE concentration measurement

In order to confirm that DCDE initial concentration was approximately 200 $mg.L^{-1}$ prior to oxidation and to verify the degree of oxidation immediately after oxidation, a Shimadzu gas chromatograph was used. The machine was equipped with a flame ionization detector that was fueled by hydrogen and air. The aqueous samples were analyzed immediately after collection by directly injection into a Nukol column (15 m x 0.53 mm with 0.5 mm film) that was obtained from Supelco (Bellefonte, PA). Helium was used as carrier gas at a flow rate of 15 $mL.min^{-1}$. The injector and detector were operated at

temperatures of 150ºC and 250ºC, respectively. The initial column temperature was 80ºC, and it was increased to 200ºC at the rate of 5ºC min^{-1}. Calibration prior to concentration measurement was performed with DCDE samples ranging in concentration from 40 to 200 $mg.L^{-1}$.

5.2.7.2. Hydrogen peroxide

Hydrogen peroxide concentration was measured using Titanium (IV) chloride reagent for low concentration and the permanganate method for high concentration.

Titanium (IV) chloride method

The titanium (IV) chloride reagent was prepared by adding 10 mL of water-white titanium (IV) chloride dropwise to 10 mL of 6N hydrochloric acid. Both of the titanium chloride and the HCl were chilled on crushed ice for 30 min prior mixing. The mixture was left standing on ice until complete dissolution of solids. The mixture was then diluted to one liter with 6N HCL. This reagent was calibrated against and H_2O_2 aliquot of known concentration prior to use. In the calibration procedure, one-to five- milliliters of H_2O_2 aliquot were transferred to 10 mL volumetric flasks and diluted to volume with the titanium (IV) chloride reagent. The absorbance of the yellow peroxytitanium acid formed was then measured at 415 nm in 10-mm quartz cells against a blank of titanium (IV) chloride reagent.

Permanganate method

Measures of H_2O_2 in the stock solution and in the aliquout used to calibrate the titanium (IV) chloride reagent was conducted by titration against potassium permanganate. In this procedure, a working solution was prepared by adding 10 mL of H_2O_2 stock solution (~ 30% H_2O_2) to 1 liter of distilled water. 25 mL of the working solution was acidified with 10 mL of 1:5 sulfuric acid and titrated against 0.1 N potassium permanganate. The titration was repeated four times and the concentration in the working and stock solutions were calculated accordingly:

$$5\ H_2O_2 + 2\ MnO_4^- + 6\ H^+ \rightarrow 5O_2 + 2\ Mn^{2+} + 8\ H_2O$$

5.2.7.3. Total organic carbon (TOC)

The total organic carbon (TOC) was measured in this case by direct injection of the filtered samples into a using a Shimadzu 5000A, TOC analyzer with an ASI automatic sample injector.

5.2.7.4. Chemical oxygen demand (COD)

The chemical oxygen demand (COD) of the samples was measured by the closed reflux, colorimetric method according to the Standard Methods, 5220-D (1995).

5.2.7.5. Total suspended solids

Total suspended solids in samples were measured by the gravimetric method (Standard Methods, 2540-D) (1995).

5.3. Range of experimental variables for DCDE oxidation experiments

DCDE solutions were prepared with Milli-Q water at 200 $mg.L^{-1}$ with no pH adjustment and using no carbonate. Hydrogen peroxide was added at the beginning of the three experiments and the DCDE/H_2O_2 $mol.L^{-1}$ ratios were 1.2, 0.75 and 0.65, respectively. In other experiments hydrogen peroxide was added in a stepwise procedure, in order to attain a slow reaction rate. For this procedure 0.97 $mmol.L^{-1}$ of H_2O_2 was added every five minutes. When it was added at the beginning, the reaction was very fast. The most significant removal of DCDE occurred in a short period of time and it was function of H_2O_2 concentration. The remaining H_2O_2 concentration was measured by titanium (IV) chloride method. Finally, pH and temperature were also monitored during the experiments.

5.4. Results and discussion for DCDE chemical oxidation experiments

Several experiments were performed to oxidize DCDE by means direct photolysis and H_2O_2/UV systems. In these oxidation experiments the objective was to find the optimal conditions of the process in order to obtain 25 %, 50 %, 75%, and 100% removal of DCDE in a reasonable irradiation time.

5.4.1. Direct photolysis

First of all, direct photolysis experiments were performed to know the influence of UV radiation in the oxidation of DCDE. Concentration of DCDE was monitored with irradiation time. The results, indicate significant reduction in DCDE concentration. DCDE concentration was reduced by 25 % after 60 minutes and by 55% after 120 minutes of irradiation time (see Fig. 5.7).

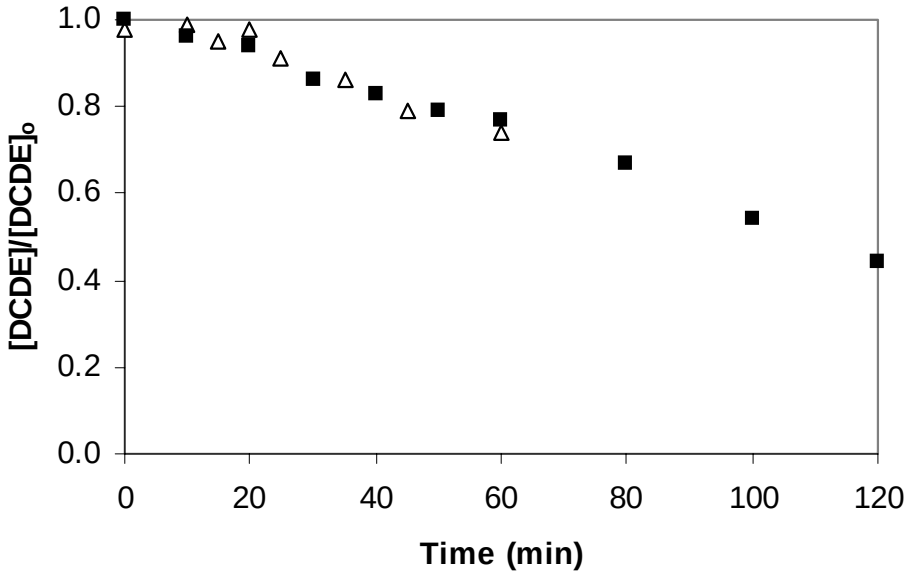

Figure 5.7. Removal of DCDE by means of direct photolysis. $[DCDE]_o = 200$ mg L^{-1}. (△) 1 h irradiation time, (■) 2 h irradiation time

On the contrary, by monitoring Total Organic Carbon (TOC) during direct photolysis experiments revealed that there was no significant change in total carbon content of the solution as shown in Fig.5.8.

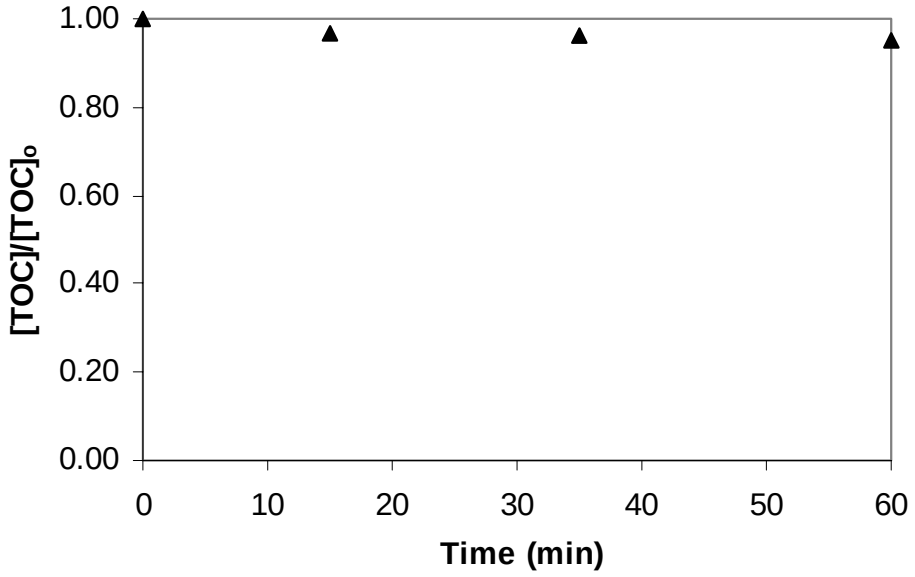

Figure 5.8. TOC removal by means of direct photolysis $[DCDE]_o = 200$ mg.L^{-1}

Changes in pH and the temperature were also monitored during the experiments. An increase of 5.3 degrees Celsius was observed in the case of temperature and a decrease in the case of pH from 6 to 4. The temperature increase was attributed to the heating effect of UV light in spite of the cooling system with air of reactor H. The pH change should be probably to formation of some carboxylic acids.

5.4.2. Influence of H_2O_2 concentration

Experiments were conducted to determine the effect of H_2O_2 concentration in presence of UV (254 nm) radiation in the oxidation of DCDE. Hydrogen peroxide was added at the beginning of the experiments at DCDE/H_2O_2 molar ratios of 1.2, 0.75 and 0.65 (40, 65, 75 mg.L^{-1} H_2O_2 respectively). A high oxidation rate was reached at higher H_2O_2 concentration because the quantity of hydroxyl radicals production increased when increasing the concentration of H_2O_2 (see Fig.5.9). However, as it has been already demonstrated in chapter 4, above certain concentration of H_2O_2, this effect is considered negligible and in some cases it could be negative. In this case above 65 mg.L^{-1}of H_2O_2 the oxidation rate is the same, indicating that 65 mg.L^{-1} was the optimal H_2O_2 concentration under the experimental conditions. As it has been expected, very fast reaction rates were

observed with H_2O_2/UV system as shown in Fig.5.9 in comparison with direct photolysis rate presented in Fig. 5.7. This shows that DCDE reacts with hydroxyl radicals faster than it photolyzes.

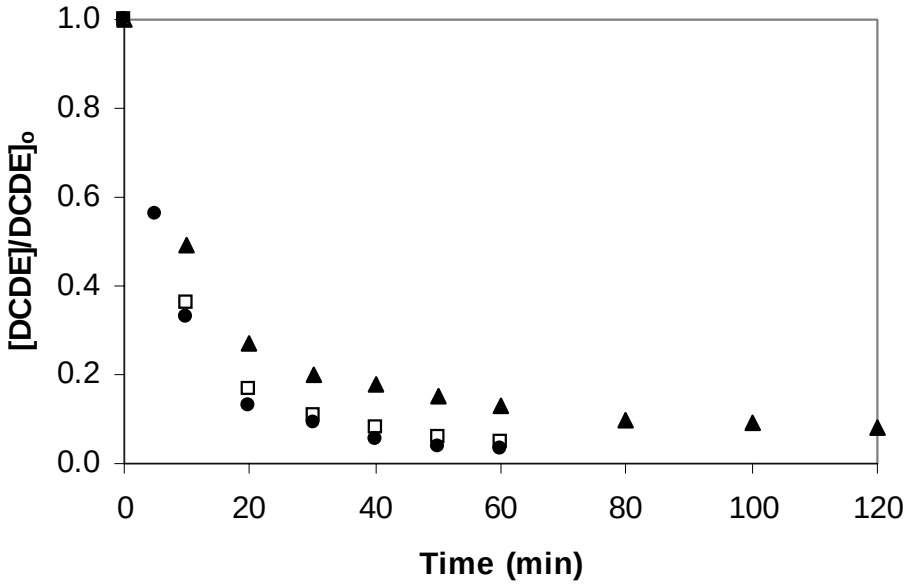

Figure 5.9. Removal of DCDE by means of H_2O_2/UV system. $[DCDE]_o = 200$ mg.L^{-1}.(▲) $[H_2O_2]$ = 40 mg.L^{-1}, (□) $[H_2O_2]$ = 65 mg.L^{-1}, (●) $[H_2O_2]$ = 75 mg.L^{-1}.

Considering that the presence of hydrogen peroxide concentration remained in solution after oxidation process could affect the microorganisms, its concentration determined by titanium (IV) chloride method was monitored and quantified. In Fig. 5.10, H_2O_2 remaining versus time is shown.

These preliminary results showed that a very fast initial kinetic removal of DCDE is obtained even lower H_2O_2 concentrations (see Fig. 5.10). For this reason, and taking into account that the objective of this pre-oxidation step was to obtain different DCDE oxidation levels (25, 50, 75 and 100%), additional experiments were necessary and H_2O_2 was added in a stepwise procedure in order to attain a slower reaction rate. For this procedure 0.97 mmol.L^{-1} of H_2O_2 was added to the solution every five minutes. The lamps were turn off before each adding. The largest drop in DCDE concentration occurred initially, and the rate was directly proportional to the H_2O_2 concentration. This stepwise procedure allowed us to oxidize DCDE by 25 %, 50 %, 75%, and 100% in a reasonable

irradiation time around 60 minutes. These results are presented in Fig. 5.11. The oxidation grade in all the experiments was obtained within ± 5 %. All the experiments were performed several times in order to check its reproducibility as it can be seen in the two examples show in this figure. Therefore, DCDE solutions pre-oxidized at 25, 50, 75 and 100% has been used as model solutions in all biodegradability tests in this work.

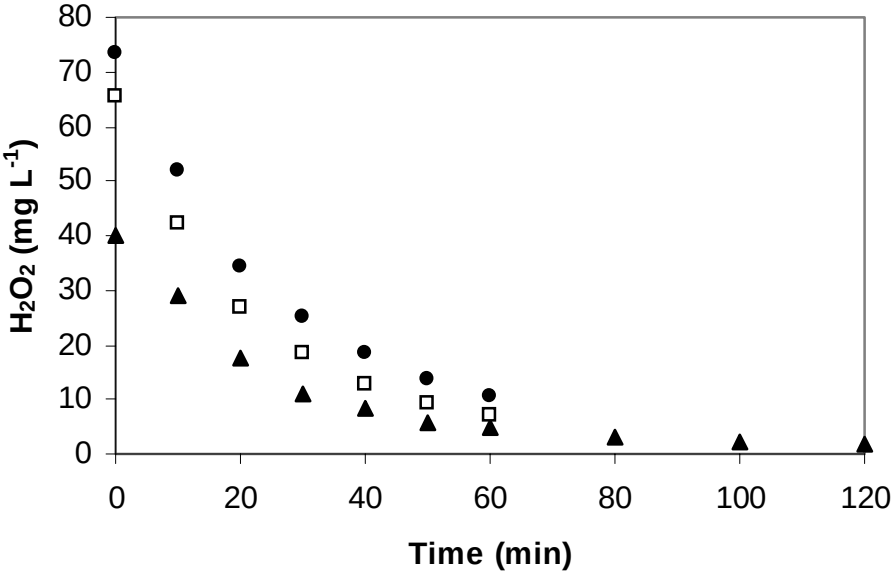

Figure 5.10. Hydrogen peroxide remaining after DCDE removal. $[DCDE]_o$ = 200 $mg.L^{-1}$. (•)$[H_2O_2]$ = 75 $mg.L^{-1}$,(□)$[H_2O_2]$ = 65 $mg.L^{-1}$(▲)$[H_2O_2]$ = 40 $mg.L^{-1}$.

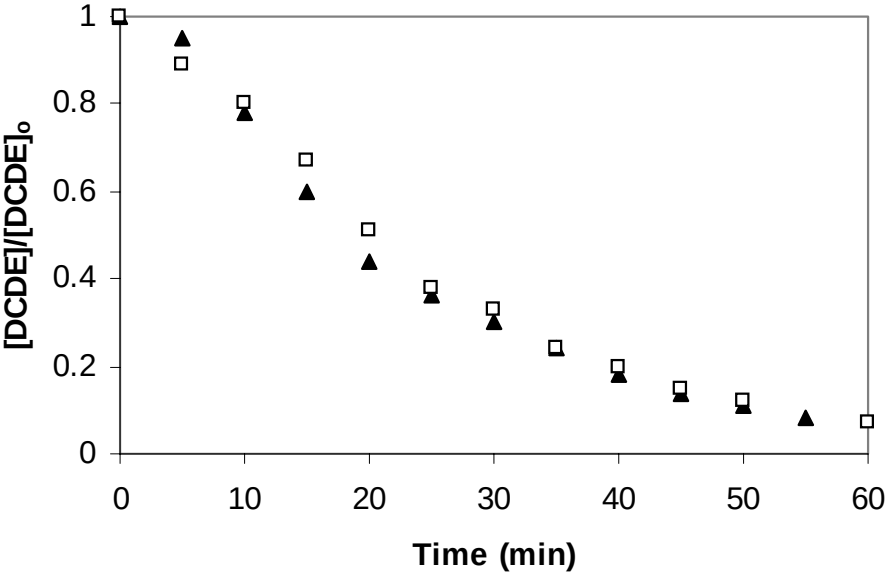

Figure 5.11. Removal of DCDE by means of H_2O_2/UV system by stepwise H_2O_2 addition.$[DCDE]_o$= 200 $mg.L^{-1}$

5.5. Results and discussion for inhibition tests

In each inhibition study, six bottles were set up to measure three different respiration rates. Bottle 1, containing only 400 $mg.L^{-1}$ biomass exhibited the endogenous respiration rate of activated sludge. Endogenous respiration rate is taken as the measurement of oxygen depletion over time for activated sludge in its "resting state". The microorganisms are not very active because they have no food, or substrate, so their oxygen demand is minimal. In bottles 2 and 3, 20 $mg.L^{-1}$ acetate was added to 400 $mg.L^{-1}$ biomass so exogenous respiration rate could be measured. Exogenous respiration rate is measured by monitoring oxygen depletion of a system with microorganisms and a readily biodegradable substance, such as acetate. Since the microorganisms are actively biodegrading the substrate, their oxygen demand is high and the concentration of dissolved oxygen in a closed system drops dramatically. Bottles 4, 5 and 6 contained 400 $mg.L^{-1}$ biomass, 20 $mg.L^{-1}$ acetate and the pre-oxidized solution to monitor inhibited exogenous respiration rate. Inhibited exogenous respiration rate represents the decrease in oxygen concentration over time for a system with microorganisms and a readily biodegradable substance in the presence of a potentially inhibitory compound or combination of compounds. Percent exogenous inhibition was found by comparing respiration rates. First, endogenous respiration rate was subtracted from exogenous respiration rate to get net exogenous respiration rate. Then, endogenous inhibition was subtracted from inhibited exogenous respiration rate to get net inhibited exogenous respiration rate. These net values were used in calculations in order to exclude the irrelevant activity of microorganisms in their resting state. Finally, these two values were compared by subtracting net inhibited exogenous from net exogenous respiration rate, and by dividing the difference by net exogenous respiration rate and multiplying by 100. This gives percent exogenous inhibition, meaning the degree to which the test solution inhibited the microorganisms from biodegrading acetate. The following is a sample calculation referring to the hypothetical slope values in Fig. 5.12.

average net exogenous respiration rate = $[(0.18 + 0.22)/2] - 0.020 = 0.18$

average net inhibited exogenous respiration rate = $[(0.12 + 0.11 + 0.10)/3] - 0.020 = 0.09$

average percent exogenous inhibition = $[(0.18 - 0.09)/0.18] \times 100 = 50\%$ inhibition

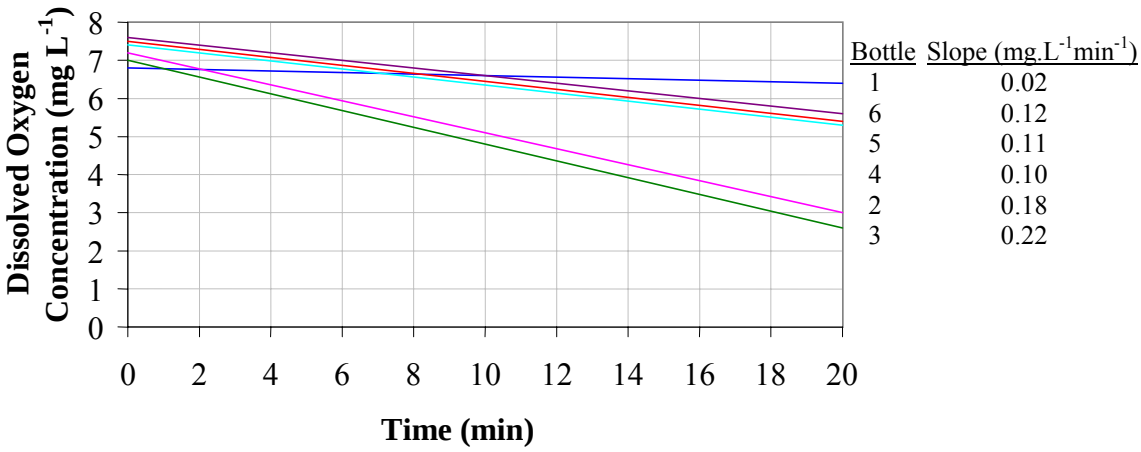

Figure 5.12. Typical respiration rates represented as slopes

Obviously, for inhibited exogenous slopes that were steeper, or greater in value, than exogenous slopes, percent inhibition was calculated as a negative value. This was interpreted as no detectable inhibition. In such cases, the test solution was assumed to provide a secondary substrate that increased the overall activity of the microorganisms.

5.5.1. Inhibition of DCDE solution

To check the inhibition of DCDE alone, four experiments were performed using DCDE concentrations of 25, 50, 75 and 100 $mg.L^{-1}$, activated sludge concentration of 400 $mg.L^{-1}$ and acetate concentration of 20 $mg.L^{-1}$. Respiration rates were monitored for 15 to 20 minutes. These experiments were performed for non-acclimated and acclimated cultures. Table 5.1 and Fig. 5.13 show the inhibition measured when exposing activated sludge cultures to various concentrations of DCDE.

In the concentration range studied, DCDE produced some inhibition at concentrations higher than 50 $mg.L^{-1}$. Although the extent of inhibition is small, preoxidation by means of H_2O_2/UV has been performed in order to see if the oxidation byproducts still have effects on activated sludge systems.

Table 5.1. Exogenous inhibition of acclimated and non-acclimated activated sludge cultures by DCDE

DCDE Concentration ($mg\ L^{-1}$)	*Acclimated*	*Non-Acclimated*
	Inhibition (%)	
0	0.0 ± 0.0	0.0 ± 0.0
25	0.47 ± 3.3	-1.1 ± 2.6
50	0.52 ± 3.4	4.5 ± 2.7
75	17 ± 2.6	10 ± 5.2
100	23 ± 3.7	18 ± 2.5

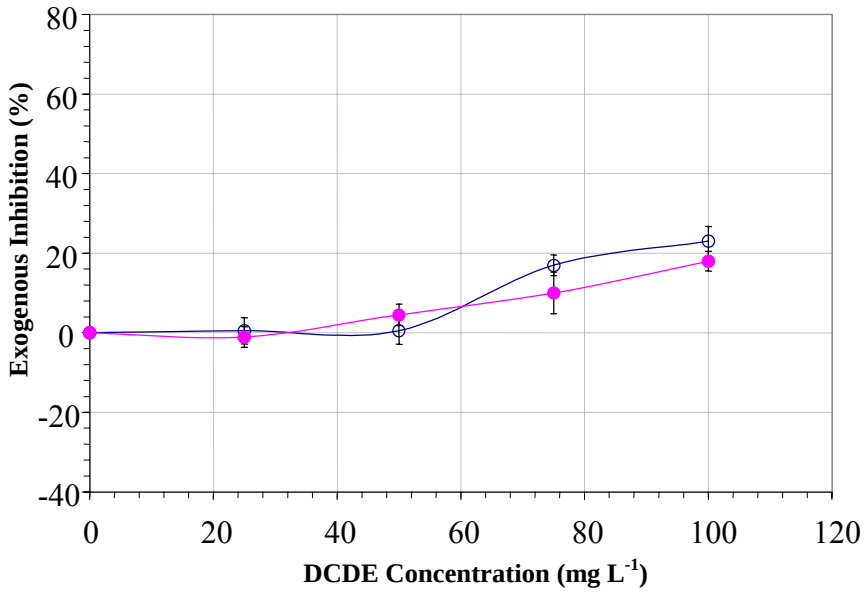

Figure 5.13. Exogenous inhibition of acclimated (○) and non-acclimated (●) activated sludge cultures by DCDE

5.5.2. Inhibition of preoxidized DCDE solutions

DCDE solutions (200 $mg.L^{-1}$) preoxidized at 25, 50, 75 and 100% were subjected to inhibition test. Table 5.2 and Fig. 5.14 present the exogenous inhibition results of studies using UV/H_2O_2-treated DCDE as a test solution.

The obtained results were very favorable for solutions oxidized with UV/H_2O_2. Not only was little or no detectable inhibition, but also the oxidized solution served as secondary substrate. Samples that contained both acetate and the test solution showed an increase in oxygen consumption over the samples with acetate and no test solution. The negative inhibition values indicated that not only was there no detectable inhibition but that some of the DCDE byproducts were actually readily biodegradable. Besides, no significant different was observed in the exogenous inhibition by using acclimated or non- acclimated biomass.

Table 5.2. Exogenous inhibition of acclimated and non-acclimated activated sludge cultures by DCDE and its oxidation byproducts (after UV/H_2O_2 treatment)

Percent Oxidation (%)	***Acclimated***	***Non-Acclimated***
	Inhibition (%)	
25 ± 5	7.0 ± 4.7	-0.77 ± 1.6
50 ± 5	7.4 ± 3.9	6.6 ± 2.4
75 ± 5	-17 ± 4.2	-14 ± 6.2
100 ± 5	-25 ± 3.2	-23 ± 3.7

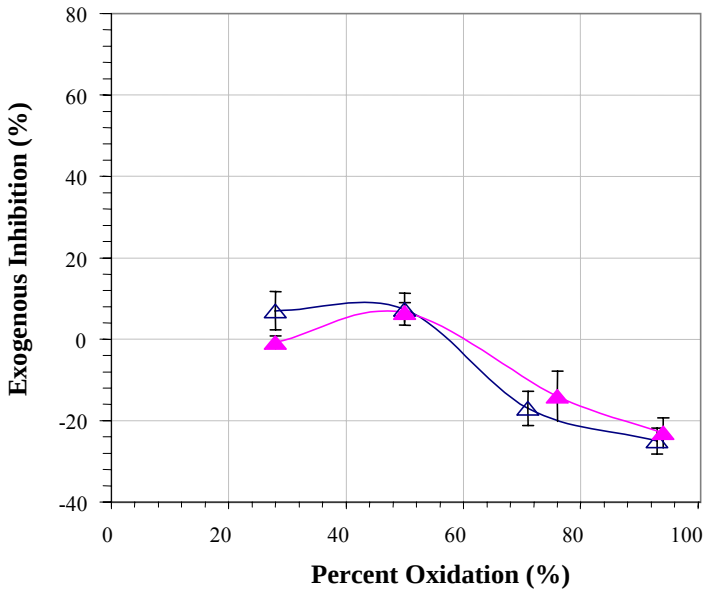

Figure 5.14. Exogenous inhibition of acclimated (∆) and non-acclimated (▲) activated sludge cultures by DCDE and its oxidation byproducts.

5.6. Results and discussion for biodegradation used tests

5.6.1. Short-term biodegradation test

The experiments were conducted for five levels of oxidation: 0, 25, 50, 75 and 100 percent oxidation of DCDE by means of H_2O_2/UVsystem. DCDE solutions preoxidized at 25, 50, 75 and 100% were subjected to short-term biodegradation experiments after diluting with mineral salt solution and distilled water at different proportions. The proportions were adjusted to results in a wide range of substrate. The net exogenous respiration rate were measured and reported as a function of the DCDE concentration remaining in solution after oxidation. The biodegradation experiments were performed with acclimated and non-acclimated cultures of microorganisms. In each biodegradability study, five bottles were set up to measure four different respiration rates. Bottle 1, containing only 400 $mg.L^{-1}$ biomass exhibited the endogenous respiration rate of activated sludge. The microorganisms are not very active because they have no food, or substrate, so their oxygen demand is minimal. In bottles 2 and 5, different concentrations of DCDE according to oxidation grade of the pre-oxidized solution was added to 400 $mg.L^{-1}$ biomass so exogenous respiration rate could be measured.

As has been already mentioned in the experimental section, the respiration rate of the microorganisms in each bottle was determined by measuring the oxygen concentration as a function of time, and by calculating the corresponding slopes using Microsoft Excel program. Fig. 5.15 shows typical raw data obtained for an experiment at different dilutions, where time is in real minutes. The endogenous respiration rate of microorganisms was obtained by running a control experiment with microorganisms alone. The net exogenous respiration rates for DCDE solutions were obtained by subtracting the endogenous rate from the observed exogenous respiration rates.

In Table 5.3 and 5.4, the experimental conditions in terms of DCDE oxidation percentage and the remaining concentration of DCDE are listed together with the net exogenous respiration rate and its corresponding standard deviations samples for acclimated and non-acclimated cultures respectively.

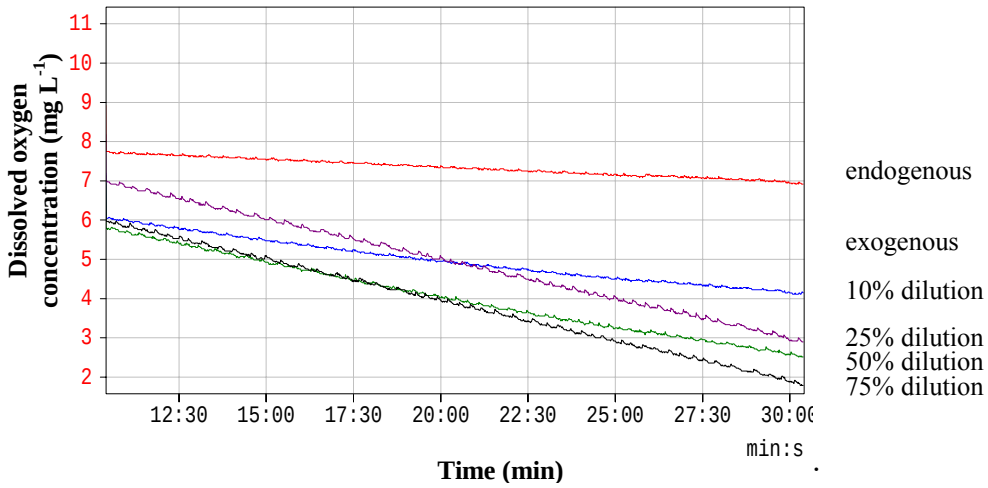

Figure 5.15. Respiration rates of microorganisms with different dilutions of DCDE after 75% oxidation by H_2O_2/UV

Table 5.3. Oxidation by H_2O_2/UV of DCDE, Biodegradation by acclimated culture

H_2O_2/UV acclimated			
% of oxidation	DCDE (mg L^{-1})	net exo. resp. (mg O_2 L^{-1})	St.Dev.
0%	0	0.000	0.002
	50	0.001	0.001
	100	0.000	0.001
25% ± 5	0	0.000	0.000
	25	0.042	0.005
	50	0.065	0.006
	75	0.077	0.001
	100	0.091	0.003
50% ± 5	0	0.000	0.000
	10	0.024	0.001
	25	0.041	0.002
	50	0.072	0.001
	75	0.086	0.002
75% ± 5	0	0.000	0.000
	5	0.031	0.003
	10	0.046	0.012
	25	0.106	0.005
	40	0.122	0.026
100% ± 5	0	0.000	0.000
	0.10	0.026	0.001
	0.25	0.056	0.002
	0.50	0.106	0.001
	0.75	0.137	0.004

Table 5.4. Oxidation by H_2O_2/UV of DCDE, Biodegradation by non-acclimated culture

H_2O_2/UV non acclimated			
% of oxidation	DCDE (mg L^{-1})	net exo. resp. (mg O_2 L^{-1})	St.Dev.
0%	0	0.000	0.009
	25	0.001	0.001
	50	0.002	0.002
	75	0.003	0.001
	100	0.004	0.001
25% ± 5	0	0.000	0.000
	25	0.014	0.003
	50	0.040	0.002
	75	0.057	0.006
	100	0.069	0.003
50% ± 5	0	0.000	0.001
	10	0.024	0.002
	25	0.052	0.006
	50	0.104	0.013
	75	0.127	0.006
75% ± 5	0	0.000	0.000
	5	0.039	0.000
	10	0.051	0.010
	25	0.118	0.002
	40	0.139	0.002
100% ± 5	0	0.000	0.000
	0.10	0.039	0.006
	0.25	0.090	0.012
	0.50	0.121	0.015
	0.75	0.173	0.014

Fig.s 5.16 and 5.17 show the net exogenous respiration rates of DCDE treated solutions for acclimated and non-acclimated culture with the abscissa presented in remaining DCDE concentration. The results obtained in both cases clearly indicate that while DCDE without oxidation exerts no oxygen demand at all, increasing levels of oxidation produces dramatic improvement in oxygen consumption, obviously due to formation of more biodegradable reaction products. It is also interesting to observe that different levels of oxidation produce different maximum respiration rate for acclimated and

non-acclimated culture. In fact for lower oxidation grade (25%), respiration rate of acclimated culture was significant higher than non-acclimated culture.

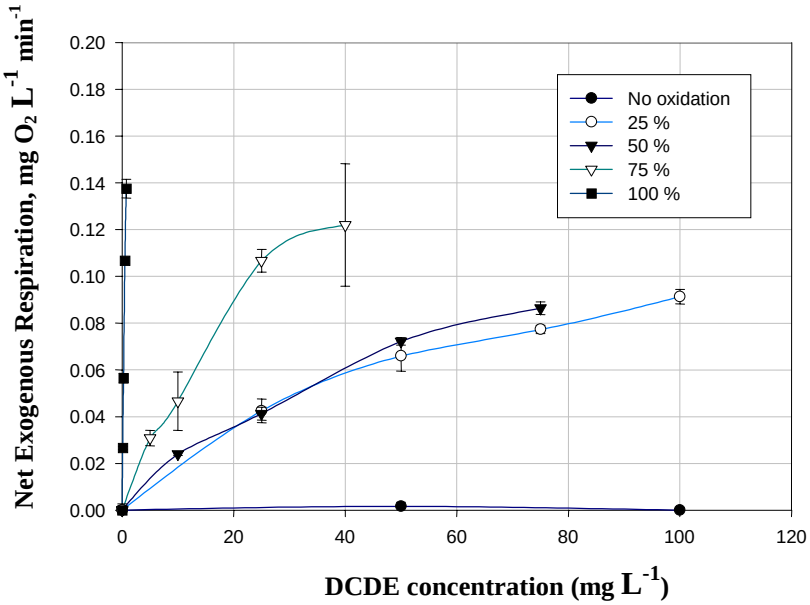

Figure 5.16. Biodegradability of DCDE treated by H_2O_2 using acclimated culture, with x-axis as DCDE concentration.

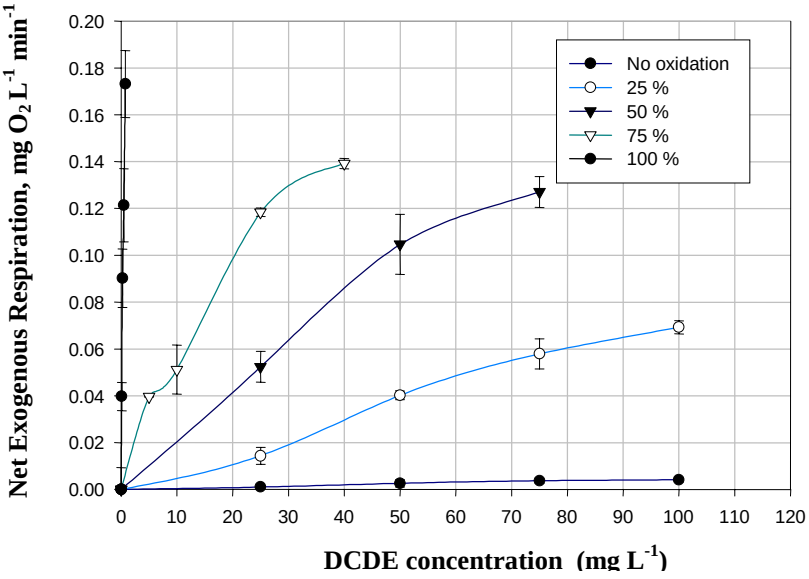

Figure 5.17. Biodegradability of DCDE treated by H_2O_2 using non-acclimated culture, with x-axis as DCDE concentration.

When 50% and 70% of DCDE was oxidized, respiration rate of non-acclimated culture was higher that acclimated one. It could be indicate that for higher pre-oxidation grade, sewage sludge acclimatation would not be necessary in order to increase biodegradability.

After acknowledging the values of respiration rates, it has been possible to calculate kinetic parameters of Monod equation that were already described in experimental section. Kinetic parameters are shown in Tables 5.5 and 5.6.

Table 5.5. H_2O_2/UV non-acclimated culture. Kinetic parameters

(%) oxidation	DCDE (mg L^{-1})	net exo. resp (mg O_2 L^{-1})	1/DCDE	1/net resp	$1/\mu_{max}$ (s)	K_s/μ_{max}	μ_{max} (s^{-1})	K_s ($g.cm^{-3}$)
0%	0	0.000						
	25	0.001						
	50	0.002						
	75	0.003						
	100	0.004						
25%	0	0.000			7.98	1898	0.125	200.4
	25	0.014	0.04	69.6				
	50	0.040	0.02	24.9				
	75	0.057	0.01	17.2				
	100	0.069	0.01	14.4				
50%	0	0.000			2.48	393.34	0.159	62.89
	10	0.024	0.10	41.6				
	25	0.052	0.04	19.1				
	50	0.104	0.02	9.55				
	75	0.127	0.01	7.86				
75%	0	0.000			5.42	106.13	0.175	18.63
	5	0.039	0.20	25.2				
	10	0.051	0.10	19.5				
	25	0.118	0.04	8.4				
	40	0.139	0.02	7.2				
100%	0	0.000			3.05	2197	0.195	0.43
	0.10	0.039	10.00	25.2				
	0.25	0.090	4.00	11.1				
	0.50	0.121	2.00	8.2				
	0.75	0.173	1.33	5.7				

Table 5.6. H_2O_2/UV acclimated culture. Kinetic parameters

(%) oxidation	DCDE (mg L^{-1})	net exo. resp (mg O_2 L^{-1})	1/DCDE	1/net resp	$1/\mu_{max}$ (s)	K_s/μ_{max}	μ_{max} (s^{-1})	K_s ($g.cm^{-3}$)
0%	0	0.000						
	50	0.001						
	100	0.000						
25%	0	0.000						
	25	0.042	0.040	23.52				
	50	0.065	0.020	15.18	7.09	410.63	0.114	48.85
	75	0.077	0.013	12.94				
	100	0.091	0.010	10.95				
50%	0	0.000						
	10	0.024	0.100	41.61				
	25	0.041	0.040	19.61	7.88	344.34	0.107	36.94
	50	0.072	0.020	13.86				
	75	0.086	0.013	11.57				
75%	0	0.000						
	5	0.031	0.200	32.48				
	10	0.046	0.100	21.45	4.87	142.55	0.154	22.08
	25	0.106	0.040	9.37				
	40	0.122	0.025	8.19				
100%	0	0.000						
	0.10	0.026	10.00	37.63				
	0.25	0.056	4.000	17.70	2.79	3.50	0.159	0.55
	0.50	0.106	2.000	9.36				
	0.75	0.137	1.333	7.27				

The net exogenous respiration rate for all levels of oxidation by H_2O_2/UV process are significantly higher than the rate of non-oxidized DCDE, which is zero. This increase in the respiration rate is clearly due to existence of biodegradable chemicals produced as intermediates of DCDE oxidation by means of H_2O_2/UV system. In fact, at higher percentage of DCDE oxidation, the values for Ks are smaller, what means that the organic matter in solution is more biodegradable. For the same reason, q_{max} is higher when increasing the oxidation grade. In addition, the kinetics for non-acclimated culture was faster than acclimated one. That fact could be explained taking into account that in the case of the non-acclimated culture, a higher diversity of microorganisms exists and therefore

major capacity to eliminate a complex substrate. On the contrary, the acclimated culture produces a very specific biomass just for one of the components of the substrate (in our case DCDE), diminishing its capacity for degrading different compounds.

5.6.2. Long-term biodegradation test

The long-term respirometric test described in the experimental section was also followed to study the biodegradability of DCDE treated by H_2O_2 system to oxidize DCDE by zero (no oxidation), 25, 50, 75 and 100%. The results of the long-term tests were presented in terms of oxygen consumption and carbon dioxide formation and all of these were performed by duplicate. The concentration of the biomass used in these studies was 400 $mg.L^{-1}$. Raw data for DCDE pre-oxidize solution used for long-term respirometric test for acclimated culture is shown in Table 5.7. The total volume of solution in each bottle (250-mL size) was 50 mL. In Fig. 5.18, the decrease in oxygen concentration due to consumption was presented in $\mu g.L^{-1}$ on the y-axis as a function of time that is presented on x-axis in units of hours for acclimated culture.

Table 5.7. Raw data for DCDE preoxidized solution used in long-term respirometer test for acclimate culture.

Percent Oxidation (%)	***$DCDE_o$ ($mg\ L^{-1}$)***	***COD_o ($mg\ L^{-1}$)***
0	212.8	260
25 ± 5	162.6	247
50 ± 5	114.9	223
75 ± 5	46.5	222
100 ± 5	5.6	185

For acclimated culture, within the first 120 hours, oxygen consumption for the endogenous control was significantly lower than the oxygen consumption observed for non-oxidized DCDE and the rest of pre-oxidized solution tested. This observation could indicate that acclimated culture seemed to tolerate the presence of DCDE up to 100 $mg.L^{-1}$. However, after about 120 hours, oxygen consumption observed for non-oxidized DCDE

and 24% pre-oxidized solution was lower than endogenous one. It could imply that the toxicity of DCDE affected acclimated culture at longer period of exposition time. Moreover, the oxygen consumption increased as the oxidation level increase resulting in an overall oxygen consumption of about 11 $mg.L^{-1}$ within 13 days for the two highly oxidized samples. These results are confirmed by CO_2 production, as shown in Fig. 5.19.

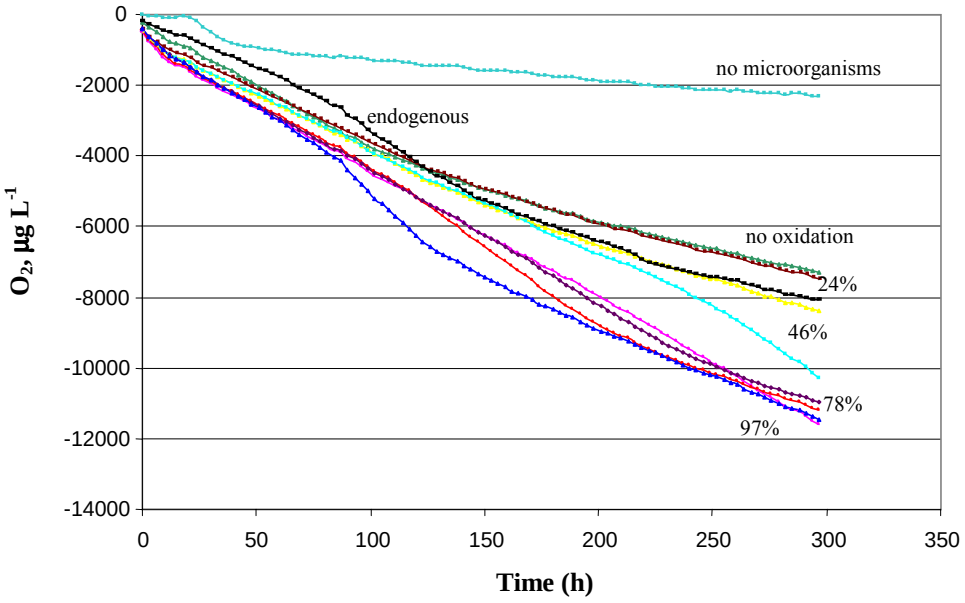

Figure 5.18. Oxygen consumption during long-term respirometric test for H_2O_2/UV-treated DCDE with acclimated culture

In Fig. 5.19, the decrease in oxygen concentration due to consumption and increase in CO_2 due to production is also shown for acclimated culture. The CO_2 production for the endogenous control was in this case lightly smaller in the firsts 120 hours in comparison with CO_2 production have observed for no oxidized DCDE. However, the no oxidized DCDE solution exhibited reduced CO_2 production after this initial period of time. On the other hand, the biggest production in CO_2 corresponds to the most oxidized samples. These results are completely compatible with that obtained for he oxygen consumption of most oxidized samples.

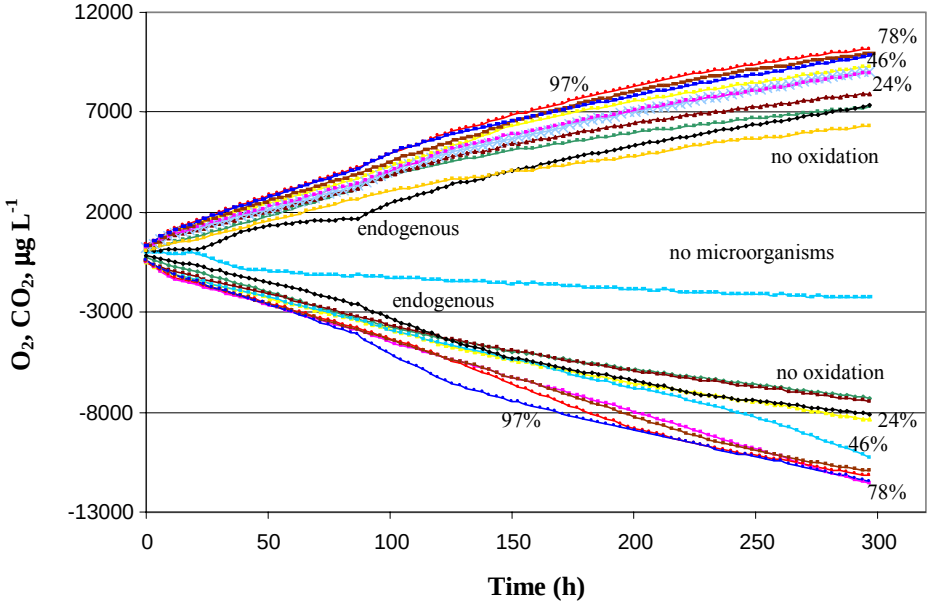

Figure 5.19. Oxygen consumption and carbon dioxide production during long-term respirometric test for H_2O_2/UV-treated DCDE with acclimated culture

Long-term biodegradation test was also performed with non-acclimated culture. In Fig. 5.20, the decrease in oxygen concentration due to consumption was presented in µg L^{-1} as a function of time. Raw data for DCDE pre-oxidize solution used for long-term respirometric test for non-acclimated culture is shown in Table 5.8.

Table 5.8. Raw data for DCDE preoxidized solution used in long-term respirometer test for non-acclimated culture

Percent Oxidation (%)	***$DCDE_o$ ($mg.L^{-1}$)***	***COD_o ($mg.L^{-1}$)***
0	185.2	213
25 ± 5	142.5	216
50 ± 5	85.9	205
75 ± 5	36.7	193
100 ± 5	3.17	200

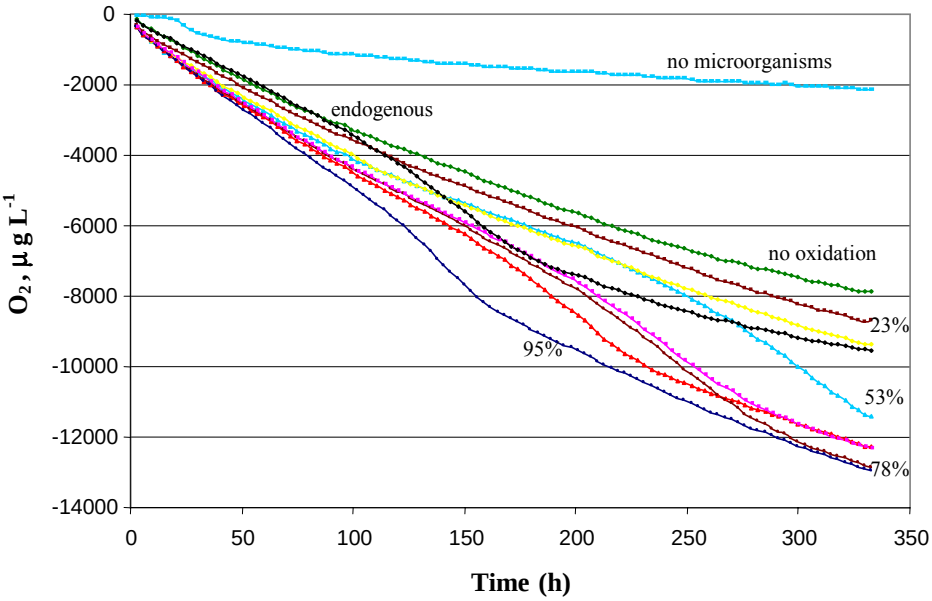

Figure 5.20. Oxygen consumption during long-term respirometer test for H_2O_2/UV-treated DCDE with non-acclimated culture.

In this case, similar profiles of oxygen consumption were obtained compared to acclimated culture although the capability of the non-acclimated biomass to tolerate DCDE presence is diminished. This effect is reflected in the lower oxygen consumption during the first 120 hours of the experimentation. At higher reaction time toxicity effect of DCDE are higher for non-acclimated culture since oxygen diminished significantly respect to endogenous respiration. Again, the oxygen consumption increase when increasing the oxidation rate, resulting in an overall oxygen consumption of about 13 $mg.L^{-1}$ within 13 days for the two highly oxidized samples.

In Fig. 5.21, the decrease in oxygen concentration due to consumption and increase in CO_2 due to production is also show for acclimated culture. The CO_2 production for the endogenous control was in this case lightly higher in comparison with CO_2 production has observed for no oxidized DCDE. On the other hand, the highest production in CO_2 corresponds to the most oxidized samples. These results are completely compatible with that obtained for the oxygen consumption of most oxidized samples.

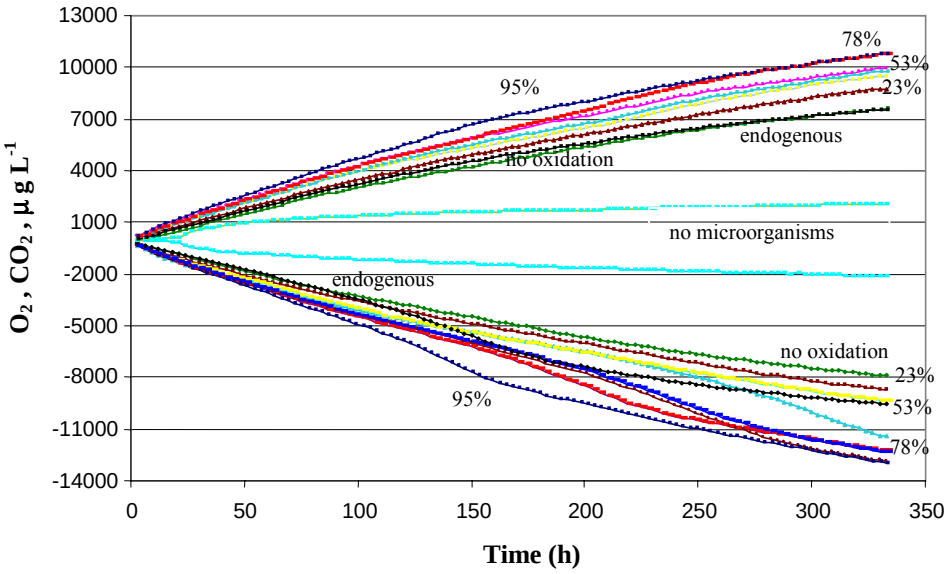

Figure 5.21. Oxygen consumption and carbon dioxide production during long-term respirometric test for H_2O_2/UV-treated DCDE with non-acclimated culture.

Long-term biodegradation test shown the viability of H_2O_2/UV process for enhancement of biodegradability of DCDE in aqueous solution.

5.6.3. Mid-term biodegradation test

The mid-term biodegradation experiments were conducted with DCDE solutions preoxidized at 100%. This level of oxidation was chosen because of the higher rate of respiration obtained with the short and long term tests. In fact, industry might need to oxidize recalcitrant chemicals by 100%. Otherwise, the effluent stream could still contain concentrations higher than is permitted by the law, especially since these recalcitrant compounds are expected to pass through the treatment sequence without being removed.

During the first 6 hours, samples were withdrawn every 1.5 hours and analyzed for COD and TOC concentrations.

The experimental results are presented in Tables 5.9 and 5.10 for duplicated during a 24-hour period and acclimated and non-acclimated culture respectively.

Table 5.9. Mid-term biodegradation experiments with acclimated culture for 100% oxidation of DCDE by means of UV/H_2O_2

Time (h)	COD_1 ($mg.L^{-1}$)	TCO_1 ($mg.L^{-1}$)	COD_2 ($mg.L^{-1}$)	TCO_2 ($mg.L^{-1}$)	COD average	TOC average
0.0	98.0	29.3	77.0	27.7	87.5	28.5
1.5	74.0	26.5	76.0	25.3	75.0	25.9
3.0	75.0	23.2	71.0	21.7	73.0	22.5
4.5	67.0	34.0	61.0	32.6	64.0	33.3
6.0	69.0	33.7	69.0	31.4	69.0	32.6
21.0	63.0	31.3	69.0	31.8	66.0	31.6
24.0	62.0	0.0	59.0	0.0	60.5	0
% removal	36.7	100	23.3	100	**30.8**	**100**

Table 5.10. Mid-term biodegradation experiments with non-acclimated culture for 100% oxidation of DCDE by means UV/H_2O_2 system.

Time (h)	COD_1 ($mg.L^{-1}$)	TCO_1 ($mg.L^{-1}$)	COD_2 ($mg.L^{-1}$)	TCO_2 ($mg.L^{-1}$)	COD average	TOC average
0.0	80.0	37.6	74.0	33.8	77	35.7
1.5	75.0	24.8	79.0	23.3	77	24.05
3.0	76.0	22.8	74.0	21.3	75	22.05
4.5	76.0	32.1	66.0	32.9	71	32.5
6.0	60.0	32.1	84.0	33.2	72	32.65
21.0	62.0	27.3	60.0	7.1	61	17.2
24.0	38.0	0.00	59.0	0.00	48.5	0.00
% removal	52.5	100	20.3	100	**37.01**	**100**

These results indicate that higher pre-oxidation of DCDE produce higher concentration of intermediates compounds that are more readily biodegradable, and that leads to the mineralization of larger fraction of organic matter. Although intermediates were not follow, the results are agree with expectation that higher levels of chemical oxidation would lead to formation of more oxygenated and smaller weight products, e.g., carboxylic acids that can easily be converted to CO_2 by microorganisms (Ertas and Gurol, 2002, 2003).

Based on TOC removal values, it can be concluded that both cultures were capable to oxidize 100% of organic matter content, which demonstrated that H_2O_2/UV process is an optimal pre-treatment method for DCDE solutions.

From short, long, and mid-term biodegradation tests, sewage sludge process could be integrate with advanced oxidation process (AOP) based on H_2O_2/UV to completely mineralization of DCDE.

6. Chemical and biological coupled system for the treatment of wastewaters generated in textile activities

6.1. Introduction

As it has been commented in the introduction of this thesis, the aim of this chapter is to explore the feasibility of combining the photo-Fenton process with biological oxidation (chemical and biological coupled system) and the development of a general strategy to be followed in industrial wastewater treatment. Among them, textile wastewater was selected taking into account that these type of waters use to contain high organic matter amount and the biological treatment is normally included in wastewater treatment facilities. However the difficulties and even failures in biological plant operation make the integration of chemical and biological processes specially recommended for this kind of industry (Scott and Ollis, 1995). On the other hand, textile industry represents one of the process in which water is used extensively and therefore textile effluents discharge creates problems in terms of water quality protection. Moreover, the discharge of colored or contaminated textile industry waste streams remains a contentious issue in many regions throughout the world. Residual textile dyes, particularly those of the reactive type, are invariably very difficult to remove with traditional methods. Although not normally, directly toxic colored dye residues may shield the lowest depths of watercourses from sunlight, inhibiting plant life, and other non-colored pollutants can present high oxygen demands, both being a threat to a "living river". For all of that, it is important to study the application of an advanced oxidation process, such as photo-Fenton coupled with an aerobic biological treatment for textile wastewater disposal

In order to develop this idea, effluents coming from a French textile industry were studied at the laboratory facilities of Ecole Politechnique Federal de Laussane (EPFL), (Switzerland).

Globally, the French textile finishing industry confronts not only low-cost textile from Asia and the Mediterranean basin, but also the rise of new countries that have made sizeable investments in order to develop a high quality industry (for example, western Europe). This industry has lost more than 40 % of its manpower against 10 % of the other manufacturing industries. Nevertheless, despite an unfavorable overall economic situation, the specific field of textile finishing resists to the crisis, more particularly in going on with a high level of export. It seems that the small companies offer more resistance than big societies. The small companies (0 to 20 employees) from French textile finishing represented up to 66 % of the whole sector in 1997 (that is to say 10 % of the manpower

and 10 % of the turnover). The investments engaged by those companies remain very low (≈ 5 %), which shows the real necessity to find out suitable solutions well fitted with the specific problems and financial capacities of these small companies.

Nowadays, in France, legal organizations tend to promote the implementation of individual wastewater treatment plants rather than the connection to urban treatment facilities. Fig. 6.1 shows the great possibility of expands for the proposed scheme in the textile sector (source: Textile French Institute).

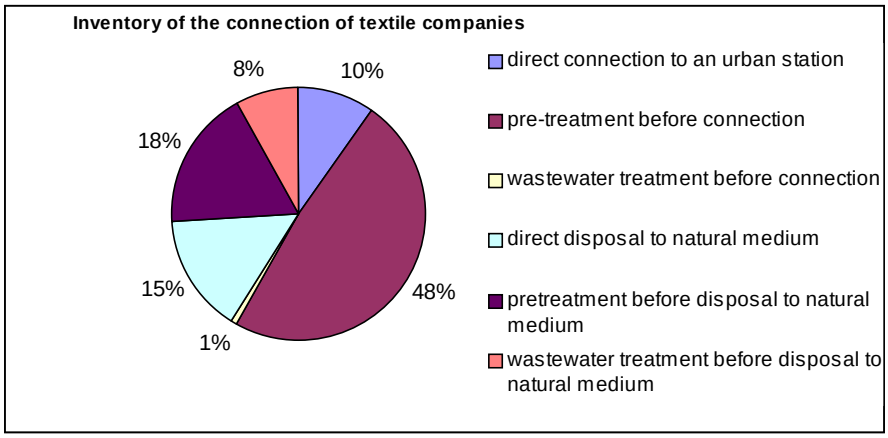

Figure 6.1. Inventory of the connection of textile French companies

In this context, solutions based on advanced oxidation processes are being investigated in order to propose an efficient process where costs are decreased as much as possible, and of quick application on the industrial field.

Thus, this research was part of a cooperation project with the French Textile Institute, which was interested in getting alternative and efficient methods for the elimination of organic recalcitrant compounds present in the French textile industry wastewaters. Effluents produced in a textile industry located in the south of France were selected to evaluate a general strategy for the treatment of the different generated wastewaters. The main objective was to find out the best operating conditions of the Photo-Fenton (pre- or post-) treatment to enhance the global removal performance. Three different wastewaters produced in this textile industry were studied. The main

physicochemical characteristics are described in section 6.4.1. Regarding its provenance, the origin of these wastewaters were:

- the outlet of an autoclave (Effluent 1).
- the mixed of different effluents produced in this industry (Effluent 2).
- the outlet of biological treatment plant (Effluent 3).

6.2. General strategy for the development of a coupled system

As it has been previously commented, coupling of photochemical and biological processes is a good alternative to minimize the treatment cost of wastewater containing biorecalcitrant and/or toxic pollutants. The chemical process could be used as pre-treatment in order to increase the biodegradability of the wastewater or as a post-treatment to remove the non-biodegradable compounds. In this sense, a general strategy is proposed and developed in the EPFL (Pulgarin *et al*, 1999) for wastewater treatment (see Fig. 6.2). First of all, due to the high cost of chemical treatments, biodegradability test should be carried out since for biodegradable compounds classical biological treatments are, at present, the cheapest and most environmentally compatible processes. From the test results three situation could be obtained:

(a) the effluent is biodegradable.
(b) the effluent is partly biodegradable.
(c) the effluent is completely non-biodegradable.

Strategy for each situation is the following:

For case (a) biodegradable non-toxic effluent could be sent directly to centralized biological treatment plant (green line, Fig. 6.2).

When the effluent is partly biodegradable (case b), it may be first treated by means of a conventional biological process and chemical oxidation process could be used in a final step to remove the biorecalcitrant part (blue line, Fig. 6.2).

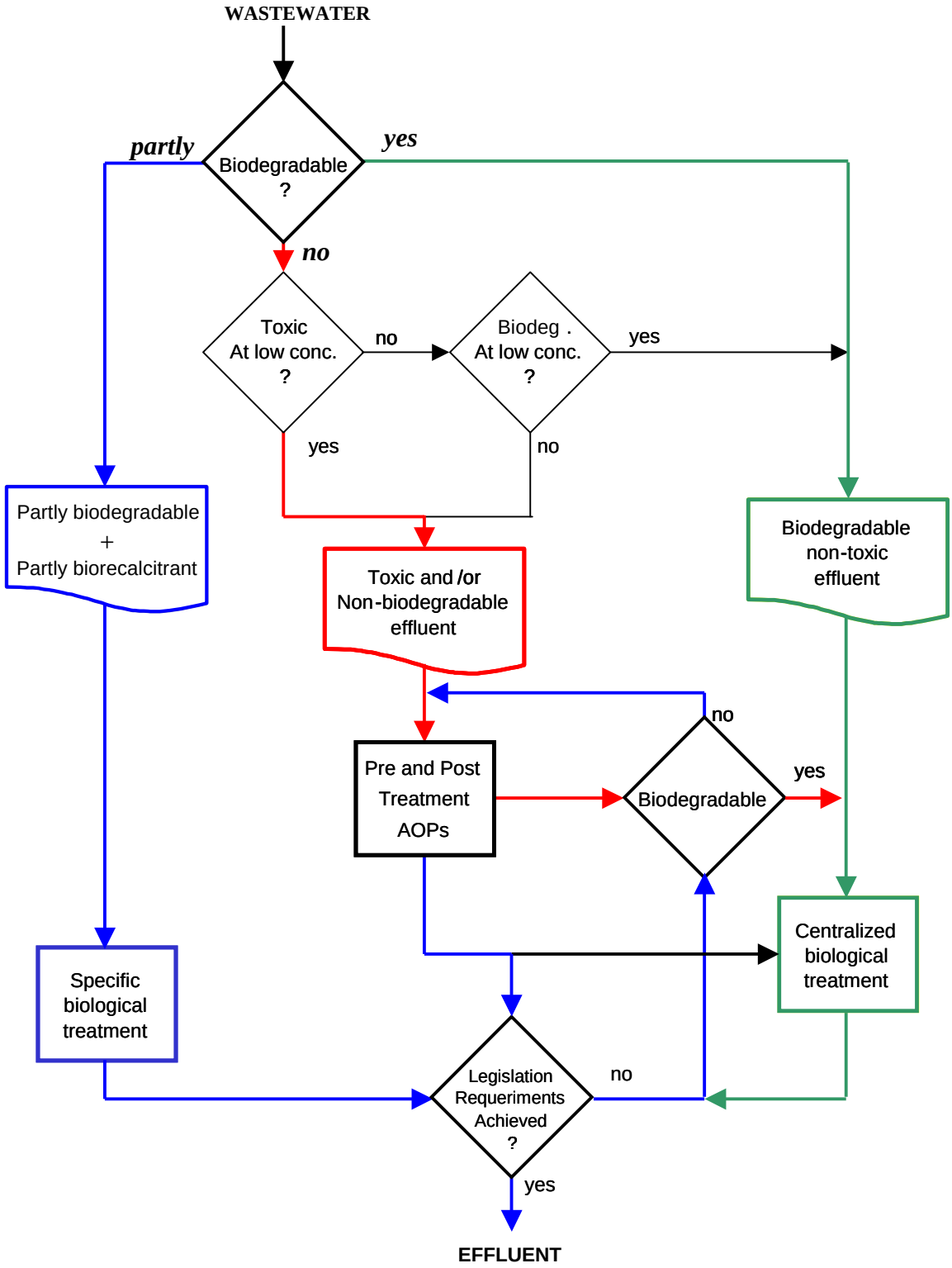

Figure 6.2. Flow diagram of the strategy for the devolopment of a coupled system

For toxic or non-biodegradable effluents (case c), the chemical oxidation as pretreatment process would increase the biodegradability and/or remove the toxicity of the wastewater. In this case, the chemical pretreatment is meant to modify the structure of contaminants by transforming them into less toxic and easily biodegradable intermediates, which allows the subsequent biological degradation to be achieved in a shorter time and in a less expensive way (red line, Fig. 6.2). The solution resulting from the phototreatment stage is considered to be biologically compatible after the elimination of:

- the initial biorecalcitrant and/or toxic compounds,
- the inhibitory and/or non-biodegradable intermediates, and
- any chemical reagent (H_2O_2, O_3 ….).

These requirements, together with information concerning the evolution of toxicity and biodegradability of the pretreated solution, allow the determination of optimal operational conditions, which corresponds to the best cost-efficiency compromise.

Finally, this strategy could be used as useful guide, as it proposes an easy way to determine the most feasibility method for any industrial wastewater treatment. Next, this strategy will be applied to the three effluents from the French industry presented before.

6.3. Experimental

6.3.1. Reagents

In Table 6.1 are shown all chemicals that were used in the experimentation. All them were used as received.

Milli-Q water is used for the preparation of aqueous solutions or as a component of the mobile phase (ammonium acetate-acetonitrile, HPLC grade) in HPLC analysis. For photo-Fenton process, HCl was used to acidify the sample to be treated. The phototreated solutions are neutralised by means of NaOH. Neutral pH of the solutions is maintained during the biological tests by adjusting with HCl or NaOH.

Table 6.1. List of chemicals used

Compound	*Formula*	*Vendor*
Ammonium chloride	NH_4Cl	Fluka
Ammoniun acetate	$C_2H_5NH_3$	Fluka
Acetronitrile		Merck
Boric acid	H_3BO_3	Fluka
Calcium chloride	$CaCl_2 \cdot 2H_2O$	Fluka
Cobalt chloride hexahidrate	$CoCl_2 \cdot 6H_2O$	Merck
Cupper chloride dihidrate	$CuCl_2 \cdot 2H_2O$	Fluka
Diethylene glycol	$C_4H_{10}O_3$	Fluka
Ferric chloride	$FeCl_3$	Aldrich
Ferric chloride hexahidrate	$FeCl_3 \cdot 6H_2O$	Fluka
Glucose	$C_6H_{12}O_6$	Aldrich
Hydrochloric acid	HCl	Fluka
Hydrogen peroxide	H_2O_2	Aldrich
Iron sulphate heptahydrate	$FeSO_4 \cdot 7H_2O$	Merck
Magnesium sulfate heptahidrate	$MgSO_4 \cdot 7\ H_2O$	Fluka
Monobasic potassium phosphate	K_2HPO_4	Fluka
Manganese chloride tetrahidrate	$MnCl_2 \cdot 4H_2O$	Fluka
Monobasic sodium phosphate	NaH_2PO_4	Aldrich
Monobasic potassium phosphate	KH_2PO_4	Fluka
Niquel chloride hexahidrate	$NiCl_2 \cdot 6H_2O$	Aldrich
Potassium hydrogen phthalate	2-(HO_2C) $C_6H_4CO_2K$	Merck
Sodium hydroxide	NaOH	Fluka
Sodium molibdate	Na_2MoO_4	Fluka
Sulfuric acid	H_2SO_4	Merck
Zinc sulfate	$ZnSO_4 \cdot 7H_2O$	Fluka

6.3.2. Experimental device and procedure

The photo-Fenton experiments were performed by means of a suntest simulator (shown in Fig. 6.3) and a coiled photochemical reactor installed in the coupled system with a biological reactor (shown in Fig. 6.4).

Figure 6.3. Reactor I (suntest simulator)

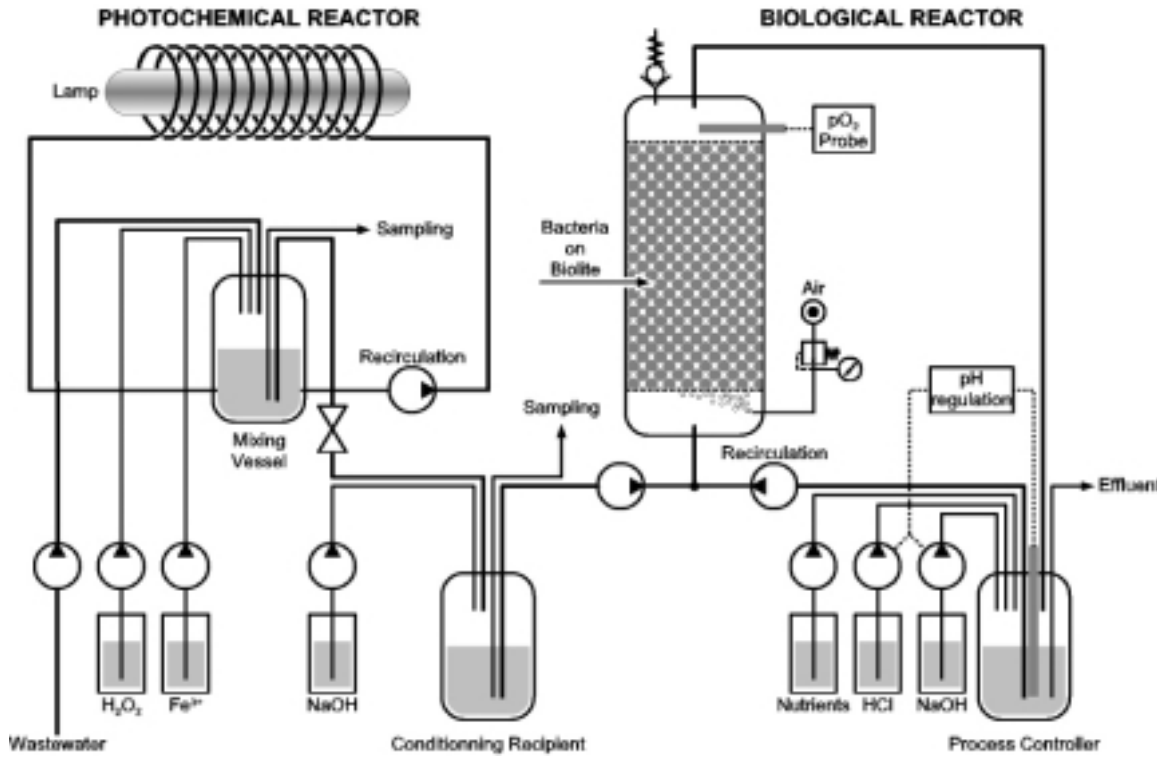

Figure 6.4. Scheme of the coupled photochemical-biological flow reactor

6.3.2.1. Suntest simulator

Several photo-Fenton experiments were performed using 40 mL Pyrex flask with wavelength cut-off at λ = 290 nm placed into a Hanau Suntest Simulator (see Fig 6.2). The radiation source employed is a xenon lamp where the total radiant flux (40 mW cm^{-2}) was measured with a YSI Corporation power meter. The lamp has a λ distribution with 0.5% of the emitted photons have wavelengths shorter than 300 nm and 7% of the emitted photons are in the range 300 and 400 nm. The photons emitted between 400 and 800 nm followed the solar spectrum. The aqueous solutions were magnetically stirred throughout irradiation, opened to air. Extreme care was taken to ensure uniform experimental conditions during the degradation rate determination. Samples were taken periodically and the Total Organic Carbon (TOC) was monitored after filtration with millipore filters (0.45 μm).

6.3.2.2. Coiled photochemical reactor

In the coiled photochemical reactor shown in Fig.6.4, the pollutant solution circulates through an 8 mm-diameter glass coil of about 20 m long. A 400 W, 40 cm long, medium-pressure Hg-lamp is positioned in such a way that its centre line passes through the axis of the coiled reactor. The predominant radiation is at 366 nm with output equivalent to ~15 W. The experiments are carried out at 30, 45 and 60^{o}C to study the influence of the temperature in the reaction rate. The pH was adjusted around 3 with HCl. The pollutant solution, H_2O_2, and Fe^{3+} solutions are added at the beginning into the mixing-vessel. The solution is in batch mode recirculated at 26 L h^{-1} through the illuminated part of the reactor. In order to prepare the phototreated water for biological treatment, the solution is neutralized and all the experiments were carried out until H_2O_2 was consumed.

6.3.2.3. Biological reactor

The Fixed Bed Reactor (FBR) shown on the right hand side of Fig.6.4 consists of a 1-L column containing biolite colonized by activated sludge coming from a municipal wastewater treatment plant (Vidy, Lausanne, Switzerland). The pH is controlled and adjusted at 7. The required nutrients N, P, K, and oligoelements for the bacterial activity are also added. The aeration is about 150 L h^{-1} and the O_2 concentration is measured by

means of an O_2 probe on the top of the column. This biological reactor was used as supplementary test to measure the biodegradability of the effluent treated.

6.3.3. Analytical determinations

6.3.3.1 Total organic carbon (TOC)

A Shimadzu, 5050A TOC analyzer was used for TOC measurements. The instrument was equipped with an ASI automatic sample injector and it uses potassium hydrogen phthalate solution as calibration standard. Acidification and stripping before analysis were sometimes necessary to keep the solutions free of atmospheric CO_2.

6.3.3.2. Chemical oxygen demand (COD)

The COD is used as a measure of the oxygen equivalent of the organic matter content of a sample that is susceptible to oxidation by a strong chemical oxidant. This analysis is carried out via a Hach-2000 spectrophotometer using dichromate solution as the oxidant in strong acid medium. Test solution (2 mL) is pipetted into the dichromate reagent and digested at 150^{o}C for two hours. Color is developed during the oxidation and measured against a water blank using a Hach DR/890 colorimeter. The optical density for the change of color of the dichromate solution was determined at λ = 430 nm.

6.3.3.3. High performance liquid chromatography (HPLC)

High performance liquid chromatography (HPLC) was carried out in a Varian 9065 unit provided with a Varian 9012 solvent delivery system, an automatic injector 9100, and a Varian ProStar variable (200-400 nm) diode array detector 9065 Polychrom. A reverse phase Spherisorb silica column ODS-2 and acetonitrile/amonium acetate as mobile phase was used to run the chromatography in gradient mode. The rapidoprint signal was detected at 258 nm with a retention time around 3.6 min.

6.3.3.4. Biological oxygen demand (BOD)

The BOD measures the oxygen required for the biochemical degradation of organic material. This analysis is made by means of a Hg free WTW 2000 Oxytop unit

thermostated at 20°C. The pH of the samples are adjusted between 6.8 and 7.5 followed by addition (20% v/v) of decanted sludge (inoculum) from the biological plant of Vidy (Lausanne, Switzerland) and of nutrient substances (solutions A, B, and C) and trace elements necessary for the bacterial activity.

Solution A:

- $FeCl_3.6H_2O$ (0.5 g)
- HCl 1N (1 mL) in 100 mL of distilled water.

Solution B:

- $MgSO_4.7H_2O$ (2.0 g)
- $CaCl_2$ (2.5 g)
- NH_4Cl (quantity depending of carbon concentration to degrade to have always a molar ratio C/N of 20) in 500 mL of distilled water.

Solution C:

- Na_2HPO_4 (6.8 g)
- KH_2PO_4 (2.8 g) in 1000 mL of distilled water.

Solution A+B:

- 50 mL of solution A, 500 mL solution B in 1000 mL of distilled water.

Trace elements solution:

- $FeSO_4.7H_2O$ (200 mg)
- $ZnSO_4.7H_2O$ (10 mg)
- $MnCl_2.4H_2O$ (3 mg)
- H_3BO_3 (30 mg)
- $CoCl_2.6H_2O$ (20 mg)
- $CuCl_2.2H_2O$ (1 mg)
- $NiCl_2.6H_2O$ (2 mg)
- $Na_2MoO_4.2H_2O$ (3 mg), in 1000 mL of distilled water.

For each BOD determination, 20 $mL.L^{-1}$of solution A+B, 50 $mL.L^{-1}$ of C and 2 $mL.L^{-1}$of trace elements are added for 400 mg C of the test solution.

6.3.3.5. Zahn-Wellens biodegradability test

The Zahn-Wellens test was adapted in 1981 as OECD Guideline 302 B for determining inherent biodegradability (OECD, 1981). A mixture containing the test substance, mineral nutrients (the same as for BOD determination), and between 1-1.5 g L^{-1} of activated sludge in aqueous medium is agitated and aerated at 20-25^{o}C in the dark or in diffuse light for up to 28 days. Blank controls, containing activated sludge with a biogenic substrate (diethylene glycol) and mineral nutrients but no test substance, are run in parallel. Another control to check the stripping effect is also carried out in parallel only with the test substance. The biodegradation process is monitored by determination of TOC. Biomass coming from the biological activated sludge plant of Vidy (Lausanne, Switzerland) is previously aerated for 24 hours and subsequently centrifuged. This test was performed in the experimental device shown in Fig. 6.5.

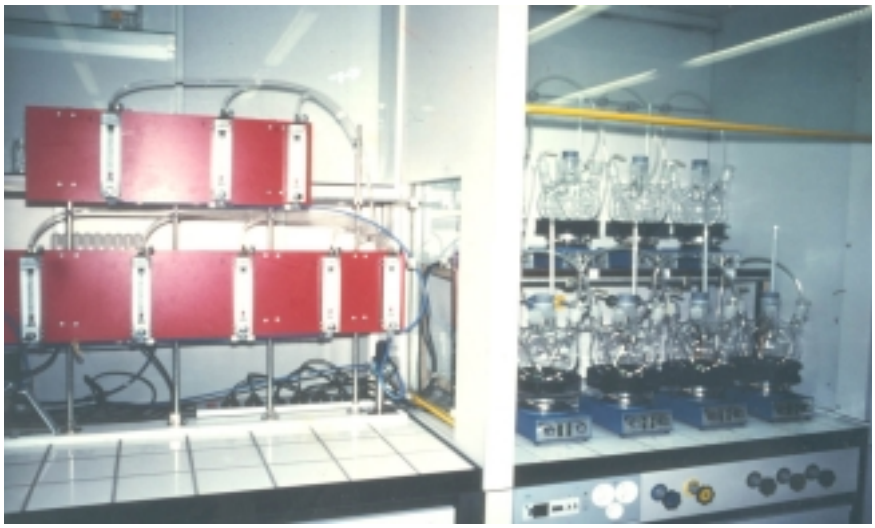

Figure 6.5. Zahn-Wellens experimental device

6.3.3.6. Hydrogen peroxide

Concentrations of H_2O_2 were determined by the Merk Merckoquant® peroxide analytical test strips and by permanganate titration.

6.4. Results and discussion

6.4.1. Wastewater characterization

Taking into account the difficulties in quickly determining and quantifying the individual constituents of the textile effluents under study, gross parameters as COD, TOC and BOD were measured. The physicochemical characteristics of the effluents are summarized in Tables 6.3, 6.4 and 6.5. Besides this, an absorption spectrum of each effluent was performed in order to know the absorption properties and therefore having a general idea about families of organic compounds that could probably be constituents of these wastewaters.

6.4.1.1. Effluent 1

As it has been commented, the effluent 1 (see Fig. 6.6) comes from the outlet of autoclave. The known composition of the mixture that enter to the autoclave and phisycochemical characteristics of the effluent are summarized in Tables 6.2 and 6.3.

Table 6.2. Initial composition of inlet autoclave

Industrial name	Concentration	Properties
Colorant A	2 %	Colorant
Colorant B	1.88 %	Colorant
Rapidoprint	1 g L^{-1}	Anti-reductor
Acid	0.3 mL L^{-1}	
Salt	30 g L^{-1}	
Carbonate	3 g L^{-1}	

Table 6.3. Physicochemical characteristics of the effluent 1

Effluent	TOC (mg L^{-1})	COD (mg O_2L^{-1})	BOD_5 (mg O_2L^{-1})	$\frac{BOD_5}{COD}$	Conductivity (mS cm^{-1})	pH	Color
1	900	4000	180	0.045	84.5	11.2	Red

This effluent exhibits low biological oxygen demand (BOD_5), high chemical oxygen demand (COD) and it is highly colored. The BOD_5/COD ratio is 0.045, indicating that this effluent is poorly biodegradable taking into account that values of this ratio higher than 0.4 for municipal wastewater are considered as biologically compatible (Metcalf & Eddy, 1995). In addition, this effluent has a high conductivity due the very high salt concentration and it also shows a high alkalinity grade.

The UV-vis absorption spectrum of this wastewater is shown in Fig. 6.7. It presents a maximum absorption band in the range of 250-340 nm. In this zone, the aromatics compounds present a characteristic absorption band. The absorbance in the visible zone (500-600 nm) is also important, which is characteristic of chromophores groups present in the effluent.

Figure 6.6. Effluent 1

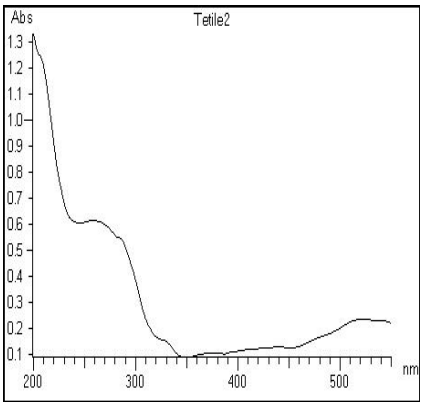

Figure 6.7. UV-vis spectra

6.4.1.2. Effluent 2

This effluent 2 (see Fig. 6.8) is the result of mixing all the wastewaters produced in the plant, such as those produced in the plants processes like dying, printing, bleaching, etc and those produced in activities like washing, washrooms and laboratories. This mixed wastewater is finally sent to the biological treatment plant placed in the same facilities. In table 6.4 the physicochemical characteristics of this effluent are summarized.

Table 6.4. Physicochemical characteristics of the effluent 2

Effluent	TOC ($mg\ L^{-1}$)	COD ($mg\ O_2L^{-1}$)	BOD_5 ($mg\ O_2L^{-1}$)	$\frac{BOD_5}{COD}$	Conductivity ($mS\ cm^{-1}$)	pH	Color
2	460	1352	526	0.39	3.36	7.10	Green

This effluent exhibits high biological oxygen demand (BOD_5), moderate COD and lightly colored. The BOD_5/COD ratio was 0.39, indicating that this effluent is potentially biodegradable, as commented before.

The UV-vis absorption spectrum of this wastewater is also shown in Fig. 6.9.

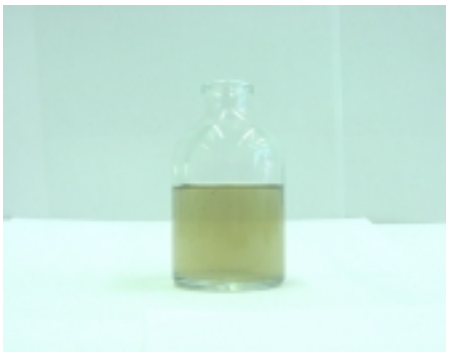

Figure 6.8. Effluent 2

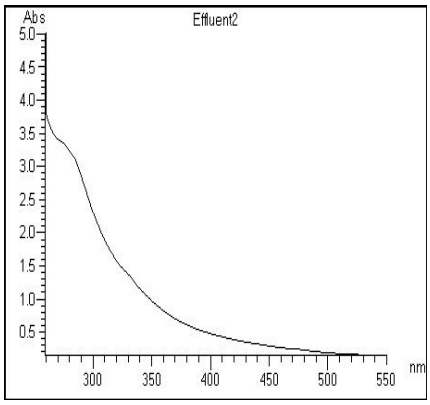

Figure 6.9. UV-vis spectrum

It presents an absorption band in the range of 250-340 nm. It could be indicative, as was mentioned before, of the presence of aromatic compounds. In this case, the absorbance in the visible zone is not important in spite of the presence of chromophore groups, as they are present in very low concentration. For this reason they do not appear registered in the spectrum.

6.4.1.3. Effluent 3

As it has been commented, effluent 3 (Fig. 6.10) is the outlet of the biological treatment plant. The physicochemical characteristics of this effluent are presented in table 6.5

Table 6.5. Physicochemical characteristics of the effluent 3

Effluent	TOC ($mg\ L^{-1}$)	COD ($mg\ O_2L^{-1}$)	BOD_5 ($mg\ O_2L^{-1}$)	$\frac{BOD_5}{COD}$	Conductivity ($mS\ cm^{-1}$)	pH	Color
3	150	170	18	0.11	3.76	7.4	No color

This effluent exhibits very low biological oxygen demand (BOD_5), low COD and no color. The BOD_5/COD ratio was 0.11, indicating that this effluent would be poorly biodegradable. Even after biological treatment the TOC and DOC values are still rather high.

The UV-vis absorption spectrum of this effluent is shown in Fig. 6.11.

Figure 6.10. Effluent 3

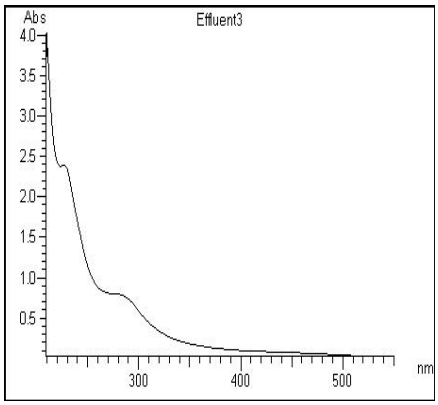

Figure 6.11. UV-vis spectrum

It presents a maximum absorption band in the range of 250-340 nm. This could clearly indicate the presence of biorecalcitrant aromatic compounds, which is in agreement with the relatively high TOC values.

6.4.2. Biodegradability assessment

As BOD_5/COD ratios give only an idea about the biodegradability of the studied waters. Moreover, Zahn-Wellens biodegradability tests were performed in order to check the biocompatible conditions of these effluents in favorable conditions.

6.4.2.1. Biodegradability of effluent 1

Fig. 6.12 shows the evolution of TOC content versus time during 25 days. The organic matter content was mostly biorecalcitrant in the tested conditions, since unacclimated biomass removed only 30% in an organic carbon basis.

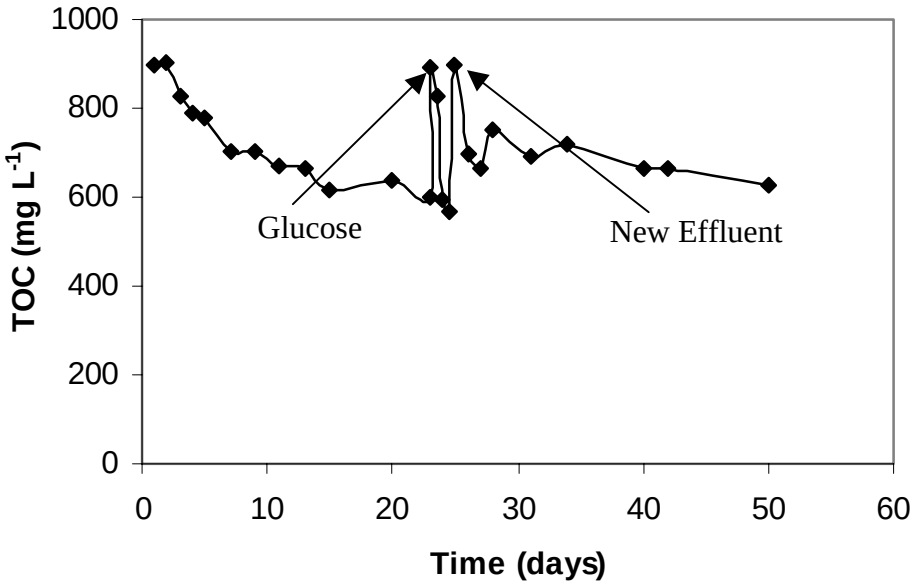

Figure 6.12. Zahn-Wellens biodegradability test of the effluent 1. Eolution of TOC as function of time

After 25 days, glucose as co-substrate was added in order to check if the microorganisms were able to eliminate a biodegradable substrate. It was observed that all the biodegradable substrate (glucose) was consumed in only 1 day, demonstrating that the biomass was no inhibited. Afterwards, the biomass was concentrated and a new batch of effluent 1 was added to test its biodegradability under acclimated culture conditions. Again, no significant TOC removal was observed. These results revealed that the

biorecalcitrance of this effluent, under the tested conditions, is associated with the structural stability of compounds towards microbiological attack but no with the toxicity of the solution (Gulyas, 1997). Therefore, this effluent is considered non-biodegradable and taking into account the proposed strategy it is recommended to be pretreated before sending it to a biological treatment plant.

6.4.2.2. Biodegradability of effluent 2

Fig. 6.13 shows TOC content evolution with time for effluent 2 during 25 days Zahn-Wellens test. Results show that organic matter is partially biodegradable since, after a short acclimatation period, the biomass removed about 50 and 75% of initial TOC within 2 and 5 days, respectively.

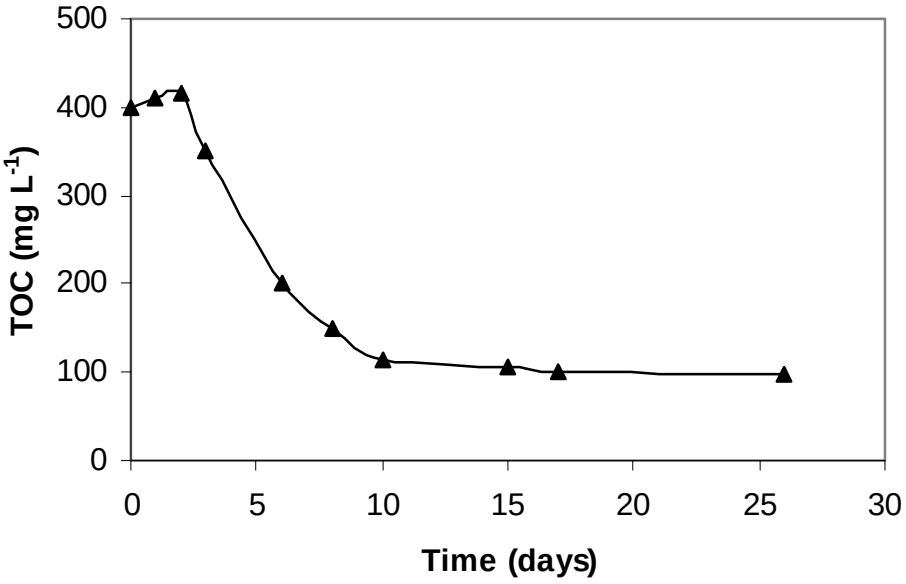

Figure 6.13. Zahn-Wellens biodegradability test of the effluent 2. Evolution of TOC as function of time

This effluent was classified as partly biodegradable because after 25 days 25% of organic carbon content still remains in solution. Taking into account that effluent 2 is a mixture of non-biodegradable effluents (e.g. effluent 1) and others mostly biodegradable (e.g. washroom wastewaters), the biorecalcitrant part must be coming from the first type of

effluents. By considering results of Zahn-Wellens test (Fig. 6.13) and the general strategy proposed for wastewater treatment, this effluent should be considered as a good candidate to be treated by biological means. In fact, this is the procedure used by the textile plant under study.

6.4.2.3. Biodegradability of effluent 3

Fig. 6.14 shows the evolution of TOC content versus time during 25 days for effluent 3.

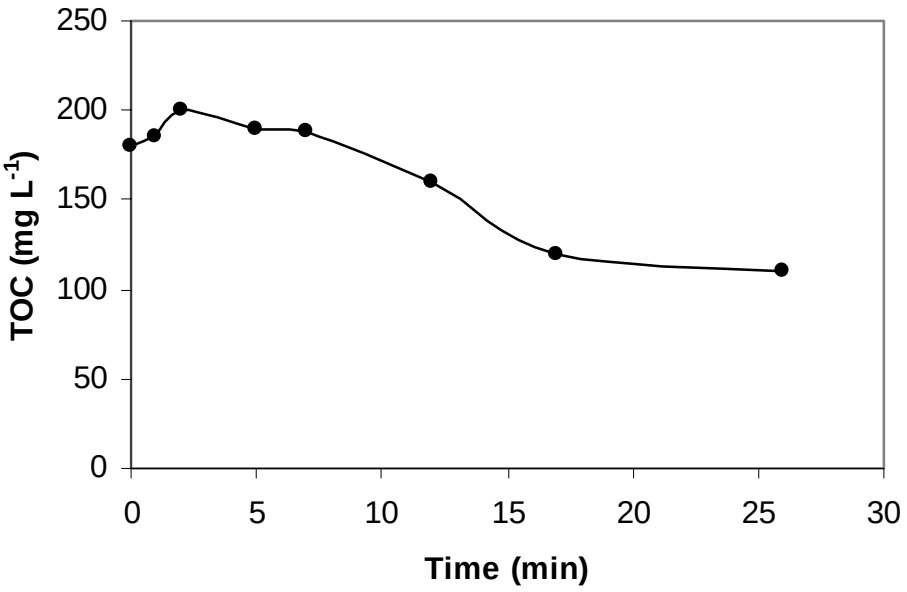

Figure 6.14. Zahn-Wellens biodegradability test of the effluent 3. Evolution of TOC as function of time

As it can be observed, organic matter is mostly biorecalcitrant under the tested conditions, since unacclimated bacteria only removed 40 % the organic carbon content within 25 days. This result is in agreement with the previous one, by considering into that in effluent 2 (the inlet to biological treatment plant) there was a significant biorecalcitrant TOC content. Therefore, the outlet of the biological treatment plant (effluent 3) confirmed this biorecalcitrance as well.

Thus, considering the proposed strategy, the effluent 3 should be post-treated by chemical process before discharge it.

6.4.3. Photo-Fenton process as pretreatment step

In this study, photo-Fenton process was selected as pretreatment in a coupled chemical biological process for effluent 1. The main objective was to find out the optimal operation conditions of the photo-Fenton reaction. For this purpose, photo-Fenton experiments were carried out using the coiled reactor operated in batch mode. Bearing in mind the high alkalinity of the effluent1 to be treated, the amount of hydrochloric acid used to bring down the pH ca. 3 (optimal pH for photo-Fenton system) would be relatively high. Furthermore, the amount of alkali needed to add before sending this effluent to a biological treatment would be high as well. This fact should be considered in the total cost of the treatment process. However, and considering the high concentration of carbonates present in this effluent, the acidification would allow the removal of these scavenging ions, permitting a better performance of the photo-Fenton system.

Temperature and both Fe^{3+} and H_2O_2 initial concentrations were optimised to enhance the biodegradability of effluent 1 by means of this process. Mineralization degree was monitored in order to determine the treatment duration. The biocompatibility of the pretreated solution was studied after 40 and 70% of TOC removal and photo-Fenton conditions were optimised to achieve these mineralization degrees in the lower possible time. In the following experiments, the mineralization of the effluent is described assuming a first order reaction already described in section 4.6.2.2 (eq. 4.26). From the $\ln(TOC/TOC_o)$ versus irradiation time plot, the first-order reaction rate constants (the slope) have been calculated and used to study the effect of different Fe^{3+}, H_2O_2, concentrations and temperature.

6.4.3.1. Effect of the initial Fe^{3+} concentration

To further elucidate the role of Fe^{3+} concentration on the mineralization of the effluent 1, a series of experiments varying the concentration of iron and keeping fixed the other parameters (H_2O_2 and temperature) were carried out. Fig. 6.15 shows a plot of first-order rate constant (k) as a function of Fe^{3+} concentration.

The best mineralization (k= 0.0067 min^{-1}) was obtained for Fe^{3+} concentration of 1.43 $mmol.L^{-1}$ at 60ºC and 150 $mmol.L^{-1}$ of H_2O_2 concentration.

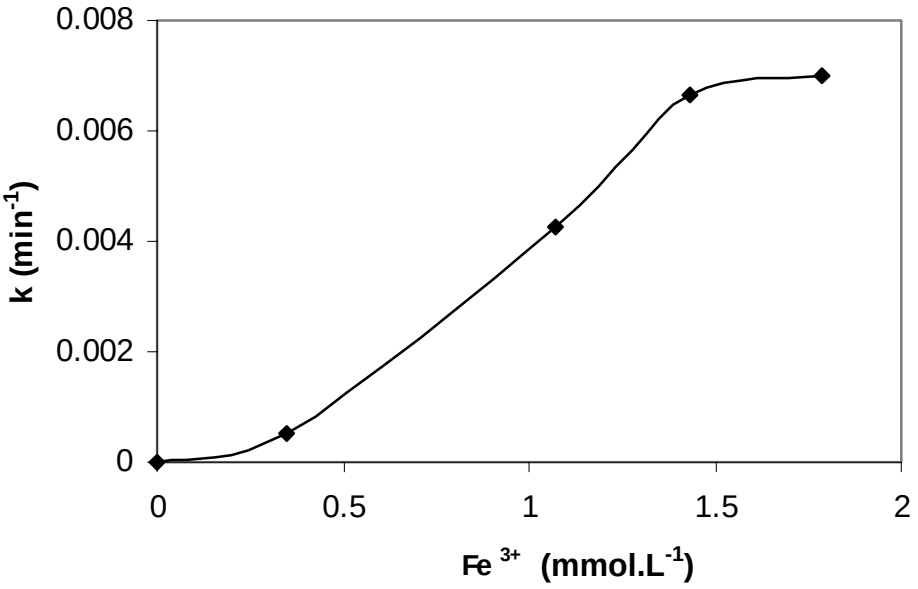

Figure 6.15. Initial rate constant of treated effluent by means of photo-Fenton process at different Fe^{3+} concentration. $[H_2O_2]$ = 50 mmol.L^{-1}, T = 60ºC

With this iron concentration, a 40% of mineralization was achieved after 120 min of phototreatment, as shown in Fig. 6.16. From that figure it can also be observed that the efficiency of the mineralization attains a plateau when the concentration of Fe^{3+} is between 1.43 and 1.8 mmol.L^{-1}. This may be due to:

(a) the increase of a brown turbidity in the solution during the photo-treatment, which hinders the absorption of the UV light required for the process.

(b) excessive formation of Fe^{2+} (eq. 1.18 and eq.1.12), which can compete with the organic carbon for $HO^{\bullet}$ radicals (eq. 1.11).

(c) H_2O_2 concentration can become the limiting factor of the oxidation-reduction reaction (eq.1.12) when high concentration of Fe^{3+} is used.

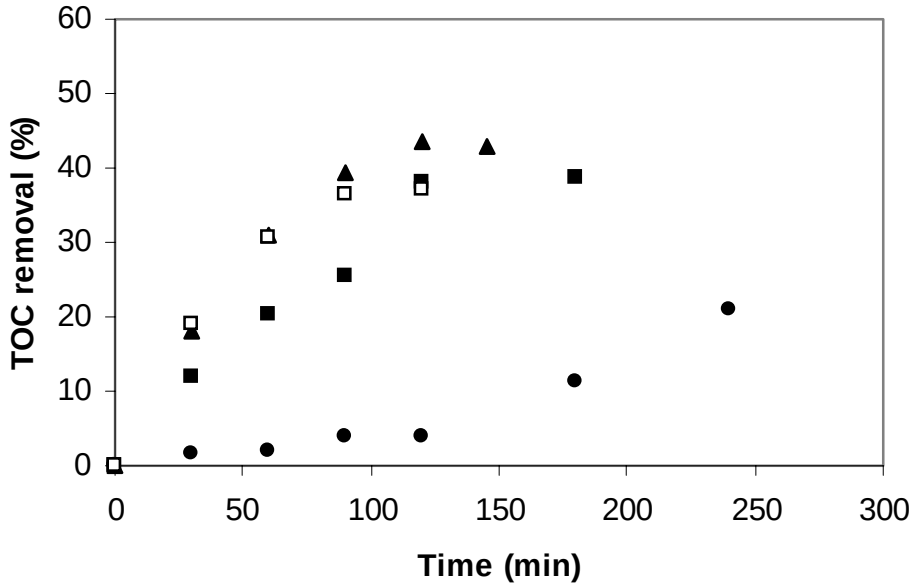

Figure 6.16. (%) TOC removal during the photo-Fenton treatment using different Fe^{3+} concentration.[H_2O_2] = 150 mmol.L^{-1}, T = 60ºC. (▲) [Fe^{3+}] = 1.43 mmol.L^{-1}, (□) [Fe^{3+}] = 1.79 mmol.L^{-1} , (■) [Fe^{3+}] = 1.07 mmol.L^{-1}, (●) [Fe^{3+}] = 0.36 mmol.L^{-1}

6.4.3.2. Effect of the initial H_2O_2 concentration

Another important parameter to consider in the photo-Fenton oxidation is the amount of H_2O_2 required to obtain the best efficiency in the treatment. In this sense, several experiments were performed fixing the optimal Fe^{3+} concentration determined before and the temperature of 60ºC (see section 6.4.3.3). As shown in Fig. 6.17, a significant enhancement of the mineralization efficiency was observed when the H_2O_2 concentration was increased from 0 to 441 mmol.L^{-1}.

Above this concentration, the oxidation rate is negatively affected by the progressive increase of H_2O_2 up to 510 mmol.L^{-1}. This is probably due to both the auto-decomposition of H_2O_2 into oxygen and water (eq. 3.33), and the scavenging effect of hydroxyl radicals by H_2O_2 (eq.3.34). This fact could be also observed in Fig. 6.18, where the mineralization above 441 mmol.L^{-1} is practically the same.

At the light of these experiments, the optimal concentration at 60ºC for H_2O_2 and Fe^{3+} were 1.43 and 441 mmol.L^{-1}, respectively.

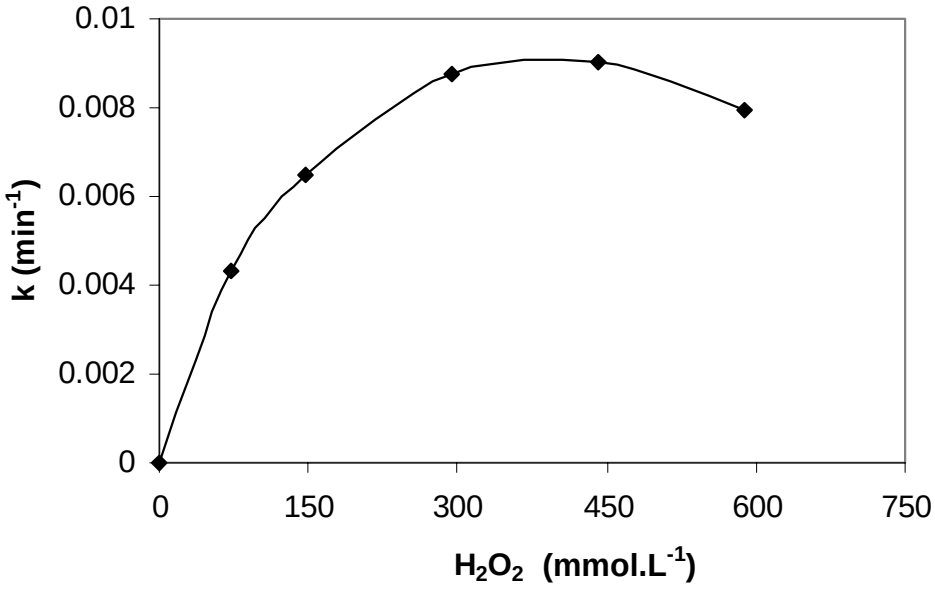

Figure 6.17. Initial rate constant of treated effluent by means of photo-Fenton process at different H_2O_2 concentration. [Fe^{3+}] = 1.43 mmol.L^{-1}, T = 60ºC

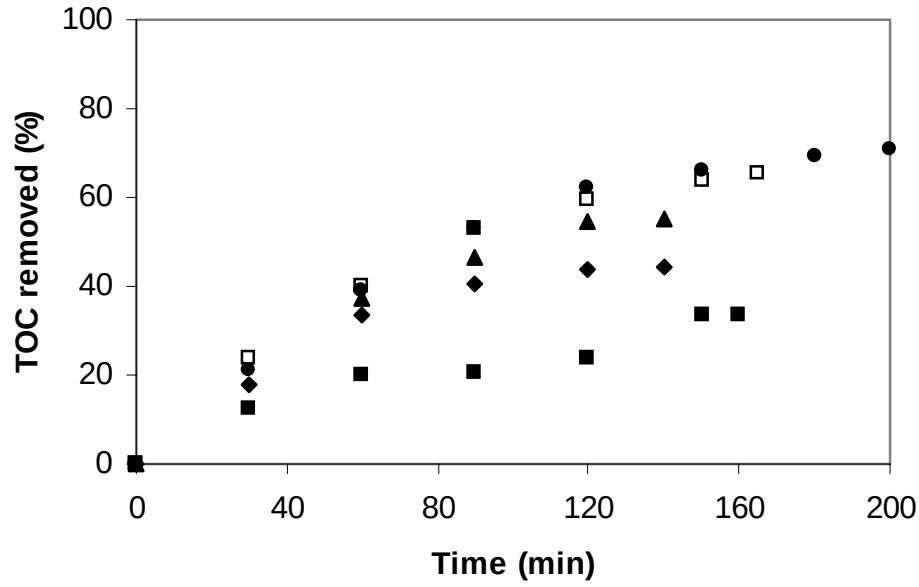

Figure 6.18. % TOC removal during the photo-Fenton treatment using different H_2O_2. [Fe^{3+}]= 1.43 mmol.L^{-1}, T = 60ºC. (●) [H_2O_2] = 588 mmol.L^{-1}, (□) [H_2O_2] = 441 mmol.L^{-1}, (▲) [H_2O_2] = 294 mmol.L^{-1}, (♦) [H_2O_2] = 147 mmol.L^{-1}, (■) [H_2O_2] = 73 mmol.L^{-1}

6.4.3.3. Effect of the temperature

Normally, the photo-Fenton process is carried out at room temperature. Nevertheless, considering that wastewaters coming from the textile industry have a temperature between 60 and 90°C, it was considered very important to test the effect of the temperature in the mineralization rate. Several experiments were performed at 30, 45, and 60ºC. As shown in Fig.6.19, a significant enhancement of the mineralization efficiency was produced when the temperature was increased.

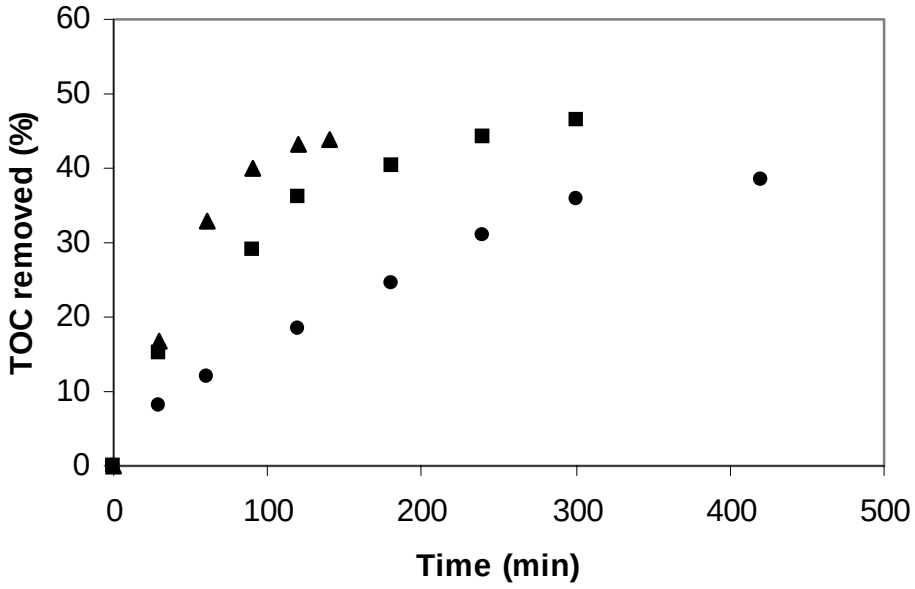

Figure 6.19. % TOC removal during the photo-Fenton treatment using different temperature. $[Fe^{3+}]$ = 1.43 mmol.L^{-1}, $[H_2O_2]$ = 147 mmol.L^{-1}. (▲) T = 60ºC, (■) T = 45ºC, (●) T= 30ºC

The treatment time necessary to achieve a 40% of mineralization was 7, 5 and 2 hours at 30, 45, and 60°C, respectively. It is also very important to make notice that the final time of reaction is marked by the exhaustion of H_2O_2, one of the key elements for the later study of biodegradability of the treated effluent.

In Fig.6.20 it is possible to observe that above 60°C a plateau is reached. From the results, photo-Fenton pretreatment process could be carried out at outlet autoclave

temperature and better efficiency would be expected when comparing with the same process at ambient temperature.

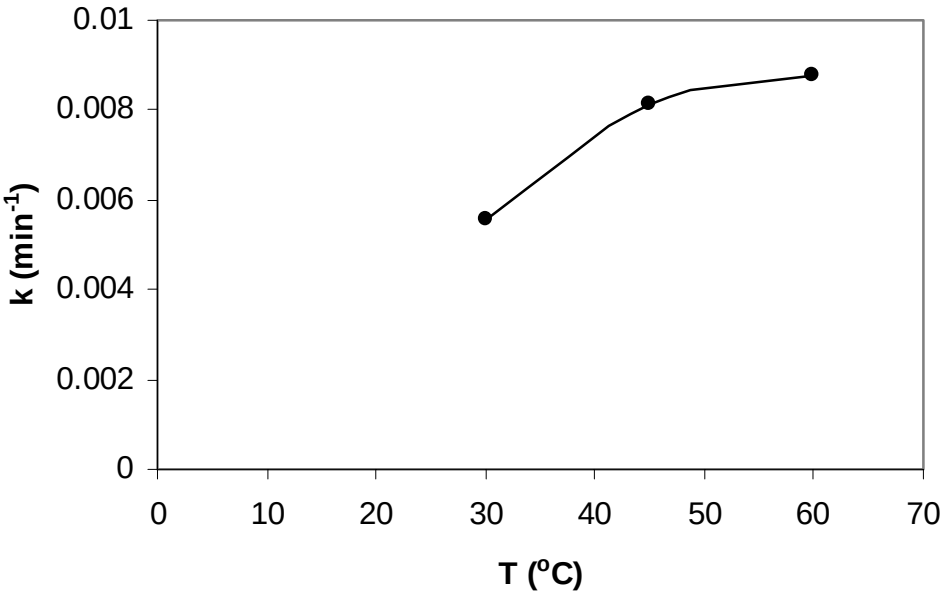

Figure 6.20. Initial rate constant of treated effluent by means of photo-Fenton process at different temperatures. $[Fe^{3+}]$ = 1.43 mmol.L^{-1}, $[H_2O_2]$ = 441 mmol.L^{-1}

6.4.4. Biodegradability evolution of photo-treated solution

From the results presented before, it was decided to fix the following condition for the pretreatment of effluent 1:

(a) for 40% of mineralization, $[Fe^{3+}]$ = 1.43 mmol.L^{-1}, $[H_2O_2]$ = 150 mmol.L^{-1}, T = 60ºC.

(b) for 70 % of mineralization, $[Fe^{3+}]$ = 1.43 mmol.L^{-1}, $[H_2O_2]$ = 441 mmol.L^{-1}, T = 60ºC.

In order to establish the biocompatibility after pre-treatment step, the biodegradability was evaluated by the Zahn-Wellens test, using unacclimated municipal sludge as initial inoculum. Fig. 6.21 illustrates TOC content evolution with time during Zahn-Wellens test for 40 and 70% of mineralization. A control experiment using diethylenglycol (400 mg.L^{-1}) as biogenic substrate is also presented.

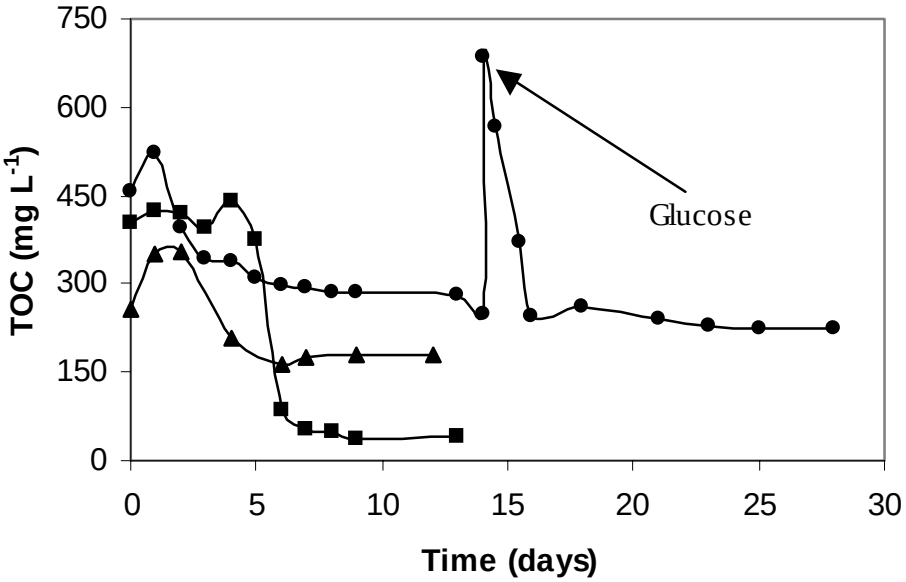

Figure 6.21. Zahn-Wellens biodegradability test with non-acclimated biomass. Evolution of TOC as a function of time: (•) after 40 % of mineralization.(▲) after 70 % of mineralization. (■) control with diethylenglycol

The figure shows that, for 40 % of mineralization, TOC removal efficiency is not very significant, since only 50 % was removed within 28 days what means that the pretreatment was not enough to produce an easily biodegradable solution. After 15 days, glucose as co-substrate was added and the biomass response was positive, since all this substrate was consumed very fast. This fact again allows confirms that the biorecalcitrance of this treated effluent is due to the absence of enzymes able to degrade the remaining organic matter and not its toxicity.

In the case of 70% of mineralization, TOC eliminated was only 30 % in 12 days. In spite of showing a faster initial TOC removal rate than previous case, the amount of TOC remaining in solution is still very important. This means that even a high mineralization degree in the pretreatment step is not enough to produce easily biocompatible solutions.

In order to check the biomass conditions, a control experiment using diethylenglycol (400 $mg.L^{-1}$) was carried out. Diethylenglycol was degraded up to 90 % within 6 days under the same conditions used to test the biodegradability of the pretreated effluent, showing that the activity of activated sludge is appropriate (see Fig. 6.21).

To verify the results shown in Fig. 6.21, a supplementary experiment attempting biodegradation of the effluent treated until 70% of mineralization was carried out in batch mode with the FBR and the results are presented in Fig.6.22. As it is illustrated, 50 % of TOC was removed within 12 days, although this test was carried out under more theoretically favorable conditions than the ones used in the Zahn-Wellens test.

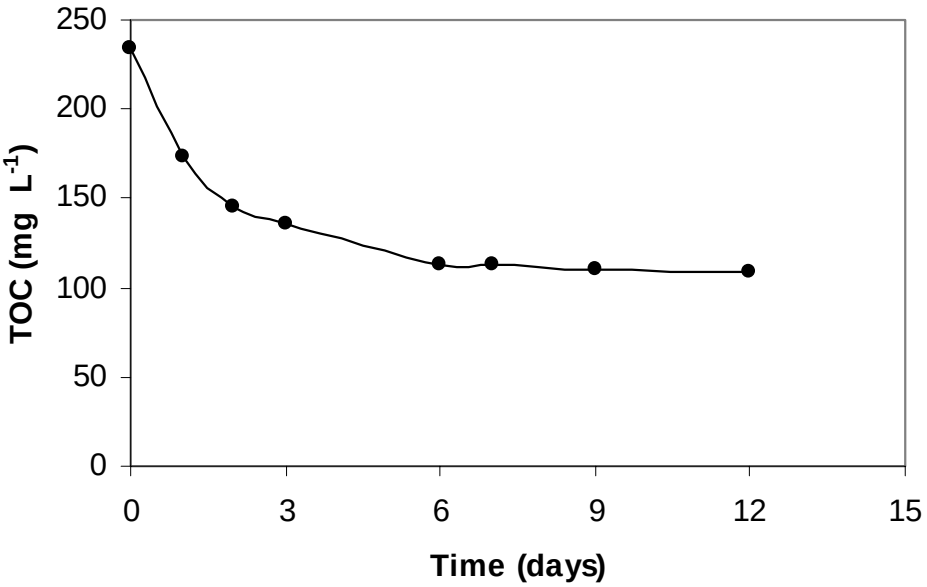

Figure 6.22. Biodegradability test of the phototreated effluent 1 after 70% of mineralization. Evolution of TOC in FBR as function of time

First of all, the concentration of available biomass was higher and secondly, fixed biomass systems give better performance in industrial wastewater biological processes. Even thought, the percentage of TOC removed was still very low, confirming the biorecalcitrance of the effluent even after 70% of photo-mineralization.

To conclude this biodegradabilility revision and to discard a possible inhibitory effect of high salt concentration present in the textile wastewater under study, the two pretreated solutions was diluted two-fold and a new Zahn-Wellens test was done for both. The results are presented in Fig. 6.23. The weak biodegradability observed confirms once again that the biorecalcitrance is due to the absence of enzymes able to degrade the organic

matter, as it was already observed, and not by the osmotic inhibiting effect that could be produced by the high concentration of salts.

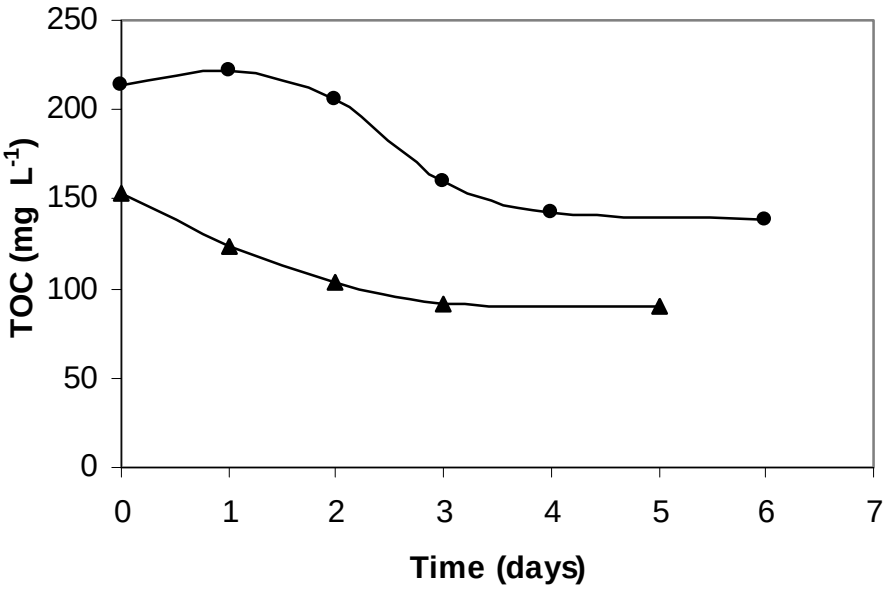

Figure 6.23. Zahn-Wellens biodegradability test of effluent 1 two-fold diluted after: (•) after 40% of mineralization; and (▲) after 70% of mineralization. Evolution of TOC as a function of time using acclimated biomass

At the light of these results, it is clear that the coupled system proposed to apply in the treatment of this effluent by means of photo-Fenton process cannot be feasible at the tested conditions. Other AOPs, like, ozone, TiO_2/UV, wet oxidation, etc, should be tested in order to make the effluent more biocompatible.

6.4.5. Causes for photo-treated solution biorecalcitrance

In order to attempt an explanation for the strong biorecalcitrance of the phototreated effluent, UV-vis spectroscopy and HPLC analysis have been made to identify and to follow the evolution of the main organic substances contained in the effluent.

Fig. 6.24 shows that initial effluent presented two absorption bands at 280 and 530 nm. The band present in the visible zone (responsible of color) disappears after 40% of mineralization. However, the absorption band at 250-280 nm is only partially eliminated.

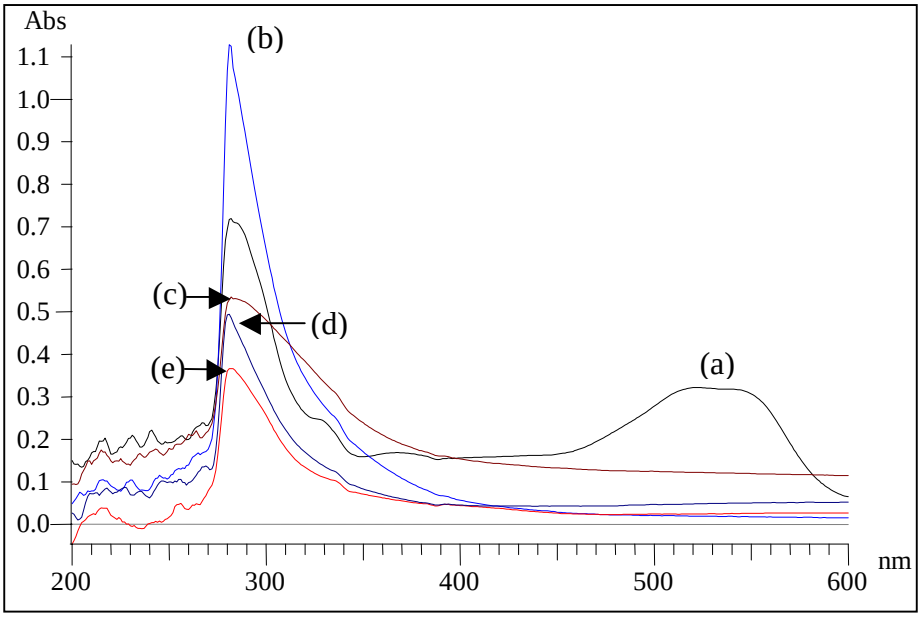

Figure 6.24. UV-vis spectra of the effluent: (a) before photo-Fenton pretreatment, (b) after 40%, (c) after 50%, after 65%, and (e) after 70% of mineralization

This means that biorecalcitrant aromatic intermediates could still be present even after 70% of photo-Fenton mineralization. These results may be used in a first approximation to explain the very strong biorecalcitrance displayed by the treated textile effluent.

Moreover, HPLC analyses were carried out and one compound present in the initial effluent was identified and quantified. This compound is rapidoprint (see Table 6.2), which is used in the textile industry as anti-reductor. Its biodegradability by means of Zahn-Wellens test can be observed in Fig.6.25. The test shows that, even though TOC removal reached 90% of initial TOC content, it took a long period of time (up to 28 days). If it compare with time needed for the same removal of diethylene glycol (less than 6 days) the effluent contained rapidoprint can be classified as low biodegradable.

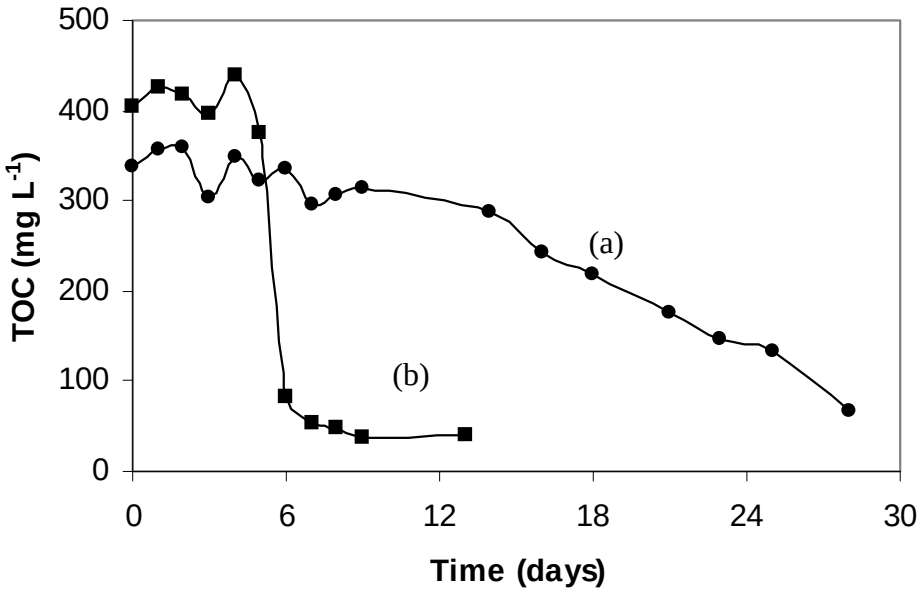

Figure 6.25. Zahn-Wellens biodegradability test with non-acclimated biomass. Evolution of TOC as a function of time: (a) Rapidoprint solution. (b) control with diethylenglycol

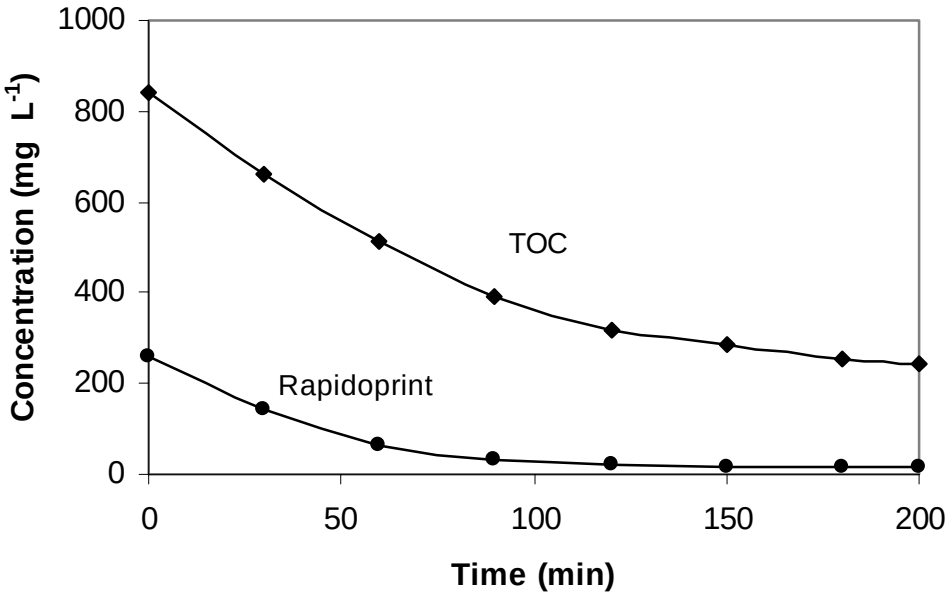

Figure 6.26. Concentration evolution ($mg.L^{-1}$) during photo-Fenton treatment of: (a) TOC , and (b) rapidoprint. $[Fe^{3+}] = 1.43 mmol.L^{-1}$, $[H_2O_2] = 441 mmol.L^{-1}$, T = 60ºC

Fig. 6.26 shows the evolution of TOC concentration in (a) rapidoprint solution and (b) in effluent 1. When 95% of rapidoprint was eliminated, about 30% of the total TOC still remained in solution, confirming that there was an important accumulation of intermediates. Nevertheless, the biorecalcitrance cannot be attributed to the presence of the biorecalcitrant rapridoprint, but to the present of aromatic compound as stated before.

6.4.6. Photo-Fenton process as post-treatment step

According to the proposed strategy, effluent 3 has been considered as potential wastewater in which chemical the post-treatment step could be very useful. In this sense several experiments by means of photo-Fenton process were carried out using a solar simulator (reactor I) and the coiled photoreactor (reactor J), both described in the experimental section 6.4.2.

In the following experiments, the mineralization of effluent 3 was also described assuming a first order kinetic reaction already described in section 3.6.2.2 (eq. 3.31). Thus, rate constants have been calculated and used to study the effect of different H_2O_2 initial concentration for the same iron initial concentration at room temperature.

As shown in Fig. 6.27, maximum mineralization efficiency was reached when the lowest H_2O_2 initial concentration (20.5 $mmol.L^{-1}$) was used. Above this concentration, the mineralization seems to be negatively affected by the progressive increase of H_2O_2. This fact has been already commented in chapter 3.

The percentage of mineralization obtained is shown in Fig. 6.28. As it can be observed, more than 80% of mineralization was reached in four hour of treatment. The use of small amount of iron contributes to avoid problems with its necessary elimination. Furthermore, as it has been commented before, the European Community directives allow 20 $mg.L^{-1}$ of iron in treated wastewater to be discharge into municipal biological treatment plant (EEC, 1992). Taking into account this directive, the resulted effluent from photo-Fenton treatment could be sent directly to municipal collectors.

It is also important to stand out that the effectiveness of photo-Fenton process using a solar simulator suggest the possibility of running the post treatment step with the direct use of solar light. Therefore, it would make the biological-photochemical coupled system proposed most attractive and less expensive.

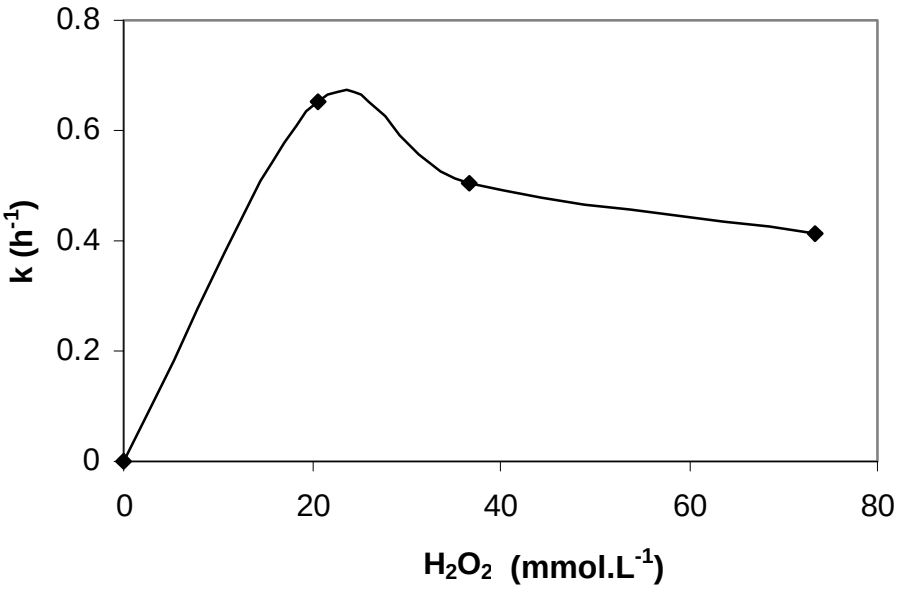

Figure 6.27. Initial rate constant of treated effluent by means of photo-Fenton process at different H_2O_2 concentration. $[Fe^{3+}]$ = 0.36 mmol.L^{-1}, room temperature

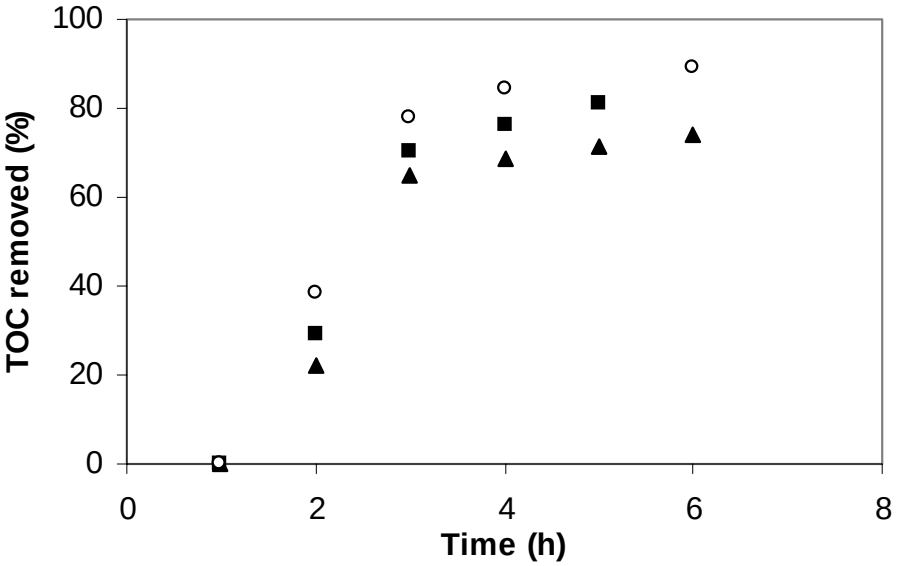

Figure 6.28. % TOC removal during the photo-Fenton treatment in reactor I using different H_2O_2. $[Fe^{3+}]$= 0.36 mmol.L^{-1}. (o)$[H_2O_2]$= 20.6 mmol.L^{-1}, (■)$[H_2O_2]$ = 36.8 mmol.L^{-1}. (▲)$[H_2O_2]$= 73.5 mmol.L^{-1}

Several experiments were also made in the coiled photoreactor (reactor J). As shown in Fig. 6.29, once more, maximum mineralization efficiency was reached when the lowest H_2O_2 concentration (2.2 mmol.L^{-1}) was used.

In this case, close to 80% of mineralization was also obtained but in less time (3 h) of treatment and using a smaller H_2O_2 concentration than the previous case.

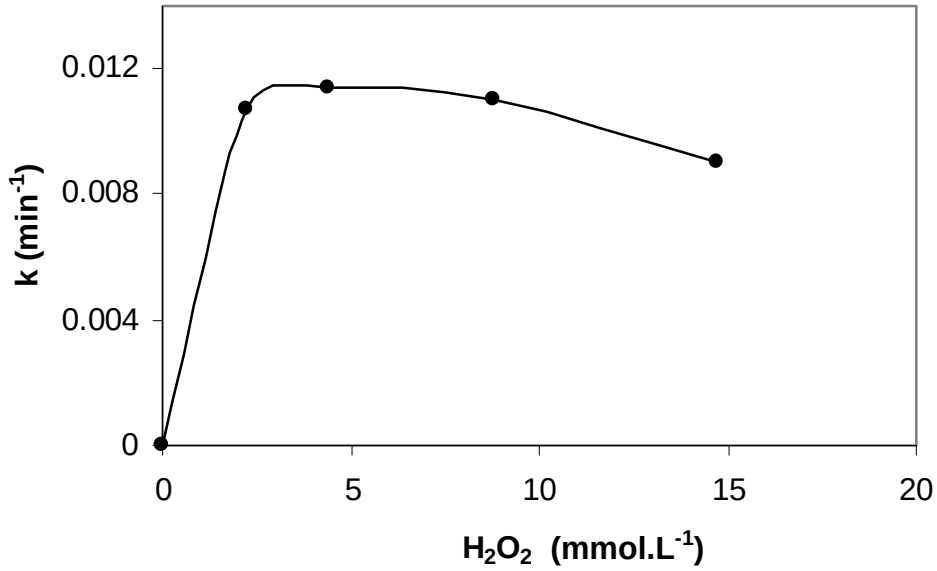

Figure 6.29. Initial rate constant of treated effluent by means of photo-Fenton process at different H_2O_2 concentration. $[Fe^{3+}]$ = 0.36 mmol.L^{-1}, T = room temperature

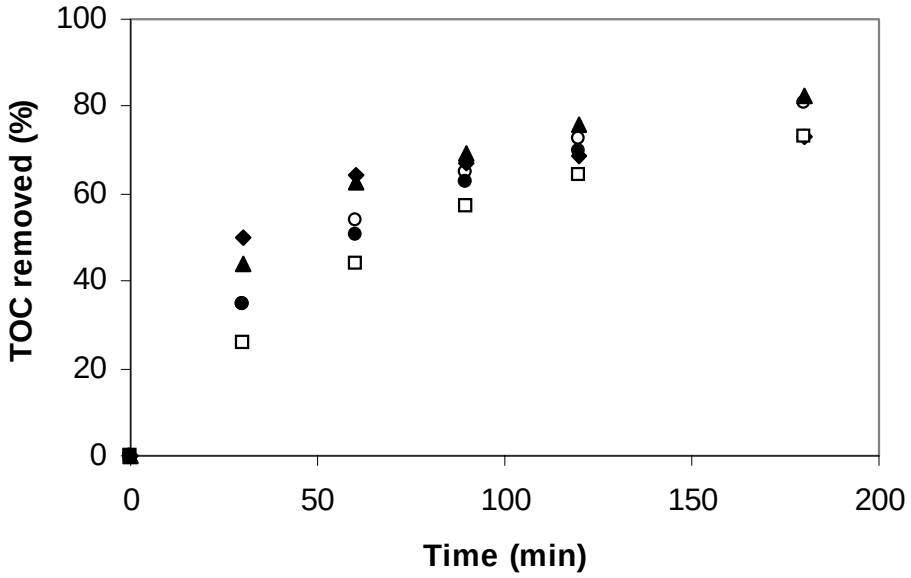

Figure 6.30. % TOC removal during the photo-Fenton treatment in reactor J using different H_2O_2. $[Fe^{3+}]$ = 0.36 mmol.L^{-1}. (o) $[H_2O_2]$ = 20.6 mmol.L^{-1}, (■) $[H_2O_2]$ = 36.8 mmol.L^{-1}. (▲) $[H_2O_2]$ = 73.5 mmol.L^{-1}, (□) $[H_2O_2]$ = 441 mmol.L^{-1}, (♦) $[H_2O_2]$ = 147 mmol.L^{-1}

7. Conclusions and Recommendations

7.1. Conclusions

The results obtained in the study lead to the following conclusions:

(1) Fenton, photo-Fenton and UV/H_2O_2 processes happened to be appropriate methods to efficiently remove nitrobenzene and phenol from aqueous solutions.

(2) Degradation rates of NB and phenol by means of Fenton process can be expressed as a first-order reaction with respect to NB and phenol concentration. The operating molar ratios of reactants concentration have been established as follow: $[Compound]_o/[H_2O_2] > 0.016$, $[Compound]_o/[Fe^{3+}]_o > 0.17$ and $[H_2O_2]_o/[Fe^{2+}]_o > 11$. This reaction rate becomes insensitive to H_2O_2 concentration when H_2O_2 to compound molar ratio is higher than ca. 16 and 5 for NB and phenol, respectively.

(3) Although the chemistry of Fenton's systems involves a rather complex mechanism, an attempt has been made to fit experimental results to simplistic kinetic model and empirical kinetic equation. Equations quantitatively predicting NB and phenol degradation rate under a wide range of experimental conditions has been established and its precision has been contrasted by comparing them with the experimental data. Furthermore, our study provided additional insight into mechanistic and kinetic factors controlling NB and phenol degradation rate in Fenton process.

(4) The identification and quantification of nitrophenols as reaction intermediates in the treatment of NB by means of the Fenton process suggests that its degradation takes place by reaction with $HO^{\cdot}$ radical as the oxidant species. Kinetic results and the comparison of initial products distribution under a wide range of experimental conditions with other oxidation process support the presence of $HO^{\cdot}$ radicals in this system.

(5) Direct photolysis of NB under the tested conditions represented a good alternative in the treatment of this compounds taking into account that e.g. 73 % of mineralization was reached in 2 hours when solar radiation was used (with artificial light, percentage of achieved mineralization was ca. 60 %). On the contrary, this method is

not recommended for the treatment of phenol, as mineralization percentage was very low and in some cases negligible. This different behavior in the studied compounds is related to their absorbing properties.

(6) Photo-Fenton process was found to be the most effective method in the treatment of phenol and NB in aqueous solution. Mineralization rate was faster in the case of phenol, probably favored by the presence of electron-donating groups like HO. The iron salts used as catalyst in this process could be Fe^{2+} or Fe^{3+}, as the degree of mineralization achieved for both species was similar.

(7) The use of solar radiation in the photo-Fenton process is a good alternative in the treatment of phenol-polluted waters. By this process, complete mineralization of these solutions was achieved. Besides this, the estimation of the intrinsic kinetic constants performed for photo-Fenton process represented a significant advance to better understand this process and the contribution of the light. As it was expected, the constants obtained in both reactors (solarbox and CPC) are practically the same since they depend neither on the radiation source nor on the geometry of the reactor. Thus, lab scale data could be used for pilot plant scale calculations.

(8) The process H_2O_2/UV has also turned out to be a good treatment method for mineralization of phenol and NB. The irradiation source presented a big influence in this process. In this sense, UV 254 nm turned out to be more efficient in comparison with polychromatic black lamp (300-400 nm) and xenon lamp (300- 560 nm). Some interesting results were reached when solar radiation was used. For example, 90% of mineralization was reached for phenol within 2 hours in a parabolic collector. In spite of these results, this method is not recommended in presence of solar radiation because the quartz tube used in the photo-reactor to perform these experiments is very expensive and it is also a type of tube difficult to manage.

(9) Regarding Fe^{3+}/UV-vis and although this process has been presented for some authors as a real alternative in the treatment of organic compounds, the results obtained for phenol and NB under the tested conditions were not satisfactory regarding mineralization of the target compounds. However, it would be feasible to

be used when the objective is the degradation, being used as pretreatment step in combination with other treatment methods, such as a biological process.

(10) The third studied compound, DCDE, was found to be non-biodegradable by the activated sludge cultures maintained in the lab. The acclimatation of the cultures to DCDE did not improve its biodegradability. Besides this, at concentrations lower than 50 mg L^{-1}, DCDE showed no significant exogenous inhibition to activated sludge cultures

(11) The intermediates of DCDE produced by H_2O_2/UV system were significantly more biodegradable than DCDE itself by both non-acclimated and acclimated to DCDE cultures. From short, long, and mid-term biodegradation tests, this study demonstrated the usefulness of the H_2O_2/UV system as pretreatment method to a sewage sludge process for the complete mineralization of DCDE.

(12) With regard to the data provided by the different biodegradation tests, results of the mid-term test would probably contribute mostly to the practical application of the coupled process by allowing the prediction of expected organic matter removal. Long-term tests, on the other hand, might predict the toxicity of the reaction intermediates products on the biomass over extended periods of exposure. Short-term test provides a rapid alternative method to the conventional 5-days BOD biodegradability test.

(13) A strategy for the use of a chemical-biological coupled system has been applied to three different effluents produced in textile industry. This strategy is considered a very useful tool to be taken into account in such a type of treatment, offering a general vision of the problem. As two of these effluents (effluent 1 and 3) were found to be non-biodegradable, photo-Fenton process was used as pretreatment in the case of effluent 1 and post-treatment in the case of effluent 3.

(13.1) Regarding effluent 1, the biorecalcitrance character was maintained even after the photo-Fenton treatment. This fact was attributed to the absence of enzymes able to degrade it and not to its toxicity, but showed that it is not always possible to successfully apply a coupled chemical-biological system.

(13.2) The post-treatment of effluent 3 by means of the photo-Fenton process showed to be a good alternative prior to its discharge.

7.2. Recommendations

According to the obtained results, the following recommendations should be taken into account in order to complete this research:

(1) Regarding the degradation of NB by means of Fenton process, the unknown intermediates should be identified in order to establish a complete mechanism of reaction. Besides, a more complete mathematical model could be developed to validate the empirical one established from Arrhenius equation in the degradation of NB and phenol.

(2) With regard to the scale-up of photo-reactors, although the estimation of intrinsic kinetic constants performed represented a significant advance, more experiments must be performed in order to corroborate the validity of the model proposed.

(3) About the enhancement of the biodegradability of DCDE solutions by means of UV/H_2O_2 and taking into account that the acclimatation of the cultures to DCDE did not improve its biodegradability, alternative approaches to ensure real acclimatation, such as acclimatation with DCDE oxidation intermediates products rather than pure DCDE should be carried out. In addition, toxicity studies as a complement to the inhibition test is to be performed in order to assure the toxicity of DCDE.

(4) Concerning the use of combined chemical-biological process for the treatment of textile wastewaters, toxicity tests should be carried out in order to determine appropriately the toxicity of the treated effluent, taking into account that toxicity test is a very important parameter in the general strategy proposed for wastewater treatment. Besides, try to identify the organic compounds responsible for the

biorecalcitrance. Finally, other advanced oxidation processes could be applied in order to study their efficiency in comparison with photo-Fenton process in the biodegradability enhancement of the textile wastewater.

8. Glossary

Symbols		Unit
A	Arrhenius equation coefficient	
A_t	Total absorbance of the effluent	
b	Optic way	cm
C	Concentration	$mol.L^{-1}$
C_o	Initial concentration	$mol.L^{-1}$
d	Inner diameter	cm^{-1}
E_a	Activation energy	$kJ.mol^{-1}$
F_λ	Source of photons factor	
I_o	Ultraviolet incident radiation	$Einsteins.L^{-1}.s^{-1}$
k_{dark}	First-order rate constant for Fenton-dark	min^{-1}
k_d	Second-order rate constant	$L.mol^{-1}s^{-1}$
$k_{illuminated}$	Intrinsic kinetic constant	$L.Einstein^{-1}s^{-1}$
k_{obs}	Pseudo-first-order rate constant	min^{-1}
K_s	Half-saturation constant in Monod	$gr.cm^{-3}$
n^o_{ox}	Amount of initials mol	mol
n_{ox}	Amount of mol	mol
Q	Accumulate energy per unit of volume	$kJ.L^{-1}$
R	Universal gas constant	$J.mol^{-1}.K^{-1}$
R_D	Degradation rate	$L.mol^{-1}s^{-2}$
R_{ox}	Intensive reaction rate	$mol.m^{-3}s^{-1}$
S	Concentration of substrate in Monod equation	$mol.L^{-1}$
t_d	Decomposition time	min
t_{99}	Time required for 99% of conversion	s
t	Time	min
T	Temperature	K, ^oC
V	Volume	L
$V_{illuminated}$	Volume of illuminated zone	L
W_{abs}	Absorbed radiation	$\mu Einsteins\ s^{-1}$
W_e	Photon flow entering to the reactor	$\mu Einsteins\ s^{-1}$

Greek alphabetic		**Unit**
ϕ	Quantum yield	mol. mol photón^{-1} = mol.Einstein^{-1}
ε_{H2O2}	The absorbency of hydrogen peroxide	L.mol^{-1}cm^{-1}
λ	Wavelength	nm
μ	Absorption; Specific growth rate	cm^{-1}, s^{-1}
μ_{max}	Maximum specific growth rate	s^{-1}
η	Fraction of light absorbed by H_2O_2	

Abbreviations		**Unit**
AOP	Advanced Oxidation Processes	
BOD	Biological Oxygen Demand	mg O_2.L^{-1}
DCDE	Dichlorodiethyl Ether	
COD	Chemical Oxygen Demand	mg O_2.L^{-1}
CPC	Compound Parabolic Collector	
FNX	Experiments with NB by means of Fenton process	
FPX	Experiments with phenol by means of Fenton process	
HPLC	High Performance Liquid Chromatography	
MLSS	Mixed Liquor Suspended Solid	mg.L^{-1}
mo	Microorganisms	
MSS	Mineral Salt Solution	
N	Normal concentration	eq.L^{-1}
NB	Nitrobenzene	
NBX	Experiments with phenol by means of UV-based processes	
PTC	Parabolic Trough Collector	
PhX	Experiments with phenol by means of UV-based processes	
RAS	Activated Sludge Reactor	

TOC	Total Organic Carbon	$mg\ C.L^{-1}$
UV	Ultraviolet radiation	
UV_G	Global Ultraviolet radiation	

9. Publications derived from this work

9.1 Publications

Rodriguez, M., Timokhin, V., Contreras, S., Chamarro, E., and Esplugas, S. (2003) "Rate equation for the degradation of nitrobenzene by Fenton-like reagent", *Advances in Environmental Research*, **7**:583-595.

Rodriguez, M., Ben Abderrazik, N., Contreras, S., Chamarro, E., Gimenez, J. and Esplugas, S. (2002) " Iron (III) photooxidation of organic compounds in aqueous solutions", *Appl. Cat. B-Environ.*, **37**:131-137.

Rodriguez, M., Timokhin, V. N., Michl, F., Contreras, S., Gimenez, J. and Esplugas, S. (2002) " The influence of different irradiation sources on the treatment of nitrobenzene", *Catalysis Today*, **76**:291-300.

Rodriguez, M., Sarria, V., Esplugas, S. and Pulgarin, C. (2002) " Photo-Fenton treatment of a biorecalcitrant wastewater generate in textile activities. Biodegradability enhancement of the photo-treated solutions", J. *Photochem. Photobiol. A:Chemistry*, **151**:129:135.

Rodriguez, M., Kirchner A., Contreras, S., Chamarro, E. and Esplugas, S. (2000) "Influence of H_2O_2 and Fe^{3+} in the photodegradation of nitrobenzene", J. *Photochem. Photobiol. A:Chemistry*, **133**:123-127.

9.2. Communications

- *8th International Conference on Advanced Oxidation Technologies for Water and Air Remediation* (Toronto (Canada), November 17-21, 2002): "Photo-Fenton treatment of a biorecalcitrant wastewater generate in textile activities. Biodegradability enhancement of the photo-treated solutions", oral presentation.

- *2nd European Meeting on Solar-chemistry and Photocatalysis: Environmental Applications.* (Saint-Avold (France), May 29-31, 2002): "Mineralization of nitrobenzene in aqueous solution using sun light", poster presentation.

- *2nd European Meeting on Solar-chemistry and Photocatalysis: Environmental Applications.* (Saint-Avold (France), May 29-31, 2002): "Limiting factors in connect of a photochemical and biological system to treat wastewater coming from the textile industry: A real case", poster presentation.

- *2nd European Workshop on Water, Air and Soil Treatment by Advanced Oxidation Technologies* (Poitiers (France), February 28- March 2, 2001): "Dark and phtoassited mineralization of phenol, aniline and nitrobenzene", oral presentation.

- *5to Congreso de Fotoquímica, COFT-5* (Torremolinos (Málaga, España), Abril 1-4, 2001):" The photo-Fenton process reaction an effective photochemical process in the treatment of phenol, nitrobenzene an aniline", oral presentation.

- *2nd International Conference on Oxidation Technologies for Water and Wastewater Treatment* (Clausthal-Zellerfeld (Germany), May 29-31, 2000): "Iron (III) photooxidation of aromatic compounds", poster presentation.

- *2nd International Conference on Oxidation Technologies for Water and Wastewater Treatment* (Clausthal-Zellerfeld (Germany), May 29-31, 2000): "Kinetic of phenol removal by Fenton's reagent", poster presentation.

- *8th Mediterranean Congress on Chemical Engineering* (Barcelona (Spain), 10-12 November 1999): "Efficiency of the degradation of phenolic compounds by the Fe^{3+}/H_2O_2 process ", poster presentation.

- *8th Mediterranean Congress on Chemical Engineering* (Barcelona (Spain), 10-12 November 1999): "Removal of phenol in aqueous solution by Fenton reagent", poster presentation.

- *4to Congreso de Fotoquímica, COFT-4* (Gandía, (Valencia, España), Marzo 21-24, 1999): "Influence of H_2O_2 and Fe^{3+} in the photodegradation of nitrobenzene ", oral presentation.

10. Bibliography

Adams, C., Randall, A. and Byung, J. (1997) "Effects of ozonation on the biodegradability of substituted phenols", *Wat. Res*., **31**: 2655-2663.

Ajona, J. and Vidal, A. (2000) "The use of CPC collectors for detoxification of contaminated water: Design, construction and preliminary results", *Solar Energy*, **68**: 109-120.

Akata, A. and Gurol, M. (1992) "Photocatalytic oxidation process in the presence of polymers", *Ozone Sci. & Eng*., **14**: 367-380.

Alaton, I. and Balcioglu, I. (2002) "The effect of pre-ozonation on the H_2O_2/UV treatment of raw and biological pre-treated textile industry wastewater", *Water Sci. Technol.,* **45**: 297-304.

Alonso y del Pino, M. (1996) " Aspectos fundamentals y practices de la aplicación de sistemas de oznación en la eliminación de contaminantes nitroaromáticos del agua", Doctoral Thesis, Departamento de Ingeniería Química, Universidad de Extremadura.

Anderson, J., Link, H., Bohn, M. and Gupta, B. (1991) "Development of U.S. solar detoxification technology: An introduction", *Solar En. Mat.,* **24**: 538-549.

Andreozzi, R., Caprio, V., Insola, A. and Marotta, R. (1999) "Advanced Oxidation Processes (AOP) for water purification and recovery", *Catalysis Today*, **53**: 51-59.

Arnold, S., Hickey, W. and Harris, R. (1995) "Degradation of atrazine by Fenton's reagent: Condition optimization and product quantification", *Environ. Sci. Technol*., **29**: 2083-2089.

ASTM: American Society for Testing and Materials, (1987a) "Standards tables for terrestrial direct normal solar spectral irradiance for air mass 1.5", Designation: E891-87.

ASTM: American Society for Testing and Materials, (1987b) "Standard Tables for Terrestial Solar Spectral Irradiance at Air Mass 1.5 for a 37º Tilted Surface", Designation: E892-87.

Bahnemann, D., Cunningham, J., Fox, M., Pelizzetti, E., Serpone, N. (1994) "*Photocatalytic treatment of waters*", Aquatic and surface photochemistry. G. R. Helz, R. G. Zepp,D. G. (eds.). Lewis Publishiers: 261-316.

Balanosky, E., Fernandez, J., Kiwi, J. and Lopez, A. (1999) "Degradation of membrane concentrates of the textile industry by Fenton like reactions in iron-free solutions at biocompatible pH values", *Water Sci. Technol.*, **40**: 417-424.

Balcioglu, I. and Arslan, I. (1999) "Treatment of textile industry wastewater by enhanced photocatalytic oxidation reaction", *Journal of Advanced Oxidation Technologies*, **4**: 189-195.

Balcioglu, I. and Arslan, I. (2001) "Partial oxidation of reactive dyestuffs and synthetic textile dye-bath by the O_3 and O_3/H_2O_2 processes", *Water Sci. Technol*. **43**: 221-228.

Bandara, J., Nadtochenko, V., Kiwi, J. and Pulgarin, C. (1997) "Dynamics of oxidant addition as a parameter in the modeling of dye mineralization (Orange-II) via Advanced Oxidation Technologies", *Water. Sci.& Technol*., **35**: 87-93.

Barb, W., Baxendale, J., George, P. and Hargrave, K. (1951) "Reactions of ferrous and ferric ions with hydrogen peroxide. Part I. The ferrous ion reaction", *Transacions of the Faraday Society*, **47**: 462-500.

Bauer, R., Waldner, G., Fallmann, H., Hager, S., Klare, M., Krutzler, T., Malato, S. and Maletzky, P. (1999) "The photo-fenton reaction and the TiO_2/UV process for waste water treatment - novel developments", *Catalysis Today,* **53**: 131-144.

Baxendale, J. and Wilson, J. (1957) "The photolysis of hydrogen peroxide at high light intensities", *Transacions of the Faraday Society*, **53**: 344-356.

Beltran, F. J., Encinar, J. M. and Alonso, M. A. (1998) "Nitroaromatic hydrocarbon ozonation in water. 2. Combined ozonation with hydrogen peroxide or UV radiation", *Ind. Eng. Chem. Res*., **37**: 32-40.

Beltrán, F., González, M. and Alvarez, P. (1997) "Tratamiento de aguas mediante oxidación avanzada (I): Procesos con ozono, radiación ultravioleta y combinación ozono/radiación ultravioleta", *Ingenieria Química*, **331**: 161-168.

Benitez, F., Beltran, F., Acero, J. and Pinilla, M. (1997) "Ozonation of phenolic acids present in wastewater from olive mills", *Ind. Eng. Chem. Res*., **36**: 638-644.

Benitez, F., Beltran-Heredia, J., Acero, J. and Rubio, F. (2000) "Contribution of free radicals to chlorophenols decomposition by several advanced oxidation processes", *Chemosphere*, **41**: 1271-1277.

Benkelberg, H. and Warneck, P. (1995) "Photodecomposition of iron (III) hydroxo and sulfate complexes in aqueous solution. Wavelength dependence of OH and SO_4^- quantum yields", *J. Phys. Chem.*, **99**: 5214-5221.

Bielsky, B., Cabelli, D., Arudi, R. and Ross, A. (1985) "Reactivity of HO_2/O_2 radicals in aqueous solution", *J.Phys.Chem.*, **14**: 1041-1100.

Bigda, R. (1995) "Consider Fenton's chemistry for wastewater treatment", *Chem. Eng. Progr.*, **91**: 62-66.

Bishop, D., Stern, G., Fleischman, M. and Marshall, L. (1968) "Hydrogen peroxide catalytic oxidation of refractory organics in municipal waste waters", *Ind. Eng.Chem. Res.*, **1**: 110-117.

Blanco, G. and Rodríguez, L. (1993) "Descontaminación de aguas residuales mediante fotocatálisis solar", *Ingenieria Química*, **286**: 129-137.

Blanco, J. and Malato, S. (1992) Proceedings of the Sixth International Symposium on Solar Termal Concentrating Technology, Mojacar, CIEMAT, Madrid.

Blanco, J. and Malato, S. (1996) "Tecnología de Fotocatálisis Solar." Cuadernos Monográficos 31. Instituto de Estudios Almerienses de la Diputación de Almería. Almería ,España.

Blanco, J. and Malato, S. (2001) "Solar detoxification", UNESCO. Natural Sciences, World Solar Programme, 1996-2005, http://www.unesco.org/science/wsp).

Blanco, J., Malato, S., Fernandez, P., Vidal, A., Morales, A., Trincado, P., Oliveira, J., Minero, C., Musci, M., Casalle, C., Brunotte, M., Tratzky, S., Dischinger, N., Funken, K., Vincent, M., Collares-Pereira, M., Mendes, J. and Rangel, C. (2000) "Compound parabolic concentrator technology development to commercial solar detoxification applications", *Solar Energy*, **67**: 317-330.

Blanco, J., Malato, S., Milow, B., Maldonado, M. I., Fallmann, H., Krutzler, T. and Bauer, R. (1999) "Techno-economical assessment of solar detoxification systems with compound parabolic collectors", *J. Phys.* **IV (9)**: 259-264.

Blesa, M. (2001) "Introducción: Eliminación de contaminantes por fotocatálisis heterogénea". Usos de óxidos semiconductores y materiales relacionados para aplicaciones medioambientales y ópticas, M.A. Blesa eds., Digital Grafic, xi-xiv, La Plata, Argentina.

Bohn, B. and Zetzsch, C. (1999) "Gas-phase reaction of the OH-benzene adduct with O_2: reversibility and secondry formation of HO_2", *Phys. Chem.*, **1**: 5097-5109.

Bossmann, S., Oliveros, E., Gob, S., Siegwart, S., Dahlen, E., Payawan, L., Straub, M., Worner, M. and Braun, A. (1998) "New evidence against hydroxyl radicals as reactiveintermediates in the thermal and photochemically enhanced Fenton reactions", *J. Phys.Chem.* **102**: 5542-5550.

Boudenne, J., Cercleir, O., Galéa, J. and Van Der Vlist, E. (1996) "Electrochemical oxidation of aqueous phenol at a carbon black slurry electrode", *Appl. Catal. B:Environ.*, 143-185.

Brand, N., Mailhot, G. and Bolte, M. (1997) "Degradation and photodegradation oftetraacetylethylenediamine (TAED) in the presence of Iron (III) in aqueous solution", *Chemosphere*, **84**: 2637-2648.

Braun, A., Maurette, M. and Oliveros, E. (1986) "Technologie photochimique", Pestic.Sci., **10**: 177-180.

Brillas, E., Calpe, J. and Casado, J. (2000) "Mineralization of 2,4-D by advanced electrochemical oxidation processes", *Wat. Res*, **34**: 2253-2262.

Brillas, E., Mur, E., Sauleda, R., Sanchez, L., Peral, J., Domenech, X. and Casado, J. (1998a) "Aniline mineralization by AOPs: anodic oxidation, photocatalysis, electro-Fenton and photo-electro-Fenton processes", *Appl. Catal. B: Environ.*, **16**: 31-42.

Brillas, E., Sauleda, R. and Casado, J. (1998b) "Degradation of 4-chlorophenol by anodic oxidation, electro-Fenton, photoelectro-Fenton and peroxicoagulation processes", *J. Electrochem. Soc.*, **145**: 2253-2262.

Cañizares, P., Dominguez, J., Rodrigo, M., Villaseñor, J. and Rodriguez, J. (1999) "Effect of the current intensity in the electrochemical oxidation of aqueous phenol wastes at an activated carbon and steel anode", *Ind. Eng. Chem. Res.*, **38**: 3779-3785.

Carter, S., Stefan, M., Bolton, J. and Amiri, A. (2000) "UV/H_2O_2 treatment of methyl ter-buthyl ether in contaminated waters", *Environ. Sci.& Technol.*, **34**: 659-662.

Catastini, C., Mohamed, S., Gilles, M. and Bolte, M. (2002) "Iron (III) aquacomplexes as effective photocatalysts for the degradation of pesticides in homogeneous aqueous solutions", *The Science of The Total Environment*, **298**: 219-228.

Catastini, C., Sarakha, M., Mailhot, G. and Bolte, M. (2001) "Direct and induced phototransformation of sulfanilamide in aqueous solution. Joint meeting of the Italian, French, and Swiss photochemistry groups, Lausanne, Switzerland.

Cervera, S. and Esplugas, S. (1983) "Obtención de hidrógeno mediante fotólisis del agua", *Energía* , **9**: 103-107.

Chamarro, E., A., M. and Esplugas, S. (2001) "Use of Fenton reagent to inprove organic chemical biodegradability", *Wat. Res.*, **35**: 1047-1051.

Chamarro, E., Marco, A., Prado, J. and Esplugas, S. (1996) "Tratamiento de aguas y aguas residuales mediante utilización de procesos de oxidación avanzada", *Química & Industria*, **1,** 28-32.

Chamberlin, N. and Griffin, A. (1952) "Chemical oxidation of phenolic wastes with chlorine", *Sewage and Industrial Wastes*, **24**: 750-756.

Chen, R. and Pignatello, J. (1997) "Role of quinone intermediates as electron shuttles in Fenton and photoassisted Fenton oxidations of aromatic-compounds", *Environ. Sci. Technol.*, **31**: 2399-2406.

Chuang, T., Cheng, S. and Tong, S. (1992) "Removal and destruction of benzene, toluene and xylene from wastewater by air stripping and catalytic oxidation", *Ind. Eng. Chem. Res.*, **31**: 2466-2472.

Ciardelli, G., Capannelli, G. and Bottino, A. (2001) "Ozone treatment of textile wastewater for reuse", *Water Sci. & Technol.*, **44**: 61-67.

Colucci, J., Montalvo, V., Hernandez, R. and Poullet, C. (1999) "Electrochemical oxidation potential of photocatalyst reducing agents", *Electrochimica Acta*, **44**, 2507-2514.

Comminellis, C. (1994) "Electrochemical oxidation of organic pollutants for waste water treatment", *Studies on Environmental Science*, 59.

Comninellis, C. and Pulgarin, C. (1993) "Electrochemical oxidation of phenol for waste-water treatment using SnO_2 anodes", *J. Appl. Electrochem.*, **23**: 108-112.

Contreras, S., Rodríguez, M., Chamarro, E., Esplugas, S. and Casado, J. (2001) "Oxidation of nitrobenzene by O_3/UV: The influence of H_2O_2 and Fe(III). Experiences in a pilot plant", *Water Sci. Technol.*, **44**: 39-46.

Costa, J., Esplugas, S. and Parejo, C. (1975) "Reactores fotoquimicos", *Ingenieria Química*, **71**: 37-48.

Curco, D., Malato, S., Blanco, J. and Gimenez, J. (1996a) "Photocatalysis and radiation absorption in a solar plant", *Solar Energy*, **44**: 199-217.

Curco, D., Malato, S., Blanco, J., Gimenez, J. and Marco, P. (1996b) "Photocatalytic degradation of phenol: comparison between pilot-plant-scale and laboratory results". *Solar Energy*, **56**: 387-400.

Davis, M., Turley, J., Casserly, D. and Guthrie, R. (1983) "Partitioning of selected organic pollutants in aquatic ecosystems", Biodeterioration 5 Oxley Ta & Barry S. Eds., 176-184.

De Laat, J. and Gallard, H. (1999) "Catalytic decomposition of hydrogen peroxide by Fe(III) in homogeneous aqueous solution: mechanism and kinetic modeling", *Environ. Sci. & Technol*., **33**: 2726-2732.

De Laat, J., Gallard, H. and Legube, B. (1999) "Comparative study of the oxidation of atrazine and acetone by H_2O_2/UV, Fe(III)/UV, Fe(III)/H_2O_2/UV and Fe(II) or Fe(III)/H_2O_2", *Chemosphere*, **39**: 2693-2706.

Dempsey, C. and Oppelt, E. (1993) "Incineration of hazardous waste: A critical review", *Air and Waste*, **43**: 25-73.

Dixon, W. T. and Norman, R. (1964) "Electron spin resonance of oxidation. Part III. Some alicyclic compounds", *J.Chem.Soc*. 4850-4860.

Duguet, J., Anselme, C., Mazounie, P. and Mallevialle, J. (1989) "Application of combined ozone-hydrogen peroxide for the removal of aromatic compounds from a ground water", *Ozone Sci. & Eng*., **12**: 281-284.

Eckenfelder, W., Argaman, Y. and Miller, E. (1989) "Process selection criteria for the biological treatment of industrial wastewaters", *Environmental Progress*, **8**: 40-45.

EEC. (1992) "List of Council Directives 76/4647", Brussels, Belgium, European Economic Community.

Eisenhauer, H. (1964) " Oxidation of phenolic wastes: I.Oxidation with hydrogen peroxide and a ferrous salt reagent", *J. Water Pollut. Control Fed*., **36**:1116-1128.

EPA "site". www.scorecard.org. visited on Octuber 2002.

Ertas, T. and Gurol, M. (2002) "Oxidation of diethylene glycol by ozone and modified Fenton", Chemosphere, **47**: 293-301.

Ertas, T. and Gurol, M. (2003) "Treatment of dichlorodiethyl ether by ozono, Fenton reagent and H_2O_2/UV", Submitted to *Environ. Sci. &Technol*.

Esplugas, S. (1981) "The elliptical photo-reactor", *Afinidad*, **38**: 315-318.

Esplugas, S. (1983) "Calculo de fotoreactores tubulares" *Cuaderns d'enginyeria*, **4**: 115-125.

Esplugas, S., Gimenez, J., Contreras, S., Pascual, E. and Rodriguez, M. (2002) "Comparison of different advanced oxidation processes for phenol degradation", *Wat. Res.*, **36**: 1034-1042.

ETPI survey. http://www.etpi.org, visited in January 2003.

Faust, B. and Hoigne, J. (1990) "Photolysis of Fe(III) - hydroxy complexes as sources of OH radicals in clouds, fog and rain", *Atmos. Environ*, **24A**: 79-89.

Feng, W. and Nansheng, D. (2000) "Photochemistry of hydrolytic iron (III) species and photoinduced degradation of organic compounds. A minireview", *Chemosphere*, **41**: 1137-1147.

Fenton, H. (1894) "Oxidation of tartaric acid in presence of iron", *J. Chem. Soc. Trans.*, **65**: 899-910.

Fernando, S., Garcia , E., Luciano, C., Capparelli, A., Braun, A. and Oliveros, E. (2002) "Degradation of nitroaromatic compounds by the UV-H_2O_2 process using polychromatic radiation sources", *Photochem. Photobiol. Sci*., **1**: 520-525.

Fisher.www.sihersci.ca/msds.nsf/96cb2019dad1311a5256670001d92b9/(visited December 2000).

Froelich, E. (1992) "Advanced chemical oxidation of contaminated water using the perox-pure oxidation system", *Water Pollut.Res.J. Canad*., **27**: 169-183.

Gallard, H. and De Laat, J. (2000) "Kinetic modelling of Fe(III)/H_2O_2 oxidation reactions in dilute aqueous solution using atrazine as a model organic compound", *Wat. Res.*, **34**: 3107-3116.

Gallard, H., De Laat, J. and Legube, B. (1999) "Spectrophotometric study of the formation of iron(III)-hydroperoxy complexes in homogeneus aqueous solutions", *Wat. Res*., **33**: 2929-2936.

García, J., Diez, F. and Coca, J. (1989) "Métodos alternativos para el tratamiento de efleuntes fenólicos industriales" , *Ingenieria Química*, **238**: 151-158.

Genium, (1993) "Material safety data sheet No.571", Genium Publishing Corporation Schenectady, NY.

Gilbert, E. (1987) "Biodegradability of ozonation products as a function of COD and DOC elimination by example of substituted aromatic substances", *Wat. Res*., **21**: 1273-1278.

Gimenez, J., Curco, D. and Queral, M. A. (1999) "Photocatalytic treatment of phenol and 2,4-dichlorophenol in a solar plant in the way to scaling-up", *Catalysis Today*, **54**: 229-243.

Gimenez, J., Curco, D., Malato, S. and Blanco, J. (1996) "Photocatalysis and radiation absorption in a solar plant", *Solar Energy Materials and Solar Cells*, **44**: 199-217.

Givens, S., Brown, E., Gelman, S., Grady, C. and Skedsvold, D. (1991). "Biological process design and pilot testing for carbon oxidation, nitrification and denitrification system", *Environmental Progress*, **10**: 133-146.

Glaze, W. and Chapin, D. (1987) "The chemistry of water treatment processes involving ozone, hydrogen peroxide and ultraviolet radiation", *Ozone Sci. & Eng*., **9**: 335-342.

Glaze, W. and Kang, J. (1989) "Advanced oxidation processes. Test of a kinetic model for the oxidation of organic compounds with ozone and hydrogen peroxide in a semibatch reactor", *Ind. Eng. Chem. Res*., **28**: 1580-1587.

Glaze, W., Lay, Y., Kang, J. (1995) " Advanced oxidation processes. A kinetic model for the oxidation of 1,2-dibromo-3-chloropropane in water by the combination of hydrogen peroxide and UV radiation", *Ind. Eng. Chem. Res*., **34**:2314-2323.

Goldstein, S. (1999) "Comments on the mechanism of the "Fenton-Like" reaction", *Am. Chem. Soc*., **32**: 547-550.

González, V. (1993) "Estudios de biodegradabilidad de efluentes industriales", *Ingenieria Química*, **260**: 97-101.

Groves, J. T. and Watanabe, Y. (1986) "Oxygen activation by metalloporhyrins related to peroxidase and cytochromo P-450. Direct observation of the O-O bond cleavage step", *J.Am.Chem.Soc*., **108**: 7834-7836.

Guittonneau, S., De Laat, J., Duguet, J. P., Bonnel, C. and Dore, M. (1990) "Oxidation of parachloronitrobenzene in dilute Aqueous solution by O_3 + UV and H_2O_2 + UV: A comparative study", *Ozone Sci. & Eng*., **12**: 73-94.

Guittonneau, S., Glaze, W., Duguet, J. and Wable, O. (1991) "Characterization of natural waters for potential to oxidize organic pollutants with ozone", *Proc. 10th Ozone World Congress*, Zürich, Switzerland.

Gulyas, H. (1997) "Processes for the removal of recalcitrant organics from industrial wastewater", *Water Sci. Technol*., **36**: 9-16.

Gurol, M. and Vastistas, R. (1987) "Oxidation of phenol compounds by ozone and ozone+UV radiation: a comparative study", *Wat. Res*., **21**: 895-900.

Gutierrez, M., Pepio, M., Crespi, M. and Mayor, N. (2001) "Control factors in the electrochemical oxidation of reactive dyes", *Coloration Technology*, **117**: 356-361.

Haber, F. and Weiss, J. (1934) "The catalytic decomposition of hydrogen peroxide by iron salts", *J. Proc. Roy. Soc*. London A, **147**: 332-351.

Hardwick, T. J. (1957) "The kinetics of the oxidation of ferrous ion by hydrogen peroxide in the presence of dissolved hydrogen and carbon monoxide", *Can. J*. Chem., **35**: 437-443.

Harrinson, R. (1992) "Pollution: Causes, effects and control", 2ª ed., The Royal Society of Chemistry , Cambridge.

Hashimoto, S., Miyata, T. and Washino, M. (1979) "A liquid chromatographic study on the radiolysis os phenol in aqueous solution", *Environ Sci.& Technol*., **13**: 71-79.

Hayward, K. (1999) "Drinking water contaminant hit-list for US EPA", *Water 21*, **September-October**, 4.

Heidt, L., Tregay, G. and Middleton, F. (1979) "Influence of the pH upon the photolysis of the uranyl oxalate actinometer system", *J.Phys.Chem*., **74**: 1876-1882.

Heinzle, E., Stockinge, H., Stern, M., Fahmy, M. and Kut, O. (1995) "Combined biological-chemical (ozone) treatment of wastewaters containing chloroguaiacols", *J.Chem. Tech. Biotechnol*., **62**: 241-252.

Henze, M. (1992) "Characterization of wastewater for modeling of activated sludge processes", *Water Sci. Technol*., **25**: 1-15.

Hislop, K. and Bolton, J. (1999) "The Photochemical generation of hydroxyl radicals in the UV-vis/ferrioxalate/H_2O_2 system", *Environ. Sci. Technol*., **33**: 3119-31226.

Hoigné, J. and Bader H. (1983) "Rate constants of reaction of ozone with organic and inorganic compounds in water. Part II. Dissociating organic compounds", *Wat. Res.*, **17**: 185-194.

Howard, P. (1989) "Handbook of environmental fate and exposure data for organic chemical. Volume I Large production and priority pollutants", Lewis Publishers, Chelsea, Michigan (USA).

Hulstrom, R., Bird, R. and Riordan, C. (1985) "Spectral solar irradiance data sets for selected terrestial conditions", *Solar Cells*, **15**: 365-391.

Hunt, J. and Taube, H. (1952) "Effect of temperature, pressure, acidity and solvent on an aquo ion exchange reaction", *J.Am.Chem.Soc*., **78**: 1273-1279.

IFTH, French Textile Instituted-Habillement, www.ifth.org (visited on Octuber 2001).

Iqbal, M. (1983) "An introduction to solar radiation", Canada, Academic Press.

Kabdasli, I. and Gurel, M. (2000) "Characterization and treatment of textile printing wastewaters", *Environmental Technology*, **21**: 1147-1155.

Kakko, R., Christiansen, V., Mikkola, E., Kallonen, R., Smith-Hansen, L. and Jorgensen, K. (1995) "Toxic combustion products of three pesticides", *J. Loss Prev. Process Ind*., **8**: 127-132.

Kaludjerski, M. (2001) "Enhancement of biodegradability of dichlorodiethyl ether by pre-oxidation", Master of Science Thesis, San Diego State University ,CA, USA.

Kameya, T., Murayama, T., Kitano, M. and Urano, K. (1995) "Testing and classification methods for the biodegradabilities of organic compounds under anaerobic conditions", *The Science of The Total Environment*, **170**: 31-41.

Kang, S., Liao, C. and Po, S. (2000) "Decolorization of textile wastewater by photo-fenton oxidation technology", *Chemosphere*, **41**: 1287-1294.

Kannan, N. (1995) "Removal of phenolic compounds by electroxidation method", *J. Environ. Sci. Health*, **30**: 2185.

Karametaxas, G., Hung, S. and Sulzberger, B. (1995) "Photodegradtion of EDTA in the presence of lepidocrite", *Environ.* Sci.& *Technol*., **29**: 2992-3000.

Kawaguchi, H. (1992) "Photooxidation of phenol in aqueous solution in the presence of hydrogen peroxide", *Chemosphere*, **24**: 1707-1712.

Kean, R. T., Oertling, W. A. and Babcock, G. T. (1987) "Characterization of six-coordinate ferryl protoheme by resonance raman and optical absorption spectroscopy", *J.Am.Chem.Soc*., **109**: 2185-2185.

Kolthoff, I. and Medalia, A. (1949) "The reaction between ferrous Ion and peroxides. I. Reaction with hydrogen peroxide in the absence of oxygen", *J. Am. Chem. Soc*., **71**: 3777-3783.

Kremer, M. (1999) "Mechanism of the Fenton reaction. Evidence for a new intermediate", *Phys. Chem*., **1**: 3595-3607.

Kremer, M. and Stein, G. (1977) "Kinetics of the Fe^{3+} ion-H_2O_2 reaction: steady-state and terminal-state analysis", *International Journal of Chemical Kinetics*, **IX**: 179-184.

Krutzler, T. and Bauer, R. (1999) "Optimization of a photo-Fenton prototype reactor", *Chemosphere*, **38**: 2517-2532.

Ku, Y. and Ho, S. (1990) "The effect of oxidants on UV destruction of chlorophenols", *Environmental Progress*, **9**: 218-221.

Kunai, A., Hata, S., Ito, S. and Sasaki, K. (1986) "The role of oxygen in the hydroxylation reaction of benzene with Fenton's reagent. O tracer study", *J. Am. Chem. Soc*., **108**: 6012-6016.

Lanouette, K. (1977) "Treatment of phenolic wastes", *Chem. Eng*., **17**: 99-106.

Ledakowicz, S. (1998) "Integrated processes of chemical and biological oxidation of wastewaters", *Environ. Protect. Eng*., **24**: 35-47.

Legrini, O., Oliveros, E. and Braun, A. M. (1993) "Photochemical processes for water-treatment", *Chem. Rev*., **93**: 671-698.

Lewis, R., Ed. (1991) "Hazardous Chemicals Desk Reference", 2[a] ed.,Van Nostrand Reinhold, New York. NY.

Li, K., Chang, S. and Yu, C. (2000) "Treatment of chlorohydrocarbon contaminated groundwater by air stripping". International Conference on Remediation of Chlorinated and Recalcitrant Compounds, 2nd, Monterey, CA, United States, May 22-25 : 293-300.

Li, L., Peishi, C. and Earnest, F. (1991) "Generalized kinetic model for wet oxidation of organic compounds", *AIChE J.*, **37**: 1687-1697.

Li, Z. and Comfort, D. (1998) "Nitrotoluene destruction by UV-catalyzed Fenton oxidation", *Chemosphere*, **36**: 1865-1865.

Liao, C. and Gurol, M. (1995) "Chemical oxidation by photolytic decomposition of hydrogen peroxide", *Environ. Sci. & Technol*., **29**: 3007-3014.

Lin, S. and Chen, M. (1997) "Treatment of textile wastewater by chemical methods for reuse", *Wat. Res*., **31**: 868-876.

Lin, S. and Chuang, T. (1994) "Combined treatment of phenolic wastewater by wet air-oxidation", *Toxical. Environ. Chem*., **44**: 243-258.

Lin, S. and Gurol, M. (1998) "Catalytic decomposition of hydrogen peroxide on iron oxide: Kinetics, mechanisms and implications", *Environ. Sci.& Technol*., **32**: 1417-1423.

Lin, S. and Lai, C. (2000) "Kinetic characteristics of textile wastewater ozonation in fluidized and fixed activated carbon beds", *Wat. Res*., **34**: 763-772.

Lin, S. and Peng, C. (1994) "Treatment of textile wastewater by electrochemical method", *Wat. Res*., **28**: 277-282.

Lin, S., Lin, C. and Leu, H. (1999) "Operating characteristics and kinetic-studies of surfactant wastewater treatment by Fenton oxidation", *Wat. Res*., **33**: 1735-1741.

Lindsey, M. E. and Tarr, M. A. (2000) "Quantification of hydroxyl radical during Fenton oxidation following a single addition of iron and peroxide", *Chemosphere*, **41**: 409-417.

Lipczynska-Kochany, E. (1991) "Degradation of aqueous nitrophenols and nitrobenzene by means of the Fenton reaction", *Chemosphere*, **22**: 529-536.

Lipczynska-Kochany, E. (1992) "Degradation of nitrobenzene and nitrophenols by means of advanced oxidation processes in a homogeneous phase: Photolysis in the presence of hydrogen peroxide versus the Fenton reaction", *Chemosphere*, **24**: 1369-1380.

Lipczynska-Kochany, E. and Bolton, J. (1992) "Flash photolysis/high-performance liquid chromatography method for studying the sequence of photochemical reactions: Direct photolysis of phenol", *Environ. Sci.& Technol*., **26**:2524-2527.

Lipczynska-Kochany, E., Sprah, G. and Harms, S. (1995) "Influence of some groundwater and surface waters constituents on the degradation of 4-Chlorophenol by the Fenton reaction", *Chemosphere*, **30**: 9-20.

Litvintsev, I., Mitnik, Y. and Mikhailyuk, A. (1993) "Kinetics and mechanism of catalytic hydroxylation of phenol by hydrogen peroxide. II. Modeling of the initial stage in the presence of catalytic system Fe^{2+}/pyrocathechol; Influence of initial reactants", *Kinetics and Catalysis*, **34**: 73-77.

Loebl, H., Stein, G. and Weiss, J. (1949) "Hydroxylation of nitrobenzene", *J.Chem.Soc*., 2704-2709.

Macfaul (1998) "A radical account of "Oxigenated Fenton Chemistry"", *Acc. Chem. Res*., **31**: 159-162.

Malaiyandi, M., Sadar, H. and Lee, P. (1980) "Removal of organic in water using hydrogen peroxide in presence of ultraviolet light", *Wat. Res*., **14**: 1131-1135.

Malato, S. (1999) "Solar photocatalytic decomposition of pentachlorophenol dissolved in water", Editorial CIEMAT, Madrid, Spain.

Malato, S., Blanco, J., Richter, C. and Maldonado, M. (2000b) "Optimization of pre-industrial solar photocatalytic mineralization of commercial pesticides Application to pesticide container recycling", *Appl. Catal. B-Environ*., **25**: 31-38.

Malato, S., Blanco, J., Richter, C., Curco, D. and Gimenez, J. (1997) "Low-concentrating CPC collectors for photocatalytic water detoxification: comparison with a medium concentrating solar collector", *Water Sci. Technol*., **35**: 157-164.

Malato, S., Blanco, J., Richter, C., Fernandez, P. and Maldonado, M. (2000a) "Solar photocatalytic mineralization of commercial pesticides: Oxamyl", *Solar Energy Materials and Solar Cells*, **64**: 1-14.

Malato, S., Blanco, J., Vidal, A. and Richter, C. (2002) "Photocatalysis with solar energy at a pilot-plant scale: An overview", *Appl. Catal. B:Environ.*, **37**: 1-15.

Malato, S., Caceres, J., Agüera, A., Mezcua, M., Vial J. and Fernández-Alba, A. (2001) "Degradation of imidacloprid in water by photo-Fenton and TiO_2 photocatalysis at a solar pilot plant: A comparative study", *Environ. Sci. & Technol*., **35**: 4359-4366.

Mansour, M. (1985) "Photolysis od aromatic compounds in water in the presence of hydrogen peroxide", *Bull. Environ. Contam. Toxicol*., **34**: 89-95.

Marco, A., Esplugas, S. and Saum, G. (1997) "How and why to combine chemical and biological processes for wastewater treatment", *Water Sci. Technol*., **35**: 321-327.

Marhaba, T. and Washington, M. (1998) "Drinking water disinfection and by-products: History and current practice", *Advanced Environ. Res*., **2**: 103-115.

Masselli, J., Masselli, N. and Burford, M. (1970) "Simplifying textile waste pollution surveys and treatment", *Proc. S. Water Resour. Pollut. Contr. Conf*., **19**: 37-48.

Matthews, R. (1990) "Purification of water with near-UV illuminated suspensions of titanium dioxide", *Wat. Res*., **24**: 653-660.

Matthews, R. and Sangster, D. (1967) "Production of isomeric nitrophenols in radiolysis of aqueous nitrobenzene solution", *J.Phys.Chem*., **71**: 4056-4062.

Mazellier, P. and Bolte, M. (1997) "Iron (III) promoted degradation of 2,6-dimethylphenol in aqueous solution", *Chemosphere*, **35**: 2181-2192.

Mazellier, P., Bolte, M. (1999) " Primary mechanism for the iron (III) photoinduced degradation of 4-chlorophenol in aquoes solution", *New J. Chem*., 133-135.

Mazellier, P., Bolte, M. (2001) " 3-chlorophenol elimination upon excitation of dilute iron (III) solution: evidence for the only involvement of $Fe(OH)^{2+}$", *Chemosphere*, **42**:361-366.

Mazellier, P., Mailhot, G. and Bolte, M. (1997) "Photochemical behavior of the Iron(III)/2,6-dimethylphenol system", *New J. Chem*., **21**: 389-397.

Mehos, M. and Turchi, C. (1992) "Measurement and analysis of near ultraviolet solar radiation", *Solar Eng*., **1**: 51-55.

Metcalf & Eddy, Inc (1995) " Wastewater engineering: treatment, disposal and reuse (Spanish version)", 3rd ed., McGraw-Hill, New York, USA.

Mieluch, J., Sadkowski, A., Wild, J. and Zoltowski, P. (1975) "Electrochemical oxidation of phenol compound in aqueous solution", *Prezm. Chem*., **54**: 513.

Minero C., Pelizzetti E., Malato S., Blanco J. (1996) "Large solar plant photocatalytic water decontamination: Effect of operational parameters", *Solar. Energy*, **56**:421-428, .

Minero, C., Pelizzetti, C., Piccini, P. and Vinceti, M. (1994) "Photocatalyzed transformation of nitrobenzene on TiO_2 and ZnO", Chemosphere, **28**: 1229-1244.

Minero, C., Pelizzetti, E., Malato, S. and Blanco, J. (1993) "Large solar plant photocatalytic water decontamination - degradation of pentachlorophenol", *Chemosphere*, **26**: 2103-2119.

Mishra, V., Mahajani, V. and Joshi, J. (1995) "Wet air oxidation", *Ind. Eng. Chem. Res*., **34**: 2-48.

Mokrini, A., Oussi, D. and Esplugas, S. (1997) "Oxidation of aromatic compounds with UV radiation/ozone/hydrogen peroxide" , *Water Sci. Technol.*, **35**, 95-102.

Munter, R., Preis, S., Kallas, J., Trapido, M. and Veressinina, Y. (2001) "Advanced oxidation processes (AOPs): Water treatment technology for the twenty-first century", *Kemia-Kemi*, **28**: 354-362.

Nansheng, D., Tao, F. and Shizhong, T. (1996) "Photodegradation of dyes in aqueous solutions containing Fe(III)--hydroxy complex I. Photodegradation kinetics", *Chemosphere*, **33**: 547-557.

Neppolian, B., Sakthivel, S., Arabindoo, B., Palanichamy, M. and Murugesan, V. (2001) "Kinetics of photocatalytic degradation of reactive yellow 17 dye in aqueous solution using UV irradiation", *J Environ. Sci. Health* Part A. Tox Hazard Subst. Environ. Eng., **36**: 203-213.

NIOSH, National Institude for Occupational Health and Safety (1985) "Registry of toxic effects of chemical substances: Dichlorodiethyl Ether", U.S. Department of Health and Human Services, Cincinnati, OH.

Norman, R. and Radda, G. (1962) "Aromatic hydroxylation: The electrophilic character of the hydroxyl radical, and its significance in biological hydroxylation", *Proc.Chem.Soc*., 138-149.

OECD. (1981), "Guidelines for Testing of chemicals", Paris, France.

Ohta, H., Goto, S. and Teshima, H. (1980) "Liquid-phase oxidation of phenol in a rotating catalytic basket reactor", *Ind. Eng. Chem. Fundam*, **19**: 180-185.

Ollis, D., Pelizzetti, E. and Serpone, N. (1989) "Heterogeneous photocatalysis in the environment: Application to water purification. Photocatalysis: Fundamentals and applications", N. Serpone, E. Pelizzetti. New York, Wiley: 603-637

Pala, A. and Tokat, E. (2001) "Color removal from cotton textile industry wastewater in an activated sludge system with various additives", *Wat. Res*., **36**: 2920-2925.

Palau, R. (1998) "Contribución al estudio de la eliminación de contaminantes acuosos mediante reacciones electroquímicas - Degradación del herbicida MCPA". Master Experimental en Química, Dpto. Ingeniería Química y Metalurgia, Universitat de Barcelona.

Parra, S., Malato, S. and Pulgarin, C. (2002) " New integrated photocatalytic-biological flow system using supported TiO_2 and fixed bacteria foe the mineralization of isoproturon", *Appl. Catal. B:Environ*., **36**: 131-144.

Parra, S., Sarria, V., Malato, S., Peringer, P. and Pulgarin, C. (2000) "Photochemical versus coupled photochemical-biological flow system for the treatment of two biorecalcitrant herbicides: metobromuron and isoproturon", *Appl. Catal. B:Environ*., **27**: 153-168.

Perez, M., Torrades, F., Domenech, X. and Peral, J. (2002) "Fenton and photo-Fenton oxidation of textile effluents", *Wat. Res*., **36**: 2703-2710.

Petersen, D., Watson, D. and Winterlin, W. (1988) "The destruction of groundwater threatening pesticides using high intensity UV light", *J.Environ.Sci.Health,Part B*, **23**: 587-603.

Peyton, G. and Glaze, W. (1988) "Destruction of pollutants in water with ozone in combination with ultraviolet radiation. 3. Photolysis of aqueous ozone", *Environ. Sci. & Technol*., **22**: 761-767.

Pignatello, J. (1992) "Dark and photoassisted Fe^{3+} catalyzed degradation of chlorophenoxy herbicides by hydrogen peroxide", *Environ. Sci. & Technol*., **26**: 944-951.

Pignatello, J. and Day, M. (1996) "Mineralization of methyl parathion insecticide in soil by hydrogen peroxide activated with iron(III)-NTA or -HEIDA complexes", *Hazardous Waste & Hazardous Materials*, **13**: 237-244.

Pignatello, J. and Sun, Y. (1993) "Photo-assisted mineralization of herbicide wastes by ferric ion catalyzed hydrogen-peroxide", *ACS Symp. Ser*., **518**: 77-105.

Pulgarin, C., Adler, N., Peringer, P. and Comninellis, C. (1994). "Electrochemical Detoxification of a 1,4-Benzoquinone Solution in Waste-Water Treatment", *Wat. Res*., **28**: 887-893.

Pulgarin, C., Invernizzi, M., Parra, S., Sarria, V., Polania, R. and Peringer, P. (1999) "Strategy for the coupling of photochemical and biological flow reactors useful in mineralization of biorecalcitrant industrial pollutants", *Catalysis Today*, **54**: 341-352.

Rahhal, R. and Richter, H. (1988) "Reduction of hydrogen peroxide by the ferrous iron chelate of diethylenetriamine-N,N,N',N'',N''-pentaacetate", *J.Am.Chem.Soc*., **110**: 3126-3133.

Renner, T., Reichelt, A., Wurdack, O. and Specht, D. (2000) "Degradation of textile dye water with Fenton process", Proceedings of the 2nd International Conference, CUTEC, Clausthal-Zellerfeld, Germany.

Rodriguez, C., Dominguez, A. and Sanroman, A. (2002) "Photocatalytic degradation of dyes in aqueous solution operating in a fluidised bed reactor" , *Chemosphere*, **46**: 83-86.

Romero, M., Blanco, J., Sanchez, B., Vidal, A., Malato, S., Cardona, A. and Garcia, E. (1999) "Solar photocatalytic degradation of water and air pollutants: Challenge and perspectives", *Solar Energy*, **66**: 169-182.

Rosen, G., Tsai, P., Barth, E., Dorey, G., Casara, P., Spedding, M. and Halpern, H. (2000) "A one-step synthesis of 2-(2-Pyridyl)-3H-indol-3-one N-Oxide: Is it and efficient spin Trap for hydroxyl radical ?", *J. Org. Chem*., **65**: 4460-4463.

Roy, C. and Volesky, B. (1977) "Physicochemical treatment of textile wastewater using activated carbon", *Canadian Textile Journal*, **94**: 47-60.

Ruiz, B., Prats, R. and Zoffmann, C. (1992) "Modelo real de flujo de una planta depuradora de aguas residuales urbanas", *Ingenieria Química*, **279**: 53-56.

Rupper, G., Bauer, R. and Heisler, G. (1994) "UV-O_3, UV-H_2O_2, UV-TiO_2 and the photo-Fenton reaction. Comparison of advanced oxidation processes for waste water treatment", *Chemosphere*, **28**: 1447-1454.

Ruppert, G., Bauer, R. and Heisler, G. (1993) "The photo-Fenton reaction - an effective photochemical wastewater treatment process", *J. Photochem. Photobiol. A*, **73**: 75-78.

Sacher, F., Karrenbrock, F., Knepper, T. and Lindneri, K. (2001) "Adsorption studies of organic compounds for the assessment of their relevancies for drinking water production", *Vom Wasser* , **96**.

Sadana, A. and Katzer, J. (1974) "Catalytic oxidation of phenol in aqueous solution over copper oxide", *Ind. Eng. Chem. Fundam*, **13**: 127-134.

Safarzadeh-Amiri, A., Bolton, J. and Cater, S. (1996) "Ferrioxalate-mediated solar degradation of organic contaminants in water", *Solar Energy*, **56**: 439-443.

Sagawe, G., Lehnard, A., Lubber, M. and Bahnemann, D. (2001) "The Insulated Solar Fenton Hybrid Process: Fundamental Investigations", *Helvetica Chimica Acta*, **84**: 3742-3759.

Sarria, V., Parra, S., Invernizzi, M., Péringer, P. and Pulgarin, C. (2001) "Photochemical-biological treatment of a real industrial biorecalcitrant wastewater containing 5-amino-6-methyl-2-benzimidazolone", *Water Sci. Technol.*, **44**: 93-101.

Schertenleib, R. and Gujer,W. (2000) *EAWAG News*, **48**: 3-5.

Scott, G. (1997) "Design, characterization and performance of a bench-scale continuous wet oxidation system", *Chem. Oxidation. Technol.*, **6**: 156-186.

Scott, J. and Ollis, D. (1995) "Integration of chemical and biological oxidation processes for water treatment : Review and recommendations", *Environ. Progr.*, **14**: 88-103.

Scott, J. P. and Ollis, D. F. (1996) "Engineering Models of Combined Chemical and Biological Processes", *J. Environ. Eng.*, **122**: 1110-1114.

Sehested, K., Rasmussen, O. and Fricke, H. (1968) "Rate constants of $HO^{\bullet}$ with HO_2, O_2, and H_2O_2 from hydrogen peroxide formation in pulse-irradiated oxygenated water", *J.Phys.Chem*., **72**: 626-631.

Serpone, N., Terzian, R., Colarusso, P., Minero, C., Pelizzetti, E. and Hidaka, H. (1992) "Sonochemical oxidation of phenol anf three of its intermediate products in aqueous media : catechol, hydroquinone, and benzoquinone. Kinetic and mechanistic aspects", *Research on Chemical Intermediates*, **18**: 183-202.

Sevener, M. (1990) "El O_3: un plan de investigación de la oxidación de compuestos sintéticos en el H_2O", *Ingenieria Química*, **250**: 239-245.

Sevimli, M. and Kinaci, C. (2002) "Decolorization of textile wastewater by ozonation and Fenton's process", *Water Sci.Technol*., **45**: 279-286.

Smith, D. S., V. and Watkinson, A. (1981) "Anodic oxidation of phenol for wastewater treatment", *Can. J. Chem. Eng*., **59**: 52-59.

Staehelin, J. and Hoigné, J. (1982) "Decomposition of ozone in water: Rate of initiation by hydroxide ions and hydrogen peroxide", *Environ. Sci.& Technol*., **16**: 676-681.

Standard Methods, APHA, AWWA and WEF, (1995), 19^{th}, Edition, Washington, DC.

Stanislav, L. and Sedlak, P. (1992) "Photoinitiated reactions of hydrigen peroxide in the liquid phase", *J. Photochem. and Photobiol. A*., **68**: 1-33.

Steverson, E. (1991) "Provoking a firestorm: Waste Incineration", *Environ. Sci. & Technol*., **25**: 1419-1427.

Stubbe, J. and Kozarich, J. W. (1987) "Mechanisms of bleomycin-induced DNA degradation", *Chem. Rev*., **87**: 1107-1136.

Sudoh, M., Kodera, T., Sakai, K., Zhang, J. and Koide, K. (1986) "Oxidative degradation of aqueous phenol effluents with electrogenerated Fenton's reagent", *J.Chem.Eng.Jap*., **19**: 513-518.

Sun, Y. and Pignatello, J. (1993). "Photochemical-reactions involved in the total mineralization of 2,4-D by $Fe^{3+}/H_2O_2/UV$", *Environ. Sci.& Technol*., **27**: 304-310.

Sundstrom, D., Weir, B. and Klei, H. (1989) "Destruction of aromatic pollutants by UV light catalized oxidation with hydrogen peroxide", *Environmental Progress*, **8**: 6-11.

Sychev, A. Y. and Isak, V. G. (1995) "Iron compounds and the mechanisms of the homogeneous catalysis of the activation of O_2 and H_2O_2 and of the ativation of organic substrates", *Russian Chemical Reviews*, **64**: 1105-1129.

Toxnet, "site". http://www.toxnet.nlm.nih.gov.visited on December 2001.

Trapido, M., Veressinina, Y. and Kallas, J. (2001) "Degradation of aqueous nitrophenols by ozone combined with UV-radiation and hydrogen peroxide", *Ozone Sci. & Eng.*, **23**: 333-342.

Turchi, C. S. and Ollis, D. F. (1990) "Photocatalytic degradation of organic water contaminants: mechanisms involving hydroxyl radical attack", *J. Catal*., **122**: 178-192.

Ullmann's (1991) "Encyclopedia of Industrial Chemistry", 5ª ed., 415-419, VCH Verlagsgesellschaft (Germany)

Urano, K. and Kato, Z. (1986) "Evaluation of boidegradation ranks of priority organic compounds", *Journal of Hazardous Materials*, **13**: 147-149.

Vian, A., Miranda, F., Agudo, J. and Rodríguez, J. (1982) "Depuración de aguas residuales mediante lodos activos: Aspectos cinéticos", *Ingenieria Química*, **216**:89-94.

Vicente, J., Rosal, R. and Diaz, M. (2002) "Noncatalytic oxidation of phenol in aqueous solutions", *Ind. Eng. Chem. Res*., **41**: 46-51.

Vicente, M. and Esplugas, S. (1983) "Calibrado del fotoreactor anular", *Afinidad*, **387**: 453-457.

Vlyssides, A., Loizidou, M., Karlis, P. and Zorpas, A. (1999) "Textile dye wastewater treatment with the use of an electrolysis system", *Hazardous and Industrial Wastes*, **31**: 147-156.

Vlyssides, A., Papaioannou, D., Loizidou, M., Karlis, P. and Zorpas, A. (2000) "Testing an electrochemical method for tratment of textile dye wastewater", *Waste Management*, **20**: 569-574.

Volman, D. and Chen, J. (1959) "The photochemical decomposition of hydrogen peroxide in aqueous solution of allyl alchohol", *J.Am.Chem.Soc*., **81**: 4141-4144.

Volman, D. and Seed, J. (1964) "The photochemistry of uranyl oxalate", *J.Am.Chem.Soc*., **86**: 331-335.

Walling, C. (1975) "Fenton's reagent revisited", *Acc. Chem. Res.*, **8**: 125-131.

Walling, C., El-Taliawi, G. and Johnson, R. (1974) "Fenton's reagent IV. Structure and reactivity relations in the reactions of hydroxyl radicals and the redox reactions of radicals", *J. Am. Chem. Soc.*, **96**: 133-139.

Wang, Y. (1992) "Effect of chemical oxidation on anaerobic biodegradation of model phenolic compounds", *Wat. Environ.Res.*, **64**.

Weber, R. and Smith, E. (1986) "Removing dissolved organic contaminants from water", *Environ.Sci.&Technol.*, **20**: 970-979.

Whitby, G. (1989) "The treatment of spa water with ozone produced by UV ligh", *Ozone Sci. & Eng.*, **11**: 313-324.

Wiesmann, U. and Putnaerglis, A. (1986) "Influence of oxygen concentration on substrate degradation in activated sludge reactors", *Ger.Chem.Eng.*, **9**: 284-291.

Wilkins, F. and Blake, D. (1994) "Use solar energy to drive chemical process", *Chem. Eng. Prog.*, **6**: 41-49.

Wu, J., Bewtra, J., Biswas, N. and Taylor, K. (1994) "Effect of H_2O_2 addition mode on enzymatic removal of phenol from wastewater in the presence of polyethylene glycol", *Can. J. Chem. Eng.*, **72**: 881-886.

Yamazaki, I. and Piette, L. (1991) "EPR spin-trapping study on the oxidizing species formed in the reaction of the ferrous ion with hydrogen peroxide", *J. Am. Chem. Soc.*, **113**: 7588-7593.

Yeh, R., Hung, Y., Liu, R., Chiu, H. and Thomas, A. (2002) "Textile wastewater treatment with activated sludge and powdered activated carbon", *International Journal of Environmental Studies*, **59**: 607-622.

Young, L. and Yu, J. (1997) "Ligninase-catalysed decolorization of synthetic dyes", *Water Res.*, **31**: 1187-1193.

Yu, Y. and Hu, S. (1994) "Preoxidation of chlorophenolic wastewaters for their subsequent biological treatment", *Water Sci. Technol.*, **29**: 313-320.

Zappi, G., Arbesman, S. and Weinberg, N. (2000) "Novel electrochemical system for the destruction of organic contaminants". Annual conference and exposition on water

quality and wastewater treatment, 73rd, Anaheim, CA, United State, **Oct.14-18**: 2966-2969.

Zepp, L., Faust, B. and Hoigné, J. (1992) "Hydroxyl radical formation in aqueous reactions (pH 3-8) of iron(II) with hydrogen peroxide: the photo-Fenton reaction", *Environ. Sci.& Technol*., **26**: 313-319.

Zoeteman, B., Harmsen, K., Linders, J., Morra, C. and Sloof, W. (1980) "Persistent organic pollutants in river water and ground water of the Netherlands", *Chemosphere*, **9**, 231-249.

11. Appendix: Estimation of absorbed radiation

11.1. Actinometric study

Before carrying out the experiments with ultraviolet radiation, an actinometric study was carried out in order to measure the photon flux entering to the reactor by the different sources of radiation used. Among the various chemical actinometers, the photochemical decomposition of aqueous solutions of oxalic acid in presence of uranyl salts was chosen (Vicente and Esplugas, 1983; Braun *et al.*, 1986).

For this reaction, it is possible to consider three competitive processes:

1) Photodecomposition of the oxalic acid yielding carbon monoxide and carbon dioxide.

$$(UO_2)^{2+} + H_2C_2O_4 \xrightarrow{h\nu} (UO_2)^{2+} + CO + CO_2 + H_2O \qquad (4.24)$$

2) Photodecomposition of the oxalic acid to formic acid and carbon dioxide.

$$(UO_2)^{2+} + H_2C_2O_4 \xrightarrow{h\nu} (UO_2)^{2+} + CO_2 + HCOOH$$

3) Redox reaction to U^{4+} and carbon dioxide.

The mechanism of this reaction is very complex according to the different products obtained: CO, CO_2, $HCOOH$, U^{4+}, H_2O.

However, the main photo-reaction, by using a solution 0.01 mol.L^{-1} in uranyl and 0.05 in oxalic acid operating in the pH range between 3 and 7 and conversion up to 20%, is the photodecomposition of the oxalic acid to carbon monoxide and carbon dioxide.

The development kinetic of this reaction may be divided in three steps:

- The first step is the activation of the uranyl ion by photon absorption

$$(UO_2)^{2+} \xrightarrow{h\nu} (UO_2^*)^{2+}$$

- The second step is the reaction between the activated uranyl and the oxalic acid yielding oxalic in excited state

$$H_2C_2O_4 + (UO_2^*)^{2+} \rightarrow (H_2C_2O_4^*) + (UO_2)^{2+}$$

- The last step is the decomposition of the activated oxalic.

$$(H_2C_2O_4^*) \rightarrow CO + CO_2 + H_2O$$

Only the first step is a photochemical reaction, and throughout the process the concentration of the compound that absorbs the radiation (uranyl ion) remains constant. Meanwhile, the oxalic acid concentration follows a zero order kinetic.

Thus, the intensive reaction rate of oxalic acid, R_{ox} ($mol.m^{-3}s^{-1}$) can be expressed as:

$$R_{ox} = -\sum_{\lambda} \phi_{\lambda} W_{abs,\lambda} \; t \tag{11.1}$$

being,

ϕ_{λ} = quantum yield

$W_{abs,\lambda}$ = absorbed radiation

t = time

In addition, the oxalic mass balance in the reactor yields:

$$V \frac{dC}{dt} = R_{ox} \tag{11.2}$$

where V is the volume of the reactor and C is the concentration of oxalic acid in the reactor at the irradiation time. The boundary condition is:

$$t = 0 \qquad C = C_o$$

C_o being the initial concentration of oxalic acid.

Equation 11.2, with its limit condition shown above, has an easy solution because it is possible to observe that the intensive reaction rate for oxalic decomposition does not varies with oxalic concentration, its only a function of uranyl concentration that remains constant (the absorbance of reacting medium and the quantum yield only depends on the uranyl concentration) during the experiments. Integration of eq. 11.2 yields:

$$V\,(C - C_o) = -\sum_{\lambda} \phi_{\lambda} W_{abs,\lambda} t \tag{11.3}$$

This means that by plotting oxalic concentration versus irradiation time a straight line must be obtained. However, in order to make calculation it is better to plot the amount of oxalic acid in moles (n = V.C), versus the irradiation time (t). In the actinometric experiments, irradiation times were adjusted so that the conversions of oxalic acid were between 3% and 20% in every run. Smaller conversions introduce uncertainties in the zero-order rate requirement, the possibility of bubble formation due to excessive formation of CO and CO_2, and the danger of reduction of UO_2^{2+}.

11.2. Experimental method

The photo-reactor was filled with 0.05 mol.L^{-1} oxalic acid and 0.01 mol.L^{-1} uranyl nitrate solutions. Lamp was turned on and samples were withdrawn at intervals of 2-5 minutes. For less powerful lamp the interval time should be longer.

In table 11.1 the characteristics of the actinometric reaction are show.

Table 11.1. Characteristics of the actinometric reaction

λ (nm)	**Φ_λ (mol Einstein^{-1})**	**μ (cm^{-1})**
240-250	0.59	9.839
250-262	0.60	6.416
262-270	0.59	5.505
270-275	0.58	4.491
275-285	0.58	3.502
285-295	0.58	2.433
295-300	0.57	1.804
300-308	0.56	1.391
308-320	0.56	0.998
329-342	0.52	0.355
360-371	0.49	0.041
395-406	0.55	0.037
430-443	0.58	0.032
481-493	0.27	0.003

Being these parameters :

λ = wavelength (nm)

Φ_λ = quantum yield (mol Einstein^{-1})

μ = absorption coefficient (cm^{-1})

11.3. Analytical determinations

The analysis of oxalic acid in each sample was done by tritration using $KMnO_4$ 0.1 N and in acidic pH and a temperature of 80-90^{o}C. The end point is easily to see by a color change.

11.4. Actinometric results

Taking into account that the actinometric method to determine the photonic emission was used in three reactors with different lamps, the results will be presented for each one. The assumption to obtain the photon-flux entering to the reactor will be in agreement with the reactor design and the kind of lamp used in each case.

11.4.1. Reactor B (Tubular photo-reactor)

As it has been mentioned before, in section 4.4.2.1, this reactor is equipped with four “germicides” low-pressure mercury lamps. These lamps emit radiation basically at 253.7 nm. In Table 11.2 and 11.3 the actinometric data obtained for this reactor are summarized.

Results of both actinometries are presented in Fig. 11.1, where the pertinent linear fittings have been performed.

Table 11.2. Actinometry 1. Reactor B.

Time (min)	n_{H2C2O4} (mol)	$n^0_{H2C2O4} - n_{H2C2O4}$ (mol)
0	0.125	0
4	0.1209	0.0041
8	0.1197	0.0053
12	0.1150	0.0101
16	0.1126	0.0125
20	0.1114	0.0136
24	0.1102	0.0149
28	0.1066	0.0184
32	0.103	0.022
36	0.101	0.024
40	0.098	0.0267

Table 11.3. Actinometry 2. Reactor B.

Time (min)	n_{H2C2O4} (mol)	$n^0_{H2C2O4} - n_{H2C2O4}$ (mol)
0	0.125	0
3	0.1209	0.0041
6	0.1197	0.0053
9	0.1150	0.0101
15	0.1126	0.0125
18	0.1114	0.0136
21	0.1102	0.0149
24	0.1066	0.0184
27	0.103	0.022
30	0.101	0.024

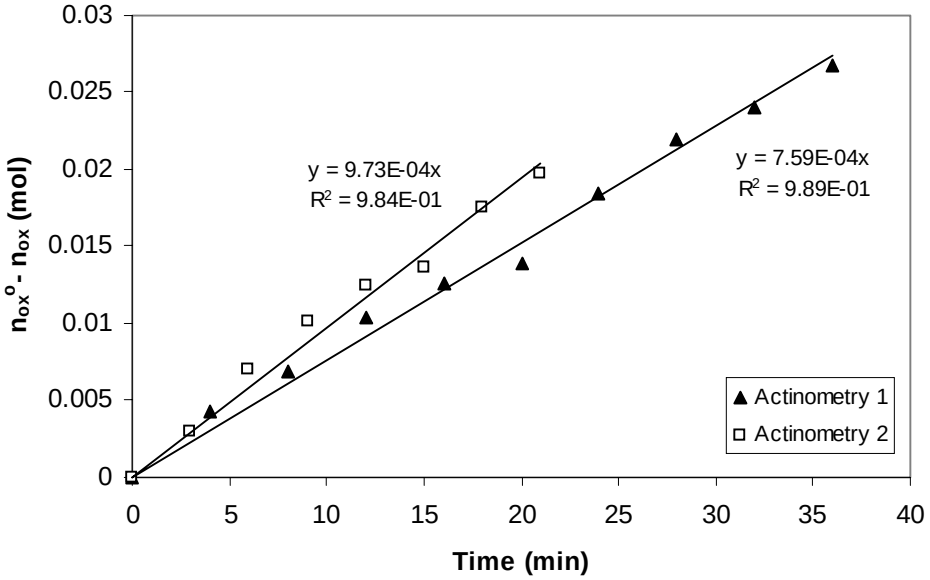

Figure 11.1. Comparison of actinometries 1 and 2 in Reactor B.

As the lamps emits mainly in a unique wavelength, eq. 11.3 can be simplified as:

$$n_{ox}^{o} - n_{ox} = - \phi_{\lambda} \; W_{abs,\lambda} \; t \qquad (11.4)$$

The value of Φ_λ in the wavelength range of between 250-262 nm is 0.6 mol Einstein^{-1} (see Table A.1). From Fig. 11.1, the slope of the graph is equal to :

slope = $\Phi_\lambda * W_{abs,\lambda}$

Therefore, $W_{abs,\lambda}$ can be obtained.

Actinometry 1, $(W_{abs,\lambda})_1$ = 22.22 μEinteins s^{-1}

Actinometry 2, $(W_{abs,\lambda})_2$ = 27.77 μEinteins s^{-1}

Average value = 24.99 μEinteins s^{-1}

11.4.1.1. Flow rate of photons absorbed by NB and phenol in reactor B

In order to describe the absorption properties of NB and phenol for direct phtolysis experiments, the following equation based in the radial field was used (Costa *et al.*, 1975; Esplugas, 1981, 1983):

$$\frac{W_{abs}}{W_e} = 1 - \exp(-\mu d) \tag{11.5}$$

being,

W_{abs} = the absorbed radiation by the compounds in the reaction medium (μEinstein.s^{-1})

W_e = the photon flow entering to the reactor (μEinstein.s^{-1})

μ = the absorbance (cm^{-1})

d = inner diameter of the reactor (cm)

To solve this equation, absorbance μ, which can be easily obtained from the absorption spectrum of NB and phenol, must be calculated. Values for μ have been inserted in Table 11.4. Thus, for 254 nm, the dependence between the energy flow entering the reactor (W_e), which has been measured by the actinometry, and the absorbed energy flow (W_{abs}) used for the mineralization process, can be calculated by means of equation 11.5. The resulting term allows the calculation of the absorbed energy flow at starting time. The radiation flow in the reactor absorbed by NB and phenol at 254 nm was 24.99 and 18.82 μEinstein.s^{-1} respectively. These values correspond to the starting time when NB and phenol concentration are maximum.

Table 11.4. Flow rate of photons absorbed by NB and phenol in reactor B

Compounds	**Wavelength** (nm)	**μ** (cm^{-1})	**W_e** (μEinstein.s^{-1})	**1-exp(-μd)**	**W_{abs}** (μEinstein.s^{-1})
Nitrobenzene	254	8.07	24.99	1	24.99
Phenol	254	0.76	24.99	0.753	18.82

Taking into account the reactor volume, the flow of photons absorbed by unit of reaction volume is 92.55 μEinstein.s^{-1} L^{-1}. and 69.70 μEinstein.$s^{-1}L^{-1}$ for NB and phenol respectively.

11.4.2. Reactor C (Annular reactor)

This reactor has been already described in chapter 4, section 4.4.2.2. It is equipped with one black lamp, which emits radiation between 300-400 nm. In Table 11.5 the actinometric data obtained for this reactor are summarized.

Table 11.5. Actinometry Reactor C

Time (h)	n_{H2C2O4} (mol)	$n^0_{H2C2O4} - n_{H2C2O4}$ (mol)
0	0.075	0
1	0.072	0.0028
2	0.0705	0.004
3	0.0682	0.0065
4	0.0667	0.0079
5	0.0652	0.0095
6	0.064	0.011
7	0.0626	0.012
8	0.0622	0.014

Results of the actinometry are presented in Fig 11.2, where the pertinent linear fitting has been performed.

This black lamp emits radiation between 300-400 nm with a maximum at 360 nm. In order to simplify the calculation, the photon flux for this lamp has been calculated assuming that it emits basically at 360 nm. Therefore, in the same way that in previous case, eq.11.3 can be simplified as eq. 11.4.

The value of Φ_λ in the range of between 360-371 nm is 0.49 mol Einstein^{-1} (see Table 11.1). From Fig. 11.2, the slope of the graph is equal to :

$$\text{slope} = \Phi_\lambda * W_{abs,\lambda}$$

Therefore, $W_{abs,\lambda}$ can be obtained.

Actinometry 3, $(W_{abs,\lambda})_1 = 0.83$ μEinteins s^{-1}.

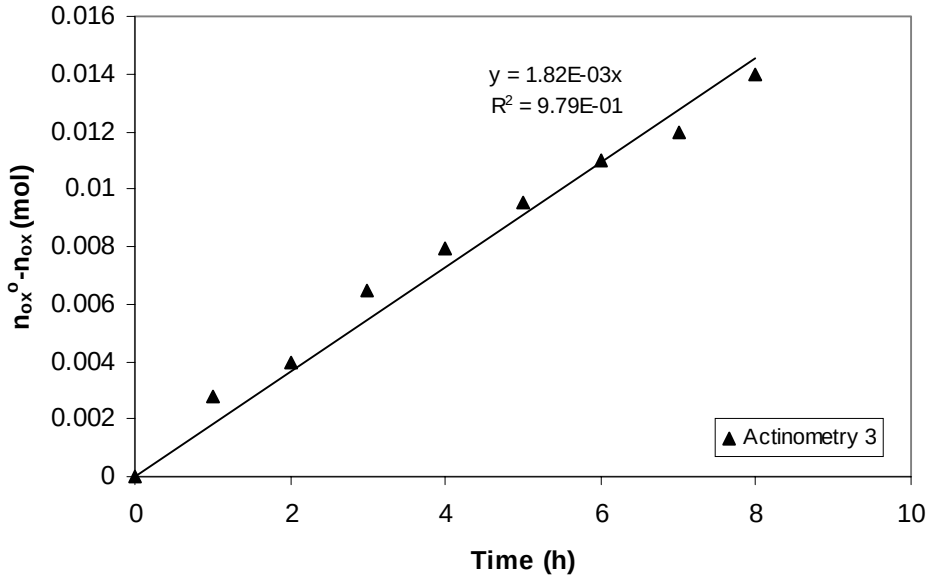

Figure 11.2. Actinometry results in Reactor C

11.4.2.1. Flow rate of photons absorbed by NB and phenol in Reactor C

The flow rate of photons absorbed by NB and phenol in reactor C was calculated using the same procedure described in section A.4.1.1. The radiation flow in the reactor absorbed by NB and phenol at 360 nm was 0.56 and 0.17 μEinstein.s^{-1} respectively (see Table 11.6). These values correspond to the starting time when NB and phenol concentration are maximum.

Taking into account the reactor volume (1.5 L), the flow of photons absorbed by unit of reaction volume are 0.37 μEinstein.s^{-1} L^{-1} and 0.11 μEinstein.$s^{-1}L^{-1}$ for NB and phenol, respectively.

Table 11.6. Flow rate of photons absorbed by NB and phenol in Reactor C

Compounds	**Wavelength** (nm)	**μ** (cm^{-1})	**W_e** (μEinstein.s^{-1})	**1-exp(-μd)**	**W_{abs}** (μEinstein.s^{-1})
Nitrobenzene	360	0.53	0.83	0.67	0.56
Phenol	360	0.11	0.83	0.21	0.17

11.4.3. Reactor D (solarbox)

This reactor has been already described in chapter 4, section 4.4.2.3 .It is equipped with one polichromatic lamp emitting radiation close to solar spectrum between 300-560 nm. In Table 11.7 the actinometric data obtained for this reactor are summarized.

Table 11.7 . Actinometry of the solarbox (Reactor D)

Time (h)	**n_{H2C2O4} (mol)**	**$n^{o}_{H2C2O4} - n_{H2C2O4}$ (mol)**
0	0.072	0
5	0.0697	0.0023
10	0.0678	0.0042
15	0.0675	0.0045
20	0.066	0.006
25	0.0648	0.0072
30	0.0637	0.0083
35	0.063	0.009
40	0.061	0.011
45	0.0603	0.0117
50	0.06	0.012
55	0.0585	0.0135
60	0.0573	0.0147

Results of the actinometry are presented in Fig 11.3, where the pertinent linear fitting has been performed.

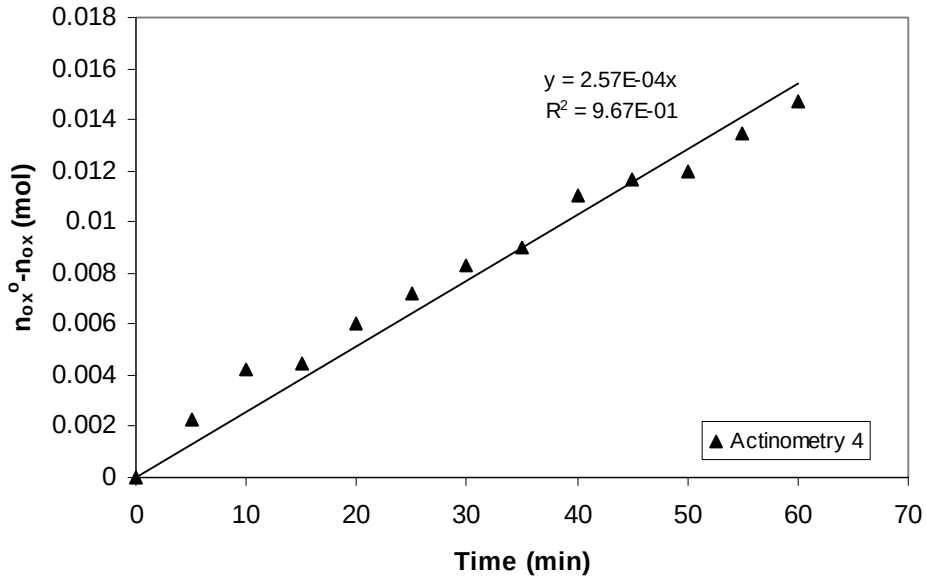

Figure 11.3. Actinometry results in Reactor D

From eq. 11.3 and taking into account the spectrum emission for this polychromatic lamp between (300 and 400), the photon flux entering the reactor (which has been measured by the actinometry) has been calculated using Microsoft Excel spreadsheet and its value was 2.17 x10^{-6} Einstein s^{-1}. This value corresponds to the total absorbed radiation by the actinometer and therefore it will be used to estimate the absorbed radiation by the reaction medium. Assuming Fe^{3+} as the main absorbing specie in the photo-Fenton reaction medium, the photon flux absorbed has been estimated according to eq. 11.6 for each wavelength.

$$W_{abs,\lambda} = W_{\text{total absorbed by actinometer}} \sum F_\lambda \left[1-\exp(-\mu_\lambda d)\right] \qquad (11.6)$$

being,

F_λ = source of photons factor (lamp factor)

μ = absorbance for Fe^{3+} (cm^{-1})

d = reactor diameter (cm)

In Table 11.8 some values are shown as example of absorbing photon flow for both actinometer and treated solutions.

Table 11.8. Flow of photons absorbed by uranyl and Fe^{3+} in reactor D

λ (nm)	Lamp Factor F_λ	μ Uranyl (cm^{-1})	$W_{abs,\lambda}$ actinomet (Einstein.s^{-1})	μ Fe^{3+} (cm^{-1})	$W_{abs,\lambda}$ Fe^{3+} (Einstein.s^{-1})
300	0	18.48	0	11.30	0
310	1.12E-4	11.99	6.14E-5	10.71	2.43E-10
320	4.93E-4	7.68	2.71E-4	9.53	1.07E-9
330	1.11E-3	4.45	6.10E-4	8.35	2.41E-9
340	1.26E-3	2.09	6.84E-4	7.76	2.74E-9
350	1.44E-3	0.98	6.92E-4	6.58	3.14E-9
360	1.59E-3	0.54	5.98E-4	5.41	3.47E-9
370	2.09E-3	0.32	5.71E-4	4.82	4.57E-9
380	2.30E-3	0.21	4.48E-4	3.64	5.01E-9
390	2.39E-3	0.20	4.64E-4	2.56	5.18E-9
400	3.45E-3	0.27	8.16E-4	2.21	7.44E-9

Thus, the photon flux absorbed by the reaction medium in the photo-Fenton process was 3.16×10^{-7} Einstein s^{-1}. With this value the intrinsic kinetic constant for photo-Fenton process carried out in reactor D can be estimated (see chapter 4, section 4.6.4.3)

11.5. Reactor G (CPC-Almería)

This reactor has been also described in chapter 4, section 4.4.2.6. In this case, for the calculation of the radiation entering the reactor, actinometry data are not available. For this reason, and provided information of the radiation captured by the radiometer, the solar useful photonic flux entering the reactor was estimated by using the radiometer measuring range between 300- 400 nm. As it has been commented in chapter 4 (section 4.6.4.3), for a photo-Fenton reaction Fe^{3+} has been assumed to be the main absorbing species between 300-400 nm. Therefore, in the desired range the photon flux entering the reactor W_t can be estimated as follow:

$$W_t = W_{radiometer} \cdot 0.83 \cdot S \qquad (11.7)$$

being,

W_t = total photon flux entering the reactor, Einstein.s^{-1} m^{-2}

$W_{riadometer}$ = radiometer measurement, W m^{-2}

S = Total collector surface, m^2

0.83 = Lost radiation factor (assumed equal to the aluminum reflectivity).

The conversion of $W_{radiometer}$ in W m^{-2} in the 300-400 nm-range can be transformed in Einstein s^{-1} m^{-2} by using the following equation (Malato, 1999):

$$I_{G,\ 300\text{-}400\ nm} = 3.403\ x10^{-6}\ UV_G \qquad (11.8)$$

being UV_G the global radiometer measurement in W m^{-2}. This equation was developed in the Plataforma Solar de Almería by means of spectrophotometer measurements to calculate the spectral distribution of each of the punctual data. For the experiment used as reference (Ph64), the UV_G average was 11.62 W m^{-2}, meaning a photon flux of $3.95x10^{-5}$ Einstein $s^{-1}m^{-2}$ (according to eq. 11.8). Besides this, they found that solar spectra measured at different times in the PSA were very closed to those given by the ASTM standard, which allows the estimation of the photon flux for each wavelength in the range (300-400 nm).

By substituting the respective values in eq.11.7:

$$W_t = 3.95\ x10^{-5}\text{Einstein}\ s^{-1}m^{-2} \cdot 0.83 \cdot 5.93\ m^{-2} = 1.94\ x10^{-4}\ \text{Einstein}.s^{-1}$$

With this value and taking into account its contribution for each wavelength (300-400 nm) in and using Microsoft Excel program, the photon flux absorbed by Fe^{3+} in the CPC can be calculated.

Finally, the absorbed radiation can be calculated according to eq. 11.6

$$\frac{W_{abs,\lambda}}{W_{e,\lambda}} = 1 - \exp(-\mu_\lambda d)$$

where $W_{e,\lambda} = F_\lambda W_t$,

Therefore,

$$W_{abs} = W_t \sum F_\lambda \left[1 - \exp(-\mu_\lambda d)\right]$$

being, F_λ the fraction of photons entering the reactor for each wavelength using, as mentioned before, the ASTM standard spectrum. In Table 11.9, some values of photons flux absorbed by the reaction medium are summarized.

Table 11.9. Photons flux absorbed by Fe^{3+} in Reactor G (CPC)

λ (nm)	**J. Einstein^{-1}**	**F_λ**	**$W_e(F_\lambda W_t)$ (Einstein.s^{-1})**	**μ (Fe^{3+}cm^{-1})**	**1-exp(-μd)**	**W_{abs} (Einstein.s^{-1})**
300	398619.28	0	0	11.30	1	0
310	385760.59	1.36E-4	2.64E-8	10.71	1	2.64E-8
320	373705.57	6.03E-4	6.57E-7	9.53	1	6.57E-7
330	322381.16	1.35E-3	2.63E-7	8.35	1	2.63E-7
340	351722.89	1.53E-3	1.68E-6	7.76	1	1.67E-6
350	341673.67	1.76E-3	3.42E-7	6.58	1	3.42E-7
360	332182.73	1.94E-3	1.12E-6	5.40	1	2.12E-6
370	323204.82	2.56E-3	4.97E-7	4.81	1	4.97E-7
380	314699.43	2.82E-3	3.07E-6	3.63	0.99	3.07E-6
390	306630.21	2.92E-3	5.67E-7	2.55	0.99	5.67E-7
400	298964.46	4.20E-3	4.58E-6	2.21	0.99	4.58E-6

Thus, the total photon flux absorbed by the CPC was 3.44 x10^{-5} Einstein.s^{-1}. With this value the intrinsic kinetic constant for photo-Fenton process can be estimated (see chapter 4, section 4.6.4.3).

Resumen

1. Introducción

Una de las características que mejor define la sociedad actual en lo que se entiende por países desarrollados es la producción de residuos. Prácticamente no hay actividad humana alguna que no genere residuos existiendo además una relación directa entre el nivel de vida de una sociedad o país y la cantidad de residuos generados. Existen actualmente registradas unos cinco millones de sustancias conocidas de las que aproximadamente 70.000 usadas son ampliamente en todo el mundo, estimándose en unas 1.000 las nuevas sustancias químicas que cada año son incorporadas a la lista.

Hasta hace relativamente pocos años, el vertido de residuos en la naturaleza ha sido el medio de eliminarlos, hasta que la capacidad auto-depuradora del medio ambiente ha dejado de ser suficiente. Éstos han sobrepasado con creces los niveles permitidos, provocando una contaminación del medio ambiente que hace inservibles nuestros recursos naturales para determinados usos y alteran sus características. El principal problema lo constituyen los vertidos procedentes de la industria y la agricultura, aunque la población también juega un papel destacado en la contaminación del medio ambiente. Plaguicidas, fertilizantes, detergentes, fenoles y otros productos químicos se vierten sin tratamiento directamente a la naturaleza, a través de vertederos, controlados o incontrolados y situados sin una estrategia de tratamiento.

Una gran parte de este tipo de residuos se generan en solución acuosa y, debido a su propia naturaleza de no biodegradabilidad, los procesos de tratamiento biológico (los más comúnmente utilizados) no tienen ninguna acción sobre ellos por lo que, si no hay ningún tratamiento específico adicional, acaban vertidos sobre el medio ambiente. Este hecho y la creciente escasez de agua potable, hacen cada vez más importante la necesidad de reciclar las aguas para nuevos usos, por lo que se hace prácticamente imprescindible el tratamiento de las aguas residuales para recuperarlas y reusarlas dependiendo del grado de calidad obtenido y del destino final que se le quiera dar.

En este marco general, se han seleccionado compuestos nitroaromáticos (nitrobenceno), fenólicos (fenol), éteres clorados (diclorodietil éter), y aguas textiles, introducidos en el medio ambiente como consecuencia de la actividad industrial, para estudiar la efectividad de tratamientos químicos, mas concretamente los Procesos de Oxidación Avanzada (POAs), en su degradación, mineralización y por otro lado en el aumento de su biodegradabilidad. Varios compuestos de estas familias, se encuentran

incluidos entre los contaminantes prioritarios seleccionados por la Unión Europea (ver **Tabla 1.1**) y han sido listados entre los 130 contaminantes prioritarios dados por la US EPA, por ejemplo, NB y fenol.

La degradación de estos compuestos mediante POAs basados en la radiación (UV-visible) y en el uso de peróxido de hidrógeno, ha sido muy estudiada en el caso del fenol, pero muy poco en el caso de NB y del diclorodietil eter (DCDE); por lo tanto ésta ha sido una de las razones para la selección de estos compuestos. El fenol sin embargo ha sido seleccionado como compuesto modelo. En cuanto a las aguas textiles, es sabido que se trata de una de las fuentes principales de vertidos líquidos y es por otro lado una de las actividades industriales con mayor consumo de agua, razón por la cual siempre representa un tema de mucho interés el buscar soluciones adecuadas para el tratamiento de este tipo de efluentes. Es de destacar, que en el caso del DCDE y las aguas textiles, han formado parte de proyectos de cooperación realizados con la Universidad de San Diego, (CA, USA) y la Ecole Politecnique Federale de Lausanne (Suiza) respectivamente.

En el primer capítulo de esta tesis (Introduction) se han descrito las características principales de los compuestos estudiados, así como las fuentes y su localización en algunas aguas. Con la excepción del fenol, tanto las aguas textiles como el DCDE y el NB, presentan una baja biodegradabilidad, lo que hace necesario el empleo de métodos de tratamiento alternativos (POAs) a los procesos biológicos convencionales.

Los POAs se definen como aquellos procesos que producen radicales altamente reactivos (especialmente radicales $HO^{\bullet}$) capaces de oxidar compuestos orgánicos principalmente por abstracción de hidrógeno (eq.3.1). La característica más positiva de estos radicales es que poseen una reactividad no selectiva con una inmensa mayoría de compuestos orgánicos, hecho que los hace muy atractivos para el tratamiento de aguas. Existen sin embargo, algunos compuestos orgánicos de cadena sencilla como los ácidos acético, maléico y oxálico, acetona o cloroformo que no son atacados por estos radicales. La versatilidad de los POAs se ve aumentada por el hecho de que estos radicales se pueden formar por medio de distintos procesos. En la sección 1.3.8 se presentan los principales POAs y las reacciones por las que se generan estos radicales. De todos ellos, los que se han utilizado en este trabajo son los basados en el uso de la radiación ultravioleta (UV) y en el peróxido de hidrógeno: Fe^{2+}/H_2O_2 (proceso Fenton), $Fe^{3+}/H_2O_2/UV$ (foto-Fenton), H_2O_2/UV y Fe^{3+}/UV.

El principal inconveniente de los POAs es su elevado coste por el uso de reactivos caros (por ejemplo, H_2O_2) y/o el elevado consumo energético (lámparas para generar radiación UV) y es obvio que nunca deben utilizarse como alternativa a tratamientos más económicos, como lo es el tratamiento biológico. De allí que una solución potencial para su uso sería la combinación de estos procesos con el tratamiento biológico, por lo que los POAs se utilizarían como pretratamiento para aumentar la biodegradabilidad del efluente o eliminar la toxicidad del mismo. Por otro lado, el uso de la radiación solar como fuente de energía en los procesos fotoquímicos a estudiar representa una alternativa mucho más económica y por lo tanto también potencia el uso de estos métodos de tratamiento.

Los objetivos de este trabajo están centrados, por lo tanto, en la aplicación de los POAs en el tratamiento del NB, fenol, DCDE y de aguas provenientes de la industria textil y su efecto en la biodegradabilidad de algunas de estas soluciones. La consecución de este objetivo general se logra mediante los siguientes objetivos particulares:

- Estudio del efecto del proceso Fenton en la degradación de NB y fenol. Se persigue además en este apartado el estudio de los parámetros principales que tienen un efecto importante en este proceso (H_2O_2, Fe^{3+}, O_2, temperatura y concentración del compuesto), y de esta forma proponer un modelo cinético que permita conocer la degradación de estos compuestos en un amplio rango de condiciones experimentales.

- Estudio del efecto que tienen diferentes fuentes de radiación en la mineralización de NB y fenol en los distintos procesos aplicados basados en el uso de la luz (foto-Fenton, H_2O_2/UV y Fe^{3+}/UV), haciendo especial énfasis en el uso de la energía solar como fuente de radiación. Se persigue además en este apartado, la determinación de constantes cinéticas intrínsecas en el proceso foto-Fenton, que puedan ser utilizadas en el escalado de reactores usados para tal fin.

- Estudio de la biodegradabilidad de soluciones acuosas de DCDE después de ser tratadas mediante el proceso H_2O_2/UV.

- Aplicación de una estrategia conducente a la aplicación de un sistema acoplado químico-biológico que permita abordar el tratamiento de aguas residuales de la

manera más adecuada. Para tal fin se escogieron aguas residuales procedentes de la industria textil y el proceso de tratamiento ha sido el foto-Fenton para estudiar su efecto en la biodegradabilidad de estas aguas.

Para ello, se han puesto a punto las siguientes técnicas analíticas: HPLC para determinar la concentración de los compuestos estudiados; TOC, DQO, DBO y análisis de H_2O_2 (ver sección de la parte experimental en cada capítulo). En cuanto a la instalación experimental utilizada, es de destacar que para cada objetivo específico se usó una instalación y las mismas están ampliamente descritas en cada sección experimental.Una breve descripción de las instalaciones utilizadas en el trabajo experimental se presenta a continuación:

- **Reactor A**: reactor tanque agitado para el estudio de la degradación de NB y fenol de volumen 1L (sección 3.3.2).

- **Reactores B, C, D, E, F y G**, foto-reactores para el estudio de la mineralización de NB y fenol cuyas principales características son:

- **Reactor B**: foto-reactor tubular, en el que se encuentran instaladas 4 lámparas (15W) de mercurio de baja presión (λ=253.7 nm) siendo el volumen de muestra tratada 2.5 L. Se operó a recirculación total con un caudal de 100 $L.h^{-1}$ (sección 4.4.2.1).

- **Reactor C**: reactor anular en el que se encuentra una lámpara negra (4W) (λ=300-400 nm), y en el que se trataron 1.5 L de muestra (sección 4.4.2.2).

- **Reactor D**: solarbox (simulador solar) con una lámpara de 150W (λ=300-560 nm). Dentro de la caja solar, hay un reactor tubular de volumen 100 cm^3 por donde circulaba la solución tratada a 100 $L.h^{-1}$. El volumen total tratado fué de 1.5 L (sección 4.4.2.3).

- **Reactor E**: es un prototipo de reactor solar parabólico construido en el laboratorio para desarrollar la fase preliminar de experimentos con uso de luz solar (sección

4.4.2.4). El volumen tratado fué de 1.5 L, sus características son similares a la caja solar (reactor D).

- **Reactores F y G**: reactores tipo CPC a escala planta piloto, con volúmenes de 100 y 190 L e instalados en la Escuela Politécnica Federal de Lausanne (Suiza) y en la Plataforma solar de Almería (España), respectivamente (secciones 4.4.2.5 y 4.4.2.6).

- **Reactor H**: es un foto-reactor tanque agitado utilizado para estudiar la efectividad del proceso H_2O_2/UV en el aumento de la biodegradabilidad del DCDE. En él se tienen instaladas 8 lámparas de mercurio de baja presión y que emiten radiación a 253,7 nm (sección 5.2.2).

- **Reactor I**: simulador solar descrito en la sección 6.3.2.1.

- **Reactor J**: se trata de un prototipo de reactor acoplado para tratamiento químico y biológico en continuo. Consta de un foto-reactor con sistema de enfriamiento que tiene instalada una lámpara de mercurio de baja presión con una potencia nominal de 400 W y que emite principalmente a 360 nm. La parte biológica la conforma una columna con relleno en el que se encuentra adherida la biomasa. El sistema acoplado cuenta con un sistema de control para regulación de caudales y del pH (secciones 6.3.2.2 y 6.3.2.3).

Es de hacer notar que en la mayoría de los foto-reactores usados se hizo previamente una actinometría para determinar el flujo de fotones emitidos por las distintas fuentes de radiación utilizadas.

2. Resultados y discusión

2.1. Degradación de NB y fenol por el proceso Fenton. Estudio cinético

Tomando como referencia el mecanismo propuesto por Haber-Weiss para el proceso Fenton (ver sección 3.1), y habiendo identificado y cuantificado tres intermedios de reacción de la degradación del NB como son el orto, meta y para nitrofenoles (ver

figura 3.6) y comparando las relaciones molares de estos isómeros con las obtenidas en diferentes sistemas químicos (ver tabla 3.4), se asume el radical hidroxilo como el principal agente oxidante en el proceso Fenton. De esta forma, se determinaron las condiciones iniciales para favorecer la reacción de estos radicales con el compuesto orgánico a tratar. Dichas relaciones son: $[compuesto]_o/[H_2O_2]_o > 0.016$, $[compuesto]_o/[Fe^{2+}]_o > 0.17$ y $[H_2O_2]_o/[Fe^{2+}]_o > 11$.

Tomando estas relaciones molares como punto de partida, se optimizaron las concentraciones del H_2O_2, Fe^{2+}, O_2, y de los compuestos estudiados, así como de la temperatura, para conocer su efecto en la degradación de NB y fenol. Como se puede observar en las figuras 3.7 y 3.19, la degradación del NB y del fenol siguen una cinética de primer orden, de tal forma que la velocidad de degradación se calcula por medio de la ecuación 3.4 y 3.14 para el NB y el fenol respectivamente. Los resultados de la velocidad de degradación para ambos compuestos calculados mediante estas ecuaciones, asi como los valores de las constantes cinéticas (k_{obs}) se muestran en las tablas 3.2 y 3.3.

Con el objeto de comparar los valores obtenidos para la velocidad de degradación de NB y el fenol, se obtuvo una ecuación empírica tomando como base la ecuación de Arrhenius que se muestra a continuación:

$$R_D = A\,[H_2O_2]_o^a\,[Fe^{2+}]_o^b\,[NB]_o^c\,[O_2]_o^d\,e^{(-Ea/RT)}$$

Los coeficientes a, b, c y d, se obtienen como se explica por ejemplo en la sección 3.3.5 para el caso del H_2O_2 en la degradación de NB. El coeficiente A se calcula a la temperatura determinada para las concentraciones iniciales de H_2O_2, Fe^{2+} y NB, y el mismo es un valor promedio de todos los experimentos realizados para cada compuesto (ver tabla 3.2 y 3.3). De la ecuación 3.11 se obtiene la energía de activación E_a graficando Lg (R_D) vs 1/T. Se obtienen entonces valores para la velocidad de degradación del NB y del fenol mediante la ecuación empírica mostrada (3.12 y 3.13) y se presentan en las tablas 3.2 y 3.3. Como puede observarse tanto en las figuras 3.18 y 3.25, así como en las tablas antes mencionadas, los valores calculados y los obtenidos experimentalmente por la ecuación empírica, son bastante concordantes para ambos compuestos. Esto permite decir que la misma puede ser usada para predecir la velocidad de degradación de los compuestos estudiados con bastante precisión.

2.2. Mineralización del NB y del fenol por medio de procesos basados en el uso de la luz. Foto-Fenton, UV/H_2O_2, y Fe^{3+}/UV

En este apartado se hace un estudio de la influencia de diferentes fuentes de radiación en los procesos antes mencionados para la mineralización del NB y el fenol. En primer lugar, por tratarse de procesos en los que está involucrada la radiación, se realizaron experimentos para estudiar el efecto de la fotólisis directa de los distintos tipos de radiación en la mineralización de los compuestos estudiados. Los resultados obtenidos para el fenol se muestran en la figura 4.21 y en la tabla 4.7. De estos resultados se desprende que la fuente de radiación más efectiva es la de longitud de onda de 253.7 nm emitida por las lámparas instaladas en el reactor B. En el resto de los casos, la lámpara negra (300-400 nm, reactor C), la lámpara de xenón (300-560 nm, reactor D) y la radiación solar directa utilizada en el reactor E, el porcentaje de mineralización es muy bajo por lo cual se puede decir que la fotólisis directa no es una vía efectiva para la mineralización del fenol. Como contraparte se tiene, sin embargo, que en el caso del NB, la fotólisis directa es un medio bastante efectivo para su mineralización como puede verse en los resultados mostrados en la figura 4.47 y en la tabla 4.9. En este caso, los mejores resultados se alcanzaron con la radiación solar, seguidos por la lámpara de xenón y las lámparas germicidas. Esto es un buen ejemplo para entender cómo puede influir la naturaleza del compuesto estudiado en el tratamiento aplicado.

Conocido el efecto de la fotólisis directa, se cosideró entonces la efectividad del proceso foto-Fenton, H_2O_2/UV-vis y Fe^{3+}/UV-vis. Para ello se estudiaron en los siguientes parámetros en los diferentes procesos:

- Foto-Fenton: Efecto de la luz incidente, [H_2O_2], [Fe^{3+}], [Fe^{2+}], [O_2]
- H_2O_2/UV: Efecto de la luz incidente , [H_2O_2]
- Fe^{3+}/UV: Efecto de la luz incidente, [Fe^{3+}]

En el caso de foto-Fenton, se observó que el proceso es muy efectivo en el tratamiento de NB y fenol, obteniéndose siempre un alto grado de mineralización (ver figuras 4.12, 4.19 , 4.26 , 4.29 y tablas 4.8, 4.10). Se obtuvo además que el uso de la luz solar representa una buena alternativa como fuente de radiación. En cuanto al análisis de las variables estudiadas, se observó que la concentración de H_2O_2 es el reactivo limitante del proceso y que cantidades en exceso no contribuyen a una mayor mineralización. Un

parámetro interesante estudiado ha sido el contenido de oxígeno en la solución tratada. De los resultados se desprende que la concentración de oxígeno es importante cuando se tratan soluciones concentradas de NB, como se puede apreciar en la figura 4.26. En cuanto a la comparación de los resultados obtenidos para ambos compuestos tratados por foto-Fenton (ver figura 4.55), se encuentra que, para las mismas condiciones de operación, la cinética de mineralización para el fenol es más rápida que para el NB, jugando una vez más un papel importante la naturaleza de los compuestos, como se explica en el apartado 4.8.2.

Los resultados obtenidos en el caso del proceso H_2O_2/UV-vis para ambos compuestos, demuestran que este sistema es también eficiente en la mineralización del NB y del fenol (ver figura 4.40 y 4.50). Sorprende sin embargo la mineralización alcanzada en presencia de la radiación solar si se tiene en cuenta que el H_2O_2 absorbe muy débilmente a estas longitud de onda. Sin embargo por los resultados obtenidos, la radiación absorbida es suficiente para producir un alto grado de mineralización. Estos resultados se ven mejorados porque el reactor utilizado es de cuarzo, lo que por supuesto permite el paso de la radiación por debajo de 350 nm. Para aplicaciones prácticas, el proceso es bastante mas lento que el proceso Fenton y no se recomiendada el uso de tubos de cuarzo.

Finalmente, se ha utilizado el proceso Fe^{3+}/UV propuesto como alternativa de tratamiento frente al proceso foto-Fenton, que emplea H_2O_2. A la luz de los resultados obtenidos, es bastante claro que no es recomendable como método de tratamiento que tenga como objetivo la mineralización de soluciones acousas de fenol, ya que la mineralización obtenida es muy baja en algunos casos y prácticamente despreciable en otros (ver figuras 4.43 y 4.45). Se puede pensar, sin embargo, en su utilización como pre-tratamiento si el objetivo es por ejemplo la eliminación del fenol. Caso distinto es el del NB, siendo este proceso bastante más efectivo (ver figuras 4.52 y 4.53). Sin embargo, todo apunta a que la efectividad más importante viene del efecto de la fotólisis directa del compuesto, como ha sido mostrado anteriormente, y no por la presencia del Fe^{3+}.

En este apartado se presenta además un modelo que permite la estimación de las constantes intrínsecas del proceso foto-Fenton asumiendo una cinética de primer orden, con lo cual se busca poder estimar la contribución individual de las etapas (oscura e iluminada) que puedan ser utilizadas en el escalado del diseño de reactores. Como se desprende de los resultados, el valor de las constantes intrínsecas obtenidas (etapa iluminada) para el reactor D (solarbox) y el reactor G (CPC-Almería) son muy cercanos, de allí que las mismas pueden ser efectivamente utilizadas para el diseño de este tipo de

reactores. Se comprueba además, que las constantes así estimadas, no dependen de la fuente de radiación ni de la geometría del reactor (ver sección 4.6.4.3). Es necesario sin embargo, realizar un mayor número de experimentos a fin de corroborar la efectividad y posible aplicabilidad del modelo propuesto.

2.3. Aumento de la biodegradabilidad del DCDE por medio de H_2O_2/UV process

En este capítulo se hace un estudio del efecto del proceso H_2O_2/UV en la biodegradabilidad del DCDE, compuesto no biodegradable ampliamente usado como disolvente y que ha sido regulado en los Estados Unidos como un contaminante prioritario debido a su carácter mutagénico y probablemente carcinogénico. El estudio se llevó a cabo en dos etapas. En primer lugar se determinaron las condiciones de operación apropiadas para el tratamiento químico y posteriormente se realizaron los distintos métodos de biodegradabilidad para determinar la biocompatibilidad de la solución tratada. El objetivo entonces, no es lograr la mineralización de la solución, sino el conseguir las condiciones de tratamiento donde la solución tratada sea biológicamente compatible. Se determinaron entonces las condiciones de tratamiento para obtener degradaciones de 25, 50, 75 y 100% de DCDE, encontrándose que la forma mas adecuada fué agregando el H_2O_2 por etapas, haciendo el proceso más lento (ver figura 5.11).

Se realizó un test para determinar la inhibición causada a una biomasa de lodos activos a concentraciones de 25, 50, 75 y 100 $mg.L^{-1}$ de DCDE. En los resultados mostrados en la figura 5.13, se observa que, en el rango de concentración estudiada, el DCDE produce inhibición a concentraciones mayores de 50 $mg.L^{-1}$. Aunque la inhibición observada es pequeña, se utiliza el proceso H_2O_2/UV como pre-tratamiento para conocer el efecto de los intermedios de degradación en un sistema de lodos activos con la biomasa aclimatada y no aclimatada.

Como métodos de determinación de biodegradabilidad se han usado los siguientes:

- “Short-term test”
- “ Long-term test”
- “ Mid-term test”

Los dos primeros (métodos respirométricos) están basados en el consumo de oxígeno por parte de la biomasa utilizada y el “mid-term test” en la evolución del carbono orgánico total (TOC). Todos estos métodos se describen ampliamente en las secciones

5.6.1.,5.6.2 y 5.6.3. En las figuras 5.16 y 5.17 se ilustran los resultados obtenidos en términos de la respiración de la biomasa aclimatada y no aclimatada en función de la concentración de DCDE para el método "short-term". De ellos se desprende que a mayor porcentaje de oxidación del DCDE, mayor es la tasa de respiración de la biomasa. Se observa también que para un alto porcentaje de oxidación (mayor de 50%) no es necesario la aclimatación de la biomasa para incrementar la biodegradabilidad. Se hizo un estudio cinético tomando como referencia la ecuación de Monod y los resultados se presentan en las tablas 5.5 y 5.6. Una ventaja importante que tiene este método es el hecho de generar un resultado en 30 minutos. Al igual que en el "short-term", en el caso de "long-term" la respiración exógena fue menor que la endógena para el caso de soluciones no oxidadas de DCDE y las de un 25 % de oxidación. Esto significa claramente que la toxicidad del DCDE afecta a la biomasa en tiempos de exposición largos. Sin embargo, el consumo de oxígeno aumenta en función del nivel de oxidación, resultados que son confirmados por la producción de CO_2 (ver figuras 5.18 y 5.19 para el caso de biomasa aclimatada). Para el caso de la biomasa no aclimatada se obtuvieron resultados muy similares (ver figuras5.20 y 5.21).

Finalmente se realizaron pruebas de biodegradabilidad con el método "mid-term" y cuyos resultados se presentan en las tablas 5.9 y 5.10 para biomasa aclimatada y no aclimatada, respectivamente. Una vez más se observa que a mayor grado de oxidación (100%) existe una mayor producción de compuestos intermedios que son mas fácilmente biodegradables, por lo que queda demostrado que el proceso H_2O_2/UV es adecuado para el pre-tratamiento de soluciones acuosas de DCDE. "El mid-term" es un método que tiene la ventaja de tener una experimental muy sencilla y por otro lado tiene la ventaja de que en la práctica puede ser de mayor utilidad al tener que seguir solamente la evolución del contenido de carbono en la solución estudiada.

2.4. Sistema acoplado químico y biológico para el tratamiento de aguas producidas en actividades textiles

En el capítulo 6, el objetivo fué desarrollar una estrategia que permitiese obtener una visión general cuando se está frente a un problema de aguas residuales industriales que deben ser tratadas con el objeto de cumplir con la regulación antes de su descarga a la red municipal de aguas. En tal sentido se propone un esquema (ver figura 6.2) en el que se

distinguen claramente tres direcciones a seguir una vez se conozca el grado de biodegradabilidad del efluente estudiado. Si las aguas son biodegradables, sencillamente deben ser descargadas a una planta de tratamiento, ya que es la forma más económica posible que existe actualmente de tratamiento. En tal caso, se sigue la línea verde señalada en el esquema. Si por el contrario se trata de un agua no biodegradable, se propone seguir la línea coloreada con rojo, en la cual se sugiere un tratamiento químico como pre-tratamiento, para luego finalizar la oxidación completa por vía biológica. Una tercera posibilidad, es que las aguas sean parcialmente biodegradables, por lo que en ese caso se sugiere seguir lo indicado por el color azul, donde el tratamiento químico puede emplearse alternativamente después del tratamiento biológico, como post-tratamiento.

Para el desarrollo de esta estrategia, se seleccionaron aguas procedentes de la industria textil, específicamente de una indistria textil del sur de Francia. Se identifican tres tipos de efluentes a tratar:

- Efluente 1, procedente de la salida de un autoclave
- Efluente 2, es una mezcla de los distintos tipos de efluentes producidos en dicha industria
- Efluente 3, se trata de un efluente que provenie de la planta de tratamiento biológico instalada en la planta.

Se empieza por caracterizar los efluentes a estudiar a través de parámetros globales como lo son la DQO, la DBO y el contenido de carbono total, (TOC) entre otros. Esto se hace, debido a la dificultad que significa el poder determinar y cuantificar los constituyentes individuales de las aguas residuales en general y de las aguas textiles en particular. Como se comentó anteriormente, de lo que se trata es conocer que tipo de efluente se tiene. En el caso estudiado, después de realizar el ensayo de biodegradabilidad (Zahn-Wellens) descrito en la sección 6.3.3.5, se observó que en el efluente 1 el contenido de materia orgánica es mayoritariamente no biodegradable a las condiciones de trabajo, utilizando biomasa no aclimatada proveniente de una planta de tratamiento biológico de aguas. Solo se eliminó el 30% del contenido de carbono en 25 días (ver figura 6.12). De igual forma se procedió con el efluente 2 y se observó que el mismo es parcialmente biodegradable (ver figura 6.13), ya que un 50 y un 75% del contenido de carbono orgánico se eliminó en un periodo de 2 y 5 días, respectivamente. En el mismo se encontró una cantidad de carbono que no se eliminó incluso después de 25 días, por lo que se considera

biorecalcitrante. En el caso del efluente 3, se observó que la mayor parte de la materia orgánica es biorefractaria, ya que después de 25 días, sólo se elimina un 40%.

A la vista de estos resultados, se decidió usar el proceso Fenton como método de pre-tratamiento del efluente 1 que sale del autoclave (ver sección 6.4.3), y como pos-tratamiento para el caso del efluente 3 que proviene del tratamiento biológico (ver sección 6.4.4). Realizado el ensayo de biodegradabilidad del efluente 1 a diferentes niveles de mineralización (40 y 70%) se observó que la materia orgánica remanente del pre-tratamiento es biorecalcitrante ya que solo el 50% del contenido de carbono fue eliminado en 28 días (ver figura 6.21). Estos resultados fueron comparados con los obtenidos para el dietilenglicol, que muestran que en sólo 6 días se elimina el 95% del contenido orgánico de una solución de este compuesto. Esto además confirma la actividad de la biomasa utilizada para la realización del ensayo. Por otro lado, se utilizó glucosa como co-sustrato para determinar la actividad de la biomasa después de estar en contacto con el efluente 1 y de los resultados obtenidos se puede deducir que la biorecalcitrancia de este efluente pudiera estar relacionada con la ausencia de enzimas en la biomasa capaces de degradarlo y no a un posible efecto tóxico del mismo. Las causas de esta biorecalcitrancia también han sido tema de estudio, llegándose a la conclusión de que el método de tratamiento usado (foto-Fenton), no es lo suficientemente efectivo para transformar el contenido de materia orgánica en fácilmente biodegradable (ver figura 6.24)

En el caso del proceso Fenton usado como post-tratamiento, se ha conseguido que las soluciones tratadas del efluente 3 puedan ser mineralizadas hasta un 90%. Además, estos experimentos se realizaron utilizando como fuente de radiación un simulador solar, por lo que hace más atractivo el método propuesto. Las concentraciones de reactivos son bastantes bajas y en concreto la del Fe^{3+} permitiría que el efluente una vez tratado pudiera ser vertido directamente sin ningún otro tipo de tratamiento. Esto significa que, ante el problema global planteado, la solución más adecuada nos lleva a pensar en aplicar el proceso foto-Fenton como post-tratamiento del efluente 3 y no como pre-tratamiento del efluente 1, donde por supuesto las cantidades requeridas de reactivo son bastante grandes, encareciendo la posibilidad de aplicación del tratamiento químico.

3. Conclusiones

Los resultados obtenidos conducen a las siguientes conclusiones:

(1) Los proceso Fenton, foto-Fenton y H_2O_2/UV han demostrado ser un método apropiado en la efectiva degradación de nitrobenceno y fenol en solución acuosa.

(2) La velocidad de degradación del NB y el fenol por medio del proceso Fenton, sigue con una cinética de primer orden con respecto a sus concentraciones. Las ralaciones molares iniciales de operación de los reactantes son las siguientes:$[Compuesto]_o/[H_2O_2]>0.016$, $[Compuesto]_o/[Fe^{3+}]_o>0.17$ and $[H_2O_2]_o/[Fe^{2+}]_o> 11$.

Se ha comprobado que la velocidad de reacción no es sensible a concentraciones de H_2O_2, cuando la relación molar (compuesto/H_2O_2) es aproximadamente mayor de 16 y 5 para NB y fenol, respectivamente.

(3) Aunque en la química del proceso Fenton está implicado un mecanismo muy complejo, se intentó partiendo de un modelo cinético muy simple obtener una ecuación empírica para así predecir cuantitativamente la velocidad de degradación del NB y el fenol. La misma ha sido establecida para un amplio rango de condiciones experimentales y su comparacion con la velocidad de degradación calculada experimentalmente la ecuacion permite decir que la misma se obtiene con bastante precisión.

(4) La identificación y cuantificación de los distintos isómeros de nitrofenoles como intermedios de reacción en el tratamiento del NB mediante el proceso Fenton, sugeriría que su degradación se da por la presencia de radicales hidroxilos ($HO^{\bullet}$) como principal especie oxidante. Los resultados cinéticos y la comparación de las relaciones molares iniciales con otros POAs en un

amplio rango de condiciones experimentales, refuerzan la presencia de estos radicales en este proceso.

(5) La fotólisis directa del NB a las condiciones estudiadas representa una buena alternativa en el tratamiento de este compuesto, ya que se obtuvo un 73% de mineralización en dos horas cuando se utilizó luz solar como fuente de radiación. Por el contrario, no se recomienda la fotólisis directa para el tratamiento de soluciones acuosas de fenol, ya que el porcentaje de mineralización obtenida fué muy bajo en la mayoría de los casos. Este comportamiento diferente en los compuestos estudiados está relacionado a sus propiedades de absorción de la luz.

(6) El proceso foto-Fenton ha sido el más efectivo en el tratamiento de fenol y NB en solución acuosa. La velocidad de mineralización fue más rápida para el fenol debido probablemente a la presencia de un grupo donador de electrones como es el OH , que favorece las sustituciones electrofilicas del radical $HO^{\bullet}$. Por otro lado, se demostroó que el uso de sales de hierro Fe^{2+} o Fe^{3+} produce el mismo grado de mineralización.

(7) El uso de la radiación solar en el proceso foto-Fenton es una buena alternativa en el tratamiento de soluciones acuosas de fenol. Mediante este proceso se obtiene una total mineralización de estas soluciones. Por otro lado, la estimación de constantes cinéticas intrínsecas para este proceso, representa un avance significativo para entender mejor este proceso y la contribución de la luz. Como era de esperar, los valores para las constantes obtenidas en los dos reactores seleccionados para su estimación (reactores D y G) son prácticamente iguales, ya que las mismas no dependen de la fuente de radiación ni de la geometría del reactor. Por lo tanto, para el escalado se podrían usar los datos obtenidos a escala de laboratorio.

(8) El proceso H_2O_2/UV ha mostrado ser también un buen método para la mineralización del fenol y el NB. La fuente de radiación usada influye de manera importante en el proceso. En este sentido, la radiación UV (254 nm) es más eficiente en comparación con la radiación de la lámpara negra (300-400 nm) y la lámpara de xenon (300-560 nm). Se obtuvieron unos resultados muy interesantes mediante el uso de la luz solar. Así por ejemplo para fenol, se alcanzó un 90 % de mineralización en dos horas en el reactor E. A pesar de estos resultados, este método no se recomienda en presencia de la luz solar.

(9) Con respecto al sistema Fe^{3+}/UV-vis, aunque este proceso ha sido presentado por algunos autores como un método alternativo para el tratamiento de compuestos orgánicos, no ha demostrado ser eficaz en la mineralización de soluciones de fenol y NB a las condiciones de trabajo. Sin embargo, si el objeto fuese la degradación de los compuestos estudiados, este proceso pudiera ser usado como pre-tratamiento, combinado por ejemplo con un tratamiento biológico.

(10) El tercer compuesto estudiado, el DCDE, ha sido caracterizado como un compuesto no biodegradable. La aclimatación de la biomasa al DCDE no mejora sustancialmente su biodegradabilidad. Además de esto, se comprobó que a concentraciones de DCDE menores de 50 $mg.L^{-1}$, no se observa una inhibición de la biomasa en términos de respiración exógena.

(11) Los intermedios del DCDE producidos al ser tratado mediante el proceso H_2O_2/UV mostraron ser significativamente más biodegradables que el mismo DCDE, tanto para el caso de la biomasa aclimatada como no aclimatada quedando demostrando así la eficiencia de de este proceso como pre-tratamiento.

(12) Con respecto a los datos obtenidos por los diferentes ensayos de biodegradabilidad, los resultados del “mid-term” test son probablemente los

que más pueden ser aprovechados en una aplicación práctica de un sistema acoplado, ya que permite saber la cantidad de materia orgánica que puede ser eliminada. Por otro lado, el "long-term" ensayo permite predecir la toxicidad de los productos intermedios sobre la biomasa utilizada en periodos de exposición largos. En cuanto al "short-term" test, resulta ser un método bastante rápido, alternativo al método de biodegradabilidad usado convencionalmente como es el de la BOD_5 .

(13) Se ha aplicado una estrategia general para el uso de un sistema acoplado químico y biológico a tres efluentes procedentes de la industria textil. Dicha estrategia es considerada una herramienta de mucha utilidad que debe ser tomada en cuenta en este tipo de tratamientos, ya que ofrece una visión general del problema y las posibles vías para solucionarlo. Debido a que dos de los efluentes estudiados resultaron ser no biodegradables, se utilizó el proceso foto-Fenton como pre-tratamiento del efluente 1 y como post-tratamiento para el efluente 3.

(13.1) En el caso del efluente 1, su carácter biorecalcitrante se mantuvo incluso después del pre-tratamiento por medio del proceso foto-Fenton. Este hecho ha sido atribuido a la ausencia de enzimas capaces de degradar la materia orgánica y no a la toxicidad de ésta, quedando en evidencia que no siempre es posible aplicar con éxito un sistema acoplado químico-biológico.
(13.2) En el caso del post-tratamiento aplicado al efluente 3 por medio del proceso foto-Fenton, los resultados muestran que el mismo es una buena alternativa de tratamiento antes de descargar este efluente.